Vol. 280, No. 1, August 2, 1993 ISSN 0003-2670

ANALYTICA CHIMICA ACTA

An international journal devoted to all branches of analytical chemistry

ELSEVIER

ANALYTICA CHIMICA ACTA

Scope. *Analytica Chimica Acta* publishes original papers, preliminary communications and reviews dealing with every aspect of modern analytical chemistry. Reviews are normally written by invitation of the editors, who welcome suggestions for subjects. Preliminary communications of important urgent work can be printed within four months of submission, if the authors are prepared to forego proofs.

Submission of Papers

Americas

Prof. Harry L. Pardue
Department of Chemistry
1393 BRWN Bldg, Purdue University
West Lafayette, IN 47907–1393
USA

Tel:(+1-317) 494 5320
Fax:(+1-317) 496 1200

Computer Techniques

Prof. J.T. Clerc
Universität Bern
Pharmazeutisches Institut
Baltzerstrasse 5, CH-3012 Bern
Switzerland

Tel:(+41-31) 654171
Fax:(+41-31) 654198

Prof. Sarah C. Rutan
Department of Chemistry
Virginia Commonwealth University
P.O. Box 2006
Richmond, VA 23284-2006
USA
Tel:(+1-804) 367 1298
Fax:(+1-804) 367 8599

Other Papers

Prof. Alan Townshend
Department of Chemistry
The University
Hull HU6 7RX
Great Britain

Tel:(+44-482) 465027
Fax:(+44-482) 466410

Prof. Willem E. van der Linden
Laboratory for Chemical Analysis
Department of Chemical Technology
Twente University of Technology
P.O. Box 217, 7500 AE Enschede
The Netherlands
Tel:(+31-53) 892629
Fax:(+31-53) 356024

Prof. Paul Worsfold
Dept. of Environmental Sciences
University of Plymouth
Plymouth PL4 8AA
Great Britain

Tel:(+44-752) 233006
Fax:(+44-752) 233009

Submission of an article is understood to imply that the article is original and unpublished and is not being considered for publication elsewhere. *Anal. Chim. Acta* accepts papers in English only. There are no page charges. Manuscripts should conform in layout and style to the papers published in this issue. See inside back cover for "Information for Authors".

Publication. *Analytica Chimica Acta* appears in 14 volumes in 1993. The subscription price for 1993 (Vols. 267–280) is Dfl. 4214.00 plus Dfl. 462.00 (p.p.h.) (total approx. US$ 2597.75). *Vibrational Spectroscopy* appears in 2 volumes in 1993. The subscription price for *Vibrational Spectroscopy* (Vols. 4 and 5) is Dfl. 700.00 plus Dfl. 66.00 (p.p.h.) (total approx. US$ 407.50). The price of a combined subscription (*Anal. Chim. Acta* and *Vib. Spectrosc.*) is Dfl. 4592.00 plus Dfl. 528.00 (p.p.h.) (total approx. US$ 2844.50). All earlier volumes (Vols. 1–266) except Vols. 23 and 28 are available at Dfl. 259.50 (US$ 144.00), plus Dfl. 18.00 (US$ 10.00) p.p.h., per volume. The Dutch guilder price is definitive. The U.S. dollar price is subject to exchange-rate fluctuations and is given only as a guide. Subscriptions are accepted on a prepaid basis only, unless different terms have been previously agreed upon.
Our p.p.h. (postage, packing and handling) charge includes surface delivery of all issues, except to subscribers in the U.S.A., Canada, Australia, New Zealand, China, India, Israel, South Africa, Malaysia, Thailand, Singapore, South Korea, Taiwan, Pakistan, Hong Kong, Brazil, Argentina and Mexico, who receive all issues by air delivery (S.A.L.–Surface Air Lifted) at no extra cost. For Japan, air delivery requires 25% additional charge of the normal postage and handling charge; for all other countries airmail and S.A.L. charges are available upon request.

Subscription orders. Subscription orders can be entered only by calendar year and should be sent to: Elsevier Science Publishers B.V., Journals Department, P.O. Box 211, 1000 AE Amsterdam, The Netherlands. Tel: (+31-20) 5803 642, Telex: 18582, Telefax: (+31-20) 5803598, to which requests for sample copies can also be sent. Claims for issues not received should be made within six months of publication of the issues. If not they cannot be honoured free of charge. Readers in the U.S.A. and Canada can contact the following address: Elsevier Science Publishing Co. Inc., Journal Information Center, 655 Avenue of the Americas, New York, NY 10010, U.S.A. Tel: (+1-212) 6333750, Telefax: (+1-212) 6333990, for further information, or a free sample copy of this or any other Elsevier Science Publishers journal.
Advertisements. Advertisement rates are available from the publisher on request.

US mailing notice – Analytica Chimica Acta (ISSN 0003-2670) is published biweekly by Elsevier Science Publishers (Molenwerf 1, Postbus 211, 1000 AE Amsterdam). Annual subscription price in the USA US$ 2597.75 (subject to change), including air speed delivery. Second class postage paid at Jamaica, NY 11431. *USA Postmasters*: Send address changes to Anal. Chim. Acta, Publications Expediting, Inc., 200 Meacham Av., Elmont, NY 11003. Airfreight and mailing in the USA by Publication Expediting.

ANALYTICA CHIMICA ACTA

An international journal devoted to all branches of analytical chemistry

(Full texts are incorporated in CJELSEVIER, a file in the Chemical Journals Online database available on STN International; Abstracted, indexed in: Aluminum Abstracts; Anal. Abstr.; Biol. Abstr.; BIOSIS; Chem. Abstr.; Curr. Contents Phys. Chem. Earth Sci.; Engineered Materials Abstracts; Excerpta Medica; Index Med.; Life Sci.; Mass Spectrom. Bull.; Material Business Alerts; Metals Abstracts; Sci. Citation Index)

VOL. 280 NO. 1 CONTENTS AUGUST 2, 1993

(Continued overleaf)

ANALYTICA CHIMICA ACTA
VOL. 280 (1993)

ANALYTICA CHIMICA ACTA

An international journal devoted to all branches of analytical chemistry
Revue internationale consacrée à tous les domaines de la chimie analytique
Internationale Zeitschrift für alle Gebiete der analytischen Chemie

Anal. Chim. Acta, Vol. 280 (1993)

ELSEVIER, Amsterdam–London–New York–Tokyo

0003-2670/93/$06.00

Analytica Chimica Acta, 280 (1993) 1–13
Elsevier Science Publishers B.V., Amsterdam

Influence of substituent and ligand electronic factors on the measurement of gas phase olefins using a surface acoustic wave oscillator coated with *trans*-$PtCl_2$(olefin)(amine) complexes

Edward T. Zellers and Guo-Zheng Zhang

Department of Environmental and Industrial Health, School of Public Health, University of Michigan, Ann Arbor, MI 48109-2029 (USA)

(Received 29th January 1993)

Abstract

Certain olefin gases and vapors can be measured selectively at low concentrations using surface acoustic wave (SAW) sensors coated with reagents of the general formula *trans*-$PtCl_2$(olefin)(amine). The sensor response depends on the steady-state rate of mass change associated with substitution of the initially complexed olefin by the free olefin analyte. This paper examines the effects of changes in the electronic nature of substituents on the free olefin and the olefin and amine ligands in the complex on the sensitivity and selectivity obtained with this class of SAW sensor coatings. For a given reagent, higher reaction rates are generally observed with electron-donating substituents on the double bond of the free olefin. For a given free olefin, varying the 4-substituent of the pyridine ligand in $PtCl_2$(ethylene)(4-X-pyridine) gives a maximum response at an intermediate degree of amine basicity. Replacing pyridine by aniline, pyridine *N*-oxide or the 4-substituted derivatives of these ligands results in reduced responses for the olefins tested. Changing the initially complexed olefin leads to large changes in response, the pattern of which varies with the nature of the free olefin. Results demonstrate the potential for controlling the response of SAW sensors through subtle structural modifications of these coating reagents.

Keywords: Acoustic methods; Gas sensor; Olefin; Surface acoustic wave sensor; Transition metal complex

Olefins comprise an industrially important class of organic compounds used primarily in the production of polymers. Adverse health effects ranging from mild respiratory tract irritation to cancer and birth defects have been associated with exposure to different olefins in humans and test animals [1]. As a result, regulatory exposure limits have been established to minimize the risk of injury and disease in production workers and the general population [2,3]. Ensuring compliance with such standards requires accurate monitoring of these compounds in the atmosphere, often in the presence of other air contaminants. Unfortunately, portable instruments suitable for routine monitoring of personnel exposures to olefin gases and vapors are limited by a lack of sensitivity and/or selectivity [4].

Surface acoustic wave (SAW) sensors and sensor arrays have the potential to address these shortcomings by providing selective measurement of a broad range of organic gases and vapors [5,6]. In the SAW sensor, a high-frequency mechanical wave is generated along the surface of a piezoelectric substrate which has been coated with

Correspondence to: E.T. Zellers, Department of Environmental and Industrial Health, School of Public Health, University of Michigan, Ann Arbor, MI 48109–2029 (USA).

a chemically sensitive film. The most common configuration used for sensing applications employs the SAW device as the frequency controlling element in an oscillator circuit. A feedback amplifier is incorporated between the input and output transducers of the device, resulting in oscillation at a fixed frequency, f_0. Small changes in the physical properties (e.g., mass) of the coating film result in a change of the velocity of the propagating wave, and hence of the oscillator frequency [6].

The following approximate expression can be used to relate the change of the SAW oscillator frequency to changes of deposited mass at the surface of the sensor [7]:

$$\Delta f = K_s f_0^2 \, \Delta m/a \qquad (1)$$

where Δf is the change of frequency (Hz), K_s is a negative substrate-dependent constant (m^2 s kg^{-1}), f_0 is the oscillation frequency of the uncoated device (Hz), and $\Delta m/a$ is the change of coating mass per unit area (kg m^{-2}). This relationship allows one to estimate both the amount of coating deposited on the sensor and the changes in the coating mass resulting from subsequent interactions with gas phase analytes.

In attempting to design sensor coatings that will respond to olefins, advantage can be taken of the ability for the C=C functional group to coordinate, often reversibly, to various transition metal compounds [8,9]. In this way selectivity for olefins in the presence of non-coordinating non-olefin organic vapors would be expected. The more difficult problem is to obtain selectivity for a given olefin in the presence of other olefins.

In a series of recent papers we have shown that a number of olefins can be measured selectivity in the presence of industrially relevant non-olefin organic solvent vapors and structurally similar olefin gases and vapors using SAW oscillators coated with the reagent complex *trans*-$PtCl_2$(ethylene)(pyridine) and related complexes [10–13]. The reaction is shown below in general form:

$$\textit{trans}\text{-}PtCl_2(OL_1)(AM) + OL_2 \rightleftarrows \textit{trans}\text{-}PtCl_2(OL_2)(AM) + OL_1 \qquad (2)$$

where OL_1 and OL_2 represent the initially complexed and free olefins, respectively, and AM is the *trans*-amine ligand. A useful property of this class of reagents is the capability for regeneration following exposure to the target olefin by brief exposure to the initially complexed olefin which drives the olefin-exchange reaction in the reverse direction.

Results from our earlier studies suggested that the selectivity observed for the target olefins in the presence of other olefins could be attributed to electronic and steric factors [11,12]. The importance of steric factors was investigated in a subsequent study where it was shown that bulky substituents on the gas phase olefin or on the pyridine ligand (i.e., in the 2 or 6 positions on the pyridine ring) dramatically reduced the rate of the substitution reaction and permitted the measurement of less sterically hindered olefins in the presence of their more sterically hindered isomers and structural analogues [13]. The influence of the electronic structural features of the free olefins and the ligands in the Pt–olefin complex has not yet been systematically explored.

The coating reagents investigated here are examples of square-planar metal-olefin π-complexes which have amine and olefin ligands in a *trans* configuration about a central Pt(II) atom [8,14]. The olefin is bound to Pt via a σ bond, involving donation of electron density from the olefin π cloud to the Pt, as well as by a π bond, involving back-bonding from the metal to the antibonding orbitals of the olefin. The relative importance of each of these bonding interactions depends on the overlaps and energies of the respective orbitals on the metal and the olefin, though it is generally accepted that the σ bond is predominant [15].

Both the rates and mechanisms of olefin-substitution reactions in these complexes are affected by the amine ligand [16,17]. The σ-bond strength of the amine is determined primarily by its basicity. In addition, where the amine has low-lying vacant p orbitals, as in pyridine and pyridine *N*-oxide, back-bonding from the metal is possible. This interaction does not occur with aniline due to the unavailability of accepting orbitals. The competitive donation (via σ bonding)

and acceptance (via π bonding) of electron density between between the amine and olefin can thus affect the overall reactivity of the complex. When a free olefin reacts it replaces the initially bound olefin without disrupting the spatial configuration of the other ligands. Where the amine is pyridine or pyridine *N*-oxide the reaction proceeds exclusively through a pentacoordinate associative transition state [16]. Where the amine is aniline both solvent-assisted and associative pathways are observed [17].

In the study described here, we examine the effect of substituents on the free olefin and the amine and olefin ligands in the complex on the relative reactivities of the complexes and the extent to which such effects might be used to adjust the sensitivity and selectivity of a SAW sensor having these complexes as coatings. Coating reagents examined include $PtCl_2$(ethylene)(AM) (AM = pyridine, aniline, pyridine *N*-oxide and their 4-substituted derivatives) and $PtCl_2(OL_1)$ (pyridine) (OL_1 = 1-butene, 1-hexene and 1-octene).

The sensor response at steady-state is a function of the change of mass accompanying the olefin substitution and it will therefore depend on the gas phase olefin concentration. Furthermore, since there is a 1:1 stoichiometry between reactants and products, the rate of frequency change of the sensor df/dt, will depend on the steady-state reaction rate according to the following equation [11]:

$$df/dt = -C(MW_2 - MW_1)\, dN/dt \qquad (3)$$

where MW_i is the molecular weight of the free or initially complexed olefin, N is the number of moles of each olefin involved in the reaction and C is a constant. Thus, for equivalent reaction rates, the greater the MW difference between the attacking and leaving olefin, the greater will be the sensor response.

TABLE 1

Analytical data for the *trans*-$PtCl_2(OL_1)$(AM) reagents

Complex X	m.p. (°C)	Calc.			Found		
		%C	%H	%N	%C	%H	%N
OL_1 = ethylene, AM = 4-X-pyridine, X =							
$-N(CH_3)_2$	124	25.97	3.39	6.73	26.01	3.44	6.68
–OH	122	21.61	2.33	3.60	21.64	2.35	3.57
$-CH_3$	117	24.82	2.86	3.62	24.90	2.90	3.60
–H	112	22.53	2.43	3.75	22.50	2.50	3.70
–Cl	120	20.63	1.98	3.44	20.80	2.00	3.40
–CN	145	24.13	2.03	7.04	24.01	1.92	6.98
OL_1 = ethylene, AM = 4-X-aniline, X =							
–H	110	24.81	2.86	3.62	24.83	2.84	3.30
$-CH_3$	114	26.94	3.27	3.49	26.82	3.26	3.67
–Cl	116	22.79	2.39	3.32	22.64	2.39	3.23
OL_1 = ethylene, AM = 4-X-pyridine N-oxide, X =							
–H	146	21.61	2.33	–	21.67	2.33	–
$-CH_3$	147	23.83	2.75	–	24.29	2.82	–
–Cl	165	19.85	1.90	–	19.77	1.82	–
AM = pyridine, OL_1 =							
Ethylene	112	22.53	2.43	3.75	22.50	2.50	3.70
1-Butene	106	26.94	3.27	–	26.77	3.33	–
1-Hexene	40	30.77	3.99	–	30.58	3.99	–
1-Octene	–	34.14	4.63	–	34.15	4.77	–

EXPERIMENTAL

Most of the starting materials, solvents and gases were obtained from Aldrich (Milwaukee, WI) and were used without further purification, with the exception of pyridine *N*-oxide which was purified by fractional distillation. Ethylene, vinyl chloride and vinyl bromide gases were obtained from Matheson Gas Products (Secaucus, NJ). Elemental analyses were performed by Galbraith (Knoxville, TN). Particle size distributions were determined according to established methods [18] using an Olympus Model BHA optical microscope.

trans-$PtCl_2$(ethylene)(amine) reagents were synthesized by the addition of 1 molar equivalent of the amine to a stirred aqueous solution of $KPtCl_3$(ethylene) (Zeise's salt) at room temperature [14]. The crude solid precipitates were recrystallized after air drying from a minimum of dichloromethane by adding an excess of hexane or petroleum ether. All of the products were isolated as yellow crystalline solids.

Conversion of the ethylene complexes to the corresponding olefin-substituted reagents was performed by combining the ethylene complex with an excess of the olefin in dichloromethane and refluxing for 1–2 h. These products were isolated and recrystallized as described above. In the case of $PtCl_2$(1-hexene)(pyridine) and $PtCl_2$(1-octene)(pyridine), the products were difficult to recrystallize and were generally isolated as viscous oils. The former complex could be obtained as a low-melting solid upon repeated recrystallizations. The complexes investigated are listed in Table 1 along with the corresponding melting points and elemental analyses.

Combining the Pt–olefin complexes with the amorphous rubbery polymer, poly(isobutylene) (PIB, Scientific Polymer Products, Ontario, NY) improved the coating uniformity and response reproducibility relative to the use of the solid complexes alone. Films were deposited on the entire active area of the sensor either by solvent casting or spray-coating from solutions containing approximately 6 mg ml^{-1} of each component in toluene : hexane (2 : 1). The mass deposited was estimated from the net frequency shift via Eqn. 1 after evaporation of the casting solvent. For all experiments described here, the frequency shift due to the coating film was in the range of 200–400 kHz, corresponding to deposited masses of 260–520 μg.

It has been shown that the reference device can be coated with an equivalent amount of PIB so that measuring the difference frequency would cancel the transient responses due to physical sorption and desorption of vapors by the polymer component of the reagent-coated sensor [10,12]. Therefore measurements collected for this study were made using a single oscillator and the response was determined after allowing a short time for equilibration: this typically required 30–90 s owing to mixing in the chamber and to establishment of steady-state reaction conditions within the sensor coating.

A 30-MHz ST-quartz SAW oscillator with Au-on-Cr metallization and an active area of 1.5 cm^2 was used for all tests [11]. Series inductors were used as tuning elements and two LM733 amplifiers provided the gain necessary to maintain oscillations in the SAW device. The sensor frequency was monitored with a digital frequency counter (Hewlett-Packard 5384A) and monitored with a personal computer via an IEEE-488 interface. Signals were collected every 10 s at a resolution of 1 Hz and the net 1-min frequency shifts were averaged over the exposure interval at a given olefin concentration to yield the rate of frequency change in Hz min^{-1}.

The sensor was placed in a stainless-steel chamber equipped with gas inlet and outlet ports. Electrical connections were made using coaxial cables and connectors in the bottom of the chamber. The chamber was wrapped with heating tape to control the temperature and a thermocouple was used to monitor the temperature at the surface of the sensor. Known concentrations of the olefin vapors were generated by bubbling N_2 gas through a flask containing the liquid solvent and then into a dilution-air stream. For gaseous olefins a syringe pump was used to introduce the pure material into the air stream. The contaminant stream was divided between the sensor exposure chamber and an infrared gas analyzer (MIRAN 1A, Foxboro, Bridgewood, CT) used for continu-

ous monitoring of solvent vapor concentrations. Dilution-air flow and temperature were controlled with a Miller-Nelson Research HCS 301 control unit. The relative humidity was maintained at 5 ± 3% for all experiments.

RESULTS AND DISCUSSION

Free-olefin substituent effects

Our current and previous [10–13] tests of the SAW sensor coated with $PtCl_2$(ethylene)(pyridine) have revealed two general features of the sensor responses to olefin gases and vapors: they vary non-linearly with the olefin concentration and they exhibit a positive Arrhenius temperature dependence. Responses to styrene, ethyl acrylate and vinyl acetate as a function of concentration and temperature are shown in Fig. 1A and B, respectively. These data are representative of the those obtained with other reactive olefins. Each point on the curves represents the average rate of frequency change obtained at a given concentration over a period of 10–30 min. Responses are generally quite constant at a given concentration for such exposures. However, prolonged exposure leads to an eventual decline in response as the reagent becomes depleted. This occurs more rapidly at higher concentrations. With careful deposition technique, intercoating response variations can be maintained below 10%.

The downward concavity in the response curves is a consequence of the heterogeneous reaction between the gaseous olefin and the solid reagent which is the rate-limiting step in the overall analyte-coating interaction. log–log plots of the sensor response versus concentration yield straight lines in accordance with a pseudo-first-order (with respect to the olefin) power-law kinetic model for the reactions [19]. For certain olefins, diffusional resistance within the reagent may also play a role in the overall interaction [13]. As mentioned above, regeneration of the $PtCl_2$(ethylene)(pyridine) is possible following exposure to the olefins

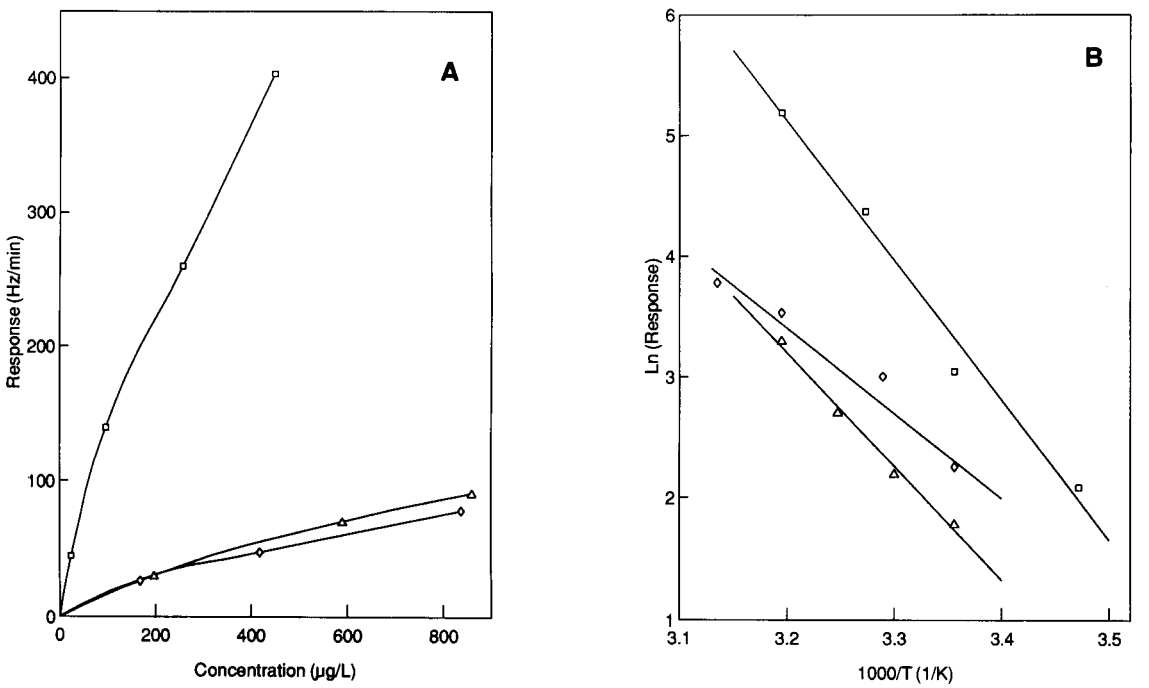

Fig. 1. Response of the $PtCl_2$(ethylene)(pyridine)-coated SAW sensor to (□) styrene (△) ethyl acrylate and (◇) vinyl acetate as a function of (A) concentration at 40°C; and (B) temperature at a fixed air concentration for each olefin. Each point represents the average response for a 10–30 min exposure.

shown in Fig. 1 and for several other olefins. However, this issue is not examined in this paper.

The Arrhenius plots in Fig. 1B show that the slopes of the lines for styrene and ethyl acrylate are quite similar, indicating a similar activation energy for reaction. The slope for vinyl acetate is significantly smaller. This suggests a possible scheme for enhancing selectivity between certain olefins by the use of a simple sensor array where all the sensors are coated with the same reagent: the ratios of responses of two or three sensors operating at different temperatures should allow discrimination on the basis of activation energies.

In Table 2, responses from the sensor coated with $PtCl_2$(ethylene)(pyridine) are summarized for exposure to each of several different olefins. The limit of detection (LOD) is defined as the concentration corresponding to 3s/sensitivity, where s = 1 Hz is the typical standard deviation of the 1-min frequency shifts measured before and after exposure. The sensitivity, in $Hz/(\mu g\ l^{-1})\ min^{-1}$, is based on the slope of the response curve at the lowest measured concentration for each olefin. The rate of reaction shown in Table 2 was determined from Eqn. 3 assuming a nominal free-olefin concentration of 1 $\mu g\ l^{-1}$. This latter measure accounts for the differences in mass change accompanying ethylene substitution.

An obvious trend in reactivity is observed between the groups listed in Table 2: olefins with strongly electron-withdrawing groups attached to the double bond (e.g., vinyl chloride, vinyl bromide, vinylidene chloride, trichloroethylene, acrylonitrile) do not react while those with moderately electron-withdrawing substituents (e.g., ethyl acrylate, methyl acrylate and vinyl acetate) or electron-donating substituents (e.g., aromatic olefins and alkenes) generally react quite readily. This inherent selectivity allows measurement of the reactive olefins in the presence of the non-reactive olefins even where the latter are present in large excess [11–13].

Within a given class of olefins, both steric and electronic factors appear to govern the relative reactivities. In the absence of such effects, sensitivity would be proportional to the difference in

TABLE 2

Limit of detection, sensitivity and molar reaction rate for various free olefins with *trans*-$PtCl_2$(ethylene)(pyridine) coatings at 40°C

Free olefin	ΔMW [a] ($g\ mol^{-1}$)	LOD ($\mu g\ l^{-1}$)	Sensitivity [$Hz/(\mu g\ l^{-1})\ min^{-1}$]	Reaction rate [b] ($pmol\ min^{-1}$)
4-Chlorostyrene	110.6	0.38	−8.0	95
4-Methylstyrene	90.1	0.65	−4.7	68
Styrene	76.1	1.4	−2.1	37
β-Methylstyrene	90.1	4.1	−0.7	11
1-Butene	28.1	15	−0.21	9.7
cis-2-Butene	28.1	20	−0.15	7.2
trans-2-Butene	28.1	45	−0.07	3.1
Isobutylene	28.1	ND [c]	–	–
1-Hexene	56.1	1.0	−2.9	68
Cyclohexene	54.1	106	−0.03	0.7
Vinyl acetate	58.0	16	−0.19	4.3
Ethyl acrylate	72.1	22	−0.14	2.5
Methyl acrylate	58.0	62	−0.05	1.1
Vinyl chloride	34.5	ND	–	–
Vinyl bromide	78.9	ND	–	–
Vinylidene chloride	68.9	ND	–	–
Trichloroethylene	103.3	ND	–	–
Acrylonitrile	25.0	ND	–	–

[a] Difference in molecular weight between free olefin and ethylene. [b] Calculated at a nominal free-olefin concentration of 1 $\mu g\ l^{-1}$. [c] Not detected.

MW between each olefin and ethylene. This is clearly not the case. Within the aromatic olefin group, the lower response for β-methylstyrene compared to styrene and the isomeric 4-methylstyrene can be attributed to the steric hindrance associated with the methyl group on the pendant double bond. The lower response for indene, however, is less easily explained. One would expect indene to give a higher response since the substituents on the coordinating double-bond are in a *cis* configuration. The anomolously low indene reactivity is apparently due to its fused ring structure. Upon coordination, the double bonded carbons in most olefins acquire some sp^3 character with a commensurate change occuring in the bond lengths and bond angles in the molecule. In addition, the substituents on coordinated olefins are bent back away from the Pt atom to minimize repulsive non-bonded interactions with the Pt or the other ligands [9]. The inflexibility of the indene ring would inhibit such structural adjustments and destabilize the transition state for the reaction.

The increase in sensitivity observed in the series styrene, 4-methylstyrene and 4-chlorostyrene is much greater than expected from the MW differences alone, and can be attributed to the electronic influence of the 4-substituent (see Fig. 2). Interestingly, the addition of either an electron withdrawing or donating group enhances the reaction rate relative to styrene. These results are consistent with those reported for the relative thermodynamic stabilities of 4-substituted-styrene complexes of Pt(II) in solution [20]. But they are in contrast to that expected from ^{13}C NMR data reported on a series of styrene complexes where it was found that the coupling constants between Pt and the olefinic carbons increased with the electron-donating strength of the 4-substituent of styrene [21,22]. It is known, however, that the coupling constant is insensitive to the strength of the π back-bonding in these complexes [21].

With respect to the alkenes and cycloalkenes in Table 2, the trend in reactivity among the butene isomers (i.e., 1-butene > *cis*-2-butene > *trans*-2-butene > isobutylene) can be ascribed to steric factors. The high reactivity of 1-hexene and low reactivity of cyclohexene were both unexpected. As shown below, use of the 1-hexene complex as the reagent coating leads to higher sensitivity for several olefins than its lower-homologue complexes. Cyclohexene adopts a so-called half-chair configuration where the methylene groups attached to the double bond are *cis* [23]. One would therefore expect the double bond to be relatively accessible for coordination, analogous to the case of *cis*-2-butene. Unlike indene, structural adjustments accompanying coordination to Pt would be relatively facile for the six-membered cyclohexene ring. While the low cyclohexene response is not completely understood, in light of the relatively high reactivity of 1-hexene and the results for indene relative to the other aromatic olefins, a high degree of selectivity against cyclic olefins is apparent.

The reactivities of vinyl acetate and ethyl acrylate are similar (see Fig. 1). This follows from the similarity in the electron-withdrawing strength of the ethoxycarbonyl and acetoxy groups as re-

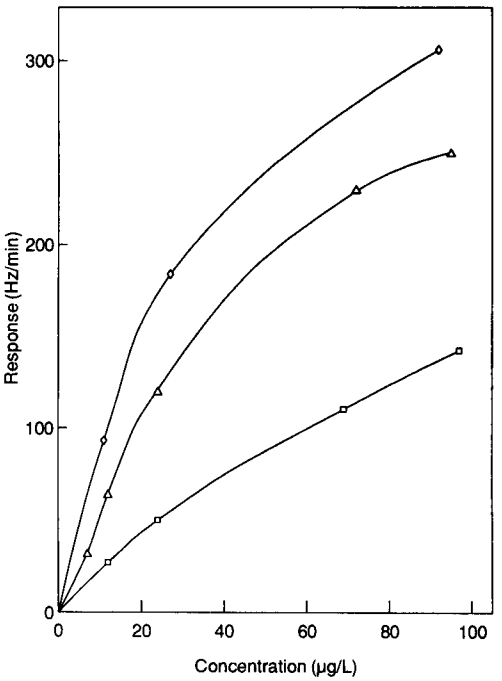

Fig. 2. Response of the $PtCl_2$(ethylene)(pyridine)-coated SAW sensor to (◇) 4-chlorostyrene, (△) 4-methylstyrene and (□) styrene at 40°C. Each point represents the average response for a 10-min exposure.

flected in their Hammet σ_p and σ_m constants [23]. Surprisingly, methyl acrylate is less reactive than both vinyl acetate (an isomer of methyl acrylate) and ethyl acrylate at all concentrations. Since steric factors can be ruled out, apparently there is a subtle difference in the electronic influence of the methyl and ethyl esters in the acrylates on the olefin double bond. It has been shown previously that the response to vinyl acetate is not affected by equivalent concentrations of methyl acrylate upon coexposure [11]. Methyl acrylate, however, will interfere with the response due to ethyl acrylate [13]. Notably, methylmethacrylate does not react to any measurable extent due to the steric hindrance of the additional methyl group on the olefin carbon.

In the absence of significant steric effects, the reactivities of the various olefins can be considered in terms of their orbital energies. As stated above, the Pt–olefin bond strength depends on the contribution of both σ-type and π-type bonding. Meester et al. [24] studied the bonding properties of a similar series of *trans*-$PtCl_2$(ethylene)(amine) complexes and determined approximate energy levels for the highest-occupied and lowest-unoccupied Pt orbitals in these complexes based on spectroscopic data. Figure 3 presents a comparison of these energies with those of the corresponding orbitals of several of the free olefins tested here (data for the remaining olefins were not available). The trend in relative energies of the occupied orbitals follows that of the observed reactivities, with the exception of vinyl chloride. That is, those olefins with closer occupied-orbital energy matches to Pt are generally more reactive. The relative energies of the unoccupied orbitals do not follow this trend. These data support the view that the σ-bonding interaction is relatively more important than the π back-bonding interaction in determining the reaction kinetics of these complexes.

$PtCl_2$(ethylene)(4-X-pyridine)

Figure 4 shows the sensor response to ethyl acrylate using the coating reagents $PtCl_2$(ethylene)(4-X-pyridine), where X = $N(CH_3)_2$, CH_3, H, Cl, and CN. Once again, each point represents the mean rate of frequency change measured over 10–30 min at a given concentration. Similar series of exposures were performed with vinyl acetate and styrene. Representative responses are shown in Fig. 5 for individual exposures to 2000

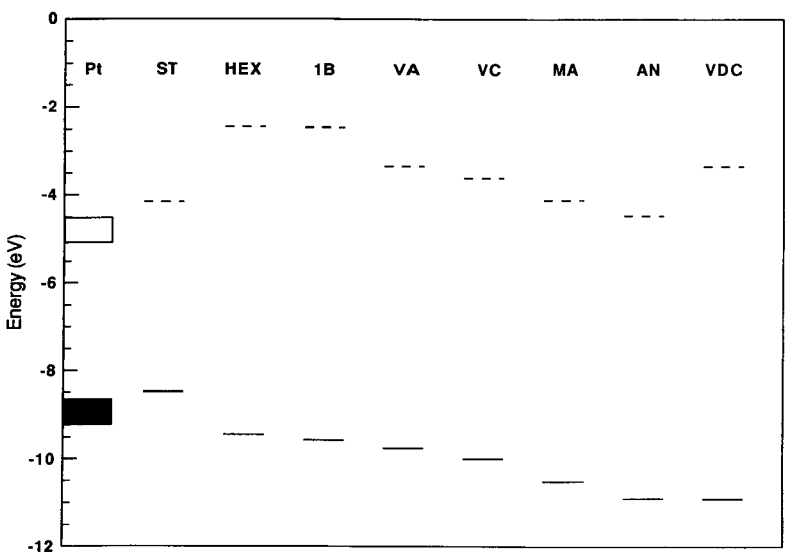

Fig. 3. Energy-level comparison of highest-occupied (———) and lowest unoccupied (— — —) orbitals for several free olefins and Pt in $PtCl_2$(ethylene)(amine); ST = styrene, HEX = 1-hexene, 1B = 1-butene, VA = vinyl acetate, VC = vinyl chloride, MA = methyl acrylate, AN = acrylonitrile and VDC = vinylidene chloride.

$\mu g\ l^{-1}$ of ethyl acrylate and vinyl acetate at 30°C and 400 $\mu g\ l^{-1}$ of styrene at 40°C. The responses have been normalized separately for each of the olefins to the coating providing the highest response.

For styrene and vinyl acetate the pyridine complex gives the highest response, whereas for ethyl acrylate the highest response is observed with the 4-chloropyridine complex. The 4-hydroxypyridine and 4-(4-nitrobenzyl)pyridine complexes were also tested and found to give no reaction. Although these olefins could be identified based on the collective response patterns, the trends in the sensor responses shown in Fig. 5 are fairly similar, with a peak in reactivity occurring at an intermediate degree of amine basicity. The patterns for a given olefin will vary somewhat with concentration because the responses do not increase at exactly the same rate with concentration. However, the same order of responses is maintained over a wide range of concentration. None of the 4-substituted pyridine complexes responded to vinyl chloride, vinyl bromide, vinylidene chloride or acrylonitrile.

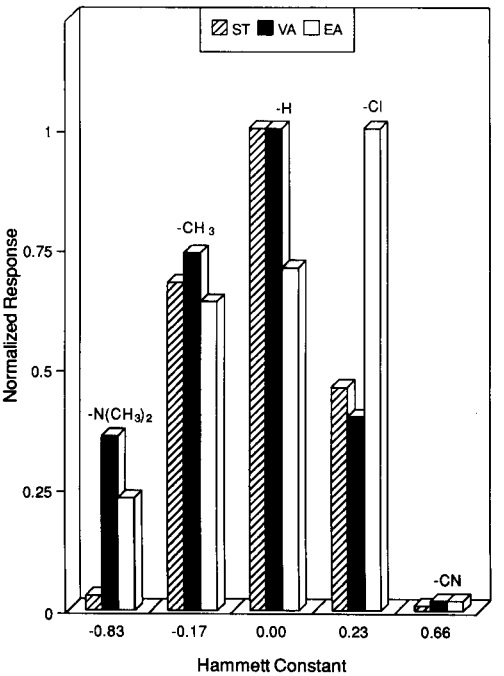

Fig. 5. Normalized responses to a given concentration of styrene (ST), vinyl acetate (VA) and ethyl acrylate (EA) as a function of the Hammett σ_p constant of X for the $PtCl_2$(ethylene)(4-X-pyridine)-coated sensor [X = $N(CH_3)_2$, CH_3, H, Cl, or CN].

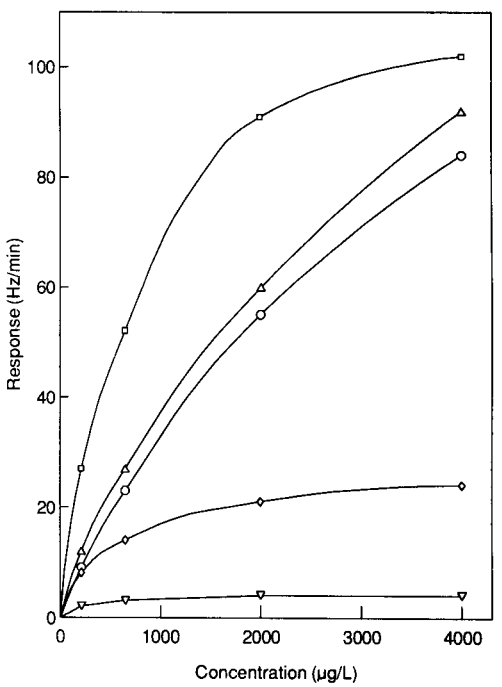

Fig. 4. Response to ethyl acrylate of the SAW sensor coated with $PtCl_2$(ethylene)(4-X-pyridine), where X = (◇) $N(CH_3)_2$, (○) CH_3, (△) H, (□) Cl, (▽) CN. Each point represents the average response for a 10–30 min exposure.

The response patterns observed are different than what would have been expected based on solution-phase kinetic studies of similar complexes. The rates of olefin substitution in the complexes $PtCl_2$(2-methyl-2-butene)(4-X-pyridine) [16] and $PtCl_2$(styrene)(4-X-aniline) [17] increased markedly with the electron-withdrawing strength of X. In the former case, the order of reactivity was X = CN > Cl > H > CH_3 > NH_2 and a linear relationship was observed between the log of the rate constant and the Hammett σ_p constant of X. It has also been shown that the ^{13}C NMR chemical shifts of the olefinic carbons and the Pt–(C=C) coupling constants also decrease in the same order, although the correlations are rather weak [22].

The reaction orders we observed are similar to the thermodynamic stabilities of olefin complexes in chloroform solution reported by Shupack and Orchin [25] where substitution of styrene by 1-dodecene in a series of *trans*-$PtCl_2$(styrene)(4-X-pyridine *N*-oxide) showed a minimum value of the equilibrium constant for X = H followed closely by the complex where X = Cl. Raman and IR data indicate that the strength of the Pt–ethylene bond in a series of $PtCl_2$(ethylene)(4-X-pyridine) complexes is not strongly affected by changes in the electron-withdrawing/donating strength of X [26]. For the same series of complexes, however, the Pt–N bond strength passes through a minimum at X = H [27].

The influence of X observed here can be rationalized broadly in terms of the relative strengths of the σ and π bonding of the substituted pyridines. For pyridines with strongly electron donating groups, the Pt–N σ bond is stronger and the Pt–ethylene π bond is also stronger, leading to a stabilization of the ethylene complex toward substitution by the attacking olefins. For complexes having electron-withdrawing pyridine 4-substituents, apparently the Pt–N π bond is strengthened and the Pt–ethylene σ bond is also strengthened, again, leading to stabilization of the ethylene complex. Only at intermediate degrees of electron withdrawal/donation by the pyridine substituents is displacement of the ethylene favorable for these olefins.

Particle size

One potential mitigating factor affecting the observed sensor responses is the particle size distributions of the solid reagents when deposited on the sensor. The active surface area of the solid Pt–olefin complex could affect the reactivity. In order to investigate this factor, the size distributions of the reagents in the coating films were characterized. While the morphologies of the deposited solids varied from reagent to reagent, approximate values of the mean diameters and surface areas could be obtained using a projected area method and assuming spherical particles. Table 3 provides summary statistics of the particle size distributions measured for several coating films of each of the reagents tested. The values for the pyridine complex are viewed with skepticism because the morphology of this reagent was particularly variable. The data shown in Table 3 were obtained using films deposited directly on the sensor that were subsequently exposed to one of the olefins.

TABLE 3

Geometric mean particle size and reagent surface area of deposited *trans*-$PtCl_2$(ethylene)(4-X-pyridine) coating reagents

X	Geometric mean diameter (μm)	Coating freqency shift (kHz)	Reagent surface area [a] (mm^2)
$-NH_3$	1.10	272	11.2
–OH	1.23	254	16.1
$-CH_3$	1.23	274	13.1
–H	1.17	247	16.5
–Cl	1.00	269	14.9
–CN	1.37	234	22.6

[a] Determined assuming approximately spherical particles within the coating.

While there is some variation in the mean particle diameters and calculated surface areas, the differences could not account for the observed differences in reactivity. The densities of the complexes may also be important, since the free olefin must diffuse into the reagent during reaction. This factor was not investigated, but is not likely to differ greatly between these complexes.

$PtCl_2$(ethylene)(4-X-aniline, 4-X-pyridine N-oxide)

Complexes having other *trans*-amine ligands were then deposited on the sensor and tested for their responses to ethyl acrylate at 30°C. In all cases, ethylene was the initially complexed olefin. It had been determined previously that the complex having NH_3 as the amine ligand showed no reactivity toward styrene, so this complex was not tested further with ethyl acrylate. Where the amine was 4-X-pyridine *N*-oxide, responses were in the order X = H > CH_3 > Cl and in all cases were significantly lower than those for the corresponding pyridine complexes. As mentioned above, the maximum response for X = H is con-

sistent with the trend in the thermodynamic stability of 4-X-pyridine *N*-oxide complexes of styrene [25]. For the 4-X-aniline series, responses were in the order $CH_3 > H > Cl$ and were greater than those for the corresponding pyridine *N*-oxides but less than those for the pyridine series. Although thermodynamic data on the aniline complexes were not available, the kinetic study cited above [17] indicated a trend opposite to that observed here, i.e., substitution rates generally increased with the electron-withdrawing strength of X. It was found for the aniline complexes, and to a lesser extent for the pyridine *N*-oxide complexes, that the sensor responses decreased rapidly at a given ethyl acrylate concentration within a few minutes of exposure.

$PtCl_2$(olefin)(pyridine)

Attempts to prepare complexes where OL_1 = vinyl chloride and trichloroethylene were unsuccessful. However, complexes of 1-butene, 1-hexene and 1-octene, with pyridine as the *trans*-amine ligand, could be prepared easily and allowed a systematic examination of the effect of progressively longer alkyl side chains on the olefin substitutional lability. Results of exposure to three different free olefins are summarized in Fig. 6 and Table 4. For exposure to ethylene, there is a steady increase in response with increasing alkyl chain length and all frequency shifts are positive because of the loss of mass from the coatings. As shown in Table 4 the response ratios are 3:2:1 for the 1-octene, 1-hexene, and 1-butene complexes, respectively, in agreement with the ratios expected based on the mass differences alone. Thus, there does not appear to be any difference due to electronic factors. In contrast, with ethyl acrylate the response pattern is quite different. The ethylene and 1-butene complexes show about the same responses, which indicates that the latter reagent is reacting at a higher rate since the net mass change is smaller. The 1-octene complex gives a large response, indicating an even higher reaction rate because of the similarity in MW between ethyl acrylate and 1-octene. In contrast to ethylene and 1-butene complexes, the response using the 1-octene complex is positive because there is a net mass loss from the surface upon

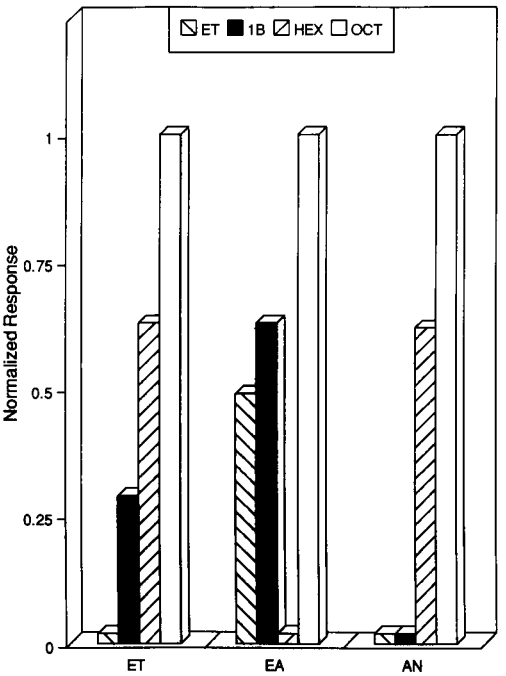

Fig. 6. Normalized responses to ethylene (ET), ethyl acrylate (EA) and acrylonitrile (AN) as a function of OL_1 for the $PtCl_2(OL_1)$(pyridine)-coated sensor where OL_1 = ethylene, 1-butene (1B), 1-hexene (HEX) or 1-octene (OCT) (note: with the exception of EA reacting with the ethylene and 1-butene complexes, all responses are positive since there is a net loss of mass from the sensor coatings).

reaction with ethyl acrylate. Surprisingly, ethyl acrylate did not react to any measurable extent with the 1-hexene complex. The reason for this is not clear. When acrylonitrile is exposed to each of these coatings, no responses are observed for the ethylene or 1-butene complexes, but large responses in the ratio of about 2:3 are obtained using the 1-hexene and 1-octene complexes, respectively (positive responses are obtained for these coatings, again, because of the net loss of mass from the sensor surface). Vinyl chloride gives small concentration dependent responses with the 1-hexene and 1-octene complexes, but vinylidene chloride could not be detected with any of the sensor coatings investigated.

Additional tests involving exposure to the butene isomers were performed using the 1-hexene complex coating. The LODs at 25°C are 1.6, 1.7, 5.3, and 49 $\mu g\ l^{-1}$ for 1-butene, *cis*-2-

TABLE 4

Comparison of sensor responses to each of several free olefins using different *trans*-$PtCl_2$(olefin)(pyridine) coatings

Initially complexed olefin	ΔMW (g/mol)	ΔMW ratio	Sensitivity [a] [Hz/(μg l^{-1}) min^{-1}]	Sensitivity ratio
Free olefin = ethylene				
Ethylene	0.0	–	–	–
1-Butene	28.0	1.0	0.64	1.0
1-Hexene	56.1	2.0	1.4	2.2
1-Octene	84.1	3.0	2.1	3.1
Free olefin = ethyl acrylate				
Ethylene	72.1	6.0	−0.031	0.5
1-Butene	44.0	3.6	−0.040	0.6
1-Hexene	16.0	1.3	ND	–
1-Octene	−12.1	1.0	0.064	1.0
Free olefin = acrylonitrile				
Ethylene	25.0	8.3	ND	–
1-Butene	3.0	1.0	ND	–
1-Hexene	−31.1	10.3	0.21	1.0
1-Octene	−59.1	19.7	0.34	1.6

[a] Evaluated at 50 μg l^{-1} for ethylene (30°C), 1000 μg l^{-1} for ethyl acrylate (30°C) and 300 μg l^{-1} for acrylonitrile (25°C). ND = Not detected.

butene, *trans*-2-butene and isobutylene, respectively. Comparison of these results with those in Table 2 shows that the 1-hexene complex is much more sensitive to these compounds than the ethylene complex.

Conclusions

The results presented here demonstrate the ability to adjust the selectivity and sensitivity of SAW sensors toward various olefin gases and vapors through subtle changes in the electronic structural features of the reagent coatings. The inherent selectivity for relatively electron-rich olefins arises from the apparent predominance of σ-bonding interactions between the olefins and Pt, though the trends observed in the data suggest that π back-bonding is also important. The exceptional behavior observed in several exposure series, however, indicates that the dynamics of these reactions cannot be fully rationalized in terms of simple variations in σ and π bonding strength alone. Still, advantage can be taken of the observed selectivities. The remarkably high response to 1-hexene relative to 1-butene and cyclohexene using $PtCl_2$(ethylene)(pyridine) and the ability to measure electron-deficient olefins by extending the alkyl side chain of the initially complexed olefin are particularly noteworthy.

The patterns of response as a function of the amine ligands in these complexes differ from those expected from previous solution-phase kinetic studies and NMR data on these and similar complexes. In contrast, fairly consistent correlations are found with thermodynamic stability data for similar systems which suggests the possibility of quasi-equilibria being established at or just beneath the surface of the solid reagents even under dynamic exposure conditions.

In some practical situations, use of a single SAW sensor coated with one of the reagents studied here could provide sufficient selectivity in the presence of non-olefins or certain other (non-reactive) olefins. The use of a simple sensor array comprising as few as two sensors coated with the same reagent complex, but operated a different temperatures, could provide selectivity based on differences in activation energy between different reacting olefins. Finally, an array of sensors having different reagent coatings could provide discrimination between a wider range of olefins on the basis of differences in steady-state response.

This work was supported by Grant No. R01-OH02663 from the National Institute for Occupational Safety and Health of the Centers for Disease Control.

REFERENCES

1 American Conference of Governmental Industrial Hygienists (ACGIH), Documentation of the Threshold Limit Values and Biological Exposure Indices, ACGIH, Cincinnati, OH, 1985.
2 Code of Federal Regulations, 29CFR1910.1000, January 19, 1989, U.S. Department of Labor, Occupational Safety and Health Administration, Occupational Safety and Health Standards.
3 American Conference of Governmental Industrial Hygienists (ACGIH), 1992–1993 Threshold Limit Values and Biological Exposure Indices, ACGIH, Cincinnati, OH, 1992.

4 J.S. Nader, J.F. Lauderdale and S.C. McCammon, in S.V. Hering (Ed.), Air Sampling Instruments for Evaluation of Atmospheric Contaminants, American Conference of Governmental Industrial Hygienists, Cincinnati, OH, 7th edn., 1989, pp. 507–582.
5 M.S. Nieuwenhuisen and A. Venema, Sens. Mater., 5 (1989) 261.
6 H. Wohltjen, D.S. Ballantine, Jr. and N.L. Jarvis, in R.W. Murray (Ed.), Chemical Sensors and Microinstrumentation, ACS Symposium Series 403, American Chemical Society, Washington, DC, 1989, pp. 157–175.
7 H. Wohltjen, Sensors Actuators, 5 (1984) 307.
8 M. Herberhold, Metal π-Complexes, Vol. 1, Parts 1, 2, Elsevier, Amsterdam, 1974.
9 F.R. Hartley, in G. Wilkinson (Ed.), Comprehensive Organometallic Chemistry – The Synthesis, Reaction and Structures of Organometallic Compounds, Vol. 6, Pergamon, Oxford, 1982, pp. 614–754.
10 E.T. Zellers, R.M. White and S.M. Rappaport, Anal. Chem., 62 (1990) 1223.
11 E.T. Zellers, in R.W. Murray (Ed.), Chemical Sensors and Microinstrumentation, ACS Symposium Series 403, American Chemical Society, Washington, DC, 1989, pp. 176–190.
12 E.T. Zellers, N.C. Hassold, R.M. White and S.M. Rappaport, Anal. Chem. 62 (1990) 1227.
13 E.T. Zellers and G.Z. Zhang, Anal. Chem., 64 (1992) 1277.
14 M. Orchin and P.J. Schmidt, Inorg. Chim. Acta. Rev., (1968) 123.
15 F.R. Hartley, Chem. Rev., 73 (1973) 163.
16 S. Miya, K. Kashiwabara and K. Saito, Inorg. Chem., 19 (1980) 98.
17 S.S. Hupp and G. Dahlgren, Inorg. Chem., 15 (1967) 2349.
18 D.G. Taylor (Ed.), NIOSH Manual of Analytical Methods, Vol. 1, USDHEW-NIOSH, Cincinnati, OH, 2nd edn., 1977, pp. 239(1)–239(21).
19 L.K. Doraiswamy and M.M. Sharma, Heterogeneous Reactions: Analysis, Examples, and Reactor Design, Vol. 1, Wiley, New York, 1984, Chap. 2.
20 J. Joy and M. Orchin, J. Am. Chem Soc., 81 (1959) 305.
21 D.G. Cooper and J. Powell, Inorg. Chem., 15 (1976) 1959.
22 D.G. Cooper and J. Powell, Inorg. Chem., 16 (1977) 142.
23 F.A. Carey and R.J. Sundberg, Advanced Organic Chemistry – Part A: Structure and Mechanisms, Plenum, New York, 2nd edn., 1984.
24 M.A.M. Meester, H. vanDam, D.J. Stufkens and A. Oskam, Inorg. Chim. Acta, 20 (1976) 155.
25 S.I. Shupack and M. Orchin, J. Am. Chem. Soc., 86 (1964) 586.
26 M.A.M. Meester, D.J. Stufkens and K. Vriese, Inorg. Chim. Acta, 14 (1975) 25.
27 M.A.M. Meester, D.J. Stufkens and K. Vriese, Inorg. Chim. Acta, 21 (1977) 251.

Analytica Chimica Acta, 280 (1993) 15–19
Elsevier Science Publishers B.V., Amsterdam

Membranes for optical pH sensors

Yordan Kostov and Stoyan Tzonkov

Central Laboratory of Bioinstrumentation and Automation, Bulgarian Academy of Sciences, Acad. G. Bonchev Str., Bl. 105, Sofia 1113 (Bulgaria)

Ljubov Yotova and Milka Krysteva

Department of Biotechnology, Technological University of Sofia, Kl. Ohhridski Bld. 8, Sofia 1756 (Bulgaria)

(Received 17th November 1992; revised manuscript received 5th February 1993)

Abstract

A method for producing membranes for optical pH sensors is described. The pH indicators (Neutral Red and Congo Red) are covalently bonded to a transparent acetylcellulose film. The membranes have good durability (> 9 months) and a short response time (ca. 30 s). The method is easy to perform and uses acetylcellulose as a carrier. The reagents for activating the cellulose support are inexpensive, non-toxic and widely available.

Keywords: Sensors; Membranes; pH sensors

The development of optical pH sensors is of great interest because of their possible application in biotechnology, ecology and medicine [1,2]. They are suitable for applications where conventional electrodes cannot be used because of their large size or because of the risk of electric shock during the in vivo measurements. The most important problem with this type of sensor relates with the stability of the binding of the reagents to the carrier. This can be improved by using an efficient procedure for immobilization of the indicator to appropriate polymer matrices [2,3].

A method for covalent binding of enzymes to a cellulose carrier was described previously [4], which includes activation of the cellulose by using urea and formaldehyde and binding the enzymes to it. This method was also used sucessfully to prepare multi-enzyme membranes for biosensors [5]. Double enzyme complexes of glucose oxidase and catalase and of glucose oxidase and invertase were produced on a cellulose matrix. A modification of this method was used for covalent binding of enzymes to synthetic membranes [6].

The purpose of this work was to investigate the possibilities for developing a modification of the above method for covalent immobilization of indicators on optically transparent acetylcellulose membranes that have been previously hydrolysed and activated using urea and formaldehyde. The characteristics of the membranes produced were investigated and the possibilities for their use in the design of optical pH sensors were evaluated.

Correspondence to: Y. Kostov, Central Laboratory of Bioinstrumentation and Automation, Bulgarian Academy of Sciences, Acad. G. Bonchev Str., Bl. 105, Sofia 1113 (Bulgaria).

EXPERIMENTAL

Materials

Phenol Red (phenolsulphonphthalein), Neutral Red (3-amino-6-dimethylamino-2-methylphenazine hydrochloride; CI 50040) and Congo

Red {3,3′-[(1,1′-biphenyl)-4,4′-diylbis(azo)]bis(4-aminonaphthalenesulphonic acid); CI 22120} were supplied by Loba-Chemie (Vienna) and urea and formaldehyde by Merck (Darmstadt). All other reagents were of analytical-reagent grade.

As a matrix for immobilization of the indicators a transparent triacetylcellulose membrane was used, produced by treating waste film tapes as described previously [7]. The average thickness of the tape was 200 ± 20 μm.

Activation of cellulose matrix

The triacetylcellulose was previously hydrolysed in order to deesterify the acetyl groups and to increase the porosity of the membrane. A 2-g amount of transparent film (separate pieces of size $33 \times 10 \times 0.2$ mm) was treated in 0.1 mol dm^{-3} KOH for 24 h [8]. The urea derivative was then prepared as follows: 2 g of hydrolysed cellulose membranes were treated with sodium periodate (0.25 mol dm^{-3}) at 22 ± 2°C and pH 5.0 for 2 h in darkness. The membranes were then washed with distilled water in a Buchner funnel until no periodate was left. The oxidized cellulose membranes were immediately treated with 15% (w/v) urea for 14 h in the presence of 0.9% (v/v) sulphuric acid at 60°C. The membranes were then washed with distilled water in a Buchner funnel until the rinsings showed a neutral reaction. The resulting urea derivative of the cellulose contained 2.8% nitrogen. The membranes were subsequently treated with 12.5% (v/v) formaldehyde in 0.1 mol dm^{-3} phosphate buffer (pH 7.5) at 45°C for 16 h with continuous stirring in a closed vessel. After careful washing with distilled water until the excess of formaldehyde had been removed, the cellulose membranes were separately treated with 0.2% (w/v) solutions of Phenol Red, Neutral Red and Congo Red in 0.1 mol dm^{-3} phosphate buffer (pH 7.5) for 20 h at room temperature with magnetic stirring. Then the membranes were washed with distilled water in a Buchner funnel until there was no absorption of the rinsings at wavelengths of 430, 540 and 600 nm respectively.

Spectrophotometric measurements

Spectrophotometric measurements were made on a Perkin-Elmer Lambda 2 spectrophotometer. The membranes with immobilized indicator were stretched vertically inside the cuvette using a special frame. The size of its opening was 7×30 mm (Fig. 1). The control sample against which the measurements were performed consisted of triacetylcellulose film treated in the same way but without indicator. The control sample was stretched in the same way inside the cuvette using a frame of the same size. The spectral characteristics of Neutral Red were measured using 0.1 mol dm^{-3} phosphate buffer in the pH range 6.0–8.2 in steps of 0.2 and those of Congo Red using 0.1 mol dm^{-3} phosphate and hydrochloric acid buffers in the pH range 1.2–4.0 in steps of 0.4. Comparative measurements under the same conditions were accomplished for the solutions of free indicators.

RESULTS AND DISCUSSION

The spectral characteristics of the free and immobilized Neutral Red are shown in Fig. 2a and b, respectively, and those of the free and immobilized Congo Red in Fig. 3a and b, respectively. The spectral characteristics of Phenol Red are not shown, as the absorption of the membranes with this indicator was lower than 0.01 throughout the whole visible and IR region and it

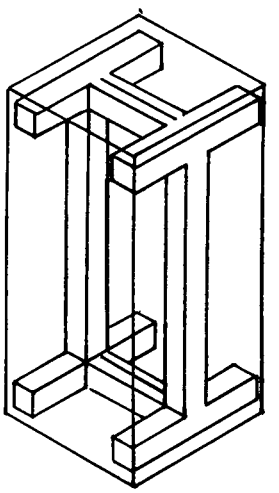

Fig. 1. Schematic diagram of the frame on which the membranes are stretched, inside the cuvette.

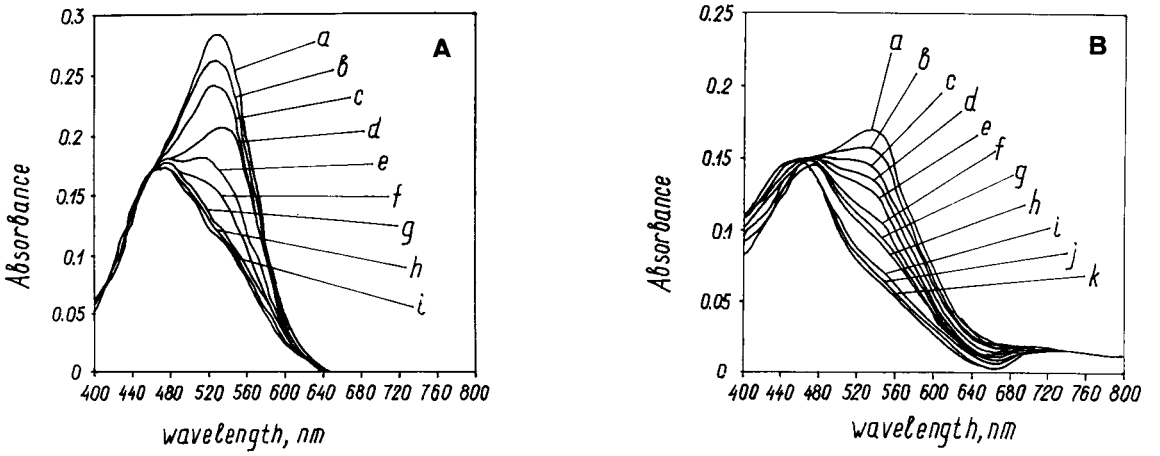

Fig. 2. (a) Absorption spectra for Neutral Red in solution at pH (a) 6.62, (b) 6.80, (c) 6.98, (d) 7.15, (e) 7.34, (f) 7.51, (g) 7.80, (h) 7.93 and (i) 8.12. (b) Absorption spectra for immobilized Neutral Red at pH (a) 6.00, (b) 6.20, (c) 6.50, (d) 6.80, (e) 7.00, (f) 7.15, (g) 7.30, (h) 7.50, (i) 7.80, (j) 8.00 and (k) 8.20.

was concluded that it is unsuitable for use in optical sensors.

As can be seen, the following specific changes in the spectra of the immobilized indicators were observed: a shift of the transition interval to the acid region; alteration of the ratio of the peak-height absorption maxima with immobilized Congo Red and the appearance of plateau with immobilized Neutral Red; and a shift of the absorption maxima (in comparison with the free dyes) towards the red with Congo Red and towards the violet with Neutral Red. The shift of the transition interval of Neutral Red is about 0.8 pH unit and thus the transition interval is pH 6.0–7.5. The apparent pK_a of the immobilized indicator was 6.7. The Congo Red transition interval shift is about 1.8 pH unit and thus the transition interval is pH 1.2–3.5. The apparent pK_a was 2.2. The ratio of the peak-height absorption maxima of immobilized Congo Red is

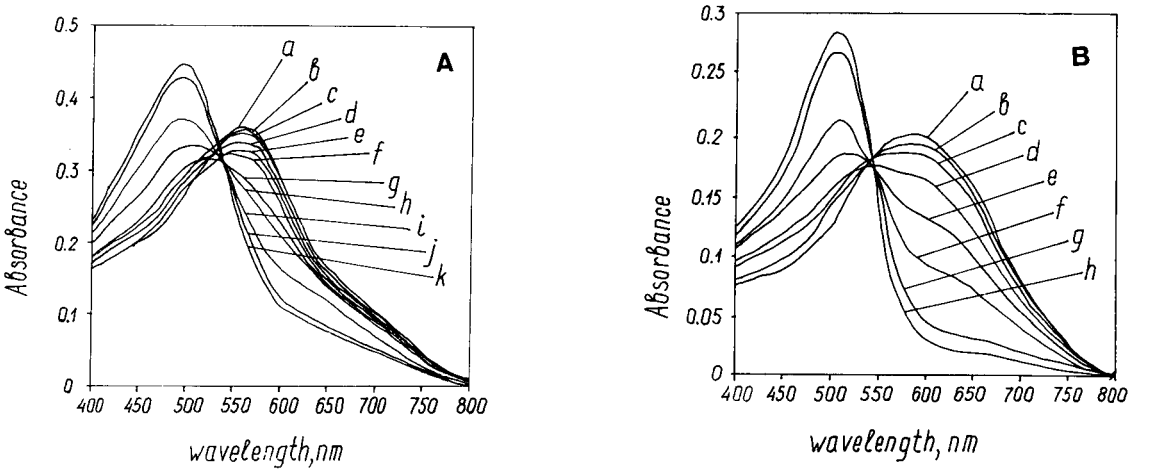

Fig. 3. (a) Absorbtion spectra for Congo Red in solution at pH (a) 2.54, (b) 2.97, (c) 3.18, (d) 3.32, (e) 3.50, (f) 3.70, (g) 3.91, (h) 4.11, (i) 4.30, (j) 4.53 and (k) 5.02. (b) Absorbtion spectra for immobilized Congo Red at pH (a) 1.27, (b) 1.61, (c) 2.13, (d) 2.54, (e) 2.97, (f) 3.18, (g) 3 .50 and (h) 4.02.

1.412 and that of the free dye is 1.256. The absorption maxima of the immobilized Congo Red are located at 507 and 588 nm and those of the free dye at 497 and 576 nm. The absorption maximum of the immobilized Neutral Red is at 535 nm and that of the free dye at 540 nm. Similar changes have been observed by others, although different immobilization methods were used [8–10].

The above results can be interpreted based on the influence of the immobilization procedure on the behaviour of the indicators. In the process of clarifying the mechanism of binding between proteins and amino acids in previous investigations [4], it was shown that the condensation between the hydroxymethyl groups of the carrier and the proteins is accomplished through the transformation of the amino groups in the alkaline pH region (ϵ-amino groups of lysine) and of amido groups in the acidic pH region (asparagine or glutamine). In addition, the reactivity of the activated carrier is so high that it was considered that an interaction is possible with low-molecular-weight compounds that have a free *ortho* position in the molecule. For this reason, indicators having amino groups or a free *ortho* position in their structure were used. A possible scheme for the reaction is shown in Fig. 4. This makes it possible to achieve covalent binding to the activated matrix at pH 7.5–8.0. In the experiments it was found that a considerable amount of indicator with amino groups was linked to the activated membrane (the maximum absorption of the membranes with immobilized Congo Red is 0.28 and of these with Neutral Red is 0.18). The low

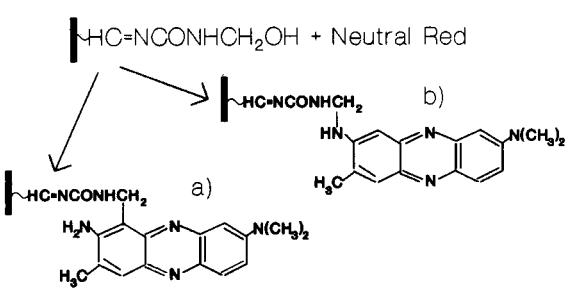

Fig. 4. Possible scheme of reaction between activated membrane and Neutral Red.

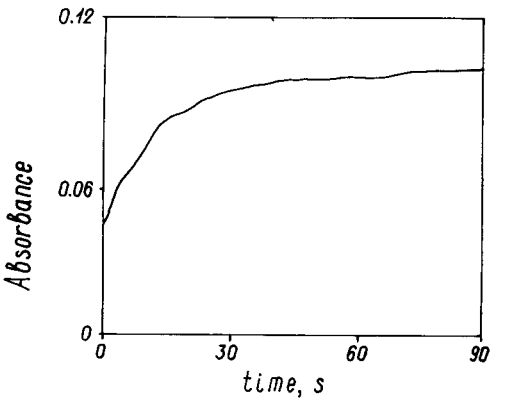

Fig. 5. Transition process of the pH sensor constructed by covalent binding of Congo Red to acetylcellulose. The initial pH was 5.0, and at $t = 0$ the pH was changed to 2.0. The absorbance was measured at 600 nm.

absorption of the membranes with Phenol Red (< 0.01 l mol^{-1} cm^{-1}) is due to the insufficient amount of linked indicator, the possible reason being spatial obstacles during the reaction.

The fact that the immobilization changes the ratio of the heights and positions of the absorption maxima of the indicators shows that the amino groups are auxochrome elements of the molecule and the loss of a proton after the covalent binding influences the charge distribution during the dissociation of the immobilized dye.

The reasons for the transition interval shift are possibly the new covalent binding and the influence of the nearby acetylcellulose carrier.

Sensor response time

The changes in the optical properties of membranes with immobilized Congo Red were measured at 600 nm. Figure 5 shows a typical curve for the transition process. As can be seen, the output signal reaches 95% of the steady-state response for about 30 s, and the average response time is 28 ± 2 s. The average response time of the membrane with immobilized Neutral Red was the same. The measurements on the membrane with Neutral Red were performed at 540 nm.

Sensor stability

The stability of the membranes with the immobilized indicators based on a recycled support

made from waste films is higher in comparison with other methods in which acetylcellulose is also used for producing optical sensors [8,9]. This is due to the higher mechanical strength of the carrier and to the covalent binding between the indicator and the matrix. Repeated measurements showed that the changes in the absorption coefficient after keeping the membranes in aqueous solutions for 9 month were less than 4%.

The membranes produced by this method possess high stability, low response times and spectral characteristics that make them appropriate for use in optical sensors for pH measurements of clear solutions in biotechnology, ecology and medicine.

The described method for producing pH-sensitive optical membranes has the following advantages in comparison with other methods: a waste cellulose material with good optical and mechanical properties is used as a matrix for immobilization; its activation is performed using widely available, inexpensive and non-toxic reagents; the membranes with immobilized Neutral Red and Congo Red have good time stability, which allows large numbers of measurements; and the immobilization of the indicator on the membrane surface reduces the diffusion limitations and allows sensors with short response times to be produced.

Future work will be directed to the investigation of the possibilities for immobilizing other indicators by this method. It is also intended to explore the application of the already immobilized indicators in luminescence spectrometry (it is known that Neutral Red shows luminescence when excited with UV radiation). The method also allows pH indicators and enzymes to be immobilized simultaneously and for this reason a study to produce optical biosensors using this method is in progress.

REFERENCES

1 G.F. Kirkbright R. Narayanaswamy and N.A. Welti, Analyst, 109 (1984) 1025.
2 J.I. Peterson, S.R. Goldstein, R.V. Fitzgerald and D.K. Buckhold, Anal. Chem., 52 (1980) 864.
3 M.J. Goldfinch and C.R. Lowe, Anal. Biochem., 117 (1983) 430.
4 M.A. Krysteva, S.R. Blagov and T.T. Sokolov, J. Appl. Biochem., 6 (1984) 367.
5 M.A. Krysteva and L.K. Yotova, J. Chem. Technol. Biotechnol., 54 (1992) 13.
6 M.A. Krysteva, B.I. Shopova, L.K. Yotova and M.I. Karasavova, Biotechnol. Appl. Biochem., 13 (1991) 106.
7 M.A. Krysteva, G.A. Peev and L.K. Yotova, Acta Biotechnol., 7 (1987) 93.
8 T.P. Jones and M.D. Porter, Anal. Chem., 60 (1988) 404.
9 Y.V. Kostov, Sensors Actuators B, 8 (1992) 99.
10 J.M. Zen and G. Patonay, Anal. Chem., 63 (1991) 2934.

Analytica Chimica Acta, 280 (1993) 21–30
Elsevier Science Publishers B.V., Amsterdam

Design, manufacture and characterization of an optical fiber glucose affinity sensor based on an homogeneous fluorescence energy transfer assay system

D.L. Meadows [1] and J.S. Schultz [2]

Department of Chemical Engineering, The University of Michigan, Ann Arbor, MI 48109 (USA)

(Received 5th November 1992; revised manuscript received 16th January 1993)

Abstract

Optical fiber biosensors based on fluorescence assays have several distinct advantages when measuring biological analytes such as metabolites, cofactors, toxins, etc. Not only are optical signals immune to electronic interferences, but the polychromatic nature of most fluorochemical assays provides more potentially useful data about the system being studied. One of the most common difficulties normally encountered with optical biosensors is the inability to routinely recalibrate the optical and electronic components of the system throughout the life of the sensor. With this in mind, an optical fiber biosensor system for glucose has been constructed along with the peripheral electronic instrumentation. The biochemical assay is based on an homogeneous singlet/singlet energy transfer affinity assay. The sensor probe indirectly measures glucose concentrations from the level of fluorescence quenching caused by the homogeneous competition assay between TRITC labeled concanavalin A (receptor) and FITC labeled Dextran (ligand). The FITC signal is used as an indicator for glucose concentrations and the TRITC signal is used for internal calibration. Chemical derivatization procedures using succinic anhydride were developed to prevent aggregation of the receptor protein in solution, and the TRITC/ConA ratios were optimized to achieve the best sensor performance. Using this sensor system, the FITC-Dextran detection limit was 0.05 μg/ml and glucose concentrations up to 1600 mg/dl could be detected with a time response of approximately 10 min.

Keywords: Biosensors; Concanavalin A; Fluorescence energy transfer; Glucose; Optical fibre biosensors

Biosensors are analytical devices that respond reversibly and specifically to the concentration or activity of a biologically important analyte. Several good reviews on biosensors have recently been published [1–6] that summarize the key developments in biosensor research. During the past several years sensor systems have been reported in the literature that are capable of measuring analytes in most of the chemical classifications important to biological systems, e.g. amino acids, cofactors, carboxylic acids, alcohols, inorganic ions, etc., in both aqueous and gaseous phases.

The application of photometric assay techniques such as fluorescence, absorbance, chemiluminescence, internal reflection spectroscopy, etc., to the biosensing area has rapidly grown over the past decade. Good reviews on the subject have been prepared by Saari [7] and Wolfbeis [8]. There are several inherent advantages to an optical fiber based sensor over an electrical based sensor, e.g., isolation from electromagnetic noise

Correspondence to: D.L. Meadows, Department of Pharmaceutical Research, Allergan Inc., 2525 Dupont Dr., Irvine, CA 92715 (USA).

[1] Present address: Department of Pharmaceutical Research, Allergan, Inc., 2525 Dupont Dr., Irvine, CA 92715 (USA).

[2] Present address: Center for Biotechnology and Bioengineering, University of Pittsburgh, 911 William Pitt Union, Pittsburgh, PA 15260 (USA).

sources, small size, use in long-distance telemetry, and the availability of spectral data [9].

In an earlier article [10], we reported on the initial results obtained with an assay system for glucose that was based on an homogeneous fluorescence energy transfer assay. The assay was developed for use in an optical fiber biosensor with geometry similar to that developed by Mansouri and Schultz [11,12]. They immobilized a glucose receptor, concanavalin A (ConA), to the inner wall of a dialysis fiber (diameter = 0.3 mm), and used fluorescein labeled dextran (FITC-Dextran) as a macromolecular ligand competing with glucose. The current sensor is based on an homogeneous fluorescence energy transfer assay and is designed to improve upon the Schultz and Mansouri sensor by eliminating the immobilization of ConA, shortening the sensor response time, and correcting for drifts in sensor components by internal calibration.

The current approach employs two labels that absorb and fluoresce visible light, FITC-Dextran as a donor (fluorescer) and tetramethylrhodamine isothiocyanate labeled ConA (TRITC-ConA) as the acceptor (quencher) [13–15]. The competing reactions for the system are given in Eqns. 1 and 2.

$$\underset{\text{(analyte)}}{\text{Glucose}} + \underset{\text{(receptor)}}{\text{TRITC-ConA}} \leftrightarrow \underset{\text{(analyte : receptor)}}{\text{Glucose : TRITC-ConA}} \quad (1)$$

$$\underset{\text{(competing analyte)}}{\text{FITC-Dextran}} + \underset{\text{(receptor)}}{\text{TRITC-ConA}} \leftrightarrow \underset{\text{(competing analyte : receptor)}}{\text{FITC-Dextran : TRITC-ConA}} \quad (2)$$

When FITC-Dextran reversibly binds to TRITC-ConA, the donor and acceptor chromophores are sufficiently close together (less than approximately 50 Å) for a significant portion of the fluorescein signal to be quenched by rhodamine. As glucose is added to the system, FITC-Dextran is liberated from the TRITC-ConA causing the fluorescein signal to increase. With this approach, the fluorescein signal is used to monitor glucose concentrations, and the TRITC signal is used for internal calibration to correct for optical and electronic drift.

The FITC/TRITC chromophore pair was selected because of the high energy transfer efficiency due to the large spectral overlap between the emission spectra of FITC and the absorbance spectra of TRITC. The absorbance and emission spectra are given in Fig. 1 for both FITC and TRITC, and the spectral overlap is indicated by the hatched region. By appropriately selecting the chromophore pair, one can increase or decrease the spectral overlap in order to optimize the efficiency of resonance energy transfer for a particular application [14].

In our most recent work, we have synthesized new TRITC-ConA conjugates that have improved the stability and dynamic range of homogeneous assays when compared with the initial work that had utilized commercially prepared ConA conjugates [10]. Synthesis of these protein conjugates successfully eliminated all ConA aggregation through chemical modification with succinic anhydride followed by labeling with TRITC. The dynamic range of assays using these new TRITC-ConA conjugates was significantly improved because of the higher dye to protein ratios. An optical and electrical instrumentation system was also constructed for evaluating the sensor perfor-

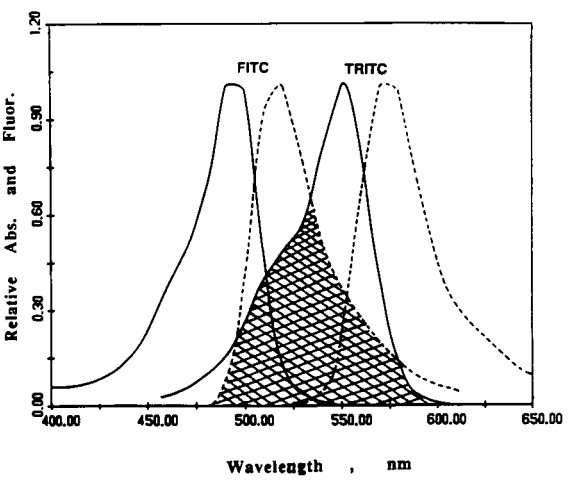

Fig. 1. Spectral overlap of FITC and TRITC. The absorbance spectra are denoted by solid lines and the emission spectra are denoted by dashed lines. The hatched region represents the spectral overlap area.

mance under various environmental conditions [16,17].

EXPERIMENTAL

Materials

Supplies of commercially prepared ConA derivatives from Sigma (St. Louis, MO) were compared against samples of chemically derivatized ConA that were prepared and purified in our laboratory. Commercially prepared samples of TRITC-ConA and succinylated ConA labeled with TRITC (TRITC-Succ-ConA) were supplied in a lyophilized form and were not purified prior to use. FITC labeled dextran, MW 7×10^4, was used as received from Sigma, Pharmacia (Piscataway, NJ), and Molecular Probes (Eugene, OR).

Equipment

An SLM (Urbana, IL) SPF-500C spectrofluorometer was used for all fluorescence measurements, and a Varian (Palo Alto, CA) DMS 200 UV–visible spectrometer was used to collect all absorbance spectra.

An instrumentation system, shown in Fig. 2, was assembled to test the homogeneous assay system in an optical fiber sensor configuration. The system was capable of multiplexing two excitation wavelengths into optical fibers that guided the light to the assay solution in the sensor probe. Fluorescence signals were collected from the sensor and carried to photon counting PMTs (multialkali photocathode with detection range 185–850 nm; Products for Research, Danvers, MA). Long pass barrier filters (50% cut off at 480 nm and 520 nm: Oriel Optics, Stratford, CT) were placed just in front of the PMTs to filter out undesired

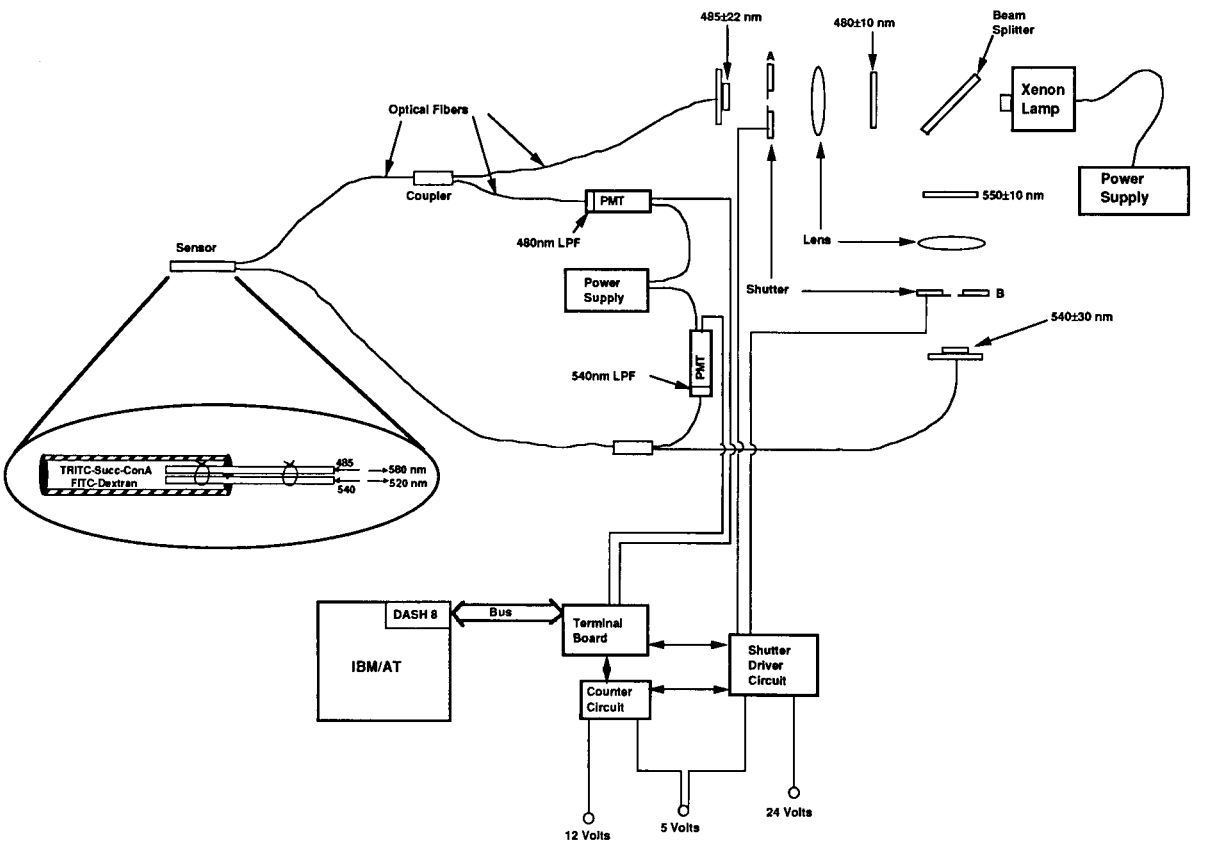

Fig. 2. A schematic diagram of the dual optical fiber sensor system.

wavelengths of light. White light from a 250 Watt Ealing Electro-Optics (South Natick, MA) xenon light source was passed through a 5 cm diameter plate beam splitter (50:50 split ratio: Melles Griot, Irvine, CA), then through a 2″ × 2″ interference filter (center wavelength 480 nm and 550 nm with FWHM of 10 nm; Oriel Optics). Two, 5 cm diameter, 10 cm focal length, double convex lenses (Melles Griot) focused each beam to the optical fiber mounts. One inch aperture electronic shutters (Melles Griot) were placed between the focusing lenses and the optical fiber mounts. The shutters were controlled by an IBM/AT microcomputer and were connected to a 24 V and a 5 V power supply. 24 V at 3 A for 8 ms were required to open the shutters, then the shutter driver circuits switched the supply voltage to 5 V to keep the shutters open. When the voltage was dropped to 0 V, the shutters closed. Just prior to entering the optical fibers, the light was filtered again using 1 in. diameter interference filters (center wavelengths 485 nm and 540 nm, FWHM 22 nm and 30 nm: Omega Optical; Brattleboro, VT). The two beams of light were guided to the sensor using 1:1 and 1:15 couplers from Canstar (Scarborough, Ont.). All fibers were multimode, graded index, with 100 μm core and 140 μm cladding. All connections were made using Amphenol 906 connectors (Lisle, IL). Hollow fiber polysulfone membranes were from AG Technologies (Needham, MA) with 0.5 mm inner diameter and 10000 molecular weight cut off. The optical fiber and hollow fiber were glued together using water activated 910 Adhesive (Permabond International, Englewood, NJ).

In summary, the sequence of events during the data acquisition process was as follows. First, shutter A was opened for a prescribed amount of time. During this interval, the excitation light intensity and the FITC fluorescence signals were measured by the two PMTs. Then shutter A was closed. Next, shutter B then opened for a prescribed amount of time and the excitation intensity and the TRITC fluorescence signal were measured. Then shutter B was closed. The cycle was repeated as many times as the experiment duration permitted. After the experiment was completed, the software computed the average and standard deviation for each sampling interval and stored the data for further manipulation. The excitation intensities were used to normalize the fluorescence signals, while the TRITC signal was used to adjust for drifts in the instrumentation hardware with time. All of the data acquisition procedures were automated using a DASH-8 (Metrabyte, Taunton, MA) A/D card and an IBM/AT microcomputer to direct all of the required steps in the proper sequence. The software was written in Basic and was designed so the operator would input only the period, the duty cycle of the shutters, and the duration of the experiment.

Assembly procedures

The first step in assembling the sensor probe was to smoothly cleave the ends of the two optical fibers that were to be inserted into the hollow fiber. The ends of the exposed fibers were then lined up flush with each other and carefully tied together with No. 00 suture thread under a dissecting microscope. A 27 gauge needle was connected to a 5 cm^3 syringe containing assay solution (TRITC-Succ-ConA/FITC-Dextran). The needle was inserted into the lumen of a one inch long section of hollow fiber. The fiber was filled with assay solution and sealed immediately at one end with cyanoacrylate adhesive. The two optical fibers were quickly inserted into the upper end of the hollow fiber and adhesive applied. The assembled sensor was then submerged in 0.05 M phosphate buffer saline at pH 7.4 (PBS) for at least one hour till the adhesive set.

Response of the sensor to various glucose concentrations was determined by first inserting the sensor into an agitated solution of PBS at 25°C to determine a baseline fluorescence signal. Then the sensor was inserted into solutions containing increasing amounts of glucose and the fluorescence signal response was monitored for ten minutes for each solution. After completion of this procedure, the sensor was inserted into a fresh solution of PBS so the sensor signal could return to baseline.

Protein derivatization

The jack bean lectin protein concanavalin A (ConA) was used as the receptor for the assay

system. Native ConA is composed of four protomers each having a molecular weight of 26 000 Daltons (pConA), and each protomer has one non-interacting sugar binding site. Acetylation or succinylation of the e-amino groups on the lysine residues of ConA can cause the dimer/tetramer equilibrium to shift to the point where tetramers are never formed, even at a pH greater than 7 and a temperature higher than 25°C [18]. The overall reactivity of ConA toward simple sugars and polysaccharides is not significantly affected by these procedures [19–21]. Utilizing this fact, a protein stabilization procedure for preventing ConA aggregation was developed based on derivatization with succinic anhydride followed by labeling with TRITC [16]. Since a dynamic equilibrium normally exists between the dimer and tetramer forms of ConA, it was essential that the dimers of ConA be prevented from aggregating in the lumen of the dialysis fiber. If aggregation was allowed to occur, then precipitation of ConA in the fiber lumen would cause rapid failure of the sensor. By reacting the lysine residues with succinic anhydride, the positive charged lysine side chains were converted to negative charges. These changes in the overall charge distribution of the protein, combined with changes in the steric interactions, caused the native ConA tetramer molecule to separate into two identical dimers that did not re-aggregate into the tetramers even at elevated temperatures. The procedures used for determining the degree of succinylation and TRITC labeling are presented elsewhere [16,22].

Fluorescence quenching

The excitation and emission wavelengths for measuring fluorescein quenching of the homogeneous energy transfer assay were 480 nm and 520 nm, respectively. All experiments were performed at 25°C with an initial starting solution of 2.0 ml of PBS containing the desired concentration of FITC-Dextran (typically 20 μg/ml) in a standard quartz spectrofluorometer cuvette. The fluorescein fluorescence intensity was first recorded at 520 nm, then an aliquot of a solution containing the ConA conjugates was titrated into the cuvette with mixing. The fluorescein signal was recorded and this procedure was repeated for each additional aliquot of ConA conjugate. Additions were made without removing the cuvette from the holder to prevent changing the cuvette alignment, and corrections were made for sample dilution. The quenching experiment was repeated a second time using the same procedure except that the 2.0 ml starting solution of FITC-Dextran also contained 1500 mg/dl glucose. These two experiments, one with glucose and one without glucose, provided what will be called the "dynamic range envelope" for the homogeneous assay between glucose concentrations of 0 and 1500 mg/dl.

RESULTS

Quenching with TRITC-ConA

Figure 3 presents a series of experiments performed to determine the extent of FITC-Dextran fluorescence quenching caused by solutions containing commercially prepared ConA conjugates, see top four curves. Results for solutions containing ConA conjugates we prepared are shown in the lower two curves. The middle two curves represent the dynamic range envelope for commercially prepared TRITC-ConA, where the lower curve of the two represents data obtained

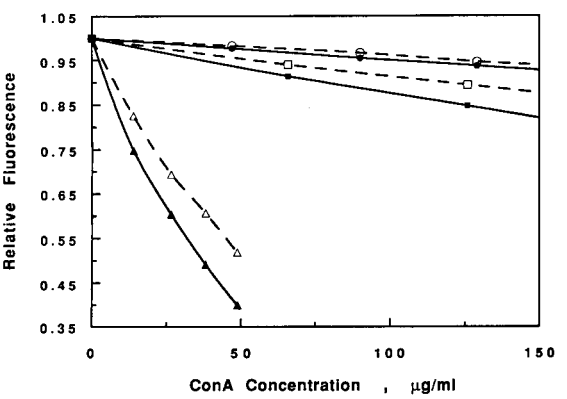

Fig. 3. Quenching of FITC-Dextran fluorescence by conjugates of TRITC-ConA and TRITC-Succ-ConA in the absence of glucose (solid lines) and in the presence (dashed lines) of 1500 mg/dl glucose. ■ and □, commercially prepared TRITC-ConA. ● and ○, commercially prepared TRITC-Succ-ConA. ▲ and △, synthesized TRITC-Succ-ConA having 6.2 and 2.8 molecules of TRITC and succinate, respectively, per pConA.

in the absence of glucose, and the upper curve of the two represents data obtained in the presence of 1500 mg/dl glucose. Comparing these two curves indicates that the fluorescence of a solution initially containing 125 μg/ml TRITC-ConA, 2.5 μg/ml FITC-Dextran, and no glucose, would increase by approximately 6% when 1500 mg/dl glucose was added to the solution. Therefore, one would expect only about a 6% increase in signal for a sensor based on the commercially prepared TRITC-ConA conjugate over a glucose concentration range of 0 to 1500 mg/dl.

The upper two curves in Fig. 3 are the fluorescence quenching results in the absence and presence of glucose for commercially prepared TRITC-Succ-ConA for the same FITC-Dextran concentration, 2.5 μg/ml. These curves indicate that there was not a significant increase in the FITC-Dextran fluorescence when glucose was added. A subsequent determination was made that the very narrow dynamic range envelope for TRITC-Succ-ConA was due to the fact that more than half of the commercially prepared material was inactive. Also, the protein molecules that still contained active glucose binding sites had very low dye/protein ratios which contributed to the low level of fluorescence quenching [16]. Because the results were so poor, we synthesized new ConA conjugates with the intention of improving the dynamic range of the homogeneous assay for use in the optical fiber sensor system.

Fluorescence quenching results for one of the TRITC-Succ-ConA conjugates we synthesized and subsequently purified are shown by the lower 2 curves of Fig. 3. This particular sample of TRITC-Succ-ConA had approximately 6.2 TRITC and 2.8 succinate molecules per ConA protomer. Other samples of TRITC-Succ-ConA were prepared with varying levels of TRITC and succinate conjugation, but the dynamic range envelopes were almost identical to the data presented in Fig. 3. This information helped to confirm that the conjugation and purification procedures were not having a significant effect on the glucose binding properties of the ConA. Comparison of the envelopes in Fig. 3 shows two important differences between the three samples. First, the higher dye/protein ratio obtained for the conjugates we synthesized resulted in a significantly wider level of total fluorescence quenching. Secondly, the dynamic range envelope was significantly greater for the synthesized TRITC-Succ-ConA when compared with either of the commercially prepared materials at the same ConA concentration (30% versus 3% and 1%, respectively at 50 μg/ml of ConA). Both of these improvements are indicative of greater specificity in the binding interactions and more efficient energy transfer which helped to significantly increase the sensitivity of the optical fiber sensor.

A series of fluorescence recovery experiments were performed over a glucose concentration range of 0 to 1500 mg/dl in order to demonstrate the reversibility of the Dextran/ConA binding interactions of the conjugates we prepared, Fig. 4. All samples had an initial FITC-Dextran concentration of 2.5 μg/ml and the degree of TRITC labeling ranged from 6.4 to 7.6 molecules per pConA and succinate ranged from 0 to 2.8 molecules per pConA. From these results, it was again clear that the Dextran/ConA binding was reversible and that there was relatively little effect of TRITC or succinate on the assay performance which in turn indicated that the conjugation procedures did not significantly affect the tertiary structure of ConA.

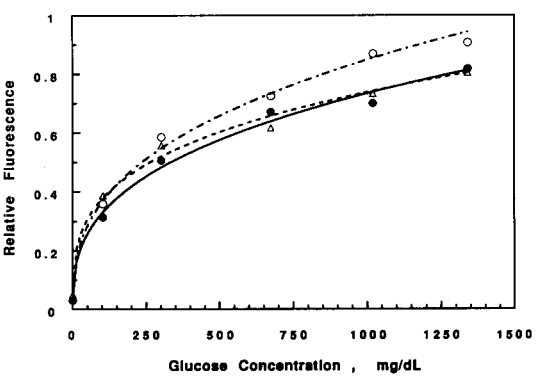

Fig. 4. Effect of conjugation on the recovery of quenched FITC-Dextran fluorescence during glucose titration. (all samples initially had 2.5 μg/ml FITC-Dextran). •, ConA concentration 0.2 mg/ml: 6.4 TRITC and 0 succinate molecules per pConA. △, ConA concentration 0.24 mg/ml: 7.6 TRITC and 1.2 succinate molecules per pConA. ○, ConA concentration 0.48 mg/ml: 6.2 TRITC and 2.8 succinate molecules per pConA.

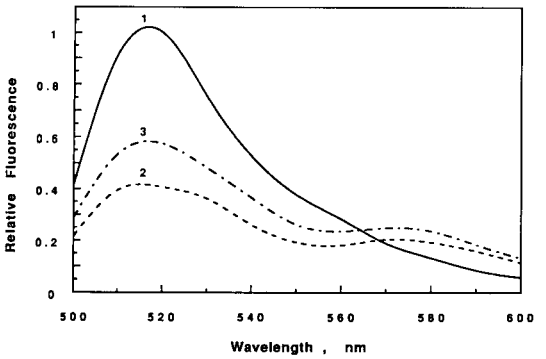

Fig. 5. The fluorescence spectra for FITC-Dextran/TRITC-ConA assay solutions with excitation at 485 nm. Curve 1 is for 2.5 μg/ml FITC-Dextran in PBS. Curve 2 is for a solution of 2.5 μg/ml FITC-Dextran and 50 μg/ml of TRITC-Succ-ConA. Curve 3 is for a solution of 2.5 μg/ml FITC-Dextran, 50 μg/ml of TRITC-Succ-ConA, and 1500 mg/dl of glucose.

Clearly the results in Figs. 3 and 4 indicate that the homogeneous assay system can specifically and reversibly respond to changes in glucose concentration up to 1500 mg/dl. However, to fully utilize all of the advantages of the system one must be able to recalibrate the instrumentation system to account for drift without the use of external glucose calibration standards. In Fig. 5, the fluorescence spectra are plotted for three solutions when the excitation wavelength was 480 nm. The first curve in Fig. 5 is the fluorescence emission spectra centered at 520 nm of a solution containing 2.5 μg/ml of FITC-Dextran. Curve 2 is the same solution after 50 μg/ml of the synthesized TRITC-Succ-ConA is added. Due to the energy transfer between FITC and TRITC when the Dextran/ConA bound complex is formed, the fluorescence signal is quenched by approximately 60%. A significant portion of this signal is recovered upon addition of 1500 mg/dl glucose, curve 3. From these results, one should expect the sensor system described in Fig. 2 to be able to monitor changes in the glucose concentration by measuring changes in the FITC signal when using 480 nm excitation light. To obtain an internal calibration signal, the fluorescence signal from TRITC can be selectively monitored using an excitation source of 540 nm.

Response of optical sensor system

Before the homogeneous assay system was tested in the optical fiber sensor configuration, the sensitivity of the dual wavelength instrumentation system shown of Fig. 2 was evaluated using FITC-Dextran standard solutions for a period of two seconds with a duty cycle of 0.4, Fig. 6. By optimizing the duty cycle and period, fluorescence bleaching was prevented. Data collection continued for at least one minute, then the average was determined. The enlarged section in Fig. 6 shows that the response was quite linear up to 10 μg/ml ($r^2 = 0.99995$), then there was a slight curvature at the higher concentration ranges probably due to the so called inner filter effect. If the fluorescein detection limit of the sensor were defined as the concentration at which the signal is twice the background noise level, then the detection limit for this dual fiber system was approximately 0.05 μg/ml. For comparison, the sensitivity of the single fiber system developed by Schultz et al. [12] was tested in solutions of 70000 MW FITC-Dextrans sourced from four different suppliers. For all four suppliers, the detection limit was approximately 4 μg/ml which is almost 100 times higher than would be obtained using the dual fiber system. An explanation for the drastically improved sensitivity of the dual fiber system was that the fluorescence signals did not return through the same fiber/connector pathway as the excitation light. By isolating the excitation and emission light signals from each other,

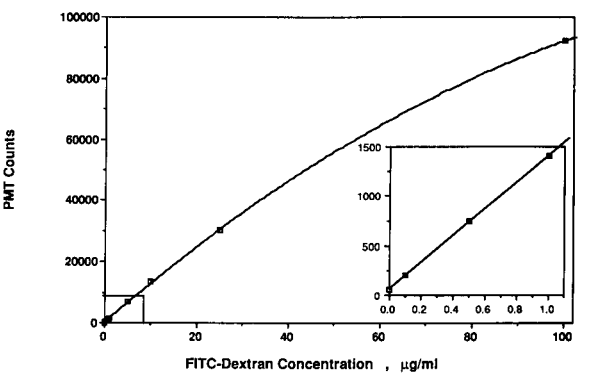

Fig. 6. Sensitivity of the dual optical fiber sensor system for 70000 MW FITC-Dextran.

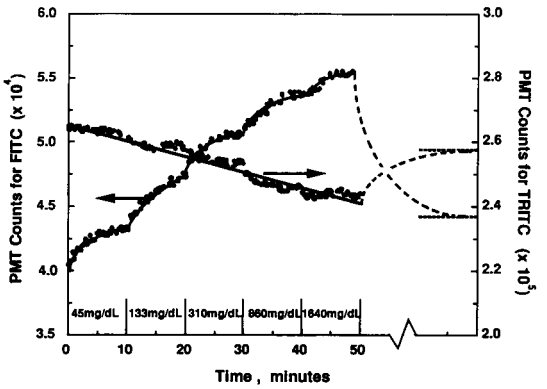

Fig. 7. Response of the dual optical fiber sensor to step changes in the glucose concentration. Glucose concentrations were monitored by changes in the FITC signal shown along the left y-axis while the internal calibration signal from TRITC is shown along the right y-axis. Glucose concentrations have been identified along the x-axis. The dashed horizontal lines indicate the new baseline signals after the sensor was inserted into PBS.

the background noise level of the dual fiber system was significantly reduced.

A sensor was then constructed with the dual fiber system using a solution containing 50 μg/ml of the synthesized TRITC-Succ-ConA conjugate and 2.5 μg/ml of FITC-Dextran. The sensitivity and signal response of the sensor was examined using a series of glucose standards, Fig. 7. Every 10 min the sensor was placed into new calibration solutions containing increasing amounts of glucose up to 1640 mg/dl. After the 50 min time point, the sensor was returned to a PBS solution and the sensor was allowed to equilibrate for approximately 60 min. The new baseline signal was measured as indicated by the dashed horizontal line near the right side axis in Fig. 7. Even after these data were corrected for slight drifts in the electronic components using the TRITC reference signal, the baseline had drifted up almost 30% in the two hours since the experiment began. The same sensor was again placed into a solution of 1640 mg/dl glucose, and the PMT counts increased only to about 55 000 indicating significant loss of dynamic range. The dynamic range continued to decrease with time until there was virtually no glucose response after twelve hours. When the sensor was disassembled, microscopic examination showed that the protein appeared to have adsorbed to the interior wall of the polysulfone membrane. It was concluded that the hydrophobic polysulfone membrane had a strong tendency to adsorb proteins, and it should be replaced with a more hydrophilic membrane, e.g., cellulose acetate. This work also indicated that the response time of a sensor based on the 0.5 mm i.d. polysulfone fiber was approximately ten minutes and the relative dynamic range was virtually the same as obtained for the cuvette experiments presented in Fig. 4. An important observation from these results is that the response of the homogeneous assay scales directly from the cuvette experiments to the sensor experiments. This should significantly shorten the time required to evaluate an assay system for use in the optical fiber sensor.

DISCUSSION

Biosensors capable of making very reliable routine measurements for a broad range of analytes, e.g., drugs, metabolites, and hormones would be a tremendous benefit to the areas of clinical medicine and biochemical process engineering. To this end, we have developed a homogeneous assay system based on fluorescence energy transfer for use in an optical fiber sensor that can detect glucose over a broad concentration range. The sensitivity of the assay using commercially prepared ConA conjugates was quite poor, but when a new succinylation procedure was used to prepare TRITC-ConA conjugates, the sensitivity and dynamic range of the assay were both significantly improved. These improvements were attributed to two factors: more than half of the commercial material was inactive, and the dye/protein ratio was too low to achieve high energy transfer efficiencies.

The chemical modification technique for stabilizing ConA using succinic anhydride proved to be successful in preventing ConA aggregation. This was essential for the homogeneous assay to perform properly. However, it was subsequently shown that there is a sub-population of Succ-ConA molecules (approximately 60% of the total)

that slowly lose their glucose binding activity over a period of several days when stored at 37°C. Even though the majority of Succ-ConA molecules loose their ability to bind glucose, protein aggregates are not formed by the deactivated material [16]. The remaining 40% of the population resists binding site deactivation and aggregation even when stored at 37°C for several weeks. Future work on the assay system should focus on isolating the more stable sub-population for use in sensors to help ensure good long-term stability.

When the homogeneous assay was used in the optical fiber sensor, another stability problem arose. Adsorption of the ConA conjugates to the inner wall of the hollow fiber made the baseline and dynamic range drift with time. It is possible that membranes made of more hydrophilic polymers such as regenerated cellulose or cellulose acetate would help to reduce the amount of adsorption. Obviously, until stability of the ConA can be ensured during the life of the sensor, the inherent advantages of the internal calibration system can not be fully realized.

In spite of the ConA adsorption problem, preliminary testing was completed to evaluate the performance of the homogeneous assay in the sensor system. The time response was found to be significantly faster for a homogeneous assay sensor than for the heterogeneous sensor developed by Schultz et al. [12]. If the diffusion constant for glucose through polysulfone was assumed to be the same as the diffusion constant through the hollow fibers used by Schultz et al. (3×10^{-6} cm^2/s), then a homogeneous sensor with the same diameter as the Schultz heterogeneous sensor would have a time response of approximately 1.5 min as compared to their reported value of 10 min. The significant improvement in the time response is probably attributable to the fact that the diffusion barrier from the immobilized ConA was eliminated. An added feature of the homogeneous assay sensor was that physical damage to the ConA from the immobilization procedure did not occur as was the case with the heterogeneous sensor.

Using a homogeneous energy transfer assay in an optical fiber biosensor had other advantages. Multiplexing two excitation sources made it possible to measure analyte concentrations while at the same time the sensor could be internally recalibrated to correct for instrumentation drifts. Also, the optimum design criteria for a specific analyte concentration range were more easily determined for the sensor because the sensitivity and dynamic range for the fluorescence quenching assay scaled down directly from the cuvette scale to the optical fiber sensor scale.

There are several design variables one can adjust to optimize the assay for a particular concentration range [23]. The bioreceptor can be changed to alter the binding constant. Also, the concentration of the bioreceptor and competing ligand can be adjusted. Finally, the efficiency of energy transfer can be changed by using donor/acceptor pairs that have different degrees of spectral overlap. Earlier work clearly showed that the donor/acceptor pair should be carefully selected in order to achieve a high energy transfer efficiency, and the donor and acceptor should have good separation between the excitation and emission spectra (Stokes shift). The large Stokes shift makes it easier to isolate the donor and acceptor fluorescence signal for sensor measurements. All of these design parameters help to make the homogeneous assay system quite versatile for other analytes.

The optical fiber sensor does have a practical lower limit of detection. Using the monovalent ligand/receptor molecular model [23], we estimated the lower detection limit for a given bioreceptor/competing ligand pair over a specific analyte concentration range. If one makes the following assumptions: (1) there is an increase in fluorescence of 35% over the analyte concentration range; (2) the mole ratio of competing ligand to bioreceptor is 1 to 10; (3) the competing ligand concentration is 10 nM; (4) the equilibrium constants of analyte and competing ligand for the bioreceptor are the same and equal to 10^8 M^{-1}, then it should be possible to detect analyte concentrations between 10^{-8} and 10^{-7} M with an adequate signal response using the dual fiber system. Because these design variables can have a wide range of values, the detection range can be quite easily shifted to the desired analyte concentration range by adjusting the design parameters.

In summary, we believe the optical fiber sensor system described here has several inherent advantages that can be capitalized on by carefully designing the homogeneous assay conditions to match the required assay conditions.

The authors wish to thank Dr. Thomas Stevenson, Evangeline Caesar, Maher Siraj, and Ed Ullman for their significant contributions to the completion of this work.

REFERENCES

1 J. Janata, Anal. Chem., 62 (1990) 33R.
2 J.N. Roe, Pharm. Res., 9 (1992) 835.
3 G.A. Rechnitz, J. Clin. Lab Anal., 1 (1987) 308.
4 R.K. Kobos, Trends Anal. Chem., 6 (1987) 6.
5 T.E. Edmonds (Ed.), Chemical Sensors, Chapman and Hall, New York, 1988.
6 R.C. Hughes, A.J. Ricco, M.A. Butler and S.J. Martin, Science, 254 (1991) 74.
7 L.A. Saari, Trends Anal. Chem., 6 (1987) 85.
8 O.S. Wolfbeis (Ed.), Fiber Optic Chemical Sensors and Biosensors, CRC Press, Boca Raton, FL, 1991.
9 W.R. Seitz, in A.P.F. Turner, I. Karube, G.S. Wilson (Eds.), Biosensors: Fundamentals and Applications, Oxford University Press, New York, 1987, Chap. 30.
10 D.L. Meadows and J.S. Schultz, Talanta, 35 (1988) 145.
11 S. Mansouri and J.S. Schultz, Bio/Technology, October (1984) 885.
12 J.S. Schultz, S. Mansouri and I.J. Goldstein, Diabetes Care, 5 (1982) 245.
13 E.F. Ullman, M. Schwarzberg and K.E. Rubenstein, J. Biol. Chem., 251 (1975) 4172.
14 L. Stryer, Ann. Rev. Biochem., 47 (1978) 819.
15 P.L. Khanna and E.F. Ullman, Anal. Biochem., 108 (1980) 156.
16 D.L. Meadows, PhD Dissertation, A Fiber Optic Biosensor for Glucose Monitoring Based on Fluorescence Energy Transfer, University of Michigan, Ann Arbor, MI, 1988.
17 D.L. Meadows and J.S. Schultz, Proc. SPIE (Fiber Optic Medical and Fluorescent Sensors and Applications), 1648 (1992) 202.
18 J.L. Wang, G.R. Gunther, and G.M. Edelman, in H. Bittinger and H.P. Schnebli (Eds.), Concanavalin A as a Tool, Wiley, New York, 1976, Chap. 57.
19 B.B.L. Agrawal, I.J. Goldstein, G.S. Hassing and L.L. So, Biochemistry, 7 (1968) 4211.
20 N.M. Young, Biochim. Biophys. Acta., 336 (1974) 46.
21 G.R. Gunther, J.L. Wang, I. Yahara, B.A. Cunningham and G.M. Edelman, Proc. Nat. Acad. Sci., 70 (1973) 1012.
22 D.L. Meadows, J.S. Shafer and J.S. Schultz, J. Immunol. Methods, 143 (1991) 263.
23 D.L. Meadows and J.S. Schultz, Biotechnol Bioeng., 37 (1991) 1066.

Analytica Chimica Acta, 280 (1993) 31–36
Elsevier Science Publishers B.V., Amsterdam

New electrocatalytic biomolecular interface for fabricating a fructose dehydrogenase-based sensing system

Anwara Begum, Eiry Kobatake, Toshiyuki Suzawa, Yoshihito Ikariyama and Masuo Aizawa

Department of Bioengineering, Faculty of Bioscience and Biotechnology, Tokyo Institute of Technology, 4259 Nagatsuta, Midori-ku, Yokohama 227 (Japan)

(Received 9th November 1992; revised manuscript received 25th January 1993)

Abstract

An enzyme electrode was fabricated by coupling a pyrroloquinoline quinone (PQQ)-containing oxidoreductase with a novel electrode material, TTF–TCNQ conducting salt in a polypyrrole matrix. The enzyme electrode was characterized by direct electron transfer between the reduced prosthetic moiety ($PQQH_2$) and the transducing material at a less extreme potential due to the electrocatalytic function of the organic conducting salt. The oxidation of the reduced enzyme occured at 0.2 V vs. Ag/AgCl. The combination of the organic conducting salt and the conductive polymer exhibited an effective molecular interface where direct electron transfer between the PQQ enzyme and the transducing electrode proceeded at a less extreme potential. Here the conductive polymer matrix played important roles, i.e., facilitation of smooth electronic communication and matrix of enzyme immobilization. On the other hand, TTF–TCNQ played another role, i.e., electrocatalysis in the regeneration of fructose dehydrogenase. The resulting amperometric fructose sensor is promising, as it was operated at a less extreme potential.

Keywords: Biosensors; Catalytic methods; Enzymatic methods; Fructose sensor; Pyrroloquinoline quinone

Advances in bioelectrochemistry have permitted the use of a variety of strategies toward the construction of bioelectronic devices in which electronic communication between electrode materials and enzymes plays an important role [1–8]. Biomolecules, especially the enzymes capable of catalyzing redox reactions (oxidoreductases), are now extensively used for the fabrication of bioelectronic devices such as amperometric biosensors. However, direct electron transfer is seldom achieved due to the deep location of active-site prosthetic groups of redox enzymes and irreversible electrochemistry of the prosthetic groups. In addition, overpotentials in the redox processes of these prosthetic groups make it difficult to fabricate amperometric biosensors which can be operated at less extreme potentials needed to reduce effects of easily oxidizable components. Recently, much attention has been paid to the fabrication of biosensors composed of FAD (flavin adenine dinucleotide) enzymes, PQQ (pyrroloquinoline quinone) enzymes and NAD (nicotinamide adenine dinucleotide) dependent dehydrogenases. Several systems have been developed which exploit synthetic redox couples for electron exchanging between prosthetic groups and transducing devices [9–11]. In such an electron-media-

Correspondence to: M. Aizawa, Department of Bioengineering, Faculty of Bioscience and Biotechnology, Tokyo Institute of Technology, 4259 Nagatsuta, Midori-ku, Yokohama 227 (Japan).

tor incorporated system, enzyme is firstly reduced by the corresponding substrate, and then regenerated either directly at transducing devices or indirectly by co-existing redox mediators. However, the sensors based on the transducing electrodes modified with ferrocene derivatives and quinone derivatives [12–14] suffer from inherent drawbacks, i.e., mediating species diffuse away from the electrode surface into bulk solution.

In previous papers, we have introduced an electrochemically polymerized conductive interface to promote electron transfer [1–5]. We have there emphasized the importance of a molecular interface where electron transfer between prosthetic groups of enzyme and transducer electrodes proceeds smoothly [4,5]. The conductive polymer-interfaced enzyme electrodes are shown to be promising with the aid of electron wiring of the conductive polymer in the determination of metabolites such as glucose and fructose, when an FAD enzyme and a PQQ enzyme were incorporated in the interface, respectively. In the case of fructose determination, it is easily understood that the prosthetic group, PQQ, is reduced to $PQQH_2$, following which $PQQH_2$ is regenerated to PQQ with liberating two electrons directly to a transducer electrode. When TTF–TCNQ complex is utilized as an electrode material, the direct electron transfer from $PQQH_2$ to the electrode is expected to proceed smoothly at a less extreme potential.

$$\text{D-fructose} + \text{FDH(PQQ)} \rightarrow$$

$$\text{5-keto-D-fructose} + \text{FDH}(PQQH_2)$$

$$\text{FDH}(PQQH_2) \xrightarrow[\text{TTF-TCNQ}]{} \text{FDH(PQQ)} + 2H^+ + 2e^-$$

In this paper, a new electron transferring system between fructose dehydrogenase and the TTF–TCNQ electrode is reported by preparing fructose dehydrogenase, the conducting organic salt in polypyrrole matrix. The concept of electrocatalytic biomolecular interface is illustrated in Fig. 1. We would like to show that the polypyrrole-interfaced TTF–TCNQ electrode can exhibit bioelectrocatalytic properties in the biosensing of fructose.

EXPERIMENTAL

Chemicals

D-Fructose dehydrogenase (E.C.1.1.99.11, grade III, 28.3 U/mg, MW 140000) from *Gluconobacter sp.* was obtained from Toyobo (Osaka) and used without further purification. Tetrathiafulvalene (TTF) and tetracyanoquinodimethane (TCNQ) were the products of Tokyo Kasei (Tokyo) and the salt TTF^+–$TCNQ^-$ complex was prepared as described by Ferraris et al. [15]. Pyrrole was purchased from Tokyo Kasei and was purified through an aluminium oxide 90 (Merck) column and distilled before use. Other chemicals were guaranteed reagent grade. The disc type glassy carbon electrode having a diameter of 4 mm was purchased from BAS (West Lafaette, IN) and was used throughout the experiment. A dialysis membrane having a pore size of 0.5 μm (thickness 30.5 μm) was employed as a semipermeable membrane to cover the thin layer of the enzyme-entrapped polypyrrole TTF–TCNQ interface. Phosphate buffer (0.1 M, pH 6.0) was prepared using KH_2PO_4 and K_2HPO_4 and mixing with 0.1 M KCl. This solution was used as the supporting electrolyte solution.

Preparation of biomolecular interface

Fructose dehydrogenase (2 mg) and TTF–TCNQ complex (3 mg) were homogeneously blended and then deposited over the surface of a

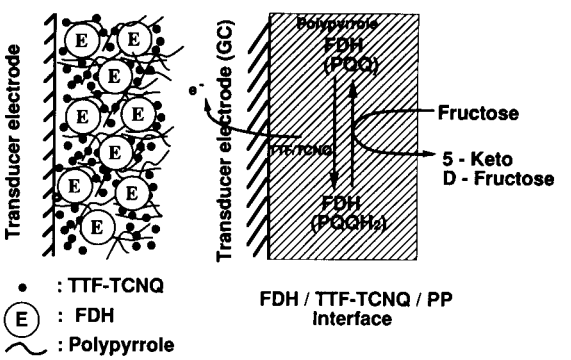

Fig. 1. Schematic representation of electron transfer between $PQQH_2$ moiety and the transducer electrode through the biomolecular interface of the FDH/TTF–TCNQ/PP electrode.

well-polished glassy carbon electrode having a diameter of 4 mm. The enzyme-entrapped TTF–TCNQ electrode was covered with the semipermeable membrane to stabilize the enzyme incorporated thin layer and to prevent the enzyme from leaking. The electrode was then immersed in 0.1 M pyrrole-containing KCl solution (0.1 M) after thorough washing with distilled water. The electrolyte was deoxygenated by bubbling nitrogen gas for 10 min. Electrochemical polymerization of pyrrole was performed in the pyrrole-containing solution using the enzyme-blended electrode as a working electrode at an applied potential of 0.8 V vs. Ag/AgCl to reinforce the composite layer. The electricity used for oxidative polymerization was 100 mC/cm^2. The biomolecular interface thus prepared is schematically illustrated in Fig. 1. In this scheme, the reduced $PQQH_2$ is expected to be electrocatalytically oxidized at the TTF–TCNQ electrode at a less extreme potential, and the electron flow among the $PQQH_2$ and the organic salts is expected to proceed smoothly with the aid of polypyrrole (PP).

Instrumentation

The surface of each glassy carbon electrode was polished with Imperial™ polishing films (Sumitomo 3M, Tokyo) with different particle sizes (30, 9, 3 and 1 μm) and with pasty alumina (0.05 μm). Sequential polishing with the polishing films and the paste made the eletrode surface smooth. Finally, the electrode surface was sonicated for 10 min to remove remaining polishing materials and then rinsed with distilled water several times. Oxidative polymerization of pyrrole was carried out with an HA-301 potentiostat (Hokuto Denko, Tokyo), and the electricity passed for the polymerization was monitored by an HF-201 coulomb meter (Hokuto Denko). All the voltammetric experiments were done in the solutions deoxygenated thoroughly by N_2 gas bubbling. All the electrode potentials were referred to an Ag/AgCl/KCl (saturated) electrode. Cyclic voltammetry was performed with an HB-104 function generator (Hokuto Denko), by which all wave forms were generated, and currents were acquired through an HA-301 potentiostat (Hokuto Denko), and a Type 3086 x,y-recorder (Yokogawa, Tokyo) was utilized to record data. All these experiments were carried out under magnetic stirring.

RESULTS AND DISCUSSION

Optimization of the mixing ratio of the TTF–TCNQ complex and fructose dehydrogenase

The conducting organic salt, TTF–TCNQ, was blended with fructose dehydrogenase at a few ratios. After covering the mixture-mounted electrode with the semipermeable membrane, the electrode was immersed in 0.1 M pyrrole-containing KCl solution (0.1 M) of pH 5.5 for 10 min and then the network formation of polypyrrole was performed by passing an electricity of 100 mC/cm^2. When 2 mg of fructose dehydrogenase and 3 mg of the complex were blended, a satisfactory response current was obtained upon the addition of 10 mM fructose. Mixing ratio of the enzyme to the complex and the polymerization charge were important factors to obtain eligible sensor response.

Voltammetric behavior of the FDH / TTF–TCNQ / PP system

Cyclic voltammetry of FDH/TTF–TCNQ/PP electrode was performed at a scan rate of 10 mV/s in a deoxygenated 0.1 M KCl containing

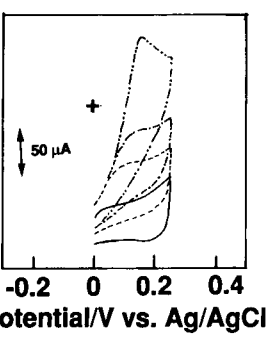

Fig. 2. Cyclic voltammograms of an electroconductive FDH/TTF–TCNQ/PP electrode in 0.1 M KCl containing phosphate buffer of pH 6.0. The electrochemical behaviors were obtained in the presence and absence of fructose at a scan rate of 10 mV/s. Fructose concentration: 0; (------) 5; (·–·–·) 10; (–··–··) 20 mM.

phosphate buffer of pH 6.0 in the presence and absence of fructose. Figure 2 shows a voltammetric behavior of a biomolecular interface of FDH/TTF–TCNQ/PP system. The electricity passed for the preparation of the interface was 10 mC. A new oxidation current increased at around 0.1 V in the presence of fructose. The dependency of the oxidation peak on fructose concentration was observed, at a higher fructose concentration, the oxidation current of fructose dehydrogenase had a distinct peak at 0.15 V, whereas those at lower fructose concentrations were less remarkable due to the overlapping of doping current of polypyrrole. The oxidation peak of FDH was observed at 100, 120 and 160 mV for 5, 10 and 20 mM fructose, respectively. It is expected that the disappearance of the corresponding reduction wave may be caused by inefficient electron transfer from the TTF–TCNQ complex to the PQQ moiety of the enzyme. Another reason can also be taken into consideration. That is, almost all fructose dehydrogenase is in the reduced form, as it is exposed to fructose. This can be partly explained from the fact that a small reduction wave was observed only in the absence of fructose. On the other hand, in the presence of fructose the electrochemically oxidized fructose dehydrogenase may be reduced by its substrate during the reverse scanning from 0.25 to 0.20 V. There was a linear relationship between the peak potential and the fructose concentration. The scan rate dependency of the FDH/TTF–TCNQ/PP system on its peak current was also studied, and it was found that the oxidation current at a higher sweep rate was superimposed on the doping current of polypyrrole. It is apparent from the cyclic voltammogram that the biomolecular interfaced electrode acts as an efficient electron transferring system from the reduced moiety ($PQQH_2$) to the transducer electrode with the aid of polypyrrole and TTF–TCNQ complex.

Potential dependency of FDH / TTF–TCNQ / PP electrode

The potential dependency of the response current of FDH/TTF–TCNQ/PP system was investigated by changing the electrode potential from 0 to 1 V. Into a magnetically stirred solution of 0.1 M phosphate (pH 6.0), a defined concentration of fructose was injected, and the resulting output current was recorded. The output current increased with the increase of electrode potential, however, it started to decrease above 0.2 V. At a potential higher than 1 V, only slight response was observed. Figure 3 shows the relationship between the response current and the electrode potential. The current decrease at a higher potential than 0.2 V seems to have been caused by the deterioration of the electron transferring system in FDH/TTF–TCNQ/PP system. In a series of our previous works concerning enzyme mediator-incorporated interfaces [1–5], the output current vs. electrode potential relationship agreed well with the redox potentials of the mediator employed, i.e., the output current increased sharply at the redox potential of the mediator incorporated in an electron transferring interface. On the other hand, in the case of enzyme incorporated TTF–TCNQ interface, the potential dependency reflected neither the oxidation behavior of FDH nor that of TTF–TCNQ, as the oxidation potential of FDH and TTF–TCNQ are around −0.1 V and 0.3 V, respectively, although the initial sharp increase from 0 to ca. 0.15 V may be ascribed to the oxidation of reduced fructose dehydrogenase.

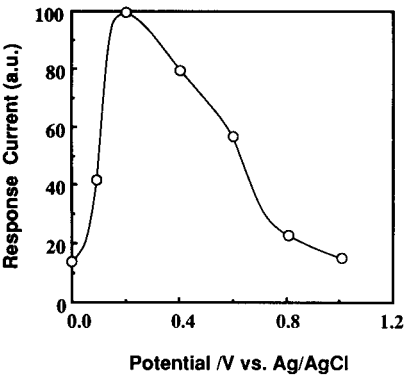

Fig. 3. Dependence of the response current of the FDH/TTF–TCNQ/PP electrode on applied potential. When the residual current reached steady state, fructose was injected to make the final concentration to 5.7 mM, and the resulting increase in anodic current was measured at various potentials.

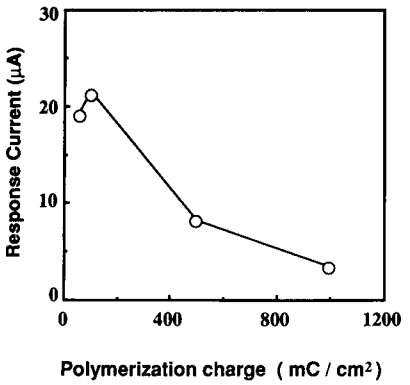

Fig. 4. Relationship between response current and polymerization charge in the preparation of an FDH/TTF-TCNQ/PP-interfaced electrode. The applied potential of FDH/TTF-TCNQ/PP was controlled at 0.2 V and the response to 5 mM fructose was compared to exhibit a synergistic phenomenon in the combination of TTF-TCNQ salt and polypyrrole.

Optimization of electron transfer in biomolecular interface with respect to polymerization charge

The relationship between the response current and the polymerization charge was investigated by changing the electricity in the preparation of the FDH/TTF-TCNQ/PP system. The output current of the resulting enzyme electrode system was measured at an applied potential of 0.2 V on the addition of 5 mM fructose in 0.1 M KCl containing phosphate buffer of pH 6.0. The greatest response current was observed when the polymerization charge was 100 mC/cm^2 as shown in Fig. 4. It seems likely that the conductive polymer thus prepared worked as a molecular wire, so that electron transfer was most effectively facilitated among TTF-TCNQ molecules and PQQ moieties of FDH. However, when the enzyme electrode was prepared at a higher electricity, very small sensor output was observed probably due to the less efficient electron transfer in TTF-TCNQ/PP matrix. Here one can easily understand that the combination of TTF-TCNQ salt and polypyrrole exhibited an synergistic function in the electron transfer of the present biomolecular interface. Besides the synergistic function, the polypyrrole played another role, i.e., as a matrix of enzyme immobilization.

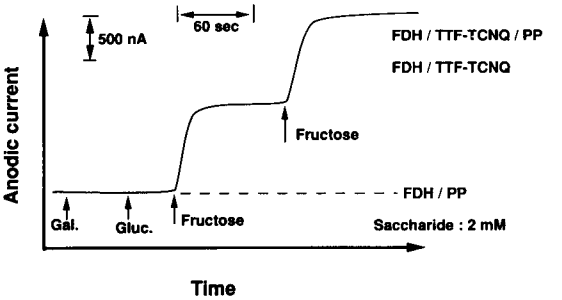

Fig. 5. Response curve of electrocatalytic biomolecular interface electrode upon the addition of saccharides. The potential of each electrode was controlled at 0.2 V. An FDH immobilized polypyrrole-interfaced electrode was employed to show the electrocatalysis of TTF-TCNQ complex. When the background current reached steady state (10–20 min), each sample was injected in a magnetically stirred buffered solution and the resulting increase in anodic current was measured as a response current.

Response behaviors of the FDH / TTF-TCNQ / PP system

The response behaviors were investigated for both FDH/TTF-TCNQ/PP and FDH/complex systems. Upon the addition of various saccharides at 0.2 V, both electrodes exhibited selective response to fructose as shown in Fig. 5. The oxidation currents of the electrodes increased upon the addition of fructose. One can easily recognize that the fructose sensor worked at less extreme potential, i.e., at 0.2 V because of the co-existence of the electrocatalytic organic conducting salt and polypyrrole. The FDH/TTF-TCNQ/PP

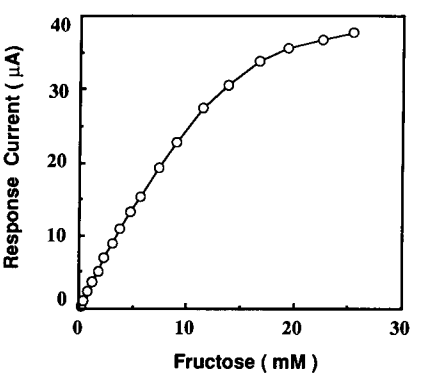

Fig. 6. Calibration curve for D-fructose obtained by the FDH/TTF-TCNQ/PP electrode. The potential of the electrode was controlled at 0.2 V, and the resulting 95% response was obtained.

electrode system was more stable than the FDH/TTF–TCNQ electrode, which indicates an active role of polypyrrole to solidify TTF–TCNQ complexes to facilitate smooth electron transfer. On the other hand, FDH-incorporated polypyrrole electrode did not respond to fructose in the absence of TTF–TCNQ at this potential. To clarify the effect of TTF–TCNQ on the oxidation of reduced PQQ moiety of fructose dehydrogenase, an FDH/PP electrode was prepared. However, the electrode having no TTF–TCNQ exhibited no response to any saccharides including fructose at 0.2 V. On the other hand, the FDH/TTF–TCNQ/PP biosensing system showed selective response only to fructose, when a series of saccharides were injected in a magnetically stirred buffer solution of pH 6.0, as shown in Fig. 5. The results showed that the electrode exhibited high selectivity to fructose. The 90% response time of the enzyme electrode was about 20 s, and the 100% response was obtained in 60 s in the determination of 2 mM fructose.

Fructose determination with an FDH / TTF–TCNQ / PP-interfaced biosensing system

The biomolecular interface-based enzyme electrode was applied for the determination of fructose. The difference in the response between FDH/TTF–TCNQ/PP biosensing system and FDH/PP system clearly indicates the electrocatalytic function of TTF–TCNQ complex in the oxidation of reduced form of FDH. The potential of the sensing system was controlled at 0.2 V in the determination of fructose. Upon the addition of fructose, the sensor response increased rapidly with 95% response of ca. 20 s. The current increase reached steady state in less than 1 min. A calibration curve was obtained between the response current and the fructose concentration from 0.2 to 20 mM, as shown in Fig. 6. The enzyme electrode provided a coefficient of variation of 4% when 10 mM fructose was determined 10 times.

REFERENCES

1 S. Yabuki, H. Shinohara and M. Aizawa, J. Chem. Soc. Chem. Commun., (1989) 945.
2 S. Yabuki, H. Shinohara, Y. Ikariyama and M. Aizawa, J. Electroanal. Chem. Interfacial Electrochem., 277 (1990) 179.
3 H. Shinohara, G.F. Khan, Y. Ikariyama and M. Aizawa, J. Electroanal. Chem., 304 (1991) 75.
4 G.F. Khan, H. Shinohara, Y. Ikariyama and M. Aizawa, J. Electroanal. Chem. Interfacial Electrochem., 315 (1991) 263.
5 G.F. Khan, E. Kobatake, H. Shinohara, Y. Ikariyama and M. Aizawa, Anal. Chem., 64 (1992) 1254.
6 A.E.G. Cass, G. Davis, D. Francis, H.A.O. Hill, W.J. Aston, I.J. Higgins, E.V. Plotkin, L.D.L. Scott and A.P.F. Turner, Anal. Chem., 56 (1984) 667.
7 M.A. Lange and J.Q. Chambers, Anal. Chim. Acta, 175 (1985) 89.
8 C. Iwakura, Y. Kajiya and H. Yoneyama, J. Chem. Soc. Chem. Commun., (1988) 1019.
9 T. Ikeda, H. Hamada and M. Senda, Agric. Biol. Chem., 50 (1986) 883.
10 T. Ikeda, T. Shibata and S. Senda, J. Electroanal. Chem. Interfacial Electrochem., 261 (1989) 351.
11 J.J. Kulys and N.K. Cenas, Biochim. Biophys. Acta, 744 (1983) 57.
12 J.J. Kulys, Biosensors, 2 (1986) 3.
13 W.J. Albery, P.N. Bartlett and D.H. Gaston, J. Electroanal. Chem. Interfacial Electrochem., 194 (1985) 223.
14 K. Mckenra and A. Brajter, Anal. Chem., 59 (1987) 954.
15 J. Ferraris, D.O. Cowan, Jr., V. Walatka and J.H. Perlstein, J. Am. Chem. Soc., 95 (1973) 948.

Analytica Chimica Acta, 280 (1993) 37–41
Elsevier Science Publishers B.V., Amsterdam

Long-term stability and improved reusability of a piezoelectric immunosensor for human erythrocytes

Bernd König and Michael Grätzel

Institut de Chimie Physique, Ecole Polytechnique Fédérale de Lausanne, CH-1015 Lausanne (Switzerland)

(Received 30th November 1992)

Abstract

The long-term stability and reusability of a recently developed piezoelectric immunosensor for the detection of purified human erythrocytes and erythrocytes in whole human blood was studied. Using polyethyleneimine–anti-glycophorin A antibody-coated gold electrodes a long-term stability of 10 weeks was found when stored dry at room temperature. Storage at 4°C did not improve this stability. To improve the reusability a synthetic peptide corresponding to the human glycophorin A sequence of the amino acids 27–39 was used for competition with the bound antigen. With this technique the number of regenerations could be increased from five to twelve without a decrease in activity.

Keywords: Biosensors; Immunoassay; Piezoelectric sensors; Blood; Human erythrocytes

The first application of a piezoelectric sensor was reported in 1964 by King [1] after Sauerbrey [2] derived the equation describing the frequency-to-mass relationship:

$$\Delta F = -2.3 \times 10^6 F^2 \Delta M/A$$

where ΔF is the change in resonance frequency of the coated crystal, F is the resonance frequency of the crystal, ΔM is the mass increase and A is the area of the coated crystal. Today the detection limit of this technique is about 10^{-12} g.

In the last decade, many reports have been described on the use of piezoelectric devices as sensors for a wide range of applications such as in the food industry, environmental monitoring and processing, biotechnology and clinical diagnostics [3], because biosensor technology offers many advantages such as real-time output, high analyte sensitivity and specificity, simplicity of use and cost effectiveness [4–6].

Correspondence to: B. König, Institut de Chimie Physique, Ecole Polytechnique Fédérale de Lausanne, CH-1015 Lausanne (Switzerland).

The biological sensing element can be an enzyme, a biological receptor molecule or antibodies. Direct enzyme biosensors convert a substrate into products that can make contact with the transducer, either directly, or through a mediator [7]. Receptor-based biosensors detect the analyte by changes in the electrical or optical fields due to receptor–analyte (antigen) interaction. The first biosensor of this type, based on the nicotinic cholineric receptor detecting ng ml^{-1} amounts of cholinergic ligands, was reported by Taylor et al. [8].

Antibody-based biosensors detect the antigen concentration either by indirect competitive and displacement reactions similar to immunoassays, or by direct changes in transducer output [9]. An example of the latter type of system is the piezo-

electric crystal detector for assays both in the gas phase and in solution. Piezoelectric devices consist of an oscillating quartz crystal with an adsorbent on its surface that interacts selectively with the analyte. Adsorption of the analyte (antigen) increases the mass of the crystal and decreases proportionally the resonance frequency of oscillation.

In a recent paper [10], the development of a piezoelectric immunosensor for human erythrocytes was reported. The strong complexation between the gold electrode and anti-glycophorin A antibody was exploited to construct a reusable immunosensor. A disadvantage of the generally used regeneration methods is that they use relatively harsh chemicals such as 8 M urea, 0.2 M glycine–HCl (pH 2.8) or 0.2 M ethanolamine (pH 8). To increase the allowable number of regenerations, the use of a synthetic peptide corresponding to the antigenic region of the anti-glycophorin A antibody was studied. Studies on the long-term stability of the immunosensor are also reported here.

EXPERIMENTAL

Materials

Anti-glycophorin A antibody was obtained from Flow Laboratories (Allschwil, Switzerland), human whole blood and erythrocytes from the Zentrallaboratorium Blutspendedienst of the Swiss Red Cross (Berne, Switzerland), polyethyleneimine from Aldrich (Buchs, Switzerland), fluoren-9-ylmethoxycarbonyl (Fmoc) amino acids from Milligen or Bachem (Heidelberg, Germany) and liquid chromatographic (LC) solvents from Merck (Darmstadt, Germany). All other reagents and solvents were of analytical-reagent grade or better (Fluka, Buchs, Switzerland).

Equipment

The PZ crystals (Microcrystal, Grenchen, Switzerland) used were AT-cut with a basic resonance frequency of 10 MHz. The crystal consists of a 14×5 mm quartz wafer which is placed between 8×2 mm gold electrodes. An identical (uncoated) crystal was used as reference to correct for temperature and humidity fluctuations. The crystal frequency was monitored with a universal counter (Hewlett-Packard).

Immobilization procedure

A methanol solution (5 ml) containing 2% polyethyleneimine was spread on the electrode of the crystal for 30 s. After air drying, the crystal was washed three times with methanol to remove unbound material. The crystal was then immersed in aqueous 2.5% glutaraldehyde solution (pH 7) for 30 min and washed with water. Subsequently, 5 μl of 4 mg ml^{-1} antibody solution was placed on each side of the crystal for 1 h. Unreacted aldehyde groups were blocked by immersing the crystal in a solution of 0.1 M glycine in 20 mM phosphate-buffered saline (PBS) (pH 7). The crystal was subsequently rinsed with PBS (pH 7) and distilled water and dried in air.

Regeneration of the crystal

For regeneration with the synthetic peptide, the crystal was placed for 10 min in 20 mM PBS (pH 7) containing 100 μM peptide (amino acids 27–39 of human glycophorin A). To remove the bound peptide, the electrode was washed several times with 20 mM PBS (pH 7). This procedure removed the bound antigen completely without desorbing the bound antibody.

Peptide synthesis

The synthesis of the peptide corresponding to the amino acids 27–39 of human glycophorin A with the sequence H_2N-D-T-H-K-R-D-T-Y-A-A-T-P-R-COOH was performed with the RaMPS multiple peptide synthesis system (DuPont) using Fmoc solid-phase chemistry [11].

Purification of the peptide

The peptide was purified with a Model 1050 LC system (Hewlett Packard) on a Vydac C_{18} reversed-phase column (250×10 mm i.d.; 5 μm particle size) at a flow-rate of 4 ml min^{-1}. The peptide (about 80 mg) was dissolved in 500 μl of starting buffer (0.1% trifluoroacetic acid in water) and injected. The column was thermostatically

controlled at 36°C and the absorbance of the effluent was monitored at 220 nm. The peptide was eluted with a linear gradient of 0.1% trifluoroacetic acid in acetonitrile. The peptide-containing fraction was collected, reinjected to check the purity, freeze-dried and stored at −20°C. Sequencing of the purified peptide yielded the predicted amino acid sequence.

Measurement procedure

ΔF_1, the frequency difference between the coated crystal and the reference crystal, was determined first. The coated crystal was subsequently dipped for several minutes in 1 ml of a solution of human red blood cells in PBS (pH 7) or human whole blood containing different concentrations of cells. After rinsing with PBS (pH 7) and air drying, the coated crystal was placed in the test chamber and a new frequency difference was measured (ΔF_2). The shift in the frequency difference ($\Delta F = \Delta F_2 - \Delta F_1$) was related to the amount of cells adsorbed on the crystal.

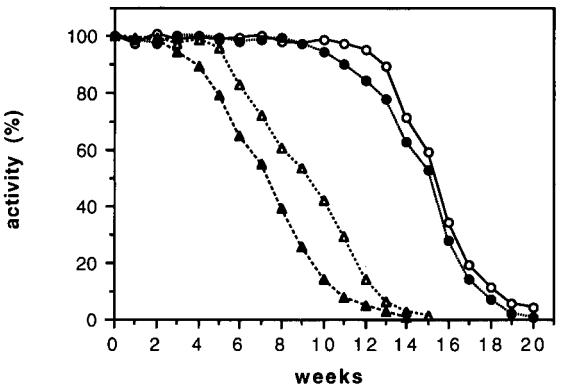

Fig. 1. Long-term stability of an anti-glycophorin A antibody-coated crystal immobilized via polyethyleneimine. Storage at room temperature, (○) dry and (△) undried; storage at 4°C, (●) dry and (▲) undried. Each point represents the average of five experiments, which were done with 2×10^4 human erythrocytes ml^{-1} with an incubation time of 10 min.

RESULTS

The stability of every biosensor for a certain period of time is an important point for the practical application and industrial commercialization of this technique. The long-term stability of the recently developed piezoimmunosensor for human erythrocytes was therefore studied. Four different methods of storage were tested for the polyethyleneimine–anti-glycophorin A-coated crystal: dry at room temperature over silica gel blue; dry at 4°C over silica gel blue; undried at room temperature; and undried at 4°C. As shown in Fig. 1 the best results were obtained when it was stored dry at room temperature. Under these conditions a long-term stability of 10 weeks was observed and a loss of 50% of the original activity occurred after 15 weeks. Storing dry at 4°C yielded nearly comparable results, but the long-term stability was reduced to 8 weeks and a 50% activity loss was seen after 14 weeks. The other two methods of storage, dust-free in air, showed the most unfavourable results with long-term stabilities of 2 and 4 weeks and a half-lives of 7 and 9 weeks for storage at 4°C and room temperature, respectively. To exclude modification of the crystals or the crystal surface due to storage, control experiments were done with polyethyleneimine-coated crystals. The results showed no evidence of direct storage effects on the crystal or its modified electrode (data not shown).

In previous work dealing with immunosensors [10,12], three methods of regeneration were reported using dissociating agents such as 8 M urea, 0.2 M glycine–HCl (pH 2.8) and 0.2 M ethanolamine (pH 8). Whereas the latter two did not remove the adsorbed erythrocytes completely, 8 M urea partly desorbed the immobilized antibody and shortened drastically the lifetime of the immunosensor. A new method was therefore developed for the regeneration step using a synthetic peptide corresponding to the known antigenic binding site of the anti-glycophorin A antibody used in these experiments. The peptide with the sequence H_2N-D-T-H-K-R-D-T-Y-A-A-T-P-R-COOH (sequence of amino acids 27–39 of human glycophorin A) increased the allowable number of regeneration cycles from five to twelve without a detectable decrease in the original activity and 50% activity loss was observed after

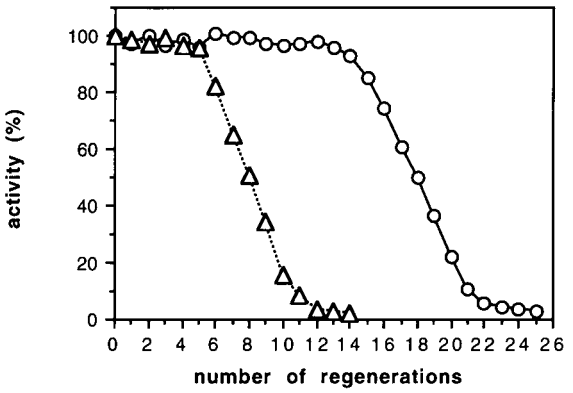

Fig. 2. Comparison of different regeneration methods. (△) Using 8 M urea with the anti-glycophorin A antibody-coated crystal. (○) Competition of the bound antigen with a synthetic peptide (100 μM for 10 min) corresponding to the antigenic region (amino acids 27–39 of human glycophorin A). Experiments were performed with 2×10^4 human erythrocytes ml^{-1}. Incubation time, 10 min. Each point represents the average of four experiments.

eighteen cycles instead of eight cycles for 8 M urea (Fig. 2).

DISCUSSION

An important point when studying long-term stability is the storage conditions. Of the four procedures employed, storing the coated crystal at room temperature and not at 4°C surprisingly gave the best results. Because from control experiments direct effects on the crystal or its modified gold electrode can be excluded, it is believed that the repeated cycles of cooling and warming destabilize the antibody–antigen interaction. When stored at room temperature these effects did not take place, resulting in a longer lifetime of the sensor.

Of the regeneration methods that have been published, that reported here seems to be the best, because it avoids the treatment of the polyethyleneimine–anti-glycophorin A-modified gold surface with harsh chemicals such as urea, glycine–HCl or ethanolamine. The disadvantage of the latter two is that they did not completely remove the bound antigen (data not shown). Urea can remove the bound antigen, but additionally during each regeneration cycle partial desorption of the immobilized antibody occurred, resulting in a decrease in sensitivity, which is in good agreement with previous results [12]. Competition with a synthetic peptide seems to be the best method for the regeneration step. It offers the possibility of completely desorbing the bound antigen without using harsh chemicals. Because such short peptides (thirteen amino acids) are very flexible, the binding constant is relatively low. This makes it possible to remove the peptides very easily from the antibody by simple washing steps. A disadvantage of this technique is that owing to the low binding constant relatively high peptide concentrations (100 μM) are necessary to compete with the bound antigen, which generally has a high binding constant, increasing the cost of each assay. On the other hand, improvement of the allowable regenerations by a factor of 2.4 (twelve vs. five) decreases the amount of antibody needed for each preparation of a new sensor.

It can be concluded that the future use of coated piezoelectric devices as immunochemical sensors is very promising and that they can be considered as an alternative to classical biochemical methods such as radioimmunoassay or enzyme-linked immunosorbent assay. This technique provides a label-free method for direct studies of antigen–antibody reactions. The use of peptide competition for the desorption of the bound antigen offers the possibility of improved reusability, which was problematic in earlier studies. This may open up the way for commercialization of this promising technique of piezoelectric immunosensing.

REFERENCES

1 W.H. King, Anal. Chem., 36 (1964) 1735.
2 G.Z. Sauerbrey, Z. Phys., 155 (1959) 206.
3 C. Kösslinger, S. Drost, F. Aberl, H. Wolf, S. Koch and P. Woias, Biosensors Bioelectronics, 7 (1992) 397.
4 C.R. Lowe, Biosensors, 1 (1985) 3.
5 A.P.F. Turner, Sensors Actuators, 17 (1989) 433.

6 R.F. Taylor, in D.L. Wise (Ed.), Bioinstrumentation: Research, Developments and Applications, Butterworths, Boston, 1990, p. 355.
7 I. Karube and M. Suzuki, Biosensors, 2 (1986), 343.
8 R.F. Taylor, I.G. Marenchic and E.J. Cook, Anal. Chim. Acta, 213 (1988), 131.
9 M.F. Cardosi and A.P.F. Turner, in A.P.F. Turner, I. Karube and G.S. Wilson (Eds.), Biosensors: Fundamentals and Applications, Oxford University Press, London, 1987.
10 B. König and M. Grätzel, Anal. Chim. Acta, 276 (1992) 329.
11 E. Atherton and R.C. Sheppard, in S. Udenfriend and J. Meierhofer (Eds.), The Peptides: Analysis, Synthesis, Biology, Vol. 9, Academic Press, San Diego, 1987, pp. 1–38.
12 M. Plomer, G.G. Guilbault and B. Hock, Enzyme Microb. Technol., 14 (1992) 230–235.

Analytica Chimica Acta, 280 (1993) 43–48
Elsevier Science Publishers B.V., Amsterdam

Determination of phospholipase D activity with a choline biosensor

E. Vrbová, I. Kroupová, O. Valentová, Z. Novotná and J. Káš

Department of Biochemistry and Microbiology, Institute of Chemical Technology, 166 28 Prague (Czech Republic)

C. Thévenot

CNRS, Laboratoire de Physiologie des Organes Vegetaux apres Recolte, 921 95 Meudon (France)

(Received 24th September 1992)

Abstract

A choline biosensor for the determination of the phospholipase D activity in rape seeds was prepared. Choline oxidase was co-immobilized with catalase on a partially hydrolysed nylon net using glutaraldehyde and cyclohexyl isocyanide. The nylon net with immobilized enzymes was fixed on the tip of a Clark-type oxygen sensor. The hydrogen peroxide formed was removed by catalase to prevent inactivation of the choline oxidase. The prepared choline biosensor was characterized by the determination of the specific activity of immobilized choline oxidase (3.24 IU mg^{-1} at pH 8.0), pH and temperature effects on the enzyme activity, the apparent Michaelis constant (1.02 mM at pH 8.0) and the range of the linear biosensor response to the choline concentration (3.34×10^{-3} to 0.167 mM). The long-term biosensor stability is shown by its use for 600 assays over an 18-month period under different pH conditions. The determination of phospholipase D activity was performed in parallel with radiochemical assay and the results obtained demonstrated the priority of the biosensor application.

Keywords: Biosensors; Enzymatic methods; Choline; Enzyme electrodes; Phospholipase D; Rape seed

Phospholipase D (PLD) has been reported to be involved in the hydrolysis of phospholipids that occur naturally in oil seeds such as soybeans [1] and peanuts [2]. The main procedures used for assaying the activity of PLD are physical, chemical and radiochemical methods [2]. Physical methods involve the application of a labelled substrate and the subsequent measurement of surface radioactivity or phase boundary potential. Chemical methods are based on the monitoring of either the products of the enzyme reaction (i.e., choline, phosphatidic acid) or the disappearance of phosphatidylcholine. The chemical determination of choline can be performed, for, instance, by using bromothymol blue [3] or choline oxidase, peroxidase and 4-aminoantipyrine [4]. Radiochemical procedures are reported to be the fastest and most sensitive assay methods [5], suitable especially for monitoring very low enzyme activities in crude plant extracts. They require the use of synthetic radiolabelled (^{14}C, ^{32}P, ^{3}H) phospholipids, many of which are available commercially, but they are often expensive. Therefore, a biosensor with co-immobilized choline oxidase and catalase was developed in order to make available a simpler and cheaper method for further research.

Various amperometric biosensors have already been described and used for the determination of choline [6–12]. To improve the accuracy and ra-

Correspondence to: E. Vrbová, Department of Biochemistry and Microbiology, Institute of Chemical Technology, 166 28 Prague (Czech Republic).

pidity of the assay and biosensor stability, choline oxidase and catalase were co-immobilized covalently on a nylon net [13,14], which was fixed on a Clark-type oxygen sensor. Optimum conditions for the biosensor performance were established and the results of biosensor assays were compared with those obtained using a radiochemical method.

EXPERIMENTAL

Materials

Choline oxidase (COD; choline:O_2 1-oxidoreductase, EC 1.1.3.17, from *Alcaligenes* sp., 4.05 IU mg^{-1}) (Sigma, St. Louis, MO) was used at a concentration 4.5 mg of the lyophilized enzyme preparation per 300 μl of 0.2 M Tris–HCl buffer (pH 8.0).

Catalase (CAT, $H_2O_2:H_2O_2$ oxidoreductase, EC 1.11.1.6, from beef liver, 2000 IU mg^{-1} of suspension, 1 g = 100 ml) (Reanal, Budapest) was used in the form of an undiluted crystalline suspension.

Phosholipase D (PLD, phosphatidylcholine phosphatidodhydrolase, EC 3.1.4.4, from cabbage, 290 IU mg^{-1}), sodium dodecyl sulphate (SDS) and L-α-phosphatidylcholine (from egg yolk) were obtained from Sigma.

Glutaraldehyde (Serva, Heidelberg was applied as a 5.0% aqueous solution. Both cyclohexyl isocyanide (CHIC), used in the form of the undiluted liquid substance, and choline chloride were obtained from Fluka (Buchs, Switzerland), 1,2-dipalmitoyl-L-3-phosphatidyl-[*N*-methyl-^{14}C]choline from Amersham International (Amersham, UK) and SLD-31 scintillator from Chemopetrol (Neratovice, Czech Republic). Other chemicals of analytical grade were from Lachema (Brno, Czech Republic).

The nylon net used (Uhelon 63, Řempo, Prague) had a mesh of 3969 cm^{-2} with a thickness of 100 μm.

Co-immobilization of choline oxidase and catalase on a nylon net and preparation of a choline biosensor

The nylon net was partially hydrolysed with 25% hydrochloric acid for 1 s, then thoroughly washed with distilled water and dried in air. A 20-μl volume of choline oxidase solution was applied to the hydrolysed surface, then 5.0 μl of catalase suspension, 5.0 μl of glutaraldehyde solution and 1 μl of cyclohexyl isocyanide were added and the mixture was incubated for 4 days at 4°C. The nylon net with the bound enzyme system was thoroughly washed with 0.1 M Tris–HCl buffer (pH 8.0), which was also used for its storage at 4°C.

The choline biosensor was prepared by fixing the nylon net with the bound enzyme system on the tip of a Clark oxygen sensor (SOPS 31, 0.8 mm cathode) (Chemoprojekt, Satalice, Czech Republic).

Determination of choline

A 1.4-ml volume of 0.1 M Tris–HCl buffer (pH 8.0 or 10.0), saturated with air oxygen, was pipetted into a 1.5-ml stirred and thermostated (30°C) reaction vessel equipped with the biosensor. The reaction was triggered by the addition of 100 μl of a choline solution of a suitable concentration. Aqueous solutions of choline chloride had to be prepared fresh every day. The biosensor response was measured with a nanommeter having a stabilized source of direct polarized voltage and a signal derivative device (Chemoprojekt). Both the single signal and its derivatives were monitored by means of a TZ 4200 recorder (Laboratory Instruments, Prague).

Characterization of the prepared biosensor

The dependence of the activity of co-immobilized enzymes on the pH of the reaction medium was determined as described above for the determination of choline, except that the buffer pH ranged from 5.9 to 10.5 and 100 μl of 5×10^{-3} M choline chloride solution were used.

The effect of temperature on the activity of the above two-enzyme system was measured in an analogous way at the same substrate concentration (100 μl of 5×10^{-3} M choline), pH 8.0 and in the temperature range 19–50°C.

The system was left to equilibrate for 10 min after each pH or temperature change.

Preparation of crude rape seed extracts

A crude extract was prepared according to Kouzeh Kanani et al. [1] with slight modifications. A 10-g amount of rape seeds was milled twice (using a kitchen poppy-seed grinder) and suspended in 50 ml of 0.05 M Tris–HCl buffer (pH 7.4), with or without adding 200 mg of sodium dodecyl sulphate. After shaking for 1 h at 4°C, the mixture was filtered through a cotton cloth and centrifuged at 10000 *g* at 4°C for 30 min in a Janetzki K 24 centrifuge (Germany).

The amount of proteins in crude extracts was determined by the biuret method [15].

Preparation of substrate emulsion

A 40-mg amount of L-α-phosphatidylcholine (from egg yolk) was dissolved in ca. 0.5 ml of ethanol, 50 μl of 100 mCi $mmol^{-1}$ 1,2-dipalmitoyl-L-3-phosphatidyl-[*N*-methyl-^{14}C]choline were added and the mixture was dried under nitrogen and resuspended in 1 ml of 1 M $CaCl_2$ plus 2 ml of 0.4 M Tris–acetate buffer (pH 5.7) containing 13 mM SDS. The mixture was then emulsified by vortex mixing for 10–15 min. The substrate emulsion for the biosensor assay was prepared in the same way except for adding the radiolabelled substrate.

Radiochemical PLD activity assay

A 1.7-ml volume of a crude rape seed extract was mixed with 0.3 ml of a substrate emulsion and incubated for 10–30 min at 30°C. The reaction was terminated with 1 ml of 0.5 M $HClO_4$ and the mixture was extracted four times with 4 ml of diethyl ether. The ether layer was removed after centrifugation. Finally, 1 ml of the aqueous layer containing released choline was mixed with 10 ml of SLD-31 scintillator and measured using a Beckman LS 5801 instrument (Beckman Instruments, Palo Alto, CA).

Biosensor PLD activity assay

A 1.7-ml volume of a crude extract was mixed with 0.3 ml of substrate emulsion and incubated for 10–30 min at 30°C. The reaction was stopped with the addition of 1 ml of 50 mM EDTA in 1 M Tris–HCl buffer (pH 8.0) and boiling for 5 min. Then 100 μl of this incubation mixture were added to the stirred reaction vessel (30°C) with an inserted biosensor, containing 1.4 ml of 0.1 M Tris–HCl buffer (pH 8.0 or 10.0). The amount of choline was calculated from a calibration graph constructed from responses of standard solutions of choline chloride.

RESULTS AND DISCUSSION

Biosensor construction

Enzymes (COD and CAT) were co-immobilized covalently on the nylon net [13,14]. The covalent attachment itself was achieved with the help of the Ugi four-component reaction [16], as described in a previous paper [13]. This method of immobilization improves the long-term stability of immobilized enzymes in comparison with other immobilization techniques [6,9–12]. The method applied was simpler and faster than covalent immobilization using a lysine spacer [6]. The mean specific activity of the immobilized choline oxidase was 3.24 IU mg^{-1} at pH 8.0. This means that 80% of the original enzyme activity was retained after this immobilization process.

Characterization

The choline biosensor prepared was characterized by the effect of pH on the activity of enzymes (Fig. 1). A certain shift of the pH optimum was observed toward the alkaline range compared with the free enzyme (pH_{opt} = 8.0 [17]) as a result of immobilization. The same phenomenon has already been described by others [10,11] and explained by the changed distribution of charges after immobilization [18].

The biosensor response to thermal changes (pH 8.0) was almost linear in the range 19–40°C. An optimum temperature of 44°C was observed under the conditions used (Fig. 2). Further temperature increases led to significant inactivation of the enzyme. Considering that the biosensor showed sufficient sensitivity at 30°C and the required long-term stability, all determinations were made at 30°C.

A linear biosensor response with respect to the substrate concentration (Fig. 3) was found from 0.05 to 2.5 mM choline in the sample solution,

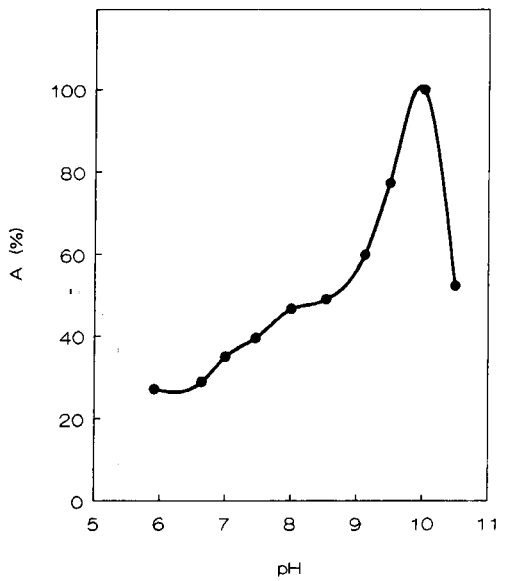

Fig. 1. Effect of pH on choline biosensor response. A = Relative activity.

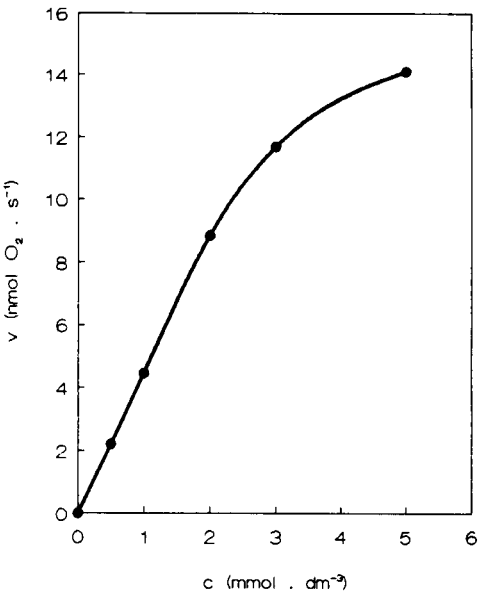

Fig. 3. Calibration graph at pH 10.0. v = Rate of oxygen depletion; c = concentration of choline in sample.

i.e., from 3.34×10^{-3} to 0.167 mM in the reaction vessel (pH 10.0). The lower limit of 0.05 mM choline was also the lowest reliably determinable concentration of choline in the sample. The correlation coefficient for the linear portion of the graph was 0.9999 ($n = 4$) for the biosensor performing at pH 10.0 (Fig. 3) and 0.9999 ($n = 6$) at

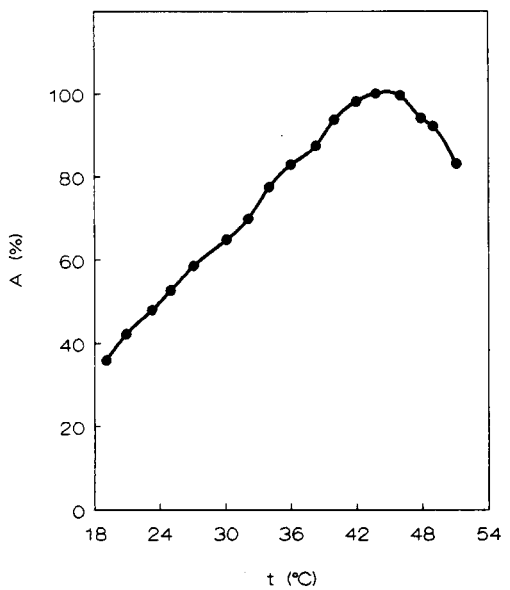

Fig. 2. Effect of temperature on choline biosensor response. A = Relative activity.

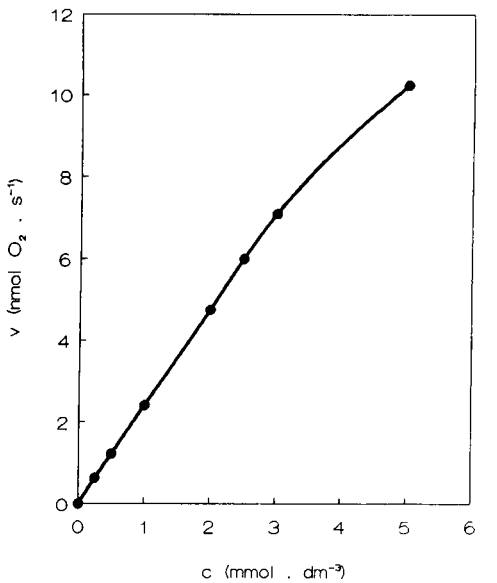

Fig. 4. Calibration graph at pH 8.0. v = Rate of oxygen depletion; c = concentration of choline in sample.

pH 8.0 (Fig. 4). The mid-range relative standard deviations were less than 2% at both pH values.

Substrate specificity of a choline biosensor (COD from the same source, Sigma) has been described previously [11]; a response comparable to that for choline was shown only in the case of betaine aldehyde (relative activity = 45%).

The apparent Michaelis constant, K_M(app.), was determined using the Gauss–Newton method of non-linear regression. With regard to the considerable difference between the optimum pH of the free and immobilized enzyme, K_M(app.) values were determined at 30°C either at pH 8.0 or 10.0. K_M(app.) = 1.02 mM was comparable to the K_M of the free enzyme at pH 8.0 (1.2 mM) [17,19]; however, K_M(app.) at pH 10.0 was four times lower (0.30 mM). The sensitivities of both enzyme systems were comparable; an enzyme electrode tested and stored at pH 10.0 gave twice the response to the choline concentration in the sample (Fig. 4).

The response time did not exceed 10 s and the time required for one analysis was about 90 s. The data obtained are comparable to those published for a similar arrangement (immobilized COD) [11]. The reason for catalase co-immobilization was to protect the choline oxidase from the toxic effect of H_2O_2 produced by COD and to maintain the high concentration of dissolved oxygen needed for the successful choline oxidation [13,14]. The stability of the prepared biosensors was investigated over 18 months at pH 8.0 and 10.0. About 600 analyses were carried out at both pH values without any detectable decrease in COD activity. Daily calibration was necessary, because the slope of the linear part of the calibration graph oscillated about a certain mean value. The long-term stability of the biosensor was not influenced by pH. After 18 months a slight decrease in enzyme activity was observed; however, this was not an obstacle for its further use. The stability of the biosensor presented here is much better than those described earlier [6,10,11,20,21].

Determination of PLD activity

The biosensor can be used at both pH 8.0 and 10.0 for the determination of PLD activity. The limited capacity of the buffer system at pH 10.0 is not a hindrance to the assay.

TABLE 1

Determination of PLD activity in rape seed crude extracts with the choline biosensor and a radiochemical method.

Sample with PLD activity	Incubation time (min)	PLD activity [a] (mIU mg^{-1} protein)	
		Biosensor	Radiochemical assay
Rape seed extract (without SDS)	10	0.0	0.2
	30	0.1	0.2
Rape seed extract (with SDS)	10	3.0	2.7
	30	5.1	4.9
Control [b] cabbage PLD activity (Sigma preparation)	30	290	300

[a] Mean values of 5 measurements (r.s.d. = 2%). The equation of the linear regression was found to be $y = 1.086x - 0.123$ ($r = 0.998$, $n = 4$), where y and x are the enzyme activities determined using the biosensor and radiolabelled substrate, respectively. [b] $y = 0.966x + 0.115$ ($r = 0.9999$, $n = 5$).

The PLD activity measured with egg phosphatidylcholine (lecithin) as substrate was found in crude extracts of rape seeds. The results obtained by the biosensor assay were compared with those of a radiochemical method (Table 1), the detection limit of which has been reported to be 1 pmol [5]. Although the sensitivity of the biosensor was lower (10 nmol of choline in the sample under the experimental conditions described above), the biosensor was preferred owing to its suitability for routine analysis, cheapness and sufficient sensitivity for assaying the samples involved. The values obtained with the biosensor correlated well with those obtained radiochemically (Table 1) and the levels of PLD activity found in rape seed extracts were similar to those reported by Kouzeh Kanani et al. [1] for soybean extracts, 3.8×10^{-3} IU mg^{-1} protein.

The commercial preparation of phospholipase D from cabbage was used for the control determination by both methods.

Conclusion

The choline biosensor prepared by a relatively simple immobilization technique showed im-

proved storage and performance stability (18 months, more than 600 assays) over earlier described sensors, sufficient sensitivity (10 nmol of choline), suitability for routine analysis (assay time ca. 90 s) and cheap performance. The accuracy and reproducibility were tested with cabbage PLD and compared with a radiochemical method using a ^{14}C-labelled substrate. The sensor was found to be suitable for assaying both choline concentrations and PLD activity and it will be used for the investigation of PLD activity levels in rape seeds.

REFERENCES

1 M. Kouzeh Kanani, J.P. Roozen, H.J.A.R. Timmermans, J. de Groot and W. Pilnik, Lebensm.-Wiss. Technol., 18 (1985) 170.
2 M. Heller, Adv. Lipid Res., 16 (1978) 267.
3 A. Barcuchová, J. Gasparič and A. Oulehlová, Cesk. Farm., 33 (1984) 343.
4 K. Shimbo, H. Yano and Y. Miyamoto, Agric. Biol. Chem., 54 (1990) 1189.
5 L.J. Reynolds, W.N. Washburn, R.A. Deems and E.A. Dennis, Methods Enzymol., 197 (1991) 3.
6 M. Mascini and D. Moscone, Anal. Chim. Acta, 179 (1986) 439.
7 U. Loeffler, U. Wollenberger, F. Scheller and W. Goepel, Fresenius' Z. Anal. Chem., 335 (1989) 295.
8 L. Campanella, M. Tomassetti, M.P. Sammartino and P. Stefanoni, J. Pharm. Biomed. Anal., 7 (1989) 765.
9 L. Campanella, M.P. Sammartino and M. Tomassetti, Anal. Lett., 22 (1989) 1389.
10 K. Matsumoto, H. Seido, I. Karube and S. Suzuki, Biotechnol. Bioeng., 22 (1980) 1071.
11 L. Campanella, M. Mascini, G. Palleschi and M. Tomassetti, Clin. Chim. Acta, 151 (1985) 71.
12 Toyo Jozo Co., and Kansai Paint Co., Jpn. Pat., 80 111 (1980) 787.
13 E. Vrbová and M. Marek, Anal. Chim. Acta, 239 (1990) 263.
14 E. Vrbová, M. Marek and E. Ralys, Anal. Chim. Acta, 270 (1992) 131.
15 A.G. Gornall, C.J. Bardavill and M.M. David, J. Biol. Chem., 177 (1949) 751.
16 I. Ugi, Angew. Chem., 74 (1962) 9.
17 S. Ikuta, S. Imamura, H. Misaki and Y. Horiuti, J. Biochem., 82 (1977) 1741.
18 L. Goldstein, Y. Levin and E. Katchalski, Biochemistry, 3 (1964) 1913.
19 H.U. Bergmeyer, H. Grassl and H.E. Walter, in H.U. Bergmeyer (Ed.), Methods of Enzymatic Analysis, Vol. 2, Verlag Chemie, Weinheim, 1983, p. 172.
20 T. Yao, Anal. Chim. Acta, 153 (1983) 169.
21 T. Yao, Y. Kobayashi and M. Sato, Anal. Chim. Acta, 153 (1983) 337.

Analytica Chimica Acta, 280 (1993) 49–52
Elsevier Science Publishers B.V., Amsterdam

Determination of glucose in instant coffee with an enzyme electrode

R. Matsukura, L.M. Aleixo, O.E.S. Godinho and G. de Oliveira Neto

Instituto de Química, Unicamp, C.P. 6154, 13081 Campinas, SP (Brazil)

(Received 2nd October 1992; revised manuscript received 25th January 1993)

Abstract

An amperometric method utilizing an enzyme electrode was developed for the determination of the glucose content of instant coffee. The electrode was constructed by combining an oxygen electrode with a β-D-glucose oxidase-immobilized collagen membrane. Samples of instant coffee were analysed and the results obtained by the proposed method and by the established AOAC method agreed well ($r = 0.9964$). The sensor was stable for more than 2 weeks and for 320 analyses.

Keywords: Coffee; Enzyme electrodes; Glucose; Amperometry; Biosensors; Enzymatic methods

One of the most common tests used to assess the purity of commercial coffee is visual defect counting [1]. The International Organization for Standardization (ISO) codified the defects that could be present such as sticks, wood, husks, parchment or whole cherries [2]. However, this procedure is not suitable for instant coffees, and a method based on screening the carbohydrate profile of soluble coffees is more appropriate [3]. Various methods for determining carbohydrates in commercial instant coffees have been proposed, such as the use of Fehling's reagent, paper chromatography and liquid chromatography, but all of them are time consuming [4].

This paper proposes a rapid, simple and economic method for distinguishing pure instant coffee products from adulterated products using a glucose oxidase-immobilized collagen membrane coupled to an oxygen electrode.

Correspondence to: G. de Oliveira Neto, Instituto de Química, Unicamp, C.P. 6154, 13081 Campinas, SP (Brazil).

EXPERIMENTAL

Glucose oxidase enzyme (EC 1.1.3.4) type VII and bovine serum albumin, fraction V, were obtained from Sigma and glutaraldehyde (25% solution, analytical-reagent grade) from Merck. Collagen membrane 0.02 mm thick was obtained from Johnson and Johnson (Brazil). All other chemicals were of analytical-reagent grade. Solutions were prepared in doubly distilled water. The working electrode was a Radelkis Type OP-9353. All experiments were performed in a thermostated cell at 28.0 ± 0.1°C.

Procedure

The collagen membrane was placed on the side of the sensing surface with a rubber O-ring. The enzyme layer was prepared by dissolving 600 U of glucose oxidase and 10 mg of bovine serum albumin in 20 μl of 0.1 M phosphate buffer (pH 6.9). Then 20 μl of 10% glutaraldehyde solution were added and homogenized. Subsequently, the membrane was exposed to "photo flood" light for

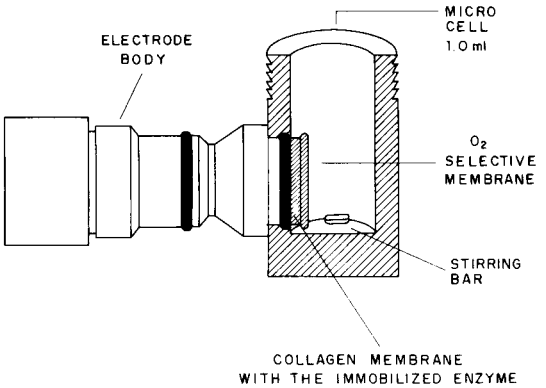

Fig. 1. Diagram of the glucose sensor in the microcell.

10 min and stored at 4°C before use. A sample of 2.00 ± 0.01 g of the instant coffee was transferred into a 100-ml volumetric flask and diluted to volume with distilled water. A 0.020-ml volume of the instant coffee solution was transferred into the micro cell and 0.5 ml of 0.1 M phosphate buffer (pH 6.89), saturated with air, was added. The signal was recorded at the steady state and the micro cell was kept at 28.0°C. The enzyme electrode was fixed in the thermostated micro cell (maximum capacity 1.0 ml) in a horizontal position. The arrangement is shown in Fig. 1. The biosensor was stored in phosphate buffer (pH 7.0) at 4°C when not in use.

RESULTS AND DISCUSSION

In order to evaluate the performance of the glucose electrode in the analysis of instant coffee, several parameters such as response time, temperature, pH, calibration, Michaelis–Menten constant, interfering sugars and stability were investigated.

The immobilized glucose oxidase in the collagen membrane was coupled to the oxygen electrode in two differents ways with the membrane: on the surface of the oxygen electrode and around the oxygen electrode membrane. The response time evaluated for the two arrangements is shown in Fig. 2. The results suggest that the enzyme membrane placed around the oxygen electrode gives a better response time (Fig. 2B) than when it is coupled on the surface (Fig. 2A). The enzyme electrode was stable for more than 2 weeks and about 320 analyses were performed with the same electrode.

The temperature dependence was studied by immersing the micro cell with the electrode in a thermostated water-bath, and the results are shown in Fig. 3. The response time of the enzyme electrode increases with increasing temperature above 28°C, so a fixed temperature was chosen for all experiments. The effect of pH was investigated in 0.1 M phosphate buffer. Figure 4 shows that the maximum response is obtained at pH 6.8–7.1.

The calibration graph was a straight line, defined by the equation $y = 55\,495x - 0.7597$ [y = electrode response; x = concentration (M)], with a correlation coefficient $r = 0.9997$ ($n = 7$). The enzyme electrode response is linear over the concentration range 8.0×10^{-5}–1.0×10^{-3} M. The apparent Michaelis–Menten constant was 3.1 mM for glucose oxidase immobilized on the collagen

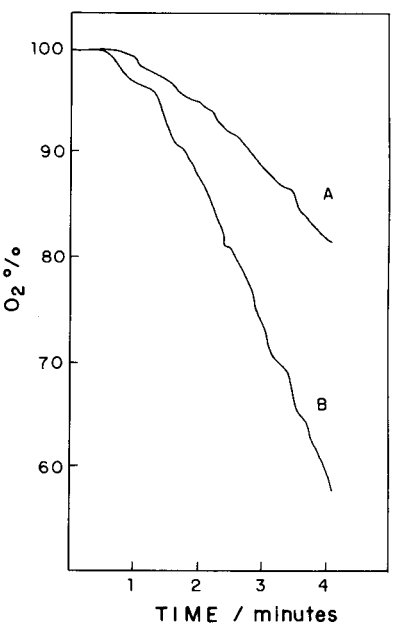

Fig. 2. Typical response curves of the glucose electrode. Glucose, 1.2×10^{-3} M in 0.1 M phosphate buffer (pH 6.8) at 28.0°C. (A) Immobilized enzyme on the surface of the oxygen electrode; (B) immobilized enzyme around oxygen electrode.

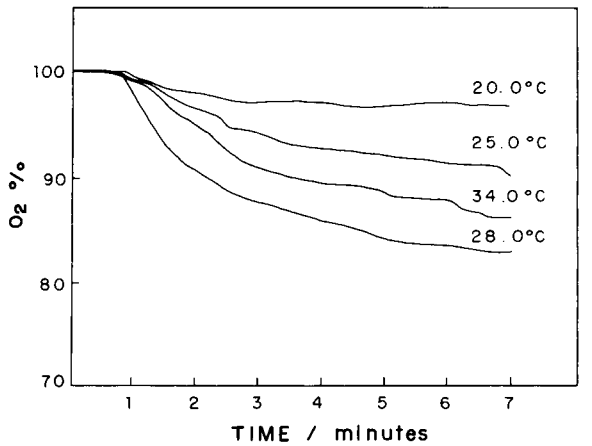

Fig. 3. Effect of temperature. Glucose oxidase immobilized on collagen membrane; 0.1 M phosphate buffer (pH 6.8); glucose, 1.6×10^{-3} M.

membrane and for the soluble enzyme it is 3.6 mM [5]. As suggested by Blanc et al. [3], pure soluble coffee is characterized by a low free sugar level. Commercial samples of instant coffee generally contain small amounts of arabinose, galactose, and mannose, together with traces of others sugars. Glucose and fructose are also sometimes found, which could be due to the addition of instant chicory [6].

The glucose concentrations in six commercial Brazilian instant coffee samples determined by

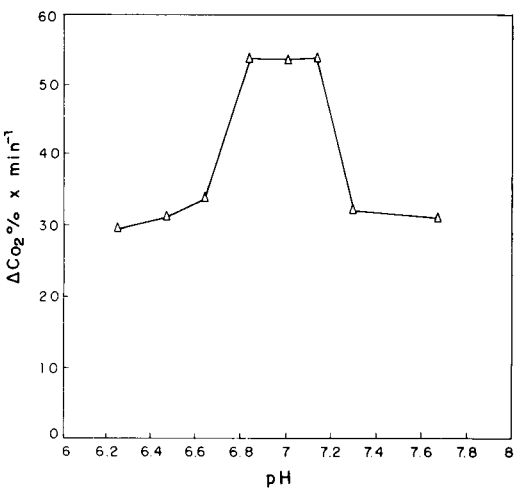

Fig. 4. Effect of pH on the glucose enzyme electrode. Temperature, 28.0°C; glucose, 2.0×10^{-3} M.

TABLE 1

Comparative study of the enzyme electrode and AOAC methods for the determination of glucose in instant coffee

Sample	Glucose found (%, w/w)			
	Proposed method		AOAC method [7]	
	Mean [a]	S.D.	Mean [a]	S.D.
A	16	0.27	15	0.22
B	2.7	0.27	2.5	0.25
B	7.3	0.22	6.9	0.16
C	5.8	0.13	6.0	0.37
C	5.8	0.18	6.0	0.28
D	5.4	0.14	5.7	0.14

[a] Means of five determinations per sample.

the present method (y) were compared with those obtained by the standard AOAC method [7] (x). The results are given in Table 1.

A straight line, defined by the equation $y = 1.053x - 0.33$, standard deviation of the slope $S_m = 0.017$ and of the intercept $S_b = 0.13$, with standard error of the estimate $s_{y,x} = 0.358$ and a correlation coefficient $r = 0.996$ ($n = 30$), was obtained. These results suggest that a glucose oxidase-immobilized collagen membrane placed around the oxygen electrode appears to offer a attractive method for the routine measurement of glucose in instant coffee. The procedure proposed here to distinguish pure instant coffee from an adulterated product is rapid and simple.

The authors thank the Fundação de Amparo à Pesquisa do Estado de São Paulo, Conselho Nacional de Desenvolvimento Científico e Tecnológico, for financial support and Dr. Fred Y. Fujiwara for correcting the English.

REFERENCES

1 P. Jobin, The Coffee Produced Throughout the World, Le Hane, France, 1982.
2 International Organization for Standardization, Coffee and its Products–Vocabulary, ISO, Geneva, 1984, ISO No. 3509.
3 B.M. Blanc, G.E. Davis, J.M. Parchet and R. Viani, J. Agric. Food Chem., 37 (1989) 926.
4 L.C. Trugo, in R.J. Clarke and R. Macrae (Eds.), Coffee Chemistry, Vol. 1, Elsevier Applied Science, Barking, 1985, p. 83.

5 D.R. Thevenot, R. Sternberg, P.R. Coulet, J. Lauret and D.C. Gautheron, Anal. Chem., 51 (1976) 96.
6 L.C. Trugo, in R.J. Clarke and R. Macrae (Eds.), Coffee Chemistry, Vol. 1, Elsevier Applied Science, Barking, 1985, p. 97.
7 S. Williams (Ed.), Official Methods of Analysis of the Association of Official Analytical Chemists, Association of Official Analytical Chemists, Washington, DC, 14th edn., 1984.

Analytica Chimica Acta, 280 (1993) 53–59
Elsevier Science Publishers B.V., Amsterdam

Specific binding of photosynthetic reaction centres to herbicide-modified grating couplers

Ralf Jockers [1], Frank F. Bier and Rolf D. Schmid

GBF – Gesellschaft für Biotechnologische Forschung mbH, Project Group Biosensors, Mascheroder Weg 1, D(W)-3300 Braunschweig (Germany)

(Received 21st December 1992; revised manuscript received 27th January 1993)

Abstract

The photosynthetic reaction centre (RC) of *Rhodobacter sphaeroides* binds not only ubiquinones, but also most of the photosystem II herbicides. This binding has been observed by several means, usually using free herbicides capable of moving into the quinone binding site. It is shown that the binding process can be observed directly, i.e., in real time, if a herbicide derivative is immobilized on a grating coupler surface and the RC is solubilized with the aid of a stabilizing detergent; it also binds if incorporated in an artificial membrane forming liposomes. The specificity of the binding is demonstrated by binding inhibition by an overdose of free quinones and photosystem II herbicides. First quantitative analyses are reported, showing the direction for a new kind of sensing device.

Keywords: Biosensors; Herbicides; Proteins

Receptors are proteins that bind their appropriate ligands normally with high affinity. Therefore, receptors have the potential to be useful as analytical tools. To quantify the binding process, enzyme-labelled or radioactively labelled components are often used. An alternative to these indirect methods are label-free methods that even visualize the binding process directly. Much effort has been put into the development of methods for the real-time analysis of biospecific interactions using optical and acoustic principles [1–3]. Despite the claims of many workers that affinity studies of any receptor–ligand pair can be carried out using these methods, they have been applied almost exclusively to monitor antibody–antigen binding [4,5].

The receptor used here is the photosynthetic reaction centre (RC) of *Rhodobacter sphaeroides*, a transmembrane protein consisting of three subunits (M_r 100 000), which is remarkably stable and has been well characterized by x-ray structural analysis [6–8]. Binding of several photosystem (PS) II herbicides to the quinone binding site (Q_B) of the RC in the bacterial system and the plant system has been confirmed [9,10].

Several herbicide derivatives were synthesized as described previously [11]. *s*-Triazines were coupled to C_{11} spacers with terminal carboxylic groups for immobilization on the sensor surface. As sensing devices grating couplers, which allow the monitoring of real-time biospecific interactions without any label were used. Originally developed for integrated optics by Tiefenthaler and Lukosz [12], it turned out to be highly sensitive to changes in the environment near the grating sur-

Correspondence to: F.F. Bier, GBF – Gesellschaft für Biotechnologische Forschung mbH, Project Group Biosensors, Mascheroder Weg 1, D(W)-3300 Braunschweig (Germany).

[1] Present address: Institut Cochin de Génétique Moléculaire, Laboratoire d'Immuno-Pharmacologie Moléculaire, 22 rue Méchain, F-75014 Paris (France).

face. This is caused by changes in the refractive index near the solid/liquid interface of the waveguide and its surrounding, which influence the propagation characteristics of the guided mode. In this paper, the specific binding of either detergent-solubilized RC or membrane-bound RC (liposomes) to grating couplers that are modified by covalently bound ligands is described.

EXPERIMENTAL

Materials

N,N-Dimethyldodecylamine *N*-oxide (LDAO) (30% aqueous solution) was obtained from Fluka (Buchs, Switzerland). Terbutryne was purchased from Riedel-de Haën (Seelze, Germany). *N*-Thiazoles (KUX 3983 and 3984) were a generous gift from Dr. Kluth (Bayer, Monheim, Germany) and ketonitrile 4 from Dr. Bühmann (Schering, Berlin, Germany). Ubiquinone-10, ubiquinone-0, L-α-phosphatidylcholine (Type III-B), L-α-phosphatidyl-D,L-glycerol, L-α-phosphatidylethanolamine (dipalmitoyl), *n*-octyl-β-D-glucopyranoside, cytochrome *c* Type VI from horse heart and *o*-phenanthroline were obtained from Sigma Chemie (Deisenhofen, Germany).

Reaction centre and chromatophore isolation

Cultivation of *Rhodobacter sphaeroides* (DSM 158) and purification of chromatophores and photoreaction centres were carried out according to Gray et al. [13].

Isolation of thylakoid membranes

Thylakoid membranes from *Spinatia* sp. were prepared according to a procedure described by Nelson et al. [14].

Synthesis of triazine derivatives

All triazine derivatives were synthesized according to the general procedure described previously [11].

Antibodies to terbutryne

The antibody used in comparative studies was a gift from Professor B. Hock (Technische Universität München); it is from the mouse IgG1 subclass and derived from clone K1F4, known to be most specific to terbutryne [15].

Oxidation of cytochrome c by isolated reaction centres

Oxidation of reduced cytochrome *c* by isolated RCs under anaerobic conditions in light (> 610 nm) was monitored spectrophotometrically at 550 nm according to Oettmeier and Preusse [16] and Clayton et al. [17]. Inhibition of electron flow, by triazine aldehydes, was measured in a 1-ml reaction mixture containing 20 mM Trizma buffer [tris(hydroxymethyl)aminomethane] (pH 7.5), 20 μg of cytochrome *c* chemically reduced with sodium dithionite, 50 μM ubiquinone-0 and 50 nM RC. Triazine aldehydes were added in ethanolic solutions (ethanol concentration < 1%).

Preparation of RC-containing liposomes

Liposomes were prepared according to Gabellini et al. [18] with slight modifications: a chloroform solution of 4 mg of L-α-phosphatidylcholine (Typ III-B), 4 mg of L-α-phosphatidyl-D,L-glycerol and 8 mg of L-α-phosphatidylethanolamine (dipalmitoyl) was dried under reduced pressure. The residue was resuspended in 8 ml of 50 mM tricine buffer {*N*-[2-hydroxymethyl-1,1-bis(hydroxymethyl)ethyl]glycine} (pH 7.8) and 1% *n*-octyl-β-D-glucopyranoside and 24 nmol of bacterial RC were added. This mixture was dialysed against 1 l of 50 mM tricine–NaOH buffer (pH 7.8)–5 mM $MgCl_2$–0.1 mM dithiothreitol with two buffer changes. The collected liposomes were centrifuged at 2500 *g* for 15 min (Heraeus Sepatech, Labofuge GL), resuspended in tricine–NaOH buffer (pH 7.8)–5 mM $MgCl_2$ and stored at −20°C until used.

Immobilization of triazine derivatives to grating couplers

11-(4-Ethylamino-6-methylthio-*s*-triazin-2-yl)-undecanoic acid (TE11S) was immobilized on a planar grating coupler consisting of a 170-nm waveguiding film on a glass substrate containing a grating of 2400 lines mm^{-1} (ASI, Zurich, Switzerland). Silanized grating couplers were prepared according to a modified method described by Weetall [19]. Prior to incubation with the silanized

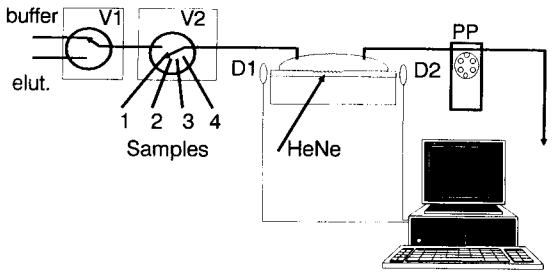

Fig. 1. Grating coupler integrated into a flow system and connected to a computer-aided data collection and data processing unit. V1 = 3/2-way valve switches between buffer and elution buffer; V2 = multi-port valve for the introduction of different samples; D1 and D2 = photodiodes to measure the incoupling light, which comes from the laser source (He–Ne, 632.8 nm, polarized); PP = peristaltic pump.

grating coupler, triazine acids had to be activated with carbodiimide [20]: 10 μmol of TE11S were stirred with 50 μmol of *N*-hydroxysuccinimide and 100 μmol of *N,N'*-dicyclohexylcarbodiimide in 200 μl of dry dimethylformamide overnight at room temperature. Precipitated urea was centrifuged and the pellet was washed with 100 μl of dimethylformamide. Activated triazine acid was incubated on the silanized grating coupler overnight at 4°C and the modified grating coupler was finally washed with ethanol and stored dry at 4°C until used.

Experimental set-up and assay procedure

The modified grating coupler waveguide was placed in a suitable flow-through cell (50 μl) connected to a simple flow system, constructed to minimize flow paths (Fig. 1). It consists of a 3/2-way valve (Lee, Westbrook, CT, USA) for buffer/elution buffer and a multi-channel valve (Latek, Heidelberg, Germany) for the samples. A peristaltic pump (Meredos, Bovenden, Germany) was used to expel all reagents through the flow cell. The grating coupler was measured with a grating coupler system (GCS-1, ASI, Zurich) by turning the sensor chip with the flow cell mechanically perpendicular to the waveguiding direction in order to determine the angle of maximum incoupling light [12]. The angle of incidence, at which the maximum intensity of the incident polarized laser light (632.8 nm) is refracted into the waveguiding film, is called the incoupling angle. It depends on the refractive index at the grating/liquid interface, i.e., amount of bound protein. The change in refractive index of the sensor surface due to antibody binding was observed by measuring the incoupling angle. From the measured change of the incoupling angle an apparent waveguide thickness was calculated, which was taken as the system response.

The measuring cycle was composed of the following steps: (1) washing with 0.08% LDAO in buffer A [20 mM Tris–HCl (pH 8.0)], (2) RC incubation (15–30 min), (3) washing with 0.08% LDAO in buffer A and (4) regeneration with 0.1 M glycine (pH 1.5). The difference in signal readout before (step 1) and after (step 3) incubation was taken as the system response, measured as the difference in apparent waveguide thickness ΔtF in nm.

RESULTS

Synthesis and characterization of triazine derivatives

Several derivatives of terbutryne, a potent PS herbicide in both plant and bacterial systems, were synthesized according to the general procedure described by Jockers and Schmid [11]. C_{11}

TABLE 1

Affinity of triazine derivatives to the Q_B site of RCs [a]

Compound [b]	K_i (μM) [c]
Terbutryne	0.048
EB11S	1
TCl11S	> 10
TE11S	0.045
TB11S	4.7

[a] Inhibition of photosynthetic electron transport in RC from *Rhodobacter sphaeroides* measured by the oxidation of cytochrome *c* by isolated RCs in the presence of triazines. [b] EB11S = 11-[4-(1',1'-dimethylethylamino)-6-ethylamino-*s*-triazine-2-yl]aminoundecanoic acid; TCl11S = 11-(4-chloro-6-methylthio-*s*-triazine-2-yl)aminoundecanoic acid; TE11S = 11-(4-ethylamino-6-methylthio-*s*-triazine-2-yl)undecanoic acid; TB11S = 11-[4-(1',1'-dimethylethylamino)-6-methylthio-*s*-triazine-2-yl]aminoundecanoic acid. [c] K_i was determined as herbicide concentration where 50% turnover was observed in the presence of 50 μM ubiquinone-0.

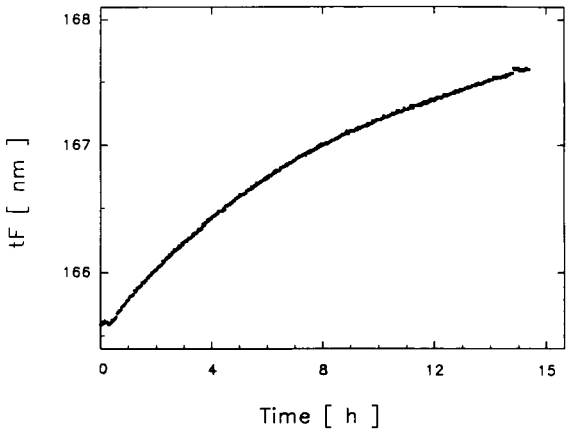

Fig. 2. Binding of RC to a TE11S-modified grating coupler. Solubilized RC (250 nM) was incubated for 15 h over the grating.

spacers were coupled at different positions to the *s*-triazine ring system. In addition, the spacers carried terminal carboxylic groups for immobilization on grating couplers.

Inhibition of photosynthetic electron transport in RCs from *R. sphaeroides* was determined by oxidation of cytochrome *c* by isolated RCs in the presence of the synthesized triazines and ubiquinone-0. Table 1 summarizes the inhibitor constants (K_i) obtained. The K_i values ranged over more than three orders of magnitude (from 0.048 to $> 10\ \mu M$). The triazine derivative TE11S was as effective as terbutryne itself and was therefore chosen for grating coupler experiments.

RC binding to modified grating couplers and comparison with antibody binding

Figure 2 shows the direct binding of RCs solubilized in LDAO over 15 h to a grating coupler that was previously modified with TE11S. RCs bind to the waveguide with a typical saturation curve. If binding was interrupted by washing with buffer without the RC, no further change in refractive index was observed and the system stabilized at the value reached. If RC incubation was interrupted at any time during the 15-h incubation, the system always stabilized at the value reached. Therefore, the real amount of bound RC is shown by the binding curve at any time during incubation. As can be seen from the slope of the curve, the binding process does not reach equilibrium even after 15 h of incubation.

In Fig. 3a the change in apparent adlayer thickness is plotted against the molar concentration of the RC. Linearity was observed over the whole detection range (40–500 nM). Less than 40 nM of the RC was still detectable after 30 min of RC incubation on modified grating couplers; in this and all subsequent experiments the binding process was stopped by washing with buffer after 30 min and thus binding was not allowed to reach equilibrium.

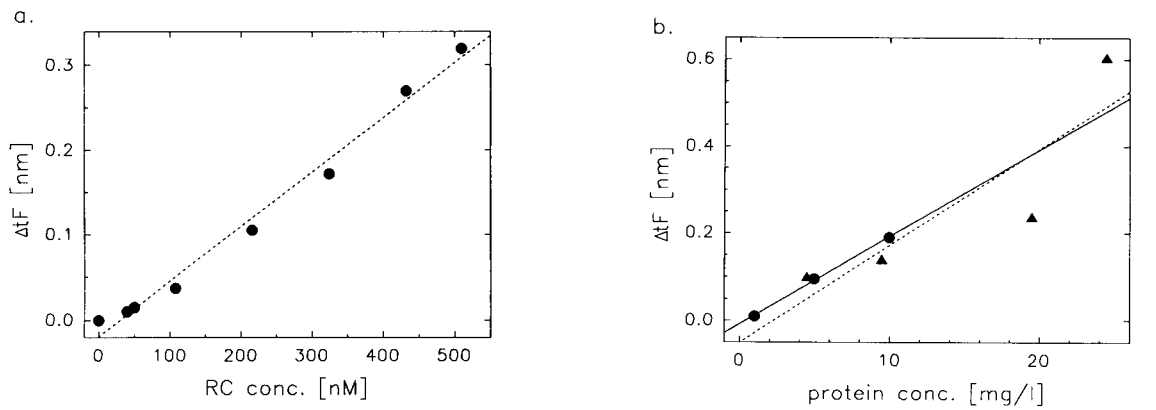

Fig. 3. (a) Calibration graph for RC binding to a TE11S-modified grating coupler. Incubation time, 30 min. (b) Comparison between (▲) RC and (●) antibody binding to modified grating couplers in terms of mass binding. Incubation time, 30 min; buffer, Tris–HCl (pH 8.0) for RC and phosphate-buffered saline (pH 8.0) for the antibody.

The obtained change in apparent adlayer thickness was nearly the same for antibodies and RCs if the protein masses are compared as shown in Fig. 3b. If one assumes that the refractive index of immunoglobulin G (IgG) (the triazine-specific antibody) and of the RC are similar, the influence of LDAO, which forms micelles, does not contribute significantly to the change in refractive index during binding of RCs to the grating coupler.

Reversibility and specificity of RC binding

Good reversibility of RC binding in less than 5 min was achieved by washing the sensor after each cycle with detergent-free acidic buffer and by decreasing the amount of RC during the incubation. Regeneration was sufficiently complete to allow several hundred incubations without any loss of binding capacity or change in background.

To examine the specificity of binding, the effect of free herbicides and quinones during RC incubation on the grating coupler was studied. Figure 4 shows a sequence of two measuring cycles out of fourteen. RC binding in the absence of terbutryne (first incubation) was decreased to 15% in the presence of 40 μM terbutryne (second incubation). This indicates that at least 85% of bound RC may be bound to Q_B sites. In addition, the binding observed in the first cycle without terbutryne [Fig. 4(I)] shows the asymptotic behaviour normally observed with specific binding. This type of binding is completely suppressed in the presence of excess of terbutryne [Fig. 4(II)].

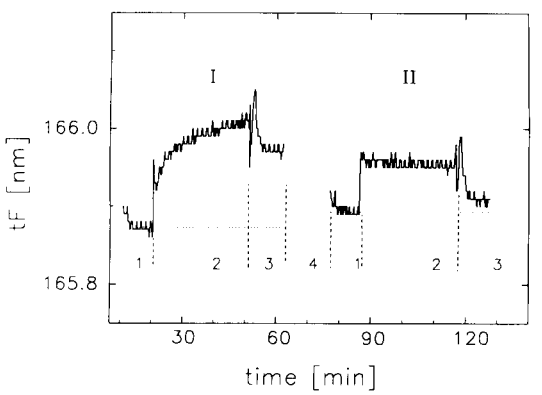

Fig. 4. Optimized binding of RC in the (I) absence and (II) presence of 40 μM terbutryne. RC, 45 nM; incubation time, 30 min. Each cycle consisted of the following steps: (1) baseline signal, (2) RC incubation, (3) washing and (4) regeneration. The change in the apparent waveguide thickness, which resulted from binding to the grating, was calculated from the values taken (1) before incubation and (3) after washing.

TABLE 2

Inhibition of RC binding to TE11S-modified grating couplers by PS-II herbicides and quinones [a]

Compound	Inhibition [b]	pI_{50} [c]
Control	–	–
Terbutryne	+	6.15
Ketonitrile 4	+	5.45 [d]
KUX 3983	+	6.40
o-Phenanthroline	–	4.15
Ubiquinone-10	+	6.00
Ubiquinone-0	–	4.00

[a] 100 nM RC were incubated on the grating coupler in the presence of 0.1 mM terbutryne, 0.1 mM ketonitrile 4 [16], 0.1 mM *N*-thiazole KUX 3983 [17], 1 mM *o*-phenanthroline, 0.1 mM uniquinone-10 and 1 mM ubiquinone-0. [b] + = Inhibition observed; – = no influence. [c] pI_{50} = negative logarithm of the concentration at which 50% bleaching of the bacteriochlorophyll dimer in the RC is observed; pI_{50} values were taken from [23]. [d] Value taken from [16].

One characteristic feature of the Q_B site is the ability to bind specifically not only quinones and one class of herbicide but also several structurally very different classes of herbicides. From Table 2 it can be seen that compounds with a high affinity for Q_B, such as ketonitriles [21], *N*-thiazoles [22] and ubiquinone-10, are able to inhibit RC binding to TE11S-modified grating couplers. The pI_{50} values of the tested compounds determined by recombination measurements [23] are also given in Table 2 for comparison. In the presence of an excess of these compounds, approximately 85% of RC binding was suppressed, which is comparable to the results obtained with terbutryne. The pI_{50} values determined using the grating coupler for terbutryne and *N*-thiazole KUX 3984 are 5.40 and 6.22, respectively. Detection of both herbicides was possible in the range 0.2–20 μM.

Weakly binding compounds such as ubiquinone-0 and *o*-phenanthroline are unable to influence RC binding, even at a ten times higher concentration than that used for strongly binding compounds.

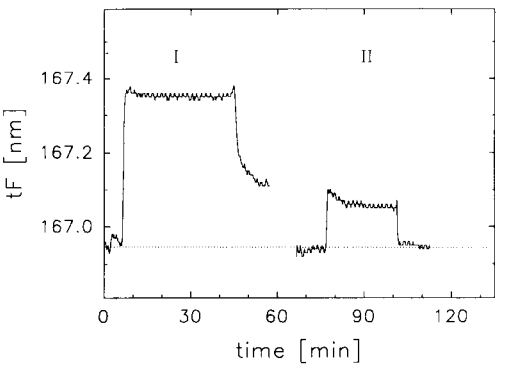

Fig. 5. Binding of (I) RC–liposomes (0.1 nmol RC) and (II) liposomes to TE11S-modified grating coupler. Measuring cycle as described in Fig. 4.

Binding of membrane-bound RCs

Isolated RCs were integrated into liposomes prepared as described by Gabellini et al. [18], with some modifications. RC-containing liposomes were incubated with TE11S-modified grating coupler [Fig. 5(I)]. As a control, the same amount of liposomes without incorporated RC was incubated in the same way [Fig. 5(II)]. Binding curves with liposomes were different from those obtained with solubilized RC. Owing to the optical density of the liposomes themselves, the refractive index changes immediately by the start of the incubation and the binding of the RC itself was not observed. The change in the apparent waveguide thickness was calculated from the values taken before incubation and after washing. RC-containing liposomes are able to bind to the grating surface, whereas after rinsing no changes in refractive index were observed with liposomes not containing the RC. Additionally, this experiment supports the view that RCs bind specifically to TE11S-modified grating couplers.

Binding of chromatophores from *R. sphaeroides* and thylakoid membranes from *Spinatia* sp. was also observed. Chromatophores at a concentration of 60 μg bacteriochlorophyll ml^{-1}, which is equivalent to ca. 0.4 μM binding sites for terbutryne [21], gave a change in adlayer thickness of 0.4 nm. This is twice of the amount observed with solubilized RCs. Complete regeneration was not possible even under more stringent conditions than used for liposomes. This limits the applications in a reusable sensing system and points to non-specific binding of chromatophores to the glassy sensor surface.

Thylakoid membranes also showed binding to the sensor surface, which was comparable to that of chromatophores. Complete regeneration was again not possible. In addition, thylakoids are unstable and degradation was observed within several hours even at 4°C.

DISCUSSION

Using the approach described here, the applicability of direct methods for biospecific binding analysis to membrane proteins has been demonstrated. In a competitive assay format, in principle performed as in immunoassays for small ligands (haptens), this approach could be used to detect ligands by binding inhibition. In the particular case investigated here, the RC is of special interest for the aim of pesticide analysis, e.g., in water designated for human usage: the RC is capable of binding many different herbicides belonging to various chemical classes, but all of them being PS-II herbicides, whereas the immunological approach would need a specific antibody for each individual compound.

A critical point in the binding of RCs to grating couplers is the chain length of the spacer. X-ray analysis showed that the Q_B lies deep in the protein, ca. ten carbon atoms away from the outside [6–8]. In the present instance the C_{11} spacer plus the aminopropyl function on the sensor surface seemed to be sufficient for the immobilized triazine to enter the Q_B site.

Evidence has been presented for the specificity of the observed binding of RCs to modified grating couplers. Five structurally different compounds that all bind to the Q_B site are able to prevent the binding of RCs to the sensor. The ability of displacing the RC and pI_{50} values obtained with recombination measurements [21] correlate fairly well. This points to a strong and specific binding of RCs via Q_Bs to TE11S covalently bound to grating couplers, which can only be suppressed by strong competitors. The results with liposomes without an RC show that a lipid

membrane does not influence either the binding or the amount of unspecific binding. Nevertheless, binding of biological membranes such as chromatophores and thylakoids to modified grating couplers was mainly unspecific.

Further, many membrane proteins are receptors of the nervous system or hormone system and many of them are of great pharmacological relevance. With the approach introduced here, receptor or drug characterization, such as binding constants and binding kinetics, may be determined easily and in real time.

REFERENCES

1 B. Liedberg, C. Nylander and I. Lundström, Sensors Actuators, 4 (1983) 299.
2 M.T. Flanagan and R.H. Pantell, Electron Lett., 20 (1984) 968.
3 P.M. Nellen, K. Tiefenthaler and W. Lukosz, Sensors Actuators, 15 (1988) 285.
4 R.P.H. Kooyman, M.H. Kolkman, J. van Gent and J. Greve, Anal. Chim. Acta, 213 (1988) 35.
5 W. Lukosz, Biosensors Bioelectron., 6 (1991) 215.
6 C.H. Chang, D.M. Tiede, J. Tang, U. Smith, J. Norris and M. Schiffer, FEBS Lett., 205 (1986) 82.
7 J.P. Allen, G. Feher, T.O. Yeates, H. Komiya and D.C. Rees, Proc. Natl. Acad. Sci. USA, 84 (1987) 5730.
8 J. Deisenhofer, O. Epp, K. Miki, R. Huber and H. Michel, Nature (London), 318 (1985) 618.
9 C.A. Wraight, Isr. J. Chem., 21 (1981) 348.
10 H. Michel, O. Epp and J. Deisenhofer, EMBO J., 5 (1986) 2445.
11 R. Jockers and R.D. Schmid, Z. Naturforsch., Teil C, 47 (1992) 573.
12 K. Tiefenthaler and W. Lukosz, Opt. Lett., 10 (1984) 137.
13 K.A. Gray, J.W. Farchaus, J. Wachtveitl, J. Breton and D. Oesterhelt, EMBO J., 9 (1990) 2061.
14 N. Nelson, Z. Drechsler and J. Neumann, J. Biol. Chem., 245 (1970) 143.
15 T. Giersch and B. Hock, Food Agric. Immunol., 2 (1990) 85.
16 W. Oettmeier and S. Preusse, Z. Naturforsch., Teil C, 42 (1987) 690.
17 R.K. Clayton, H. Flemming and E.Z. Szuts, Biophys. J., 12 (1972) 46.
18 N. Gabellini, Z. Gao, D. Oesterhelt, G. Venturoli and B.A. Melandri, Biochim. Biophys. Acta, 974 (1989) 202.
19 H.H. Weetall, Methods Enzymol., 44 (1976) 134.
20 B. Neises and W. Steglich, Angew. Chem., 90 (1978) 556.
21 A. Trebst, J. Kluth, K. Tietjen and W. Draber, in H. Frese (Ed.), Pesticide Chemistry, Advances in International Research, Development and Legislation, VCH, Weinheim, 1991, p. 111.
22 W. Oettmeier, S. Preusse and M. Haefs, Z. Naturforsch., Teil C, 46 (1991) 1059.
23 R. Jockers, F.F. Bier, R.D. Schmid, J. Wachtveitl and D. Oesterhelt, Anal. Chim. Acta, 274 (1993) 185.

Analytica Chimica Acta, 280 (1993) 61–67
Elsevier Science Publishers B.V., Amsterdam

Highly sensitive and selective measurements of lead by stripping voltammetry/potentiometry following adsorptive accumulation of the lead–*o*-cresolphthalexon complex

Joseph Wang, Jianmin Lu and Chaim Yarnitzky [1]

Department of Chemistry and Biochemistry, New Mexico State University, Las Cruces, NM 88003 (USA)

(Received 14th December 1992; revised manuscript received 26th January 1993)

Abstract

A very sensitive and selective stripping procedure for trace measurements of lead, based on the adsorptive accumulation of the lead–*o*-cresolphthalexon (OCP) complex onto various mercury electrodes is described. The technique offers enhanced sensitivity over analogous stripping measurements of lead (with a detection limit of 40 ng l^{-1} after 2 min accumulation). Even more significant is the improved selectivity in the presence of a large excess of thallium or tin (which commonly interfere in anodic stripping measurements). Both voltammetric and potentiometric stripping modes can be employed to probe the reduction of the lead–OCP complex. The reported coupling of the new method with disposable screen-printed electrodes holds a great promise for decentralized testing of lead. Applicability to assays of drinking water is illustrated.

Keywords: Potentiometry; Stripping voltammetry; Lead; *o*-Cresolphthalexon

Lead is widely distributed in nature and exhibits severe deleterious effects on human [1]. In particular, it strongly affects the mental and physical development of children. Due to new concerns regarding the toxicity of lead, there are growing needs for improved analytical methods for monitoring this metal. Such methodology may be useful for children screening and prevention programs, for assessing industrial exposure to lead, and for monitoring trace lead in (drinking and waste) water systems. Numerous analytical methods are available for trace measurements of lead [1]. Because of its remarkable sensitivity and suitability for decentralized testing, electrochemical stripping analysis has been widely used for this task [2]. Indeed, a major interlaboratory study ranked stripping analysis above other spectroscopic techniques in terms of overall reliability for blood lead determinations [3]. Yet, improved stripping procedures are desired to address resolution problems (in the presence of co-existing metals such as thallium or tin), for shortening the analysis time, and for addressing the requirements of new on-site screening and surveillance programs.

The present investigation was prompted by a desire to develop an alternative method for the determination of lead based on adsorptive, rather than electrolytic, accumulation. Stripping analysis following adsorptive accumulation of metal chelates is becoming a widely accepted analytical tool, as it extends the scope of stripping analysis toward additional trace metals, and offers an effective alternative method for monitoring other

Correspondence to: J. Wang, Department of Chemistry and Biochemistry, New Mexico State University, Las Cruces, NM 88003 (USA).

[1] Permanent address: Department of Chemistry, Technion I.I.T., Haifa (Israel).

metals [4,5]. A sensitive adsorptive stripping scheme for lead in the presence of oxine was reported [6], but did not possess the desired selectivity (particularly due to a severe copper interference). In contrast, the present scheme, based on the formation, accumulation, and reduction of the lead–*o*-cresolphthalexon (OCP) complex, offers both inherent sensitivity and selectivity, and represents an attractive alternative to conventional stripping measurements of lead. In particular, its response is not affected by a large excess of thallium, tin, or copper. OCP is a triphenylmethane dye, that was employed previously for adsorptive stripping measurements of light rare earths [7]. The improvements offered by the use of OCP for monitoring trace lead are illustrated below in connection with conventional and disposable working electrodes.

EXPERIMENTAL

Apparatus

An EG&G PAR 264A voltammetric analyzer, a PAR 303A static mercury drop electrode, and a PAR 0073 X-Y recorder were used to obtain the voltammograms. A medium-size hanging mercury drop electrode (with an area of 0.016 cm^2) was employed. A TraceLab potentiometric stripping unit (PSU 20, Radiometer), with SAM20 sample station (Radiometer) and an IBM PS/2 55SX computer, were used to obtain the potentiograms. A glassy carbon disk (Radiometer) and screen-printed carbon strip (Medisense) [8] were employed as substrates for the mercury film, in connection with the Ag/AgCl and platinum-wire reference and auxiliary electrodes, respectively of the TraceLab unit.

Reagents

All solutions were prepared from doubly-distilled water. Stock solutions (1000 mg l^{-1}) of lead (atomic absorption standard, Aldrich) were diluted daily as required. A 5×10^{-4} M stock solution of OCP (Aldrich) was prepared daily. A 1×10^{-3} M acetate buffer (pH 4.0) solution served as supporting electrolyte. Human albumin was obtained from Sigma. Drinking water samples were collected from a water fountain at NMSU.

Procedure

For adsorptive stripping voltammetry, the supporting electrolyte solution (10 ml), containing 1×10^{-6} M OCP, was pipetted into the cell and purged with nitrogen for 8 min. The preconcentration potential (usually 0.0 V) was applied to a fresh mercury drop while the solution was stirred. Following the preconcentration period, the stirring was stopped, and after 15 s, the voltammogram was recorded by applying a negative-going differential pulse scan (with 5 mV s^{-1} rate and 50 mV amplitude). The scan was terminated at −0.60 V. Aliquots of the lead standards were introduced after recording the background voltammograms. Throughout this operation, nitrogen was passed over the solution. Analogous measurements, in the presence of oxine, were carried out in accordance to Ref. 6.

Potentiometric stripping measurements were made on a mercury film electrode (MFE) covering glassy carbon or carbon strip supports. The preplated MFE was obtained by plating mercury from a 100 mg l^{-1} Hg^{2+} (in 0.05 M HCl) solution at −0.9 V for 8 to 15 min (on the glassy carbon or carbon strip electrodes, respectively). Twenty ml of the sample solution was pipetted into the cell and purged with nitrogen for 4 min (while the electrode was held at open circuit). An accumulation potential of 0.0 V was applied to the electrode while the solution was stirred for a predetermined period of time. Following the accumulation step, the stirring was stopped and after 10 s the potentiogram was recorded by applying a constant current (of −5 and −10 μA for the glassy carbon and carbon strip coated electrodes, respectively). The stripping was terminated upon reaching a potential of −0.9 V. All data were obtained at room temperature.

RESULTS AND DISCUSSION

Figure 1A shows cyclic voltammograms for 50 μg l^{-1}, in an acetate buffer solution containing 1×10^{-6} M OCP, after 0 (a) and 240 (b) s accu-

mulation at 0.0 V. One cathodic peak is observed at −0.43 V during the negative-going scan. Scanning in the reverse direction exhibits a smaller and broader anodic peak (at −0.40). The response increases dramatically (22-fold) when an accumulation period preceded the potential scan, indicating an effective interfacial accumulation of the OCP–lead complex. The rising current at potentials higher than −0.50 V is attributed to the reduction of the free ligand. No response was observed for analogous measurements without the ligand (not shown). Also shown in Fig. 1B are repetitive cyclic voltammograms for 50 μg l^{-1} lead (in the presence of OCP) in an unstirred solution. Progressive increases of the cathodic and anodic peaks are observed, until saturation is achieved. The maximum charge obtained by integrating the reduction current at saturation was found to be 7 nC (i.e. a surface coverage of 2.2×10^{-12} mole cm^{-2}). Because of the mixed adsorbed layer the area occupied by a single complex molecule cannot be estimated. The peaks at saturation remained highly stable upon continuous scanning, with no desorption over prolonged periods. The height of the complex reduction peak increased with the scan rate (v) over the 2–100 mV s^{-1} range. The plot of log i_p vs. log v was linear with a slope of 0.98. (A slope of 1.00 is expected for an ideal surface reaction.) In the case of rare-earth complexes of OCP, the reduction peak is attributed to a negative shift in the potential of the ligand reduction process (associated with the involvement of the redox functionality in the coordination) [7,9]. In contrast, the lead–OCP response is attributed to the reduction of the metal center in the complex (with a potential 70 mV more negative than that of the free metal, and ca. 150 mV positive to the ligand peak).

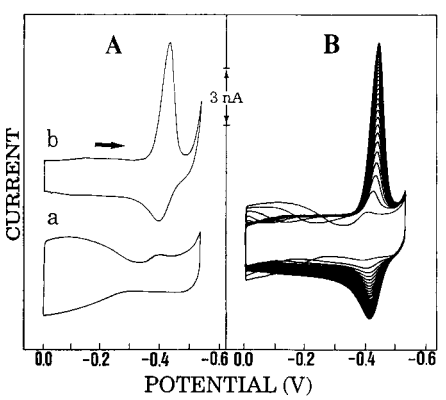

Fig. 1. Cyclic voltammetry of the Pb–OCP complex. (A) voltammograms for 50 μg l^{-1} lead after 0 (a) and 240 (b) s accumulation at 0.0 V with 300 rpm stirring. (B) Repetitive cyclic voltammograms for 50 μg l^{-1} lead in an unstirred solution. Scan rate, 50 mV s; media, 1 mM acetate buffer (pH 4.0), containing 1 μM OCP.

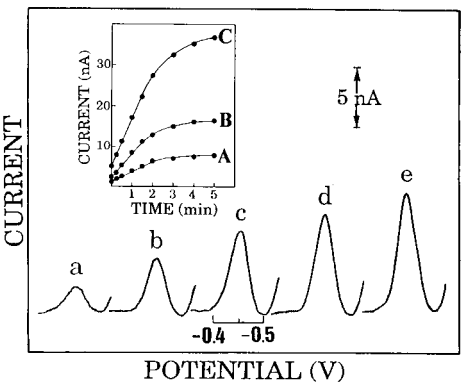

Fig. 2. Differential pulse voltammograms for 1 μg l^{-1} lead after different preconcentration times: 0 (a), 30 (b), 60 (c), 90 (d) and 120 (e) s. Inset are current vs. preconcentration time plots for (a) 1, (b) 2 and (c) 5 μg l^{-1} lead. Conditions: accumulation at 0.0 V with 300 rpm stirring, followed by a differential pulse scan with 50 mV amplitude and 5 mV s^{-1} rate. Solution, as in Fig. 1.

The spontaneous adsorption of the lead–OCP complex can be used as an effective preconcentration step prior to the voltammetric measurement. In this way, highly sensitive adsorptive stripping measurements of lead can be achieved. For example, Fig. 2 shows stripping voltammograms for 1 μg l^{-1} lead after different accumulation periods (0–120 s, a–e). The longer the preconcentration time, the more complex is adsorbed, and the larger is the peak current. For example, with 120 s preconcentration there is a six-fold enhancement of the peak relative to that obtained without preconcentration (a vs. e). As a result, excellent signal-to-background characteristics are obtained, which permit convenient measurement of μg l^{-1} lead concentrations. Also shown in Fig. 2 (inset) are plots of peak current vs. preconcentration time at three levels of lead

[1 (A), 2 (B), and 5 (C) μg l^{-1}]. In all cases, the current increases linearly with time at first (up to 2 min) and then it starts to level off [slopes of initial linear portions, 2.8 (A), 5.8 (B), and 12.5 (C) nA min^{-1}]. Such profiles reflect the kinetics of the adsorption of the lead–OCP complex.

The OCP concentration has a profound effect on the stripping current. For example, the stripping peak for 5 μg l^{-1} lead increases rapidly with increasing OCP concentration up to 8×10^{-7} M, and then more slowly (Fig. 3A). The dependence of the stripping current on the preconcentration potential was examined over the range 0.2 to −0.3 V (Fig. 3B). A slow decrease of the response is observed between 0.2 and −0.2 V, with a stable peak at more negative potentials. An accumulation potential of 0.0 V yielded the most favorable signal-to-background characteristics, and was used in all subsequent work. Similarly, the differential pulse waveform yielded better signal-to-background characteristics than corresponding linear-scan or square-wave measurements, and was used throughout this work.

The analytical utility of the adsorptive stripping procedure depends on achieving a well-defined concentration dependence. Figure 4 shows stripping voltammograms for solutions of increasing lead concentration (1–6 μg l^{-1}, a–f). Well-defined stripping peaks are observed at this low level following a short (60 s) preconcentration time. These six peaks were part of a series of ten concentration increments, up to 15 μg l^{-1}. The resulting calibration plot is also shown in Fig. 4 (inset). The response is linear over the entire range (slope, 3.1 nA l μg^{-1}; correlation coefficient, 0.999). Another calibration experiment, involving 5 μg l^{-1} increments in the lead concentration, up to 60 μg l^{-1} (60 s preconcentration) also yielded a linear dependence over the entire range (not shown). The very favorable signal-to-noise characteristics (S/N) yield extremely low detection limits following short preconcentration times. For example, detection limits of 0.1 and 0.04 μg l^{-1} were estimated from the response to 1 μg l^{-1} following 60 and 120 s preconcentrations ($S/N = 3$; Figs. 4a and 2f, respectively). The high sensitivity is coupled to high precision. The latter was estimated from twelve repetitive measurements of 5 μg l^{-1} (60 s preconcentration). This series yielded a relative standard deviation of 1.8% (mean peak current of 17.9 nA, with a range of 17.5–18.4 nA).

Perhaps the main advantage of the OCP-based adsorptive stripping procedure for lead is its inherent selectivity. Such selectivity is apparent from comparison with conventional (anodic strip-

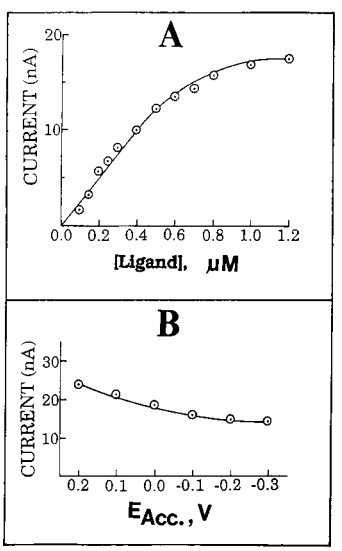

Fig. 3. Effect of OCP concentration (A) and accumulation potential (B) upon the adsorptive stripping response for 5 μg l^{-1} lead. Preconcentration for 60 s. Other conditions, as in Fig. 2.

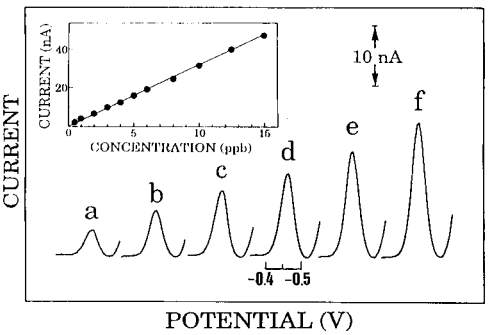

Fig. 4. Voltammograms obtained with increasing lead concentration in steps of 1 μg l^{-1} (a–f). Preconcentration for 60 s. Also shown (inset) is the calibration plot over the 1–15 μg l^{-1} range. Other conditions, as in Fig. 2.

ping) measurements of lead. Figure 5 compares voltammograms for 2.5 μg l^{-1} lead in the presence of 10 μg l^{-1} tin (top) and thallium (bottom). Due to severe peak overlap, the lead cannot be measured selectively by the conventional stripping procedure (A, B). In contrast, the two metals have no effect on the lead–OCP peak (C,D). Indeed, no interference was observed in the presence of a larger excess (100 μg l^{-1}) of tin and thallium (not shown). Besides the substantial improvement in selectivity, it is clear from Fig. 5, that the adsorption strategy offers improved sensitivity and overall detectability compared to conventional stripping measurements [C, D (a) vs. A, B (a)]. Note also the improved peak sharpness in the presence of OCP. Other metal ions were tested (at the 25 μg l^{-1} level) and found not to affect the 2.5 μg l^{-1} lead response, including iron(III), aluminum, bismuth, nickel, titanium, copper, cadmium, indium, vanadium, lanthanum, zinc, uranium, and chromium (III and VI). The lack of copper interference is of great significance, considering its major interference in the

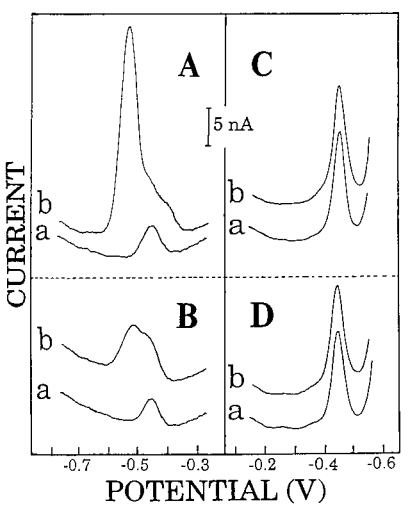

Fig. 5. Effect of coexisting metals upon the response for lead in anodic (A, B) and adsorptive (C, D) stripping measurements. (A, C) (a) 2.5 μg l^{-1} lead; (b) same as (a) but after addition of 10 μg l^{-1} tin. (B, D) (a) 2.5 μg l^{-1} lead; (b) same as (a) but after addition of 10 μg l^{-1} thallium. Solutions, (A, B) acetate buffer (10 mM, pH 4.0); (C, D) as in Fig. 1. Preconcentration potential (A, B), −1.0 V. Other conditions, as in Fig. 2C.

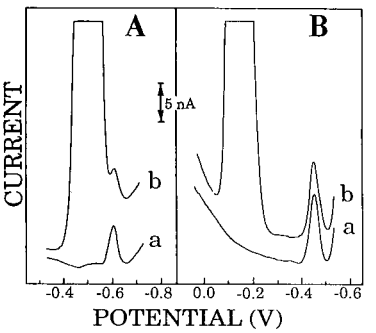

Fig. 6. Effect of copper upon the response for lead in the presence of oxine (A) and OCP (B). (a) 2.5 μg l^{-1}; (b) same as (a) but after additions of 50 μg l^{-1} copper. Conditions (A), a 0.01 M HEPES solution (pH 7.8) containing 5×10^{-5} M oxine; accumulation at −0.30 V; (B) as in Fig. 2. Preconcentration times, 60 s.

oxine-based adsorptive stripping scheme, and the presence of copper in numerous relevant samples. For example, Fig. 6 compares adsorptive stripping measurements of 2.5 μg l^{-1} lead, in the absence (a) and presence (b) of 50 μg l^{-1} copper, utilizing oxine (A) and OCP (B) as chelating agents. While the lead–oxine peak is largely obscured by the copper–oxine response, the large excess of copper has no effect upon the lead–OCP peak. Note also (from curves a) the enhanced sensitivity of the OCP-based procedure. The only major interfering metal (in the OCP method) was molybdenum, which exhibited a large overlapping signal. Hence, an appropriate separation or masking step would be required in the presence of elevated molybdenum levels. Surface-active organic materials competing for adsorption sites can also interfere with the quantitation of lead. However, albumin at 4 and 8 mg l^{-1} caused only 12 and 15% diminutions, respectively, of the 4 μg l^{-1} lead peak (60 s preconcentration).

The highly sensitive and selective response of the OCP-based procedure allows direct assays of relevant samples. Figure 7 demonstrates its suitability for monitoring lead in an untreated drinking water sample. With 1 min preconcentration time the method yields a well-defined lead peak (a), which allows convenient quantitation following standard additions (b, c). A lead sample value of 8.4 μg l^{-1} was thus estimated (considering the

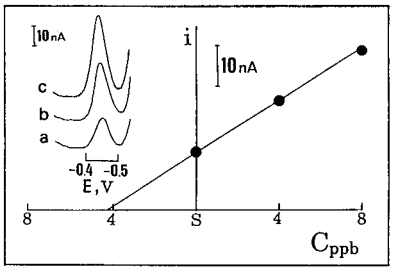

Fig. 7. Voltammograms for a drinking water sample (a) and successive concentration increments of 4 μg l^{-1} lead (b, c). Sample was diluted (1:1) with the supporting electrolyte. Preconcentration for 1 min. Other conditions, as in Fig. 2.

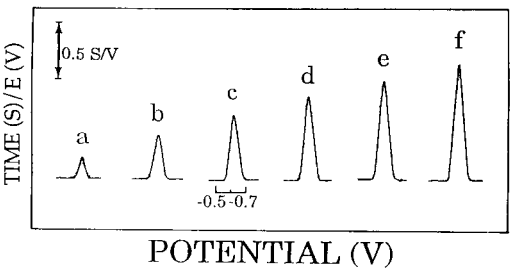

Fig. 9. Potentiograms for increasing lead levels in 5 μg l^{-1} steps at the mercury-coated carbon strip electrode. Preconcentration for 2 min followed by stripping with a current of -10 μA. Other conditions, as in Fig. 8.

1:1 dilution). Other applications (particularly clinical ones) may require the adaptation of a suitable sample pretreatment.

Besides voltammetric scanning, it is possible to employ a potentiometric stripping approach to follow the reduction of the adsorbed lead–OCP complex. For example, Fig. 8 illustrates the time-dependence (A), precision (B), and concentration dependence (C) of the potentiometric stripping response at a mercury-film electrode. Similar to its voltammetric counterpart, the constant-current potentiometric stripping operation yields a well-defined peak, which permits convenient quantitation of μg l^{-1} lead concentrations. This complex peak is highly reproducible, and increases linearly with the preconcentration time and lead concentration. A detection limit of 0.8 μg l^{-1} can be estimated based on the signal-to-noise characteristics of potentiograms C (a).

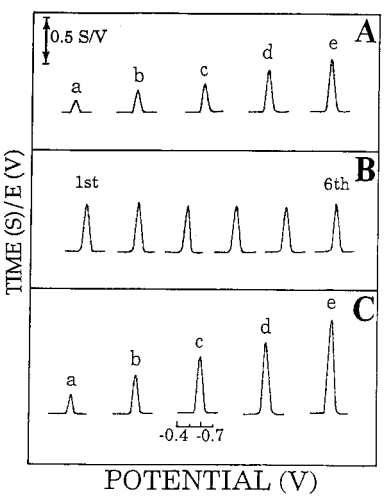

Fig. 8. Potentiograms for trace lead at the mercury-coated glassy carbon electrode. (A) Response for 10 μg l^{-1} lead following different preconcentration times: 0 (a), 15 (b), 30 (c), 45 (d), and 60 (e) s. (B) Reproducibility at the 10 μg l^{-1} level; (C) Response for increasing lead levels in 4 μg l^{-1} steps (a–e). Preconcentration time (B, C), 60 s; stripping current, -5.0 μA. Other conditions, as in Fig. 2.

The potentiometric stripping operation of mercury film electrodes facilitates the adaptation of screen-printed electrodes for adsorptive stripping measurements of trace lead. Such operation holds an enormous promise for decentralized clinical testing or environmental monitoring, because the extremely low cost of such metal sensors permits single-use applications. We reported recently that screen-printed electrodes are suitable for conventional (anodic) stripping measurement of trace lead [8]. Similarly, Fig. 9 displays potentiograms at the mercury-coated carbon strip electrode for increasing lead concentrations in 5 μg l^{-1} steps. A well-defined concentration dependence and very favorable signal-to-background characteristics are observed, indicating that the stripping performance is not compromised by the use of these disposable electrodes.

In conclusion, the present study indicates important advantages of the OCP-based stripping scheme over previously reported stripping procedures for lead. In particular, such a scheme eliminates major interference from co-existing metals (e.g. tin, thallium, copper) and offers enhanced signal-to-background characteristics. Such improvements (and particularly the new selectivity dimension) are attributed to a fundamentally dif-

ferent detection principle than that of conventional stripping analysis. The inherent sensitivity and selectivity of the OCP-based procedure along with the portable nature of the instrumentation, holds great promise for decentralized (clinical or environmental) screening for trace lead. The coupling of disposable screen-printed electrodes with the new adsorptive stripping procedure is particularly attractive in this direction. Such application will require the adaptation of a simple and rapid sample preparation (involving a lead-releasing agent).

This publication was supported by a grant from Centers for Disease Control (contract number CCR 608615-01). Its contents are solely the responsibility of the authors and do not represent the official views of CDC.

REFERENCES

1 R.L. Boeckx, Anal. Chem., 58 (1986) 274A.
2 J. Wang, Stripping Analysis: Principles, Instrumentation and Application, VCH, Deerfield Beach, FL, 1985.
3 J. Boone, T. Hearn and S. Lewis, Clin. Chem., 25 (1979) 389.
4 R. Kalvoda and M. Kopanica, Pure Appl. Chem., 61 (1989) 97.
5 J. Wang, Fresenius' Z. Anal. Chem., 337 (1990) 508.
6 C.M.G. van den Berg, Anal. Chim. Acta, 215 (1986) 111.
7 J. Wang, P.A. Farias and J. Mahmoud, Anal. Chim. Acta, 171 (1985) 215.
8 J. Wang and B. Tian, Anal. Chem., 64 (1992) 1706.
9 X. Gao and M. Zhang, Anal. Chem., 56 (1984) 1912.

Analytica Chimica Acta, 280 (1993) 69–74
Elsevier Science Publishers B.V., Amsterdam

Investigations on adsorption potentiometry

Part IX. Determination of ultratrace boron by derivative adsorption chronopotentiometry

Wenrui Jin, Li Xiao and Yan Wu

Department of Chemistry, Shandong University, Jinan 250100, Shandong (China)

(Received 21st November 1992; revised manuscript received 4th February 1993)

Abstract

A derivative chronopotentiometric method for the determination of ultratrace boron, based on adsorptive accumulation of a boron complex on the surface of a hanging mercury drop electrode, was developed. In order to form the boron(III) complex with 4-[(4-diethylamino-2-hydroxyphenyl)azo]-5-hydroxynaphthalene-2,7-disulphonic acid (Beryllon III), it is necessary to boil the solution for 1 h and to leave it at room temperature for 20 h. The dependences of the peak value of the dt/dE vs. E curve for the reduction of the adsorbed boron(III) complex with Beryllon III on the preconcentration time, the preconcentration potential and the concentration of Beryllon III are discussed. The optimum supporting electrolyte is 0.05 mol l^{-1} NaOAc + 0.025 mol l^{-1} HOAc, the optimum preconcentration potential is −0.30 V (vs. SCE) and the optimum concentration of Beryllon III is 500–5000 times the concentration of B(III). Under these optimum conditions, the detection limit is 8×10^{-12} mol l^{-1} for a preconcentration time of 30 s. The relative standard error of the method is 2.4% for 4×10^{-9} mol l^{-1} B(III). The method was applied to food samples and the recovery was 98–103%.

Keywords: Potentiometry; Stripping voltammetry; Boron; Chronopotentiometry; Foods

Adsorption potentiometry is a very sensitive electroanalytical method for ultratrace analysis [1]. In this method, organic compounds or inorganic complexes are first accumulated on the surface of the working electrode by adsorption, then the adsorbed substances are reduced or oxidized by a constant current and the curve of E vs. t or dt/dE vs. E of the working electrode is recorded. The transition time, τ, on the plot of E vs. t and the peak value of dt/dE, $(dt/dE)_p$, on the plot of dt/dE vs. E for a cathodic reversible interfacial reaction are given by the following equations [2]:

$$\tau = nFA\Gamma_0/i_0 \quad (1)$$

$$(dt/dE)_p = -(n^2F^2/4RT)A\Gamma_0/i_0 \quad (2)$$

where A is the area of the working electrode, i_0 is the constant reducing current and Γ_0 is the surface concentration of the substance adsorbed, expressed as [3,4]

$$\Gamma_0 = [Kt_a + f(t_r)]c \quad (3)$$

where K is a constant and c is the bulk concentration of the substances, which, when the substances are complexes, is proportional to the analytical concentration of metal or non-metal, and

Correspondence to: Wenrui Jin, Department of Chemistry, Shandong University, Jinan 250100, Shandong (China).

$f(t_r)$ is a function of the rest period, t_r. From Eqns. 1–3, it can be seen that τ or $(dt/dE)_p$ is proportional to the analytical concentration of metal or non-metal ions, the value of $(dt/dE)_p$ is greater than the value of τ and the smaller is i_0, the higher is the signal. Therefore, for ultratrace analysis a smaller i_0 should be used.

Adsorption potentiometry has been applied to ultratrace metal ions, such as Fe(III) [1], Bi(III) [5], V(V) [6] and Cu(II) [7], and organic compounds, such as furazolidone [8]. Up to now, adsorption potentiometry of non-metal ions has not been reported.

Boron is a very important trace non-metal element for plants. By means of liquid membrane electrodes, only 1×10^{-5} mol l^{-1} can be determined [9]. As boron is not an electroactive element, direct determining of boron is impossible by modern polarography or voltammetry. If boron is converted into molybdotungstoboric acid, determination of molybdenum gives an indirect determination of boron. By determining molybdenum by catalytic d.c. polarography, the limit of detection for determination of boron is 2×10^{-5} mol l^{-1} [10]. In the presence of 4-[(4-diethylamino-2-hydroxyphenyl)azo]-5-hydroxynaphthalene-2,7-disulphonic acid (Beryllon III), 2×10^{-7} or 4×10^{-7} mol l^{-1} boron can be measured by oscillopolarography [11–13]. When a dropping mercury electrode with a long lifetime is used, the linear range of determination is 4×10^{-8}–1×10^{-5} mol l^{-1} [14].

The mechanism of reduction of the B(III)–Beryllon III system at a dropping mercury electrode can be described by the following reaction scheme [15]:

in the solution:

$$B(III) + A \rightarrow B(III)A \quad (4)$$

at the electrode:

$$B(III)A + Hg \rightarrow B(III)A(ads)(Hg) \quad (5)$$

$$B(III)A(ads)(Hg) + 2H^+ + 2e^- \rightarrow B(III)A'(des) + Hg \quad (6)$$

where A is Beryllon III and A′ is the product of the reduction of Beryllon III.

It can be expected that derivative adsorption chronopotentiometry can be applied to the determination of ultratrace boron. In this paper, the details of the method are described. When $i_0 = 0.1$ μA was used, 8×10^{-12} mol l^{-1} B(III) could be detected for $t_a = 30$ s. So far this is the most sensitive method for the determination of boron and for adsorption chronopotentiometry.

EXPERIMENTAL

Apparatus

A Model DPSA-3 stripping analyser (Shandong Seventh Electronic Factory) for derivative adsorption chronopotentiometry was used in connection with a cell, using potentiostatic control of the electrode potential by means of a Model SH-84 hanging mercury drop electrode (HMDE) (Department of Chemistry, Shandong University) as the working electrode, a platinum plate as the counter electrode and a saturated calomel electrode (SCE) as the reference electrode connected to the analyte via a salt bridge containing the supporting electrolyte. In the preconcentration step, the solution was stirred with a PTFE-coated stirring bar, rotated by a Model 78-1 magnetic stirrer (Nanhui Telecommunication Equipment Factory). Microwave digestions were made with a Model BL-823 microwave oven (Jinan Quanli) operating at 2450 MHZ with a maximum power of 650 W.

Reagents and solutions

All reagents were of analytical-reagent grade and solutions were prepared with triply distilled water.

A 2.5×10^{-3} mol l^{-1} stock standard solution of Beryllon III was prepared by dissolving an appropriate amount of Beryllon III in water and dilute solutions were obtained by serial dilution with water. The solutions were stored in a refrigerator. A 1.00×10^{-2} mol l^{-1} stock standard solution of boron was obtained by dissolving an appropriate amount of H_3BO_3 in water. Working standard solutions were obtained by diluting the stock standard solution with water. A 1 mg ml^{-1} Bromocresol Green solution was obtained by dis-

solving 0.1 g of the indicator in 100 ml of 20% ethanol.

Procedure

A 10-ml volume of supporting electrolyte consisting of 0.125 mol l^{-1} HOAc and 0.25 mol l^{-1} NaOAc was transferred into a high and narrow PTFE vessel with a PTFE cover (3.2 cm i.d., 4.5 cm high), then a certain amount of Beryllon III solution and boron standard solution were added. The solution was heated for 1 h in a boiling water-bath and allowed to stand for 20 h at room temperature. The solution was transferred in a 50-ml volumetric flask and diluted to volume with water. The solution was ready for measurement after deaeration for 15 min with 99.9% nitrogen.

The measurement procedure is as follows: in the preconcentration step, the solution was stirred for 30 s at the chosen preconcentration potential, E_a, of −0.30 V (vs. SCE). After a rest period of 30 s, the potentiostatic circuitry was disconnected and a constant reducing current, i_0, was passed through the HMDE and the counter electrode and the plot of dt/dE vs. E was simultaneously recorded. All potentials were measured against the SCE.

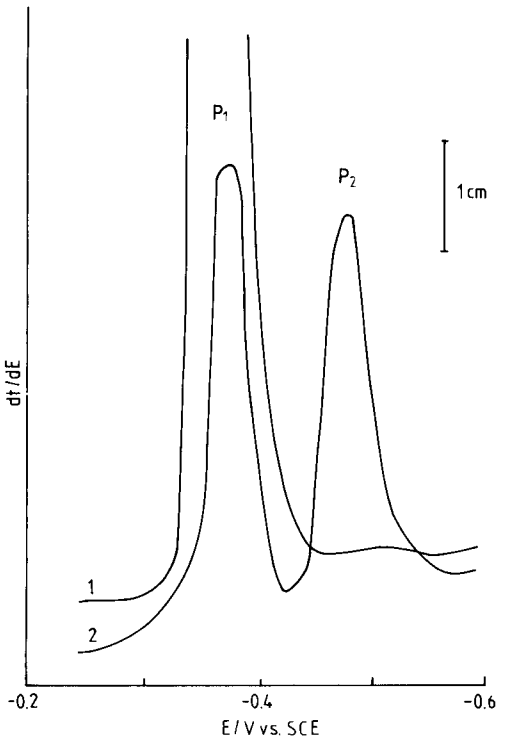

Fig. 1. Typical derivative adsorption chronopotentiograms of Beryllon III and its complex with B(III), (1) 2×10^{-7} mol l^{-1} Beryllon III; (2) (1)+2×10^{-8} mol l^{-1} B(III). Buffer, 0.025 mol l^{-1} HOAc+0.05 mol l^{-1} NaOAc; $t_b = 1$ h; $t_s = 20$ h; $E_a = -0.10$ V; $i_0 = 0.5$ μA; $t_a = 30$ s. The sensitivity of the analyser was set to 60.

RESULTS AND DISCUSSION

Derivative adsorption chronopotentiogram of the boron(III) complex with Beryllon III

In the presence of 2×10^{-7} mol l^{-1} Beryllon III, one peak, P_1, appeared at a potential of −0.38 V on the derivative adsorption chronpotentiogram (Fig. 1, curve 1). A micro-amount of boron(III) standard solution was added and the solution was heated for 1 h and then allowed to stand at room temperature for 20 h. A new peak, P_2, appeared at a potential of −0.48 V and P_1 decreased (Fig. 1, curve 2). With increasing concentration of B(III), P_1 decreased and P_2 increased correspondingly. This shows that a B(III) complex with Beryllon III is formed in the solution and P_2 is the result of reduction of the complex B(III) A adsorbed on the HMDE.

Optimum experimental conditions

It was found that the longer the boiling time, t_b, the larger is the height of P_2, but a boiling time of 1 h was adopted because otherwise too much solvent would evaporate. After boiling for 1 h, the height of P_2 varies with the standing time, t_s. The peak height reaches its maximum after 20 h; with longer times the peak height remains almost unchanged. Therefore, a t_b of 1 h and a t_s of 20 h were chosen.

The dependence of the height of P_2 on pH in HOAc + NaOAc is shown in Fig. 2. It can be seen that at pH 5.04, the peak height reaches its maximum. The optimum base solution is 0.025 mol l^{-1} HOAc–0.05 mol l^{-1} NaOAc. these concentrations were chosen as the supporting electrolyte. Figure 3 shows the derivative adsorption chronopotentiograms of B(III) A at different pre-

concentration times, t_a; the height of P_2, $(dt/dE)_p$, increases linearly with increasing t_a. This means that under these conditions, the complex can be adsorbed on the surface of the mercury electrode. The adsorption of the complex is dependent on the potential, E_a; the relationship between $(dt/dE)_p$ and E_a is presented in Fig. 4. At $E_a = -0.30$ V the adsorption of B(III) A is stronger. In Fig. 5 it can be seen that under the same experimental conditions, the smaller the reducing current, i_0, the larger is the height of P_2.

The limit of detection of the method was governed by the concentration of Beryllon III. If the concentration of Beryllon III is too low, the amount of the complex formed will be very small. If the concentration of Beryllon III is too high, peak P_2 is still small because of the competitive adsorption of Beryllon III. It was found that the optimum concentration of Beryllon III is 500–5000 times the concentration of B(III).

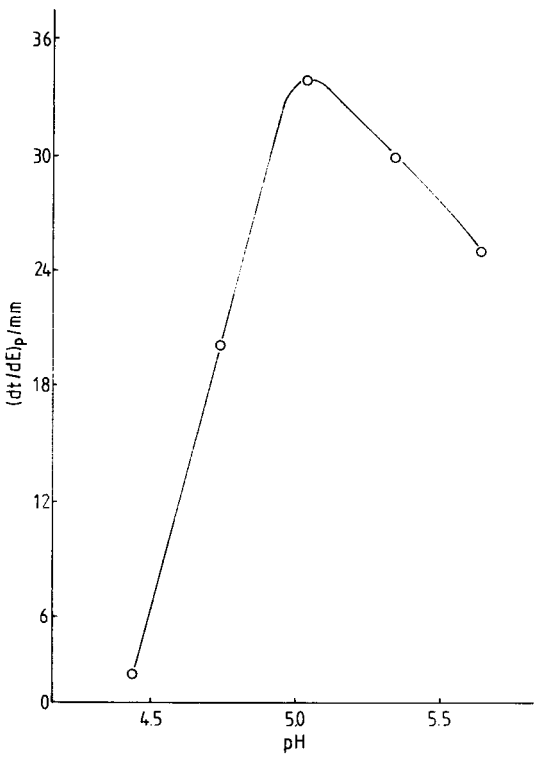

Fig. 2. Dependence of the peak height of B(III)A adsorbed on pH in the buffer solution of HOAc+NaOAc. 4×10^{-9} mol l^{-1} B(III); 2×10^{-6} mol l^{-1} Beryllon III; $E_a = -0.30$ V. Other conditions as in Fig. 1.

Linear range, detection limit and reproducibility

In principle, on increasing t_a, the amount of B(III)–Beryllon III complex accumulated adsorptively on the surface of the working electrode increases, but the height of P_2 decreases with increasing t_a for lower concentrations of B(III) when $t_a > 30$ s. It was found that $t_a = 30$ s is an optimum. The linear range of derivative adsorption chronopotentiometry is 1.0×10^{-11}–8.0×10^{-9} mol l^{-1} and the limit of detection is 8.0×10^{-12} mol l^{-1} for a reducing current $i_0 = 0.1$ μA. Figure 6 shows the dependence of peak height on the concentration of B(III) at levels of 10^{-11}, 10^{-10} and 10^{-9} mol l^{-1}. The precision calculated from ten successive measurements of 4×10^{-9} mol l^{-1} B(III) is 2.4%.

Analytical application

Metal ions such as Fe(II) and Cu(II) may interfere in the determination of B(III), as they form complexes with Beryllon III. These interferences can be overcome by adding EDTA to the sample solutions, because EDTA may form complexes with these metal ions but not with B(III).

Samples of food were digested with the microwave technique prior to derivative adsorption chronopotentiometric measurement. The procedure for the digestion of flour and millet is as follows: ca. 0.5-g samples were weighed to an accuracy of 0.1 mg in individual PTFE digestors [16], 4 ml of nitric acid and 6 ml of perchloric acid were added to each and the digestors were covered. Four digestors with samples and acids were placed on the plate in the microwave oven for 50 min at 30% power. The digestors were removed from the oven and allowed to cool to room temperature. Each sample solution digested was transferred into a 50-ml volumetric flask and diluted to volume with water. A 100-μl volume of sample solution was transferred into a high, narrow PTFE vessel and 2 ml of 0.1 mol l^{-1} EDTA and 1 drop of 1 mg ml^{-1} Bromocresol Green solution were added. Then 0. 1 mol l^{-1} KOH solution was added until the colour of the solution changed from yellow to blue. A total volume

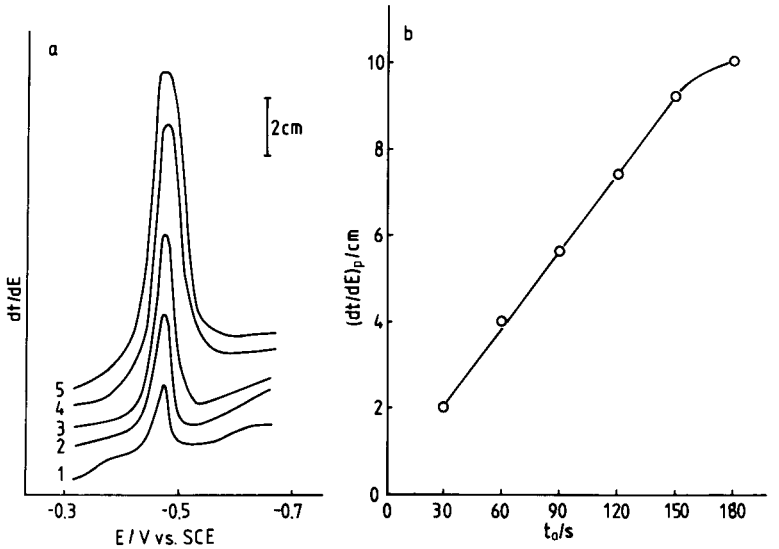

Fig. 3. (a) Derivative adsorption chronopotentiograms of B(III)A adsorbed at different preconcentration times, t_a, of (1) 30, (2) 60, (3) 90, (4) 120 and (5) 150 s. (b) Relationship between $(dt/dE)_p$ and t_a. 2×10^{-7} mol l^{-1} Beryllon III. Buffer, 0.025 mol l^{-1} HOAc + 0.05 mol l^{-1} NaOAC. Other conditions as in Fig. 2.

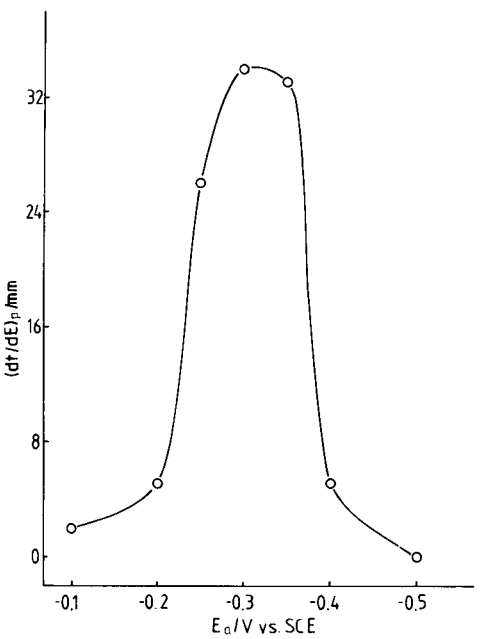

Fig. 4. Relationship between the peak height of B(III)A and preconcentration potential. Buffer, 0.025 mol l^{-1} HOAc + 0.05 mol l^{-1} NaOAc; $t_a = 30$ s. Other conditions as in Fig. 2.

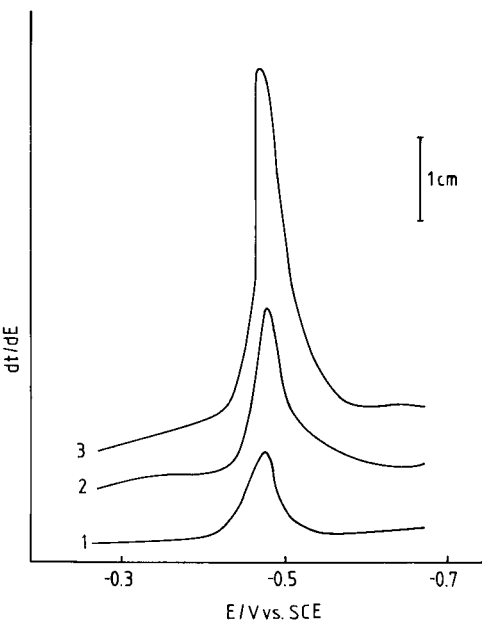

Fig. 5. Derivative adsorption chronopotentiograms of B(III)A at different reducing currents, i_0, of (1) 2, (2) 1 and (3) 0.5 μA. Buffer, 0.025 mol l^{-1} HOAc + 0.05 mol l^{-1} NaOAc; $t_a = 10$ s. The sensitivity of the analyser was set to 120. Other conditions as in Fig. 2.

TABLE 1

Results for determination of boron in samples of food and recoveries of boron added to the samples

Sample	Content determined in sample ($\mu g\ g^{-1}$)	Concentration determined in solution (mol l^{-1})	Concentration of B(III) added (mol l^{-1})	Concentration of B(III) found (mol l^{-1})	Recovery (%)
Flour A	0.100	9.25×10^{-9}	2.00×10^{-9}	11.2×10^{-9}	98
Flour B	0.095	8.75×10^{-9}	2.00×10^{-9}	10.8×10^{-9}	103
Millet A	0.051	4.70×10^{-9}	2.00×10^{-9}	6.70×10^{-9}	100
Millet B	0.046	4.20×10^{-9}	2.00×10^{-9}	6.25×10^{-9}	103

of 10 ml of 0.125 mol l^{-1} HOAc and 0.25 mol l^{-1} NaOAc solution and 100 μl of 1×10^{-5} mol l^{-1} Beryllon III were also added. The mixed solution was heated for 1 h on a boiling water-bath and then kept at room temperature for 20 h. The solution was diluted to 50 ml.

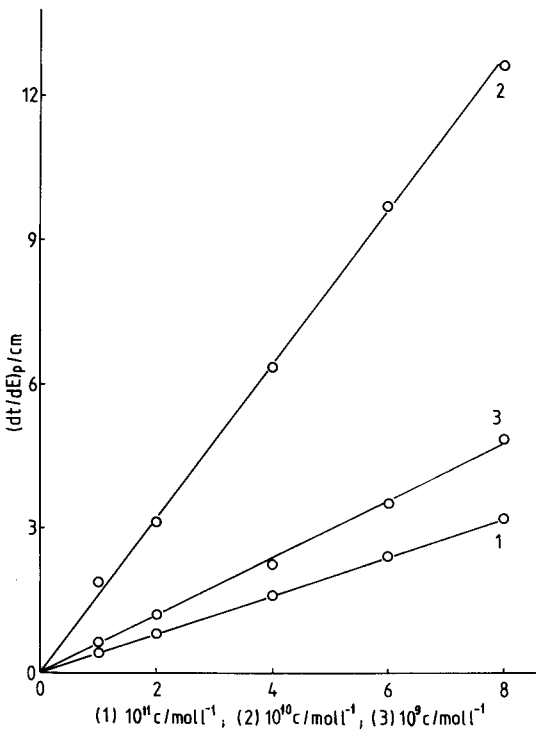

Fig. 6. Dependence of the peak height on the concentration of B(III) at levels of 10^{-11}, 10^{-10} and 10^{-9} mol l^{-1}. Concentration of Beryllon III, (1) 5×10^{-8}, (2) 5×10^{-7}, (3) 5×10^{-6} mol l^{-1}; i_0 = (1) 0.2, (2) 0.2, (3) 1.0 μA; sensitivity of the analyser set to (1) 10, (2) 30, (3) 60; $E_a = -0.30$ V. Other conditions as in Fig. 1.

The solution was transferred into a cell and the derivative adsorption chronopotentiogram of B(III)A was recorded. The results obtained by derivative adsorption chronopotentiometry with two successive standard additions for samples of food and the analysis of samples spiked with known amounts of B(III) are summarized in Table 1. The recoveries of added B(III) were 98–103%.

REFERENCES

1 W.-R. Jin and J.-Y. Wang, Anal. Chim. Acta, 245 (1991) 77.
2 W.-R. Jin and J.-Y. Wang, J. Electroanal. Chem., 306 (1991) 31.
3 W.-R. Jin, Y.-C. Hou, C.-T. Yan, J.-Y. Wang and C.-L. Sun, Electroanalysis, 4 (1992) 233.
4 W.-R. Jin, Y.-C. Hou, C.-T. Yan, J.-Y. Wang and C.-L. Sun, Electroanalysis, 4 (1992) 239.
5 W.-R. Jin and J.-Y. Wang, Electroanalysis, submitted for publication.
6 W.-R. Jin, X. Zhao and Y.-X. Liu, Anal. Lett., 25 (1992) 1741.
7 L. Xiao and W.-R. Jin, Talanta, in press.
8 W.-R. Jin, Y.-H. Zheng and X. Qu, Anal. Chim. Acta, 262 (1992) 123.
9 S.S.M. Hassan, Qatar Univ. Sci. Bull., 6 (1986) 41.
10 R. Kannan, T.V. Ramakvishna and S.R. Rajagopalan, Indian J. Techol., 24 (1986) 482.
11 M.-S. Mo, Fenxi Huaxue, 15 (1987) 414.
12 K.-Q. Zheng, YanKuang Ceshi, 6 (1987) 100.
13 J.-Q. Wu and N.-X. Deng, Zhongnan Kuangye Xueyuan Xuebao, 18 (1987) 573.
14 W.-R. Jin, K. Jiao and H. Metzner, Electroanalysis, in press.
15 W.-R. Jin, K. Jiao and H. Metzner, Electroanalysis, in press.
16 W.-R. Jin, D. Liu and B.-Y. Gao, unpublished work.

Analytica Chimica Acta, 280 (1993) 75–83
Elsevier Science Publishers B.V., Amsterdam

Standardization of potentiometric cells in propan-2-ol–water

Clara Ràfols, Martí Rosés and Elisabeth Bosch

Departament de Química Analítica, Universitat de Barcelona, Diagonal 647, 08028 Barcelona, Catalonia (Spain)

(Received 23rd November 1992)

Abstract

Equations for the standardization of potentiometric systems in binary solvent mixtures of moderate permittivity are proposed. The equations were applied to the standardization of a potentiometric system in propan-2-ol–water (70 + 30, w/w). Different standardization methods were tested: titration of a strong and a weak acid (hydrochloric and phthalic acid, respectively) with a basic titrant solved in the studied binary solvent or in pure propan-2-ol, or addition of hydrochloric acid to the pure binary solvent. The dissociation constants of the acids and their salts were previously determined conductimetrically. The advantages and disavantages of the methods for standardization of potentiometric systems in binary solvents of moderate permittivity were evaluated.

Keywords: Potentiometry; Titrimetry; Binary solvent mixtures; Dissociation constants; Propan-2-ol–water; Standardization

Aqueous–organic solvent mixtures have interesting applications in synthesis, electrochemistry, mechanistics and biophysical studies. Aqueous–organic solvent mixtures are widely used in important analytical techniques such as liquid chromatography and capillary electrophoresis. However, the acid–base behaviour of many substances in most solvent mixtures is not well known. In recent years, the International Union of Pure and Applied Chemistry has highlighted the importance of the knowledge of the acid–base constants in these media and it has endorsed rules and procedures for the determination of reference value standards and primary standards for pH measurements in binary aqueous–organic solvent mixtures [1,2]. Within the framework of that project, the behaviour of some substances (considered as primary standards) in methanol–water, ethanol–water, propan-2-ol–water, acetonitrile–water, 1,4-dioxane–water and dimethyl sulphoxide–water has been studied [1–10].

The main problem in determining pH and pK values in mixed solvents is the determination of the standard potential of the cell used. In previous papers a method was proposed for standardization of potentiometric systems in non-aqueous solvents [11–13]. The method involves titration of an acid or a base and it takes into account all the possible relevant equilibria in the solvent (acid, base and salt dissociations) and the variations caused by addition of other solvents with the titrant or the formation of water in the neutralization reaction.

In this work the method was applied to the standardization of a potentiometric cell in a bi-

Correspondence to: M. Rosés and E. Bosch, Departament de Química Analítica, Universitat de Barcelona, Diagonal 647, 08028 Barcelona, Catalonia (Spain).

nary propan-2-ol–water solvent mixture (70 + 30, w/w) as a preliminary study for extension to other propan-2-ol–water mixtures and to other relevant organic solvent–water mixtures.

Propan-2-ol–water (70 + 30, w/w) is a solvent of moderate permittivity ($\epsilon = 28.7$) [14]. The formation of ionic aggregates does not occur in mixtures with a lower content of propan-2-ol, and therefore salts and strong acids and bases can be considered to be completely dissociated in them. However, ionic associations seem to be considerable in mixtures with a propan-2-ol content higher than 70% (w/w) [15].

Standardization of the potentiometric cell was performed by titration of a strong and a weak acid (hydrochloric and phthalic acid, respectively) with a strong base (tetrabutylammonium hydroxide) dissolved in the same propan-2-ol–water mixture or in pure propan-2-ol and compared with the results obtained with addition of hydrochloric acid to the pure studied solvent, the acid also being dissolved in the same solvent. From the results obtained, the influence of the different factors on the determined standard potential was evaluated, and standardization methods are proposed.

IONIC EQUILIBRIA OF ACID–SALT MIXTURES IN BINARY SOLVENTS OF MODERATE PERMITTIVITY

In solvents of moderate permittivity, the formation of ionic pairs should be taken into account, and the dissociation equilibria of acids (HA) and salts (B^+A^-) are

$$HA \rightleftharpoons H^+A^- \rightleftharpoons H^+ + A^-$$

$$K_a = \sum [H^+][A^-]y^2/([HA] + [H^+A^-]) \quad (1)$$

$$B^+A^- \rightleftharpoons B^+ + A^-$$

$$K_{salt} = [B^+][A^-]y^2/[B^+A^-] \quad (2)$$

where y is the mean activity coefficient, K_a and K_{salt} are the dissociation constants of the acid and salt, respectively, and $\Sigma[H^+]$ means the total hydrogen ion concentration (solvated by water or by the organic solvent).

From Eqns. 1 and 2 and the mass and charge balances, general equations for the calculation of $[A^-]$ and $\Sigma[H^+]$ have been derived [12]:

$$(K_{salt}^{-1}K_a^{-1}y^4)[A^-]^3 + (K_{salt}^{-1}y^2 + K_a^{-1}y^2)[A^-]^2 + (1 - K_a^{-1}c_{salt}y^2 - K_{salt}^{-1}c_a y^2)[A^-] - (c_{salt} + c_a) = 0 \quad (3)$$

$$\sum [H^+] = c_a/(1 + K_a^{-1}[A^-]y^2) \quad (4)$$

where c_a and c_{salt} are the analytical concentrations of acid and salt, respectively.

To calculate the pH value of an acid–salt mixture, $[A^-]$ is calculated from Eqn. 3 by an iterative procedure, i.e., the Newton–Raphson method, $\Sigma[H^+]$ from Eqn. 4 and the pH from

$$pH = -\log\left(\sum [H^+]y\right) \quad (5)$$

The pH of a solution of an acid alone can be calculated from the same equations taking $c_{salt} = 0$.

In weak acid–salt mixtures, $K_{salt} \gg K_a$ and Eqns. 3 and 4 can be combined to obtain [16]

$$pH = pK_a - \log(c_a/c_{salt}) + \log y - \log\left\{(1/2) + \left[(1/4) + (c_{salt}y^2/K_{salt})\right]^{1/2}\right\} \quad (6)$$

If the permittivity is high enough to consider the salt to be completely dissociated, $K_{salt}^{-1} = 0$ and Eqn. 3 becomes

$$K_a^{-1}y^2[A^-]^2 + (1 - K_a^{-1}c_{salt}y^2)[A^-] - (c_{salt} + c_a) = 0 \quad (7)$$

which is the equation usually employed in water.

For weak acid–salt solutions with $K_a^{-1} \gg c_{salt}^{-1} \approx c_a^{-1}$, Eqn. 7 can be simplified to

$$K_a^{-1}y^2[A^-]^2 - K_a^{-1}c_{salt}y^2[A^-] = 0 \quad (8)$$

or

$$[A^-] = c_{salt} \quad (9)$$

and substitution in Eqn. 4 leads to

$$\sum [H^+] = c_a/K_a^{-1}c_{salt}y^2 \quad (10)$$

or

$$pH = pK_a - \log(c_a/c_{salt}) + \log y \quad (11)$$

which is the equation used for buffered solutions in water, taking into account the activity coefficients.

If the acid is also completely dissociated, $K_a^{-1} = 0$, and Eqns. 3, 4 and 5 become

$$\sum[H^+] = c_a \quad (12)$$

$$[A^-] = (c_{salt} + c_a) \quad (13)$$

$$pH = -\log c_a - \log y \quad (14)$$

which are the equations used for strong acids in water.

STANDARDIZATION OF POTENTIOMETRIC SYSTEMS FROM TITRATION OF ACIDS IN BINARY SOLVENTS OF MODERATE PERMITTIVITY

Standardization of a potentiometric cell can be performed from the potential values (E) otained through titration of an acid. The pH of acid–salt mixtures can be calculated from Eqns. 3–5 (or the simplified Eqns. 6, 11 and 14 in some particular instances) if the dissociation constants of the acid and the salt are known (e.g., determined by an independent method such as conductimetry or spectrophotometry). These pH values are related to the measured potential through the Nernst equation:

$$E = (E^\circ + E_j) - g\,pH \quad (15)$$

where the term $(E^\circ + E_j)$ is the reference potential [12] of the potentiometric system. The reference potential is composed of two independent terms, the standard potential E° and the junction potential E_j (assumed to be constant). In a cell without liquid junction the reference potential coincides with the standard potential.

Equation 15 applies when the solvent composition does not change during titration. However, in many titrations the titrant is a tetralkylammonium hydroxide, and therefore water is formed in the neutralization reaction. Moreover, titrants are not stable in every solvent, and often they are used dissolved in a solvent different from the titration medium. Therefore, the titration medium cannot, in general, be considered as a solvent of fixed composition. The addition or formation of other solvents changes the permittivity of the medium, changing the dissociation of electrolytes and reference potentials. It has been demonstrated that for small additions of a co-solvent, the change in pK values can be considered to be proportional to the volume fraction (v) of co-solvent added [17,18]:

$$pK_a = pK_{a(S)} + s_a v \quad (16)$$

$$pK_{salt} = pK_{salt(S)} + s_{salt} v \quad (17)$$

where the subscript (S) refers to the value in the pure solvent studied (unique or mixed) and s are the proportionality coefficients. Assuming that the reference potential of the system $(E^\circ + E_j)$ also changes linearly with v according to

$$(E^\circ + E_j) = (E^\circ + E_j)_{(S)} + g s_E v \quad (18)$$

a method for the calculation of reference potentials and dissociation constants of acids in pure tetrahydrofuran from titration with a titrant dissolved in propan-2-ol has been developed [11]. This method has been generalized to any non-aqueous solvent [12], and it implies calculation of the reference potential for all the points of the titration curve $[(E^\circ + E_j)_{comp}]$ and extrapolation of these values to the pure main solvent according to the equation

$$(E^\circ + E_j)_{comp} = (E^\circ + E_j)_{(S)} + gsv \quad (19)$$

where

$$s = s_E - s_a + s_{salt}/2 \quad (20)$$

The plot of the calculated reference potential through a potentiometric acid–base titration against the volume fraction of titrant added should give a straight line with the reference potential in the pure mixed solvent $[(E^\circ + E_j)_{(S)}]$ as intercept and a slope gS. This method has been proposed as a general method for the standardization of potentiometric systems in non-aqueous solvents [12] and it will be used in this work.

EXPERIMENTAL

Apparatus

For conductivity measurements a Radiometer CDM 83 conductimeter and a CDC 304 cell (cell

constant 1.03 cm^{-1}) were used. A Crison MicropH 2002 pH meter and a Methrom 665 Dosimat autoburette were used for potentiometric titrations. The titration assembly was controlled by means of the VALORA program [13]. The potentiometric cell consisted on a glass electrode and an AgCl/Ag/Pt reference electrode similar to that used by Mussini and co-workers [4–10]. The reference electrode was made of platinum wire 0.040–0.045 cm in diameter sealed through the end of a glass tube, leaving about 1 cm of wire outside of the tube. The platinum wire was coated with silver by electrolysis of 1% $KAg(CN)_2$ solution for about 6 h at a total current of 0.3 mA cm^{-2}. The electrode was then carefully rinsed and kept in distilled water until it was chloridized. This was performed by electrolysis for 30 min in 0.1 M hydrochloric acid at a total current of about 0.6 mA cm^{-2}.

Reagents

A 0.1 M solution of tetrabutylammonium hydroxide in propan-2-ol from Carlo Erba (RPE grade, containing 8% of methanol by gas chromatography) was used for titrations of hydrochloric acid (Merck, 25%) and phthalic acid (Carlo Erba, RPE, > 95%). The titrant was standardized by titration of benzoic acid (Scharlau, > 99.9%) using thymol blue as indicator. The binary solvent was prepared by mixing the appropriate weights of propan-2-ol (Carlo Erba RPE-ACS; water content < 0.5%) and triply distilled water.

Procedure

For conductimetric measurements, different measured amounts of a 5×10^{-2} M solution of electrolyte were added to 50 ml of the pure binary solvent in the conductivity cell and the conductivity was measured after each addition. Tetrabutylammonium chloride and hydrogenphthalate were prepared by exact neutralization of the acid with the 0.1 M tetrabutylammonium hydroxide solution.

For potentiometric titrations, 20 ml of a ca. 8×10^{-3} M or 4×10^{-3} M solution of acid were titrated with 0.1 M tetrabutylammonium hydroxide in propan-2-ol or with 0.05 M tetrabutylammonium hydroxide in propan-2-ol–water (70 + 30, w/w) prepared from the 0.1 M solution in propan-2-ol. In the titration of phthalic acid the solution was also 5×10^{-4} M in potassium chloride to obtain a suitable response of the reference electrode. Potentiometric measurements were also obtained by addition of measured amounts of a 1 M solution of hydrochloric acid in propan-2-ol–water (70 + 30, w/w) to 25 ml of the same pure binary solvent.

All the measurements were done in vessels externally thermostated at 25.0 ± 0.1°C with a water jacket.

Calculation methods

The dissociation constants of hydrochloric and phthalic acid and their tetrabutylammonium salts in the studied binary solvent were determined conductimetrically by using the Debye–Hückel–Onsager and Shedlovsky equations [19]. The Λ_0 and pK parameters which best fit the conductivity equations to the experimental data were determined by non-linear regression.

The reference potential of the potentiometric system was calculated from the measured potentials by means of the Nernst equation (Eqn. 15) modified to take into account the response of the reference electrode to the chloride ion:

$$E = (E^\circ + E_j) - g\,\mathrm{pH} + g\,\log([\mathrm{Cl}^-]y) \qquad (21)$$

The pH was calculated from Eqns. 3–5 using the dissociation constants of the acid and the salt previously determined conductimetrically. $[Cl^-]$ was calculated from Eqn. 3 for hydrochloric acid titration or addition or from the potassium chloride concentration for phthalic acid titration. Activity coefficients were calculated from the Debye–Hückel equation with the constants $A = 2.13$ and $a_0B = 2.30$ according to the Bates–Guggenheim convention [20,21].

The calculated $(E^\circ + E_j)$ values were plotted against the volume fraction of titrant added according to Eqn. 19 and the value in pure propan-2-ol/water (70 + 30, w/w) determined by linear regression with the POTENCI program described previously [13].

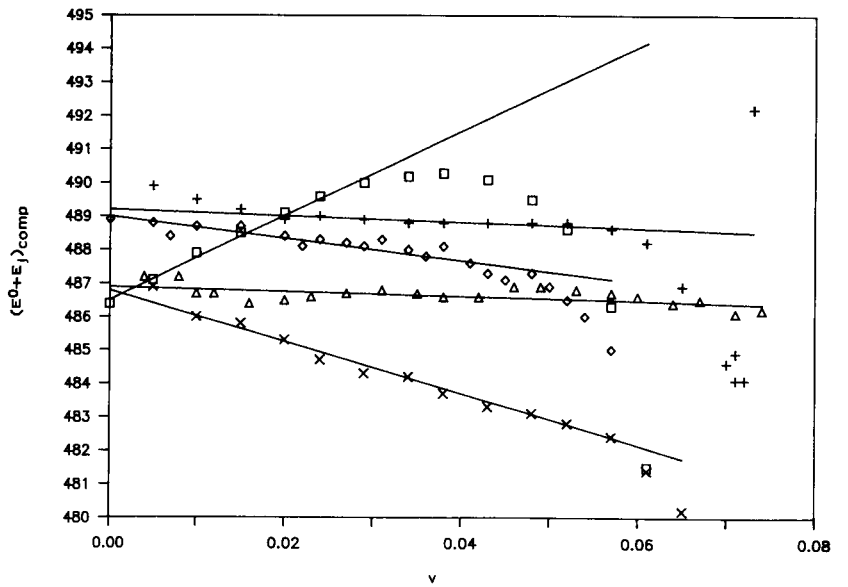

Fig. 1. Standardization of the potentiometric system with various methods. △ = Addition of 1 M hydrochloric acid in propan-2-ol–water (70 + 30, w/w); ◇ = titration of hydrochloric acid with 0.05 M tetrabutylammonium hydroxide in propan-2-ol–water (70 + 30, w/w); □ = titration of hydrochloric acid with 0.1 M tetrabutylammonium hydroxide in propan-2-ol; + = titration of phthalic acid with 0.05 M tetrabutylammonium hydroxide in propan-2-ol–water (70 + 30, w/w); × = titration of phtahlic acid with 0.1 M tetrabutylammonium hydroxide in propan-2-ol. v is the volume fraction of titrant or solvent added.

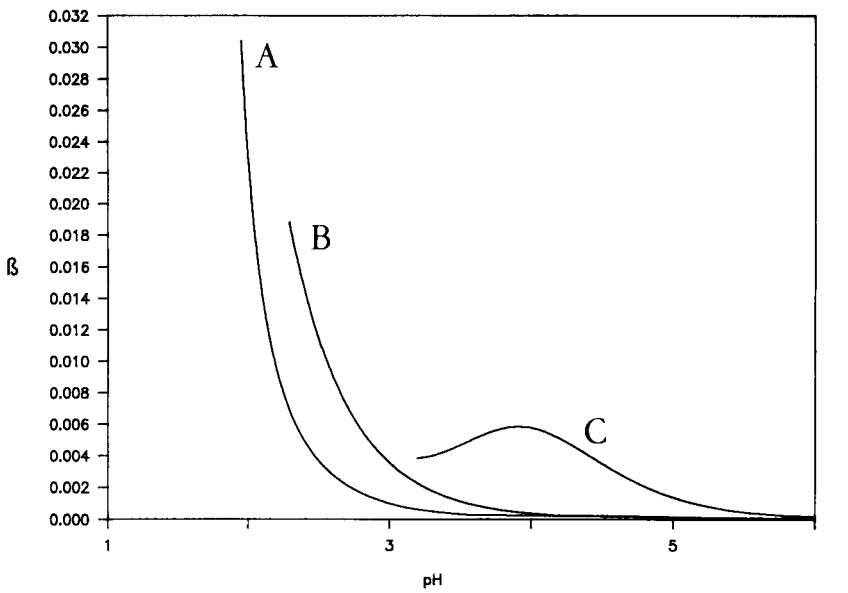

Fig. 2. Variation of buffer capacities (β) with pH during addition or titration of acids. (A) Addition of 1 M hydrochloric acid to 25 ml of the pure binary solvent (the real β value is ten times higher than that represented); (B) titration of 20 ml of 8×10^{-3} M hydrochloric acid with 0.1 M tetrabutylammonium hydroxide; (C) titration of 20 ml of 8×10^{-3} M phthalic acid with 0.1 M tetrabutylammonium hydroxide.

RESULTS AND DISCUSSION

The pK values of hydrochloric and phthalic acid and their tetrabutylammonium salts determined conductimetrically are presented in Table 1. Hydrochloric acid and tetrabutylammonium chloride are completely dissociated in the studied range of concentrations ($< 10^{-2}$ M). However, tetrabutylammonium phthalate suffers appreciably from ion-pair formation except in very dilute solutions. The conductimetric pK value of phthalic acid agrees well with the potentiometric value determined by Rondinini et al. [9] (4.16 on the molal scale, which correspons to 4.23 on the molar scale used here).

By using the determined pK values, the potentiometric system was standardized according to the proposed method. Figure 1 presents the $(E^\circ + E_j)$ values calculated for each point of the titration of hydrochloric and phthalic acid against the volume fraction of titrant added, the latter being tetrabutylammonium hydroxide in propan-2-ol or in propan-2-ol/water (70 + 30, w/w), and also the values calculated for the addition of the hydrochloric acid solution to the pure binary solvent. It can be observed that straight lines are obtained in the best buffered part of the titration or addition. In order to determine which is the best buffered part, the buffer capacity during titration of hydrochloric and phthalic acid or addition of hydrochloric acid were calculated by means of the CORVAL program [13].

TABLE 1

Dissociation constants and molar conductivities of acids and their tetrabutylammonium salts in propan-2-ol–water (70 + 30, w/w)

Electrolyte	pK	Λ_0 (Ω^{-1} cm^2 mol^{-1})
Hydrochloric acid	d [a]	64.8
Tetrabutylammonium chloride	d	28.2
Phthalic acid	4.24 ± 0.02	56.8
Tetrabuylammonium hydrogenphthalate	2.19 ± 0.09	21.3

[a] d = Completely dissociated.

Figure 2 shows the variation of buffer capacities with pH during titration or addition of the acids. On the one hand, a typical strong acid exponential curve is obtained for titration or addition of hydrochloric acid. On the other, a bell-shaped curve, typical of a weaker acid, is ob-

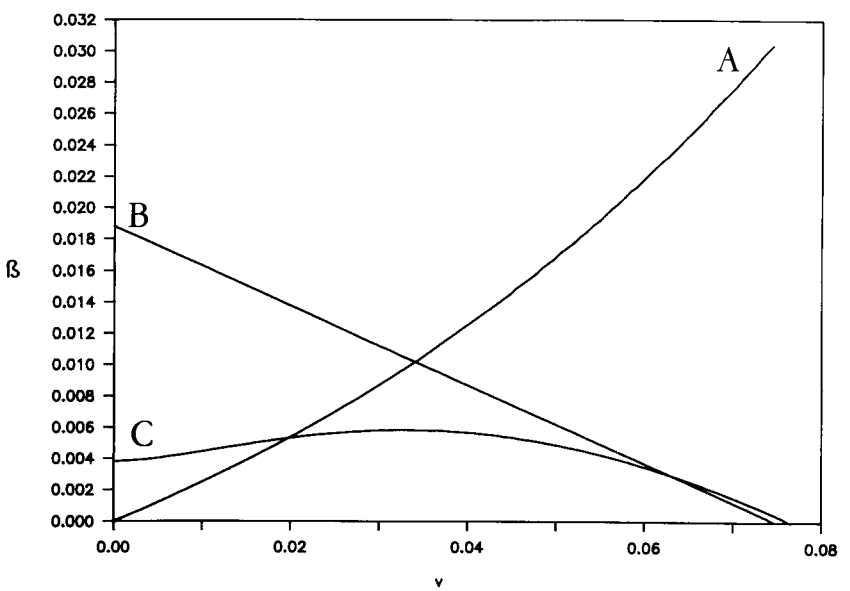

Fig. 3. Variation of buffer capacities (β) with the volume fraction of solvent added during addition or titration of acids. (A)–(C) as in Fig. 2.

tained for phthalic acid. However, the latter is not centered at pH = pK = 4.24 as expected, because of salt ion-pair formation which enhances the strength of the acid and moves the maximum buffer capacity toward lower pH values. This effect has been observed previously in solvents such as *tert*-butanol [22,23], tetrahydrofuran [13] and anhydrous acetic acid [24].

In order to determine the variation of buffer capacity during titration or addition of an acid, it is more useful to plot the buffer capacity against the volume fraction (v) of solvent added (Fig. 3) than the more usual β vs. pH plot. The buffer capacity increases on addition of hydrochloric acid. However, the solution is well buffered almost from the beginning, and a straight line is obtained for all the points in Fig. 1. The buffer capacity in the titration of hydrochloric acid is high for the first titration points but decreases along the titration (Fig. 3). As a consequence, straight lines are obtained in Fig. 1 for low v values in the titration of hydrochloric acid with tetrabutylammonium hydroxide in propan-2-ol or in propan-2-ol–water (70 + 30, w/w). For higher v values the solution is less buffered and the points deviate from the line. According to Fig. 3, the best buffered part in titration of phthalic acid is between $v = 0.015$ and 0.050 ($\beta > 0.005$), which agrees with the limits of linearity in Fig. 1 for the titration of phthalic acid.

Another factor that can influence the linearity of the plots in Fig. 1 is the errors in c_a and c_{salt}, which can arise from random errors in measuring initial, equivalence and added volumes. On addition of hydrochloric acid for $c_{salt} = 0$, c_a increases with increasing v. Therefore, points with a lower relative c_a error are obtained for high v values. In the titration of hydrochloric or phthalic acid, c_{salt} increases with increasing v but c_a decreases. However, as hydrochloric acid is completely dissociated at the working concentrations, the general cubic Eqn. 3 becomes Eqn. 14 and c_{salt} has no influence on pH calculations. Therefore, the points with a lower error will be obtained for low relative c_a errors, that is, for high c_a values. However, in the titration of phthalic acid the general Eqn. 3 tends to become Eqn. 6 or 11 and both c_a and c_{salt} errors should be considered. Lower errors in pH calculation are obtained for points with c_a values close to c_{salt}. The parts with lower errors in calculations of concentrations are the same as those with lower errors in potential measurements (the best buffered) and the best parts for relating pH values with experimental potentials can be summarized as follows: the last points for addition of a strong acid, the first points for titration of a strong acid and the middle points for titration of a weak acid.

From these parts the calculated ($E^\circ + E_j$) reference potentials were extrapolated to $v = 0$, which correspond to the values in propan-2-ol–water (70 + 30, w/w) and the results are presented in Table 2 together with the slopes s of the plot.

There is no significant difference between the extrapolated ($E^\circ + E_j$) values to propan-2-ol–water (70 + 30, w/w) solvent, but the slopes s of the plots are quite different. For addition of hydrochloric acid dissolved in propan-2-ol–water or titration of hydrochloric or phthalic acid with tetrabutylammonium hydroxide in propan-2-ol–water, the slopes are close to zero because the addition of hydrochloric acid or tetrabutylammonium hydroxide hardly changes the titration

TABLE 2

Standardization of the potentiometric system with various methods

Method	Acid added or titrated	Solvent of the acid added or of the titrant	$(E^\circ + E_j)_{(S)}$ (mV)	s
Addition	Hydrochloric acid	Propan-2-ol–water (70 + 30, w/w)	486.9 ± 0.2	−0.12 ± 0.04
Titration	Hydrochloric acid	Propan-2-ol–water (70 + 30, w/w)	489.0 ± 0.2	−0.56 ± 0.06
Titration	Hydrochloric acid	Propan-2-ol	486.5 ± 0.1	+2.13 ± 0.08
Titration	Phthalic acid	Propan-2-ol–water (70 + 30, w/w)	489.2 ± 0.1	−0.16 ± 0.03
Titration	Phthalic acid	Propan-2-ol	486.8 ± 0.1	−1.31 ± 0.05

medium. The small values of s can be attributed to water formation during the titration or to errors in solvent preparation (e.g., because of the methanol present in the commercial titrant), concentration calculations or pK determinations. However, titrations of hydrochloric and phthalic acid with tetrabutylammonium hydroxide dissolved in pure propan-2-ol show appreciable values of s because the solvent content in propan-2-ol increases during the titration. The increase in propan-2-ol content should increase $(E^\circ + E_j)$, pK_a and pK_{salt} values, which results in positive values of s_E, s_a and s_{salt}. However, as hydrochloric acid is completely dissociated, $s_a = 0$, $s_{salt} = 0$ and $s = 2.1 \approx s_E > 0$, as expected. In the titration of phthalic acid s depends on the s_E, s_a and s_{salt} values according to Eqn. 20 and if $s_a > (s_E + s_{salt}/2)$, s should be negative. Assuming $s_E \approx 2.1$, and as $s = -1.3$, s_a should be about 3.4 units higher than $s_{salt}/2$, which is a reasonable value.

It can be concluded that the five methods (addition of hydrochloric acid and titrations of hydrochloric and phthalic acid with the titrant dissolved in the same solvent or directly with the commercial titrant) allow accurate standardization of the potentiometric system. Direct titration with the commercial titrant is more facile but produces higher s values because of the medium change, which can result in a less accurate extrapolated value of $(E^\circ + E_j)$. Titration of a strong acid is preferred to titration of a weak acid because of the higher buffer capacity and because the extrapolation to obtain the reference potential in the pure binary solvent is made from the first few points instead of the points in the middle part of the titration. On the addition of a strong acid the extrapolation should be made from the last points of the addition, but if the acid is concentrated enough the first points can also be used. Therefore, the most recommendable methods for standardization of electrode systems in binary solvent mixtures, similar to that studied here, are titration or addition of a strong acid, with the titrant dissolved in a solvent as similar as possible to the main titration medium.

The proposed methods have been used for every-day standardizations of potentiometric systems. Figure 4 shows the results obtained over a period of more than 2 months after preparation of the reference electrode. A constant $(E^\circ + E_j)$

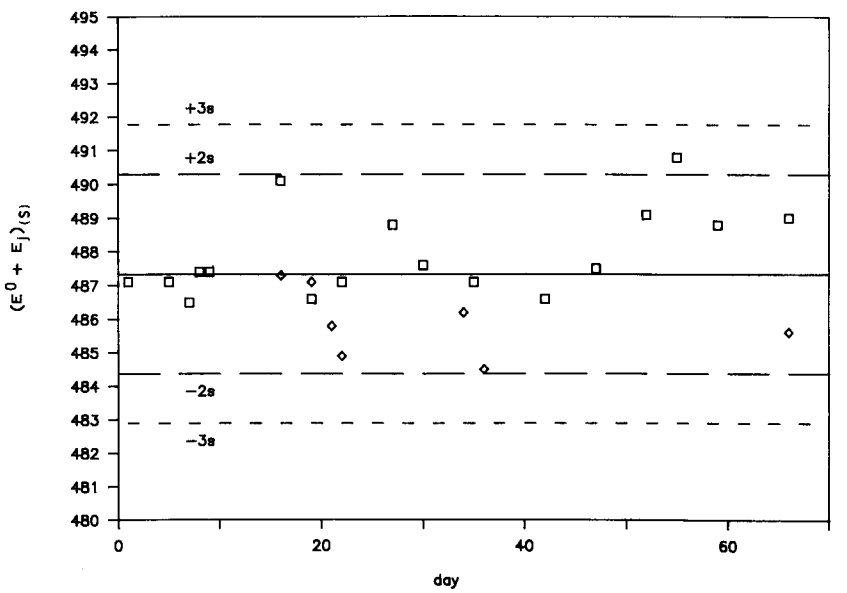

Fig. 4. Control chart for standardization of the potentiometric system. □ = Titration of hydrochloric acid with 0.05 M tetrabutylammonium hydroxide in propan-2-ol–water (70 + 30, w/w); ◇ = addition of 1 M hydrochloric acid in propan-2-ol–water (70 + 30, w/w).

value of 487.3 ± 1.5 mV was obtained for propan-2-ol–water (70 + 30, w/w) binary solvent.

Financial support from the DGICYT (Project PB88-0194) of the Spanish Government is gratefully acknowledged.

REFERENCES

1 T. Mussini, A.K. Covington and S. Rondinini, Pure Appl. Chem., 57 (1985) 865.
2 S. Rondinini, P.R. Mussini and T. Mussini, Pure Appl. Chem., 59 (1987) 1549.
3 M.J. Taylor, J. Chem. Eng. Data, 24 (1979) 230.
4 T. Mussini, A.K. Covington, F. Dal Pozzo, P. Longhi, S. Rondinini and Z.-Y. Zou, Electrochim. Acta, 28 (1983) 1593.
5 T. Mussini, M. Cicognini, P. Longhi and S. Rondinini, Anal. Chim. Acta, 162 (1984) 103.
6 T. Mussini, P. Longhi, S. Rondinini, M. Tettamanti and A.K. Covington, Anal. Chim. Acta, 174 (1985) 331.
7 P. Longhi, T. Mussini and S. Rondinini, Anal. Chem., 58 (1986) 2290.
8 S. Rondinini and A. Nese, Electrochim. Acta, 32 (1987) 1499.
9 S. Rondinini, P. Longhi, P.R. Mussini, A. Nese, M. Pozzi and G. Tiella, Anal. Chim. Acta, 207 (1988) 211.
10 P. Longhi, P.R. Mussini, T. Mussini and S. Rondinini, J. Chem. Eng. Data, 34 (1989) 64.
11 J. Barbosa, D. Barrón, E. Bosch and M. Rosés, Anal. Chim. Acta, 264 (1992) 229.
12 M. Rosés, Anal. Chim. Acta, 276 (1993) 211.
13 M. Rosés, Anal. Chim. Acta, 276 (1993) 223.
14 G. Åkerlöf, J. Am. Chem. Soc., 54 (1932) 4125.
15 R.N. Roy and A. Bothwell, J. Chem. Eng. Data, 15 (1970) 548.
16 E. Bosch and M. Rosés, Talanta, 36 (1989) 615.
17 E. Bosch and M. Rosés, Anal. Chem., 60 (1988) 2008.
18 E. Bosch, C. Ràfols and M. Rosés, Anal. Chem., 62 (1990) 102.
19 H.S. Harned and B.B. Owen, The Physical Chemistry of Electrolytic Solutions, Reinhold, New York, 3rd edn., 1958.
20 R.G. Bates, Determination of pH. Theory and Practice, Wiley, New York, 2nd edn., 1973.
21 R.G. Bates and E.A. Guggenheim, Pure Appl. Chem., 1 (1960) 163.
22 E. Bosch and M. Rosés, Talanta, 36 (1989) 623.
23 E. Bosch and M. Rosés, Talanta, 36 (1989) 627.
24 J. Barbosa, E. Bosch, J.L. Cortina and M. Rosés, Anal. Chim. Acta, 256 (1992) 211.

Analytica Chimica Acta, 280 (1993) 85–92
Elsevier Science Publishers B.V., Amsterdam

Determination of 2-chloro-4,5-difluorobenzoic acid and related impurities by liquid chromatography

Lee Elrod, Jr., Stephen G. Spanton, Mike Cirovic, Dean I. Shaffer, Timothy G. Golich, Cathie L. Linton and Douglas R. Vievia

Pharmaceutical Products, Analytical Research Division, Abbott Laboratories, 1401 Sheridan Road, North Chicago, IL 60064 (USA)

Panos Kalaritis [1]

Chemical Development Department, Chemical and Agricultural Products Division, Abbott Laboratories, 1401 Sheridan Road, North Chicago, IL 60064 (USA)

Horst Schmand

Riedel-de Haën AG, Postfach, D-3016 Seelze (Germany)

(Received 16th November 1992; revised manuscript received 28th January 1993)

Abstract

2-Chloro-4,5-difluorobenzoic acid (CDFBA) and related impurities are determined using liquid chromatography (LC). Separations are achieved using a reversed-phase isocratic system with an ion-pair reagent (tetrabutylammonium hydroxide). Unique isomeric impurities observed in commercially produced CDFBA were isolated and identified by NMR and single crystal x-ray diffraction. The method has relative standard deviations of $\pm 0.55\%$ to $\pm 1.26\%$ for the CDFBA determination and from $\pm 4.3\%$ to $\pm 12\%$ for impurities below 0.3% in CDFBA. Impurities are determinable to at least 0.03% by weight.

Keywords: 2-Chloro-4,5-difluorobenzoic acid; CDFBA

Halogenated benzoic acids are key intermediates in the preparation of fluoroquinolone antibacterial agents. In the general synthetic scheme for the preparation of the fluoroquinilone drugs, an intramolecular nucleophilic displacement of the halogen substituent at position 2 is followed by a nucleophilic displacement at position 4 of the original benzoic acid ring [1–3]. The purity of the halogenated benzoic acid must be carefully controlled to minimize the formation of undesired products which react in a similar manner as the main component in the synthesis and which are potentially carried through to the finished drug.

Halogenated benzoic acids have been used in the evaluation of various column packings. Few attempts, however, have been made to separate polyhalogenated isomers of benzoic acid by liquid chromatography. Several authors report the separation of isomeric monosubstituted benzoic acids having either fluoro-, amino-, hydroxy- or nitro-functional groups [4–8]. Separation of these compounds is often achieved using a mixed-mode of ion-exchange and adsorption chromatography. This approach provided baseline resolution of *o*-, *m*- and *p*-aminobenzoic acid and near-baseline

Correspondence to: L. Elrod, Jr., Pharmaceutical Products, Analytical Research Division, Abbott Labs., 1401 Sheridan Road, North Chicago, IL 60064 (USA).
[1] Current address: Hoffman-LaRoche, Nutley, NJ 07110 (USA).

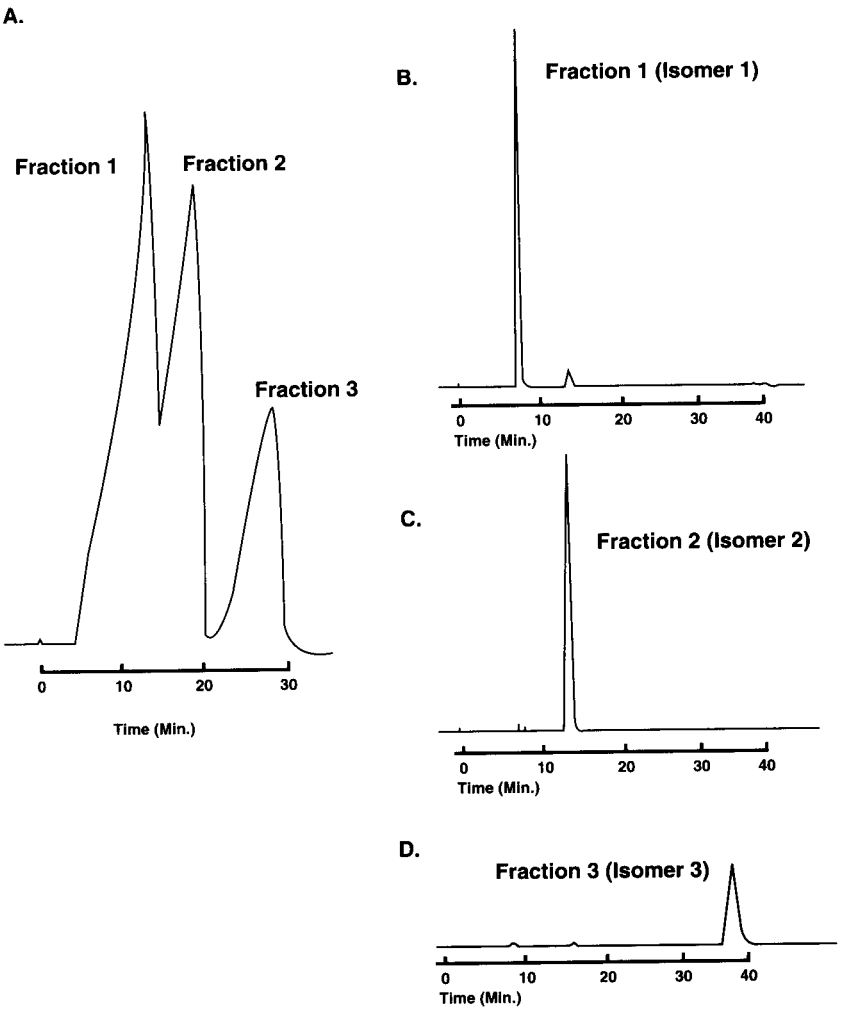

Fig. 1. Chromatograms for synthetic CDFBA isomer mixture by semi-preparative and analytical systems. Conditions stated in text. A = Semi-preparative separation, Benson OA 850 organic acid column. B–D = Analytical separations of collected fractions.

resolution of *o*-, *m*- and *p*-chlorobenzoic acid [9]. Separation of 2,6-difluorobenzoic acid, pentafluorobenzoic acid, and *o*-(trifluoromethyl)benzoic acid has been reported using an ion-exchange packing [10]. Reverse-phase separation and quantitation at ppb levels of pentafluorobenzoic acid and *m*-(trifluoromethyl)benzoic acid has been reported [11]. Separation of 2,4-, 2,5-, 2,6-, and 3,4-dichlorobenzoic acids has been achieved using a column packed with octadecyl vinyl alcohol copolymer gel [12].

In this work we describe the determination of 2-chloro-4,5-difluorobenzoic acid (CDFBA) by liquid chromatography (LC). Separations are achieved using a reversed-phase isocratic system containing an ion-pair reagent. This approach provides better selectivity of isomeric analogs of CDFBA than achieved by ion-suppression on reversed-phase packings and eliminates the need for ion-exchange or mixed-mode stationary phases. Quantitation of CDFBA and potential impurities is performed by the internal standard method.

Observed impurities in commercially produced CDFBA are identified as lower halogenated benzoic acids and positional isomers. Three chloro-

difluoro positional isomers were independently synthesized as a three-component mixture. Pure samples of the impurities were isolated by preparative LC and characterized using single crystal x-ray diffraction and NMR.

EXPERIMENTAL

Apparatus

The liquid chromatograph used typically consisted of a Model SP-8800 pump and autosampler and a Model Spectra 100 UV detector (Spectra-Physics, San Jose, CA). A Model C-R4A data system was used (Shamadzu, Kyoto). Analytical separations were made using either a Nucleosil C_{18} chromatographic column (5 μm particle size, 100 Å pore size) measuring 150 mm × 4.6 mm i.d. (Alltech Associates, Deerfield, IL) or a Techsphere C_8 chromatographic column (5 μm particle size, 100 Å pore size measuring 250 mm × 4.6 mm i.d. (Serva Biochemicals, Paramus, NJ). Preparative or semi-preparative scale separations were made using a Shandon C_{18} column measuring 250 mm × 25 mm (Alltech, Deerfield, IL) or a Benson OA 850 organic acid column measuring 300 mm × 7.8 mm i.d. (Benson Polymeric, Reno, NV). X-Ray diffraction patterns were obtained on a Rigaku Model AFC5R diffractometer.

Chemicals

Acetonitrile, methanol and dichloromethane were HPLC grade (Fisher Scientific, Fair Lawn, NJ). Tetrabutylammonium hydroxide (TBAOH) was reagent grade and was purchased as a 1 M solution in methanol (Southwestern Analytical Chemicals, Austin, TX). The internal standard used was 3,5-dinitrobenzoic acid (Baker, Phillipsburg, NJ). Throughout this work, CDFBA was prepared in-house or purchased in bulk from commercial sources. Authentic standards of the following materials were prepared in-house and were purified by recrystallization or sublimation: 2,4,5-trifluorobenzoic acid (TFBA), 5-chloro-2,4-difluorobenzoic acid (5-C-2,4-DFBA), and 4-chloro-2,5-difluorobenzoic acid (4-C-2,5-DFBA). The following materials were reagent grade from Aldrich (Milwaukee, WI): 2,5-difluorobenzoic acid (2,5-DFBA), 3,4-difluorobenzoic acid (3,4-DFBA), 2,4-difluorobenzoic acid (2,4-DFBA), 2-chlorobenzoic acid (2-CBA) and 4-chlorobenzoic acid (4-CBA).

A three-component mixture of positional isomers of CDFBA was synthesized starting from 2,3-difluoroaniline. 1-Chloro-2,3-difluorobenzene was prepared from this material by the Sandmeyer reaction. Dichloroacetylation of 1-chloro-2,3-difluorobenzene by the Friedel-Crafts reaction and subsequent haloform reaction resulted in a three-component mixture of isomeric chloro-

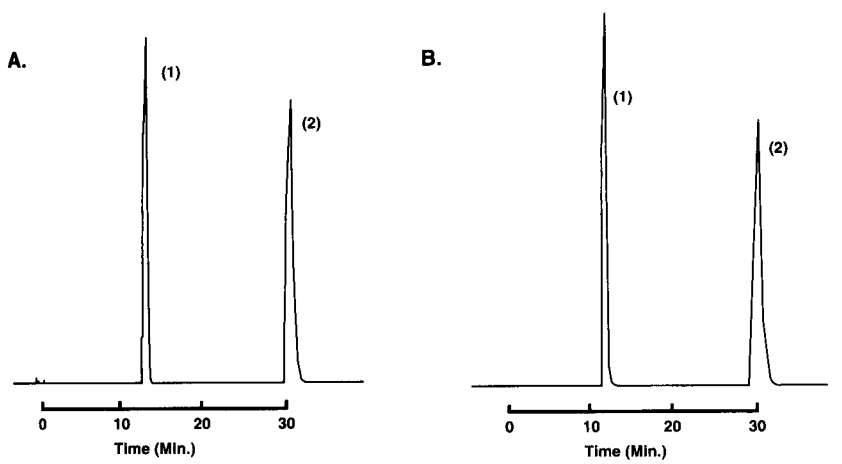

Fig. 2. Typical chromatograms for CDFBA determinations. Conditions stated in text. A = Standard preparation, B = Sample preparation, Peak identities: (1) CDFBA, (2) Internal standard.

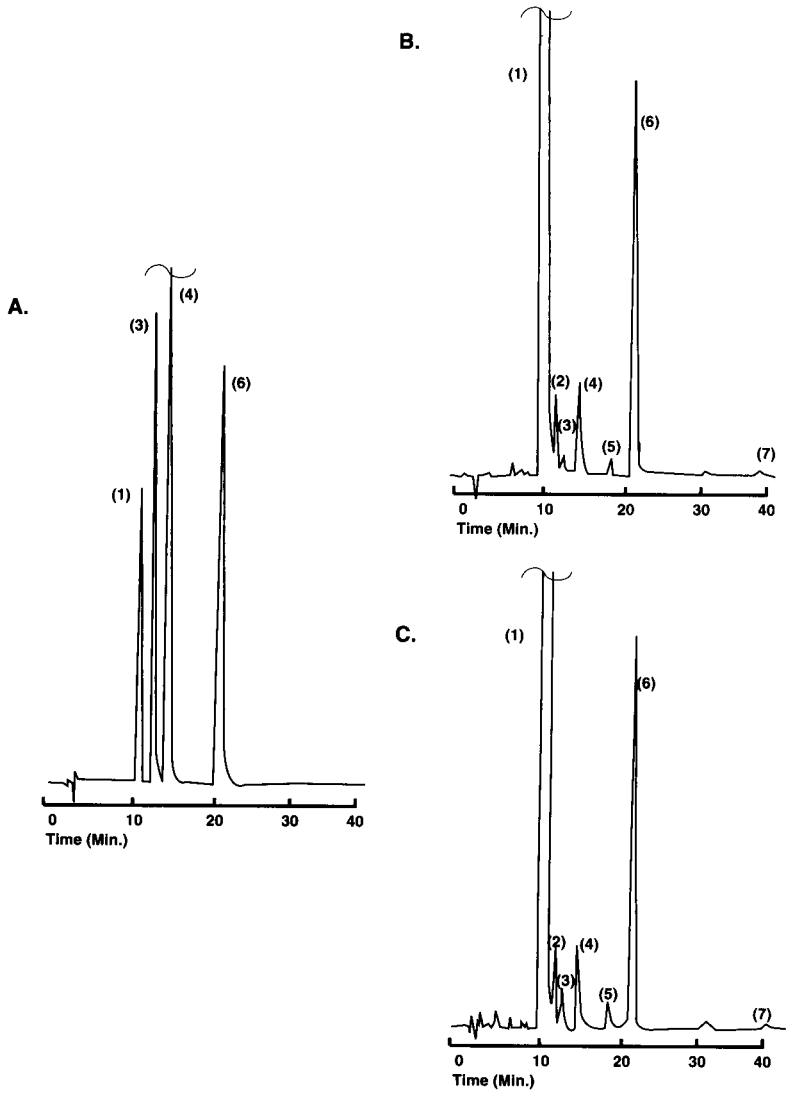

Fig. 3. Typical chromatograms for CDFBA impurities. Conditions stated in text. A = Quantitation standard, B = CDFBA lot 1, C = CDFBA lot 2. Peak identities: (1) CDFBA, (2) 2-C-3,4-DFBA, (3) 3,4-DFBA, (4) 4-CBA, (5) 4-C-2,3-DFBA, (6) Internal Standard and (7) 5-C-3,4-DFBA.

difluorobenzoic acids which was separated by preparative LC.

1-Chloro-2,3-difluorobenzene. Into 120 ml of 25% (w/w) hydrochloric acid, 29.6 g (0.23 mole) of 2,3-difluoroaniline was added. The suspension was cooled to 0°C and afterwards maintaining this temperature, 15.8 g (0.23 mole) of sodium nitrite dissolved in 30 ml of water was added dropwise with stirring. Subsequently, the diazonium salt solution was decomposed at 100°C by adding it to a previously prepared solution of 9.3 g (0.09 mole) of copper(I)chloride and 30 ml of 25% (w/w) hydrochoric acid. Rapid evolution of nitrogen ensued spontaneously. The crude reaction mixture was steam distilled and vacuum distilled. Yield: 22.1 g of 1-chloro-2,3-difluorobenzene (64.7% of the theoretical amount). Assay (GC) 99%; assay (GC–MS) 99% (M^+, m/e =

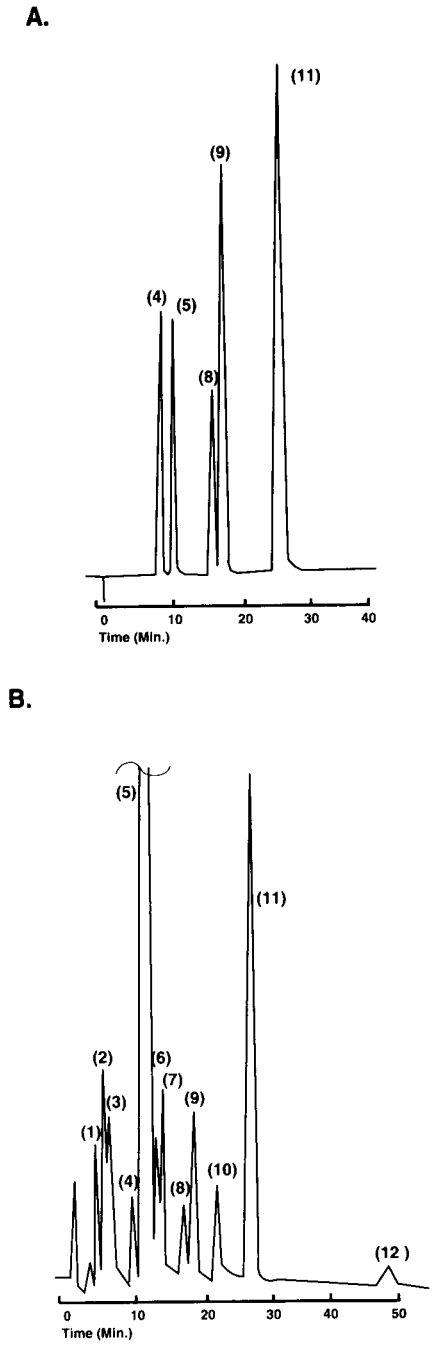

Fig. 4. Typical chromatograms of CDFBA, synthetic mixtures of CDFBA and some possible impurities. Conditions stated in text. A = Mixed standard preparation, B = Synthetic mixture of CDFBA and possible impurities. Peak identities: (1) 2-CBA, (2) 2,5-DFBA, (3) 2,4-DFBA, (4) TFBA, (5) CDFBA, (6) 2-C-3,4-DFBA, (7) 3,4-DFBA, (8) 5-C-2,4-DFBA, (9) 4-C-2,5-DFBA, (10) 4-C-2,3-DFBA, (11) Internal standard and (12) 5-C-3,4-DFBA.

148/150), ^{19}F NMR (60 MHz), ($CDCl_3$) ppm, related to C_6F_6: −22.8 ppm to −23.7 ppm (1 F, m), −26.7 ppm to −27.5 ppm (1 F, m).

Chlorodifluoro-α,α-dichloroacetophenone, mixture of isomers. To 22.1 g (0.149 mole) of 1-chloro-2,3-difluorobenzene was added 29.8 g (0.224 mole) of anhydrous aluminum chloride at an initial temperature of 20°C. The suspension was heated to 65°C. In the course of 3 h 26.5 g (0.18 mole) of dichloroacetyl chloride was added to the suspension dropwise with stirring and under exclusion of moisture. During this period the temperature was maintained at 65°C. The reaction mixture was stirred for an additional 4 h at 65°C and then the green viscous liquid was poured into 300 ml of water. The temperature rose to about 60°C. The organic bottom layer was separated in a separating funnel at 50°C. A yield of 37.3 g of chloro-difluoro-α,α-dichloroacetophenone as a mixture of three positional isomers was obtained (96.4% of the theoretical amount). Isomeric assays by GC: 19.8%, 56.7%, 22.2%. ^{19}F NMR (60 MHz) ($CDCl_3$) δ ppm, related to C_6F_6: isomer −26 ppm to −26.6 ppm (1 F, m), −34.7 ppm to −35.8 ppm (1 F, m); isomer −27.6 ppm to −28.3 ppm (2 F, m); isomer −30.3 ppm to −31.8 ppm (1 F, m), −34.7 ppm to −35.8 ppm (1 F, m). ^{13}C NMR (75 MHz) (DMSO-d6) δ ppm: $ArC(O)\underline{C}HCl_2$, isomer 70.32 ppm, isomer 70.48 ppm, isomer 70.54 ppm. $Ar\underline{C}(O)CHCl_2$, isomer 182.4 ppm, isomer 183.5 ppm, isomer 185 ppm.

Chlorodifluorobenzoic acid, mixture of three isomers. To 374.6 g of sodium hypobromite solution (prepared from a mixture of 34 g of sodium hydroxide and 293 g of water to which was added 47.6 g of bromine at 0–10°C) was added dropwise with stirring 37.3 g of chlorodifluoro-α,α-dichloroacetophenone, mixture of isomers at 30°C in 2 h. Afterwards, stirring was continued 45 min at 30°C and then for an additional 3 h at 50°C. After separation of halomethane species and impurities as liquid (bottom phase) the alkaline aqueous phase was acidified with 140 ml of 32% (w/w) hydrochloric acid to pH 1 and sodium disulfite was added in order to reduce excessive sodium bromite. Working-up by standard procedure yielded 24.4 g of chlorodifluorobenzoic acid mixture of isomers (88.1% of the theoretical amount

related to the dichloroacetophenone, mixture of isomers and 85.2% related to 1-chloro-2,3-difluorobenzene). Isomeric assays by LC: 37.8%, 43.5%, 18.1%. ^{13}C NMR (75 MHz) ($CDCl_3$, DMSO-d_6) δ ppm. O<u>C</u>OH, isomer 163.42 ppm, isomer 164.48 ppm, isomer 164.83 ppm.

Isolation of isomeric chlorodifluorobenzoic acids

Isolation of the isomeric chlorodifluorobenzoic acids was performed using either preparative or semi-preparative LC systems. Small scale isolation of the isomers was achieved using a Benson OA 850 organic acid column (300 mm × 7.8 mm i.d.) with an eluent containing 5×10^{-4} M H_2SO_4–acetonitrile (90:10) at a flow-rate of 1.0 ml/min. Detection was by UV at 230 nm with an injection volume of 200 μl. The three-component isomer mixture prepared synthetically was chromatographed from a solution containing 5 mg/ml prepared in eluent. Collection of the peak fractions were made and pooled. The pooled fractions were acidified using conc. H_2SO_4 and extracted into dichloromethane. Evaporation of the dichloromethane layer provided 0.8–2.0 mg quantities of the clean isomeric acids (Fig. 1). Larger quantities of these materials were obtained preparatively using a Shandon ODS 5 column (250 mm × 25 mm) and an eluent containing 0.1% acetic acid–methanol in a three step gradient at (50:50), (40:60) and (20:80) ratios. A flow-rate of 8 ml/min was used with UV detection at 240 nm. Collected fractions were pooled and evaporated, providing individual isomeric acids for identification.

Procedure for CDFBA and impurities determination

The eluent used for all determinations consisted of 77% aqueous buffer which was 0.02 M TBAOH and 0.02 M potassium phosphate dibasic (pH adjusted to 6.0 with phosphoric acid) and 23% acetonitrile. Separations were performed using a flow-rate of 1.0 ml/min, 50 μl injection volume and UV detection at 230 nm. Nucleosil C_{18} or Techsphere C_8 columns (15 cm × 4.6 mm i.d. or 25 cm × 4.6 mm i.d.), respectively, are equivalent for the analytical separations with the stated conditions. Determination of CDFBA was made by chromatographing sample and standard solutions containing approximately 100 μg/ml of CDFBA and 35 μg/ml of internal standard. Quantitation of CDFBA was made by the internal standard method using peak area ratios of CDFBA to internal standard and the known concentrations of standard and sample. Determination of impurities was made by chromatographing mixed standards containing approximately 10 μg/ml of known impurities and CDFBA and 5.8 μg/ml of internal standard. The CDFBA sample preparation was approximately 1.0 mg/ml and contained 5.8 μg/ml of internal standard. Quantitation was made by the internal standard method using peak area ratios and known concentrations of standard and sample. Unknown impurities were based on the CDFBA standard. All preparations were made in the HPLC eluent.

RESULTS AND DISCUSSION

The halogenated benzoic acids studied can be retained on reversed-phase columns by simply suppressing the ionization of the acids at low pH. However, by this approach, various lower halogenated isomers co-eluted and were incompletely resolved from CDFBA. As an alternative to ion suppression, the described ion-pair LC system was developed to more completely resolve possible isomeric mono-chlorodifluorobenzoic acids and lower halogenated benzoic acids which are potential impurities in CDFBA.

When commercially produced CDFBA was chromatographed using the conditions stated, impurities were identified by GC–MS techniques and matched to commercially available or independently synthesized standards. Three major chlorodifluorobenzoic isomeric impurities of CDFBA were traced to the starting material and were isolated preparatively (Fig. 1). The structures of the isolated materials were assigned based on ^{13}C NMR. The spectral characteristics for the isolated isomers are summarized in Table 1 and, as indicated, fractions (isomers) **1**, **2** and **3** were assigned as 2-chloro-3,4-difluorobenzoic acid (2-C-3,4-DFBA), 4-chloro-2,3-difluorobenzoic acid

TABLE 1

^{13}C NMR (75 MHz) data for isolated CDFBA isomers
(All spectra are broad band decoupled)

Isomer **1** (fraction 1, Fig. 1)		Isomer **2** (fraction 2, Fig. 1)		Isomer **3** (fraction 3, Fig. 1)	
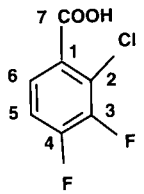		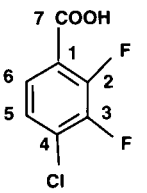		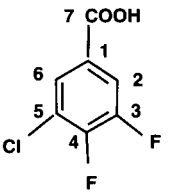	
δ_c (ppm) values in parentheses are coupling constants J_{FC} in Hz		δ_c (ppm) values in parentheses are coupling constants J_{FC} in Hz		δ_c (ppm) values in parentheses are coupling constants J_{FC} in Hz	
166 br	C_7	166.7 br	C_7	164.6	C_7
150.8 dd (12.9, 251.4)	C_4	149.8 dd (13.0, 260.6)	C_3	151.2 dd (16.4, 254.4)	C_4
146.4 dd (14.7, 247.0)	C_3	146.8 dd (15.3, 247.4)	C_2	147.8 dd (17.3, 256.3)	C_3
132.5 br	C_2	126.7	C_1	128.7 triplet not resolved ($\approx$ 2)	C_5
126.2	C_1	125.9 d (3.1)	C_6	121.8 d (2.3)	C_1
120.8 d (13.3)	C_6	124.5 d (14.4)	C_5	121.6 d (14.7)	C_6
115.7 d (17.2)	C_5	122.2 br	C_4	117.4 d (18.3)	C_2
(br = broad signals)		(br = broad signals)		(br = broad signals)	

(4-C-2,3-DFBA) and 5-chloro-3,4-difluorobenzoic acid (5-C-3,4-DFBA) respectively.

Proposed structures for isomer **1** and **2** were unambiguously confirmed by single crystal x-ray diffraction. Both isomers were crystallized from methanol by slow evaporation. The data sets were collected on a Rigaku AFC5R diffractometer. The structures were solved using SHELXS76 [13]

TABLE 2

Single crystal x-ray experimental results for CDFBA isomers **1** and **2**

	Isomer **1**	Isomer **2**
Crystal system	Triclinic	Triclinic
Lattic parameters	$a = 7.407(1)$ Å	$a = 7.258(1)$ Å
	$b = 7.773(2)$ Å	$b = 8.5656(6)$ Å
	$c = 6.846(1)$ Å	$c = 6.0159(6)$ Å
	$\alpha = 103.54(2)^0$	$\alpha = 97.273(8)^0$
	$\beta = 95.19(2)^0$	$\beta = 91.62(1)^0$
	$\gamma = 109.72(1)^0$	$\gamma = 73.224(9)^0$
	$V = 354.5(1)$ Å	$V = 355.20(8)$ Å
Space group	P-1	P-1
Z value	2	2
Radiation	Cu K_α ($\lambda = 1.54178$ Å)	Cu K_α ($\lambda = 1.54178$ Å)
$2\Theta_{max}$	110.0^0	120.0^0
Number of reflections measured	Total: 980	Total: 1154
	Unique: 895 ($R_{int} = 0.008$)	Unique: 1057 $R_{int} = 0.028$)
Number of observations (I > 3.00 δ)	821	753
Residuals	$R = 0.037$	$R = 0.061$
	$R_w = 0.055$	$R_w = 0.078$
Goodness of fit indicator	2.92	3.07

and refined by full-matrix least-squares method (TEXSAN) [14]. The results are shown in Table 2. Single crystals for isomer **3** could not be successfully grown.

Typical chromatograms for CDFBA determinations are presented in Fig. 2. Detector response was linear to at least 207 μg/ml [CDFBA concentration (μg/ml) = x versus peak area ratio of CDFBA to internal standard = y]; slope = 6.07×10^{-3}, y-intercept = 8.37×10^{-3}, correlation coefficient > 0.9999. Precision data were generated by two analysts performing the determination in triplicate ($n = 6$). Three different lots of CDFBA gave mean values of 100.1, 99.6 and 101.2% with standard deviations of ± 0.55, ± 1.25 and ± 1.27%, respectively. The relative standard deviations ranged from ± 0.55 to ± 1.26%.

Typical separations for CDFBA impurities are presented in Figs. 3 and 4. Precision data for the determination of minor impurities were generated by two analysts performing the determinations replicately on three days ($n = 10$). Two lots of CDFBA were used. Assay values (mean weight% $\pm$ standard deviation) for lot 1 were: 2-C-3,4-DFBA = 0.32 ± 0.023; 3,4-DFBA = 0.03 ± 0.003; 4-CBA = 0.11 ± 0.0068; 4-C-2,3-DFBA = 0.11 ± 0.012. Assay values (mean weight% $\pm$ standard deviation) for lot 2 were: 2-C-3,4-DFBA = 0.31 ± 0.023; 3,4-DFBA = 0.06 ± 0.007; 4-CBA = 0.11 ± 0.0063; 4-C-2,3-DFBA = 0.20 ± 0.0084. Relative standard deviations ranged from ± 4.3% to ± 12% for these lots of commercially produced CDFBA. Known minor impurities were determinable to at least 0.03% by the method.

The authors thank Prof. G. Hägele for interpreting the ^{13}C NMR spectra, D.C.G. Plein for development of the preparative LC method, and Ms. D. Horgen for her assistance in preparation of the manuscript.

REFERENCES

1 D.T.W. Chu, C.W. Nordeen, D.J. Hardy, R.N. Swanson, W.J. Giardina, A.G. Pernet and J.J. Plattner, J. Med. Chem., 34 (1991) 168.
2 S.E. Hagen, J.M. Domagala, C.L. Heifetz and J. Johnson, J. Med. Chem., 34 (1991) 1155.
3 W. Xiao, R. Krishnan, Y.I. Lin, E.F. Delos Santos, N.A. Kuch, R.E. Babine and S.A. Long, Jr., J. Pharm. Sci., 78 (1989) 585.
4 S. Coppi, A. Getti and S. Caldari, J. Chromatogr., 395 (1987) 159.
5 C. Guinchard, J. Masson, T. Truong and M. Porthault, J. Liq. Chromtogr., 5 (1982) 1123.
6 D. Pietrzyk, Z. Iskondorani and G. Schmitt, J. Liq. Chromatogr., 9 (1986) 2633.
7 A. Sugii, K. Harada and N. Obawa, J. Chromatogr., 354 (1986) 211.
8 L. Pohiti, M. Moiggi, R. Nicoletti and J. Scandurra, J. Chromatogr., 267 (1983) 403.
9 K. Naikwadi, S. Rokushika and H. Hetano, Chromatographia, 18 (1984) 633.
10 R. Bowman, J. Chromatogr., 285 (1984) 467.
11 K. Stetzenbach, S. Jensen and G. Thompson, Environ. Sci. Technol., 16 (1982) 250.
12 Y. Arai, M. Hirokawa, J. Hanai, J. Chromatogr., 400 (1987) 27.
13 G.M. Sheldrick, SHELXS76, Program for Crystal Structure Determination, University of Cambridge, 1976.
14 TEXSAN, Structure Analysis Package, Molecular Structure Co., 1985.

Analytica Chimica Acta, 280 (1993) 93–101
Elsevier Science Publishers B.V., Amsterdam

Efficient determination of the pK_a values of six chlorinated phenols by reversed-phase liquid chromatography

P. Chaminade, A. Baillet and D. Ferrier

Laboratoire de Chimie Analytique III, Faculté de Pharmacie, 1 Avenue Jean-Baptiste Clément, F-92296 Chatenay-Malabry Cedex (France)

B. Bourguignon and D.L. Massart

Fakulteit Geneeskunde en Farmacie, Farmaceutisch Instituut, Dienst Farmaceutische en Biomedische Analyse, Laarbeeklaan 103, B-1090 Brussels (Belgium)

(Received 8th February 1993)

Abstract

A non-linear regression algorithm is used to compute acidity constants from capacity factors recorded at various pH values using a standard reversed-phase column and acetonitrile as organic modifier. An application is presented for six chlorophenols and the pK_a values calculated for those compounds compare favourably with literature data obtained by other methods in aqueous media. This pK_a determination method is also suitable for mobile phase optimization; a resolution map based on pK_a values from the literature and liquid chromatography-related pK_a values is presented.

Keywords: Liquid chromatography; Acidity constants; Chlorophenols; Mobile phase optimization

In reversed-phase liquid chromatography (RPLC), the retention of a weak acid or base is a function of both the ionized and non-ionized species of the compound [1]. Consequently, the optimization of chromatographic selectivity can be achieved by taking into account the ionization constants and the capacity factors of the ionized and non-ionized forms of the analytes [2]. As the chromatographic selectivity is linked to the solute capacity factor ratio, the accuracy of pK_a determination in an aqueous–organic mobile phase plays a major role in the prediction of the optimum location. pK_a determination is usually realized by potentiometric titrations or spectrophotometric measurements in aqueous or aqueous–alcoholic mixtures. However, such methods require relatively large amounts of pure substance. Consequently, they are unsuitable for determining the ionization constants of all the compounds in the small amounts of samples used in LC. The theoretical basis of pK_a determination using LC measurements were proposed by Horváth et al. [1], who demonstrated the ability of curve fitting to determine pK_a values from capacity factors recorded at different pH. A recent study [3] dealt with pK_a determination of chlorinated phenols in LC using methanol–water mobile phases but used a graphical method for acidity constant calculation.

Correspondence to: P. Chaminade, Laboratoire de Chimie Analytique III, Faculté de Pharmacie, 1 Avenue Jean-Baptiste Clément, F-92296 Chatenay-Malabry Cedex (France).

This paper reports the results obtained with a computer program designed to compute acidity constants from LC measurements. This program is part of a software package developed for mobile phase optimization which requires pK_a values of each ionizable compound in a mixture. The pK_a determination procedure is similar to previously published methods [1,3] and uses a numerical method for the calculation of pK_a values. As the aim of optimization procedures is to minimize the number of experiments, the purpose is to demonstrate that pK_a values can be determined with good precision from a limited number of data points.

THEORETICAL BACKGROUND

Influence of pH on capacity factor

An equation expressing the dependence between the capacity factor of a weak acid and the mobile phase pH was proposed by Horváth et al. [1]:

$$k'(\mathrm{pH}) = \frac{k'_{(\mathrm{AH})} + k'_{(\mathrm{A}^-)}\dfrac{K_a}{[\mathrm{H}^+]}}{1 + \dfrac{K_a}{[\mathrm{H}^+]}} \qquad (1)$$

where $k'_{(\mathrm{AH})}$ is the capacity factor of the molecular species AH, $k'_{(\mathrm{A}^-)}$ is the capacity factor of the ionized species A^-, K_a is the acidity constant of the corresponding acid base equilibrium $AH \rightleftharpoons A^- + H^+$ and $[H^+]$ is the concentration of the solvated proton in the mobile phase.

As the quantities K_a and $[H^+]$ are usually small, the following form [4] of the Eqn. 1 is more practical to link the capacity factor k' of an ionizable compound and the pH of the mobile phase:

$$k'(\mathrm{pH}) = \frac{k'_{(\mathrm{AH})} + k'_{(\mathrm{A}^-)}10^{(\mathrm{pH}-pK_a)}}{1 + 10^{(\mathrm{pH}-pK_a)}} \qquad (2)$$

A similar equation can be developed for a base B considering the BH^+–B system:

$$k'(\mathrm{pH}) = \frac{k'_{(\mathrm{BH}^+)} + k'_{(\mathrm{B})}10^{(\mathrm{pH}-pK_a)}}{1 + 10^{(\mathrm{pH}-pK_a)}} \qquad (3)$$

TABLE 1

Values of pK_s, pK'_s and ϵ for common LC solvents [6]

Solvent	pK_s	pK'_s	ϵ
Acetonitrile	−5.00	−9.00	36.2
Methanol	−1.2	−1.5	32.6
Tetrahydrofuran	5.0	−2.1	7.40

pH scale in organic solvents and solvent mixtures

In contrast to water, the pH range of a solvent varies according to its own acidity or basicity. The difference of the pH scale in organic solvents compared with pure water is quantified by the parameters pK_s and pK'_s, where pK_s expresses the extension to more basic pH and pK'_s that to more acidic pH.

The pH range of a solvent s with respect to water, whose pK_i is equal to 14.0, can be written as

$$pK_{i_{(S)}} = pK_{i_{(H_2O)}} - (pK_s + pK'_s) \qquad (4)$$

For a solvent mixture the pK_i will be

$$pK_{i_{(m)}} = \sum_{j=1}^{n} \phi_j pK_{i_j} \qquad (5)$$

where ϕ_j is the volume fraction of the component j.

The values of pK_s and pK'_s for the commonly used LC solvents are summarized in Table 1 together with the dielectric constant ϵ which expresses the dissociating ability of the solvent.

Non-linear regression algorithm

The Marquardt–Levenberg algorithm is used to fit parameters from Eqn. 2. This non-linear regression algorithm is considered as a standard method of data modelling [5] and is especially convenient when the partial derivatives with respect to the fitted parameters can be calculated (see Appendix for details).

Starting from initial values of k'_{AH}, k'_{A^-} and pK_a, the algorithm proceeds while minimizing the weighted chi-squared (χ^2), where χ^2 represents the sum of the square of differences between experimental k' values and k' values calculated from Eqn. 2. Each difference is divided by the experimental error σ.

χ^2 can be expressed as

$$\chi^2 = \sum_{i=1}^{n} \left[\frac{k_i' - k'(\mathrm{pH}_i)}{\sigma_i} \right]^2 \quad (6)$$

The σ weighting is especialy interesting since it allows the influence of experimental error on the calculation of parameters in Eqn. 2 to be minimized. In RPLC, the experimental error σ can be approximated easily, considering that the measurement of retention times can be assumed to be accurate and reproducible within a capacity factor range of about 1–10. Consequently, σ can be approximated according to the following rule:

if $1 < k_i' < 10$ then $\sigma_i = 0.01 k_i'$

else $\sigma_i = 0.05 k_i'$

Contraints due to organic modifiers

The three organic modifiers commonly used in RPLC are methanol, acetonitrile and tetrahydrofuran (THF). Among these, methanol appears to be the most valuable for pK_a determination as its behaviour is similar to that of water with respect to acids and bases [6]. Consequently, pK_s and pK_s' are weak and its pK_i is near the value of water, as shown in Fig. 1, which represents the pH scale for several volume fractions of methanol.

Acetonitrile, which is often used in LC, exhibits a more complex behaviour towards the acid–base systems. Acetonitrile appears to be an aprotic solvent with a high dielectric constant in which acids and bases are not completely dissociated [7]. This solvent is slightly acidic and slightly basic so $K_i \approx 10^{-20}$ [6]. The values of pK_s and pK_s' imply some important pK_a differences from the values observed in water. The acid–base phenomena are complicated by the slow transformation of the solvated hydrogen ion $[H^+,CH_3CN]$ and by the weak solvation of the anionic species. In the same way, the more strongly basic species in acetonitrile should be $[CH_3CN^-]$ while $[NC–CH_2–C(CH_3)N^-]$ is formed.

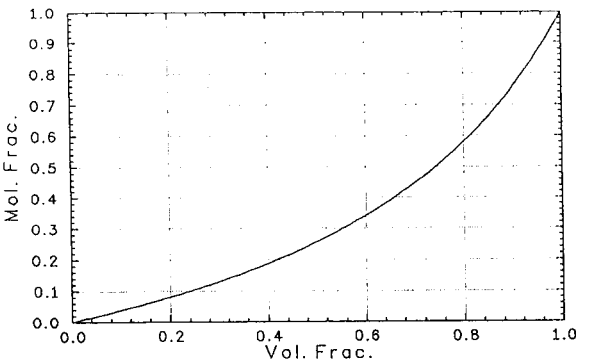

Fig. 2. Mole ratio vs. volume fraction of acetonitrile in water.

However, in the specific case of acetonitrile–water mixtures which are usually used as mobile phases, Fig. 2 shows that acetonitrile has the largest molar fraction above a volume fraction of 0.75. This suggested that the pH will be mainly governed by the H_3O^+–OH^- system until a volume fraction of 0.75 is reached. Consequently, the solvent mixture will be comparable to water despite its pK_s and pK_s' values (Fig. 3).

THF is a slightly dissociating solvent ($\epsilon = 7.6$). It is very weak acid but some very basic pH values

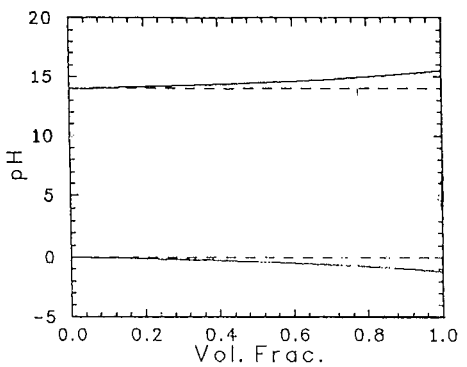

Fig. 1. pK_i for methanol–water mixtures.

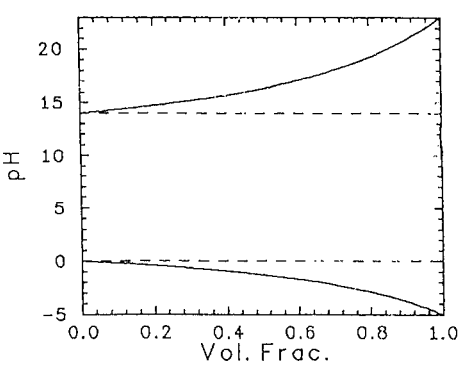

Fig. 3. pK_i for acetonitrile–water mixtures.

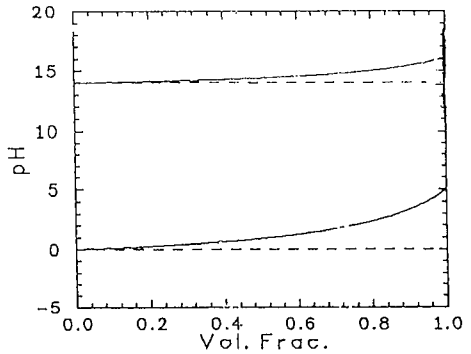

Fig. 4. pK_i for THF–water mixtures.

can be attained (fig. 4). This property is of little interest in the specific case of LC where the apparatus is not resistant to extreme pH values.

EXPERIMENTAL

The programming and calculations of acidity constants were done with a Chronosoft 486-33 IBM-AT compatible microcomputer with built-in math coprocessor. The computer program is written in Pascal using Borland's Turbo Pascal.

Measurements were made with a Varian Model 5000 liquid chromatograph equipped with a Rheodyne injection valve (5-μl sample loop). Detection at 260 nm was effected with a Shimadzu SPD-2A UV detector. The attenuation was set at 0.04 a.u.f.s. The chromatograms were recorded with a Spectra-Physics SP 4290 integrator. The column used was LiChrospher RP-18 (250 × 4 mm i.d.) from Merck with a particle size of 5 μm. The flow-rate was maintained at 1 ml min^{-1}. During chromatography, the column temperature was maintained at 30°C with a Prolabo Sup-Rs Stabitherm column thermostat. pH measurements of buffer solutions were made with a Corning model 240 pH meter.

All chlorophenols were of reference grade and were obtained from Aldrich. Standard solutions of ca. 300 mg l^{-1} were prepared in the mobile phase. Acetonitrile of LC gradient quality was purchased from Distrilab. The water used was purified in a Milli-Q system (millipore). Sodium dihydrogenphosphate, phosphoric acid, citric acid, trisodium citrate and sodium hydroxide of analytical-reagent grade were obtained from Prolabo.

Citrate and phosphate buffers of pH 3, 4, 5, 5.5, 6, 6.5, 7 and 7.5 and ionic strength 0.05 mol l^{-1} were prepared with purified water. The electrode was calibrated with standard solutions of pH 4 and 7. After adjusting the pH, the buffers were filtered through a 0.45-μm Millipore filter under vacuum. At each pH value, stoichiometric mixtures of the two buffers were applied.

The measurements were made at 30°C with six chlorophenols at pH values ranging from 3 to 7.50 using a classical analytical column. The pH was fixed using a phosphate–citrate buffer; the acetonitrile concentration in the mobile phase was 38% for 2,3,6- and 2,4,6-trichlorophenol and 48% for other chlorophenols. The limits of pH were chosen with respect to the stability of the column packing.

RESULTS AND DISCUSSION

The acidity constants calculated for compounds **1**, **2**, **4**, **5** and **6** (Table 2) are close to

TABLE 2

Literature data and pK_a values for six chlorophenols.

No.	Compound	Literature values	LC [3]	LC (ACN) [a]
1	2,3,6-Trichlorophenol	5.8 [11], 5.90 [8]	6.10	5.89 ± 0.012
2	2,4,6-Trichlorophenol	6.20 [9], 5.99 [8]	6.51	6.05 ± 0.441
3	2,3,4,5-Tetrachlorophenol	5.64 [11], 5.64 [9]	5.92	6.23 ± 0.014
4	2,3,4,6-Tetrachlorophenol	5.22 [10], 5.22 [8]	5.53	5.20 ± 0.009
5	2,3,5,6-Tetrachlorophenol	5.01 [11], 5.03 [8]	5.76	5.05 ± 0.011
6	Pentachlorophenol	4.74 [8]	4.93	4.59 ± 0.012

[a] ACN = acetonitrile

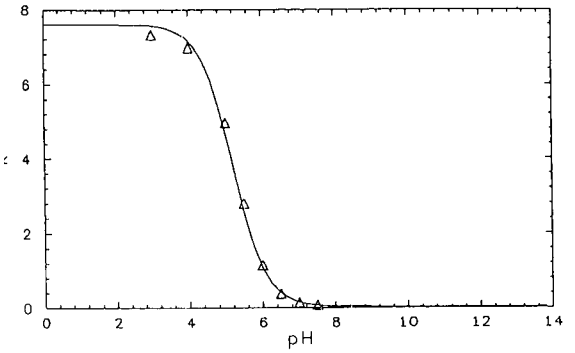

Fig. 5. k' vs. pH curve for 2,3,4,6-tetrachlorophenol.

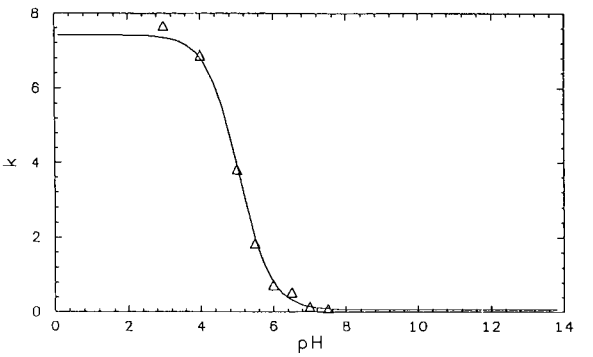

Fig. 7. k' vs. pH curve for 2,3,5,6-tetrachlorophenol.

literature values obtained by UV spectrophotometric [8] or potentiometric measurements [9–12] with a relative error of less than 2%. The calculation accuracy is about 0.01 pH unit for most compounds, which indicates a good quality (see Figs. 5–10). However, with a relative error of about 11%, the pK_a value calculated for the 2,3,4,5-tetrachlorophenol (**3**) is significantly different from the published values [9,11].

Compared with literature data, Horváth et al. [1] reported a relative error of 5% for three of four monofunctional acids. This difference was ascribed to the high ionic strength of the mobile phase ($I = 3$ due to 1 M Na_2SO_4), whereas literature data refer pure water ($I = 0$). In this work, the ionic strength is substantialy lower since it varies between 0.05 and 0.20 given the pH of the mobile phase. This allows a more direct comparison of the present pK_a values with water-related literature data, despite the possible effect of the ionic strength of the retention of both the ionized and non-ionized species [1,4].

An important difference from literature data was also noted by Horváth et al. [1] for one of the four monofunctional acids. However, for this compound, the LC-determined pK_a agrees with the value obtained from potentiometric measurements in the mobile phase. In this work, owing to the high buffering capacity between pH 3 and 7 of the phosphate–citrate buffer used in the mobile phase, such a procedure could not be applied to verify the ionization constant of **3**. This difference is difficult to explain, especially as this behaviour was not reported by Li et al. [3] using methanol as mobile phase and a graphical pK_a determination. Moreover, according to the ionization constants that they compiled, the pK_a value of **3** should lie between 5.64 and 6.96.

As the study by Li et al. [3] was done at 20°C, and other literature data were obtained at 25°C,

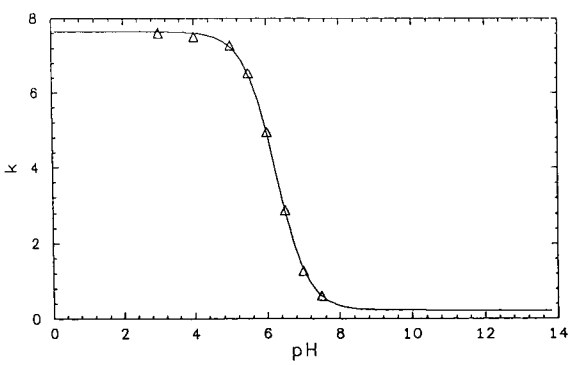

Fig. 6. k' vs. pH curve for 2,3,4,5-tetrachlorophenol.

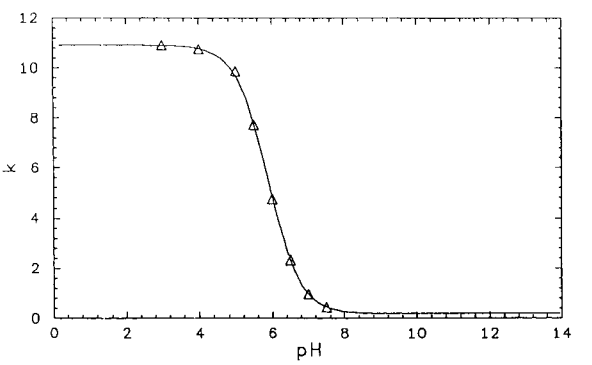

Fig. 8. k' vs. pH curve for 2,3,6-trichlorophenol.

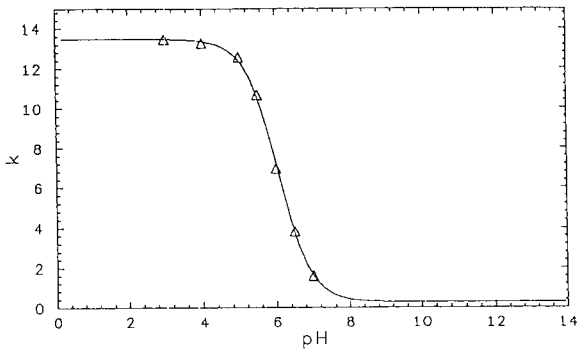

Fig. 9. k' vs. pH curve for 2,4,6-trichlorophenol.

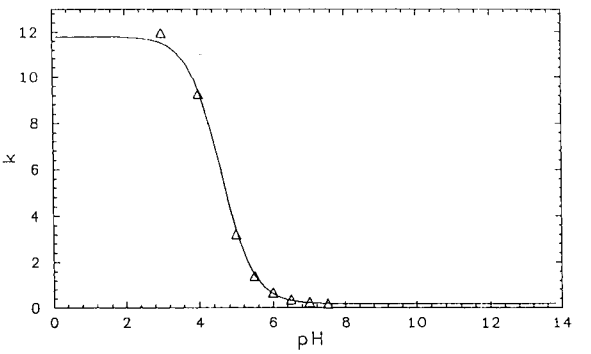

Fig. 10. k' vs. pH curve for pentachlorophenol.

the pK_a dependence on temperature may be corrected assuming that the pK_a of phenol decreases by 0.012 pH unit for a temperature rise of 1°C [13]. Under those conditions, each pK_a value in this study must be increased by 0.06 pH unit for comparison with the data in [8–11] and by 0.12 pH unit for comparison with the data in [3]. The revised data are summarized in Table 3. This temperature correction does not reduce the deviation from the literature and LC-determined pK_a values. Moreover, the pK_a values determined in this study are about 5% lower than values given in [3] for a methanol–water mobile phase. Li et al. [3] explained the deviation between their measurements and literature data by the difference in the dielectric constants in water alone in the aqueous alcoolic mobile phase leading to a systematic overestimation of pK_a values. The pK_a values obtained in methanol–water mobile phase must then be corrected to agree with those relative to water alone.

In this study, the difference between LC-determined pK_a values and literature data is randomly distributed. Consequently, despite the characteristics of acetonitrile with regard to methanol for acid–base equilibrium, it seems that the results obtained on the restricted set of compounds in this work are closer to those reported for aqueous solutions than LC measurements performed in methanol–water mobile phases. This tends to confirm the previous asumption made about the acid–base phenomena in acetonitrile–water mixtures which may have a behaviour comparable to that of water alone with volume fractions of acetonitrile less than 0.75. It should be pointed out that this hypothesis is proposed only for the specific case of the capacity factor vs. pH relationship in LC.

Likewise, the non-linear regression allows the preceding relationship to be modelled in a sufficiently accurate way whereas the analytical column used does not allow to a pH to be reached

TABLE 3

Temperature-corrected pK_a values

No.	Literature values (aqueous)	25°C correction LC (ACN–H_2O) [a]	LC [3] (MeOH–H_2O)	20°C correction, LC (ACN–H_2O) [a]
1	5.8 [11], 5.90 [8]	5.95	6.10	6.01
2	6.20 [9], 5.99 [8]	6.11	6.51	6.17
3	5.64 [11], 5.64 [9]	6.29	5.92	6.35
4	5.22 [10], 5.22 [8]	5.26	5.53	5.32
5	5.02 [11], 5.03 [8]	5.11	5.76	5.17
6	4.74 [8]	4.65	4.93	4.71

[a] ACN = acetonitrile.

where the ionized or non-ionized form of the compound is fully obtained. It is emphasized that this kind of procedure is less influenced by the data point spacing in the neighbourhood of the pK_a value than the graphical methods. For example, if the graphical derivative procedure is used to calculate the pK_a value from the k' vs. pH plot, a data point spacing of 0.10 pH unit near the pK_a value is needed to approximate it with the same precision. On the contrary, with non-linear regression methods, the precision will depend on the description of the whole curve which allows the use of a set of equally spaced data points. Consequently, if data points are well distributed along the k' vs. pH curve, an adequate guess of the three parameters in Eqn. 2 can be obtained with a minimum number of measurements.

This allows this method to be used for rapid optimization of the mobile phase pH, suitable even if the absolute pK_a values are unknown. According to Foley and May [2], four capacity factors recorded at four different pH values are sufficient to determine the parameters k'_{A^-} and k'_{AH} with an a priori knowledge of the solute pK_a using a graphical transformation of Eqn. 2. This number of four data points is also the minimum needed in the Marquardt algorithm to fit a three-parameter equation. Table 4 shows that the present algorithm allow these two parameters and the solute pK_a in the mobile phase to be estimated with this restricted number of data points. The pK_a values so obtained differ by 0.10 unit compared with those calculated from eight measurements. Also, the difference in the values of the parameters k'_{A^-} and k'_{AH} compared with values obtained from eight measurements are not significant.

Finally, to illustrate the importance of the use of LC-determined pK_a values mobile phase optimization, two resolution maps were constructed in the separation of the tetra- and pentachlorinated phenols (compounds **3**, **4**, **5** and **6**) using the pK_a values from the literature and those previously calculated. The chosen optimization criterion was the TC-CNRP from Drouen et al. [14], which accounts for the overall resolution and the analysis time. This criterion also accounts for the presence of an unretained peak in the chromatogram by including the resolution between the first peak and a hypothetical peak located at the column dead time. The dependence between capacity factors and the acetonitrile content of the mobile phase was established using the classical log-linear model [15,16] for both parameters k'_{A^-} and k'_{AH} according to the following equations:

$$\ln k'_{A^-}(\varphi) = \ln k_{w_{A^-}} - S_{A^-}\varphi$$

$$\ln k'_{AH}(\varphi) = \ln k_{w_{AH}} - S_{AH}\varphi \qquad (7)$$

where $\ln k_w$ refers to the logarithm of the hypothetical value of the solute capacity factor for an aqueous mobile phase, φ is the volume fraction of organic modifier, S is the slope of the relationship and the subscripts A^- and AH refer to the ionized and non-ionized form of the same compound, respectively.

As shown in Fig. 11 the optimum location differs according to the source of the pK_a values. For Fig. 11A, constructed from literature values,

TABLE 4

Parameters of Eqn. 2 obtained from four or eight measurements

No.	LC (ACN) [a], 8 measurements			LC (ACN) [a], 4 measurements, pH = 3, 5, 6, 7.5		
	pK_a	k'_{AH}	k'_{A^-}	pK_a	k'_{AH}	k'_{A^-}
1	5.89 ± 0.012	10.91 ± 0.116	0.19 ± 0.016	5.86 ± 0.014	11.04 ± 0.117	0.20 ± 0.011
2	6.05 ± 0.441	13.47 ± 0.191	0.28 ± 0.06	5.99 ± 0.013	13.61 ± 0.18	0.40 ± 0.04
3	6.23 ± 0.014	7.65 ± 0.112	0.22 ± 0.023	6.25 ± 0.016	7.64 ± 0.107	0.22 ± 0.01
4	5.20 ± 0.009	7.60 ± 0.115	0.04 ± 0.002	5.25 ± 0.010	7.49 ± 0.107	0.04 ± 0.002
5	5.05 ± 0.011	7.41 ± 0.12	0.06 ± 0.003	4.98 ± 0.011	7.73 ± 0.11	0.06 ± 0.002
6	4.59 ± 0.012	11.78 ± 0.21	0.18 ± 0.005	4.58 ± 0.011	12.01 ± 0.196	0.16 ± 0.004

[a] ACN = acetonitrile.

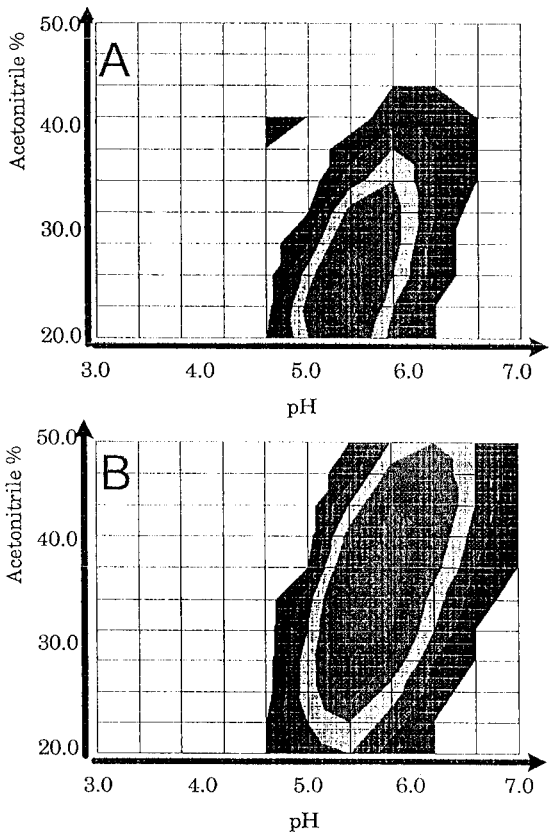

Fig. 11. Resolution map for compound **3**, **4**, **5** and **6**. (A) pK_a from literature; (B) LC-measured pK_a.

the optimum location is ($\varphi \approx 0.25$, pH ≈ 5.3), whereas the optimum appears to lie in a wider area centred at ($\varphi \approx 0.37$, pH ≈ 5.7) using the LC-determined pka (Fig. 11B).

Conclusion

The advantages of LC for the determination of acidity constants, such as the small amount of sample needed and the possible use of impure compounds, have been pointed out recently [3]. However, LC takes longer than the classical potentiometric or UV, spectrophotometric determinations because of the numerous mobile phases needed and the equilibration time that ensues. Therefore, the use of a numerical method such as the application of the Marquardt–Levenberg algorithm allows an acceptable precision to be achieved with a set of less than ten equally spaced data points. Moreover, this method also permits the simultaneous measurement of capacity factors for a set of compounds that exhibit similar retention characteristics, i.e., a quicker determination of their acidity constants. It is believed that the use of LC-related methods in pK_a determinations, will grow in the future. With some restrictions concerning the ionic strength and the organic content of the mobile phase, LC-determined pK_a values appear to be comparable to literature data. This, in addition with the previous considerations about solute purity and sample amount, enables this method to be of particular interest for the determination of the pK_a values of metabolites and biogenic compounds.

In the field of mobile phase pH optimization, pK_a determination by LC is usefull even if pK_a values are known from the literature and/or compounds are available in high purity. This method provides pK_a values in the mobile phase and allows the capacity factors of the ionized and non-ionized forms of the compound to be calculated.

The authors thank J.R. Desmurs and F. Marcenac (Centre de Recherches des Carrières, Rhône-Poulenc Recherches, Saint-Fons, France) for valuable technical help and extensive comments on this work.

APPENDIX

Partial derivative forms of Eqn. 2 with respect to the parameters k'_{AH}, k'_{A^-} and pK_a

$$k'_{pH} = \frac{k'_{AH} + k'_{A^-}10^{(pH-pK_a)}}{1 + 10^{(pH-pK_a)}} \quad (2)$$

Partial deriative with respect to k'_{AH}:

$$\frac{\partial k'_{pH}}{\partial k'_{AH}} = \frac{1}{1 + 10^{(pH-pK_a)}}$$

Partial derivative with respect to k'_{A^-}:

$$\frac{\partial k'_{pH}}{\partial k'_{A^-}} = \frac{10^{(pH-pK_a)}}{1 + 10^{(pH-pK_a)}}$$

Partial deriative with respect to pK_a:

$$\frac{\partial k'_{pH}}{\partial pK_a} = \frac{(k'_{AH} - k'_{A^-}) \ln(10) \times 10^{(pH - pK_a)}}{[1 + 10^{(pH - pK_a)}]^2},$$

Development of pK_a derivative

Let

$$pH - pK_a = u$$

Hence

$$\frac{\partial u}{\partial pK_a} = u' = \frac{\partial(pH - pK_a)}{\partial pK_a} = -1$$

and

$$\frac{\partial 10^u}{\partial pK_a} = \ln(10) \times u' \times 10^u = -\ln(10) \times 10^u$$

$$= -\ln(10) \times 10^{(pH - pK_a)}$$

Equation 2 can be expressed as

$$\frac{k'_{AH} + k'_{A^-} \times 10^u}{1 + 10^u} = \frac{f}{g}$$

Hence

$$\frac{\partial\left(\frac{f}{g}\right)}{\partial pK_a} = \frac{f'g - fg'}{g^2}$$

with

$$f = k'_{AH} + k'_{A^-} \times 10^u$$

$$f' = \frac{\partial f}{\partial pK_a} = -k'_{A^-} \ln(10) \times 10^u$$

$$g = 1 + 10^u \quad g' \frac{\partial g}{\partial pK_a} = -\ln(10) \times 10^u$$

which yields

$$\frac{\partial k'_{pH}}{\partial pK_a} = (-k'_{A^-} \ln(10) \times 10^u (1 + 10^u)$$

$$- (k'_{AH} + k'_{A^-} \times 10^u)[-\ln(10) \times 10^u])$$

$$\times \left((1 + 10^u)^2\right)^{-1}$$

$$= (\ln(10) \times 10^u (k'_{AH} + k'_{A^-} \times 10^u - k'_{A^-}$$

$$- k_{A^-} \times 10^u))\left((1 + 10^u)^2\right)^{-1}$$

$$= \frac{\ln(10) \times 10^u (k'_{AH} - k'_{A^-})}{(1 + 10^u)^2}$$

REFERENCES

1 C. Horváth, W. Melander and I. Molnár, Anal. Chem., 49 (1977) 142.
2 J.P. Foley and W.E. May, Anal. Chem., 59 (1987) 102.
3 S. Li, M. Paleologou and W.C. Purdy, J. Chromatogr. Sci., 29 (1991) 66.
4 P.J. Schoenmakers, Optimization of Chromatographic Selectivity (Journal of Chromatography Library, Vol. 35), Elsevier, Amsterdam, 1986, p. 71.
5 W.H. Press, B.P. Flannary, S.A. Teukolsky and W.T. Vetterling, Numerical Recipes in Pascal, Cambridge University Press, Cambridge, 1989, pp. 572–590.
6 G. Charlot and B. Trémillon, Les Réactions dans les Solvents et les Sels Fondus, Gauthier-Villard, Paris, 1963, pp. 303–305, 373–374, 438–439.
7 R.G. Bates, Determination of pH, Wiley-Interscience, New York, 1973, pp. 205–206.
8 J. Drahonovsky and Z. Vacek, Collect. Czech. Chem. Commun., 36 (1971) 3431.
9 A. Fisher, G.J. Leary, R.D. Thopsom and J. Vaughan, J. Chem. Soc. B, (1967) 686.
10 P.D. Bolton, J. Ellis and F.M. Hall, J. Chem. Soc. B, (1970) 1252.
11 K. Lyland, E. Lundanes and T. Greibhl, Chromatographia, 213 (1981) 83.
12 V.A. Dandali, B.V. PanChenks and L.M. Litrinenko, J. Org. Chem. USSR, 16 (1980) 1725.
13 A. Albert and E.P. Serjeant, The Determination of Ionisation Constants, Chapman and Hall, London, 1971, p. 7.
14 A.C.J.H. Drouen, P.J. Schoenmakers, H.A.H. Billiet and L. de Galan, Chromatographia, 16 (1982) 48.
15 P.J. Schoenmakers, H.A.H. Billiet and L. de Galan, J. Chromatogr., 185 (1979) 179.
16 L.R. Snyder, J.W. Dolan and J.R. Gant, J. Chromatogr., 23 (1979) 3.

Analytica Chimica Acta, 280 (1993) 103–109
Elsevier Science Publishers B.V., Amsterdam

Monitoring the mobile phase composition in supercritical fluid chromatography

Dongjin Pyo and Hoon Hwang

Department of Chemistry, Kangweon National University, Kangweon-do, Chuncheon 200-701 (South Korea)

(Received 15th November 1992; resubmitted 22nd January 1993)

Abstract

Adding additional components to supercritical CO_2 in supercritical fluid chromatography can extend or significantly alter the fluid solvating properties. Polar samples that are difficult to analyse using pure supercritical CO_2 because of their high polarity can be separated by adding polar modifiers to the supercritical CO_2. A method for monitoring the mobile phase composition in modified supercritical fluid chromatography is introduced. The amount of water or methanol dissolved in supercritical CO_2 was measured using an amperometric microsensor made of a thin film of perfluorosulphonate ionomer.

Keywords: Supercritical fluid chromatography; Mobile phase modification

The use of compressed (dense) gases and supercritical fluids as chromatographic mobile phases in conjunction with liquid chromatographic (LC)-type packed columns was first reported by Klesper et al. in 1962 [1]. During its relatively short history, supercritical fluid chromatography (SFC) has become an attractive alternative to GC and LC in certain industrially important applications. SFC gives the advantage of high efficiency and allows the analysis of non-volatile or thermally labile mixtures.

The density of the mobile phase in SFC is about 200–500 times that in gas chromatography. The effect of shorter intermolecular distances and the resulting increase in molecular interactions is an enhanced solubilizing capability of the solvent towards various solutes. Compounds with much higher molecular weights than gas chromatography normally allows can therefore be chromatographed. However, the most commonly used mobile phases in SFC are all relatively non-polar fluids. Carbon dioxide, the most widely used fluid, is no more polar than hexane [2], even at high densities. Solute polarity should be between that of the stationary phase and the mobile phase in order to have a well behaved separation. Few real samples contain only non-polar solutes, so a major objective of research in SFC has been directed toward increasing the range of solute polarity that can be handled by the technique. To bring the SFC technique into routine use, mobile phases that are more polar than the commonly used carbon dioxide are necessary.

The solvent strength of supercritical CO_2, even at high density, is not sufficient for the elution of polar solutes. Polar mobile phases such as NH_3 [4] exhibit useful properties, but a more practical way to extend the range of compounds separable by SFC is to use a mixed mobile phase. The solubility of the solute in the supercritical phase can be influenced considerably by adding modifiers to the mobile phase. The use of modifiers

Correspondence to: D. Pyo, Department of Chemistry, Kangweon National University, Kangweon-do, Chuncheon 200-701 (South-Korea).

has been reported by Jentoft and Gouw [3] and by Novotny et al. [4]. The latter group showed that adding 0.1% 2-propanol to pentane as the mobile phase decreases the observed partition coefficient (K) values for many polynuclear aromatic hydrocarbons by 20–35%. Thus, the addition of modifiers (generally organic solvents) to a supercritical mobile phase changes the polarity of the mobile phase and also leads to deactivation of the column packing material. In capillary SFC, most separations are made with pure CO_2 because of its compatibility with an flame ionization detection (FID); except for formic acid and water, the addition of any common modifier precludes the use of FID [5]. Modifiers are essential in packed-column SFC for the elution of polar compounds [6] and are extensively used.

Several workers [6–8] have reported the influence of modifiers on peak shape, selectivity and retention time in capillary and packed-column SFC. A simple and effective way to add modifiers to a supercritical fluid mobile phase is to use a saturator column [9,10], which is usually a silica column saturated with polar modifiers. The column is inserted between the pump outlet and the injection valve. During the passage of the supercritical fluid mobile phase through the silica column, polar modifiers can be dissolved in the pressurized supercritical fluid. A disadvantage with this system is that the amount of modifier dissolved in the mobile phase varies as the mobile phase passes through the saturator column as the modifier holding capacity of the silica column is limited. Therefore, the monitoring of the amount of polar modifiers dissolved in a supercritical fluid is essential. In this paper, a method for the accurate determination of modifiers in the mobile phase in modified SFC is introduced.

EXPERIMENTAL

A CCS (Computer Chemical Systems, Avondale, PA) Model 5000 supercritical fluid chromatograph was used with a 100 mm × 2 mm i.d. packed column (Nucleosil diol). This system was equipped with a C14W loop injector (Valco) and a flame ionization detector. SFC-grade carbon dioxide (Scott Specialty Gases) was used as a basic mobile phase. Experimental conditions for SFC separations are as follows: supercritical CO_2 at 150°C, pressure programmed from 27.58 to 34.47 MPa at 0.276 MPa min^{-1}, detector at 300°C and 10 ml min^{-1} restrictor flow-rate at 10.34 MPa. For the addition of modifiers to supercritical CO_2, a μPorasil column (250 mm × 4.6 mm i.d.) which is manufactured for normal-phase HPLC by Waters was used. Its functional group is a silanol (SiOH) group. The μPorasil column was saturated with modifiers using a Model 600 syringe pump (Lee Scientific) and placed between the pump and injector. To measure the amount of modifier dissolved in the supercritical fluid, an amperometric microsensor was designed and made of perfluorosulphonate ionomer (PFSI) [11]. A constant-current power supply (0.1 μA) (Sungeun, Seoul, South Korea) was used to measure the voltage drop across the sensor. The sensor output was recorded on a strip-chart recorder (Knauer). Figure 1 shows the cross-section of the modifier sensor used. Platinum wire was wrapped with PFSI thin film and another platinum wire was wound in a coil over the assembly. The sensor made in this way was placed in a plastic tube and the entire modifier measuring device was assembled as shown in Fig. 2.

RESULTS AND DISCUSSION

When modifiers are used with supercritical CO_2 in order to chromatograph more polar substances, the binary mixture of eluents can contaminate the instrument. Especially when water or formic acid is used as a modifier, the modifier remaining in a pump may cause corrosion of the pump, and when methanol is used as a modifier, methanol remaining in the pump can be eluted slowly during the next run. This may affect the time required to achieve chemical equilibrium for the subsequent separations, and also many modifiers can evaporate and contaminate the air in the laboratory. A good way to overcome these problems is to use a saturator column [9,10,12] to add polar modifiers to supercritical CO_2.

For the first experiment, water was used as a

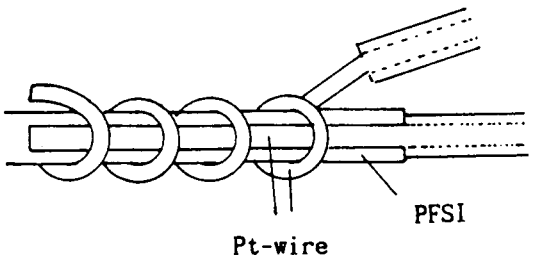

Fig. 1. Diagram of the modifier sensor.

modifier and a μPorasil column was used as a saturator column with system design similar to that described by Engelhardt et al. [9]. With this design, a polar modifier (water) can be added to pressurized CO_2 after the pump, and thus no modifier remains in the pump. Supercritical CO_2 is delivered from the pump to the μPorasil column which is saturated with water. When supercritical CO_2 passes through the μPorasil column, water molecules held on the OH groups of the μPorasil by hydrogen bonding can dissolve in the pressurized supercritical fluid. Thus non-polar supercritical CO_2 can have the characteristics of a polar mobile phase because it can absorb a polar solvent, i.e., water. Therefore, after passing through the μPorasil column, supercritical CO_2 is changed into a new mobile phase with different polarity, and it is possible to separate polar samples using this modified mobile phase.

Mixtures of insecticides and fungicides were analysed with this modified mobile phase (supercritical carbon dioxide–water phase) using a μPorasil column as saturator column. The chromatograms are shown in Figs. 3 and 4. As expected, good separations were obtained. When only CO_2 was used as a mobile phase with these samples, unseparated and very broad peaks were observed in about 25 min. The addition of a small amount of water to supercritical CO_2 decreased the retention time and improved the peak shapes. These results agree well with those reported by Engelhardt et al. [9], Schwartz et al. [10] and Blilie and Greibrokk [7]. The molecular struc-

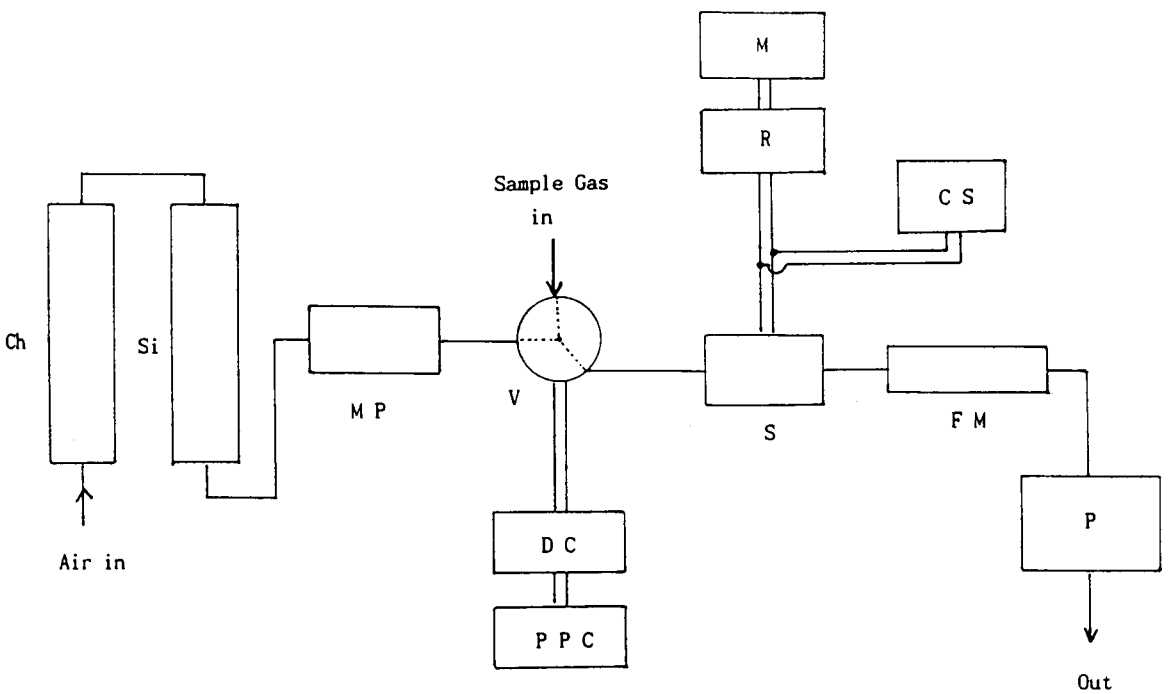

Fig. 2. Schematic diagram of the water content measuring device: P = pump; V = solenoid valve; S = sensor; FM = flow meter; MP = magnesium perchlorate; R = recorder; M = multimeter; DC = 12-V power supply; PPC = programmable process controller; Ch = charcoal; Si = silica gel; CS = current source.

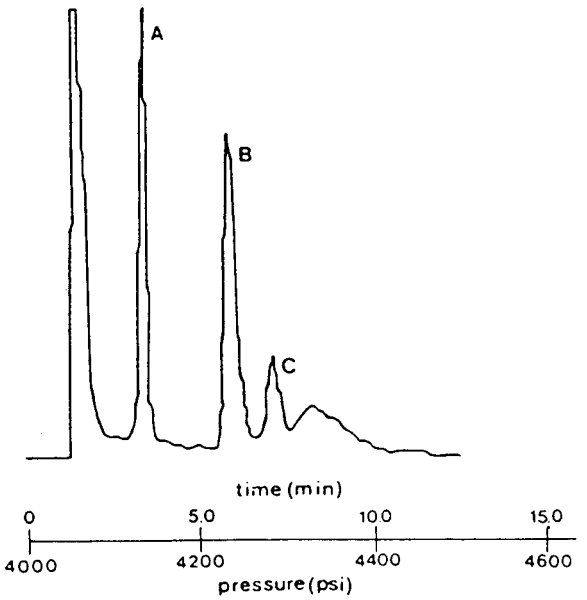

Fig. 3. Chromatogram of a mixture of insecticides and fungicides. Peaks: A = Thiolix; B = Kitazine; C = Captan.

tures corresponding to the peaks are shown in Table 1.

However, when dealing with the use of a saturator column, a serious problem always arises, namely the bad reproducibility of the amount of modifier dissolved in the supercritical CO_2. When the same experiments were repeated several times, it was very difficult to obtain reproducible results for the chromatograms as the amount of modifier in the mobile phase does not remain constant with time. For these reasons, it was decided to monitor the exact amount of modifier in the supercritical CO_2 mobile phase as a function of time. To measure the amount of water dissolved in supercritical CO_2 in the water-modified system, the PFSI polymer, film [9], which has a high affinity for water, was used. When the PFSI film was in contact with two electrodes and a constant current flowed through the film, the water that partitioned into the film from the surrounding environment was electrolytically de-

TABLE 1

Identification of peaks in the chromatograms

Chromatogram	Peak	Commercial name	Chemical name	Structure
Fig. 3	A	Thiolix (insecticide)	1,4,5,6,7,7-Hexachloronorborn-5-ene-2,3-dimethanol sulphide	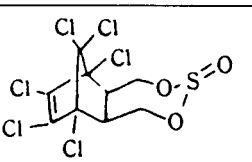
	B	Kitazine (fungicide)	*S*-Benzyl-*O*,*O*-diisopropyl phosphorothioate	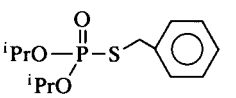
	C	Captan (fungicide)	*N*-(Trichloromethylthio)cyclohex-4-ene-1,2-dicarboximide	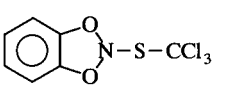
Fig. 4	A	Hinosan (fungicide)	*O*-Ethyl-*S*,*S*-diphenyl dithiophosphate	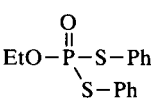
	B	Parathion (insecticide)	*O*,*O*-Diethyl-*O*-4-nitrophenyl phosphorothioate	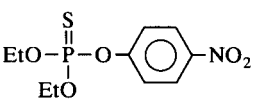
	C	DDVP (insecticide)	2,2-Dichlorovinyldimethyl phosphate	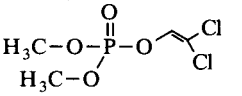

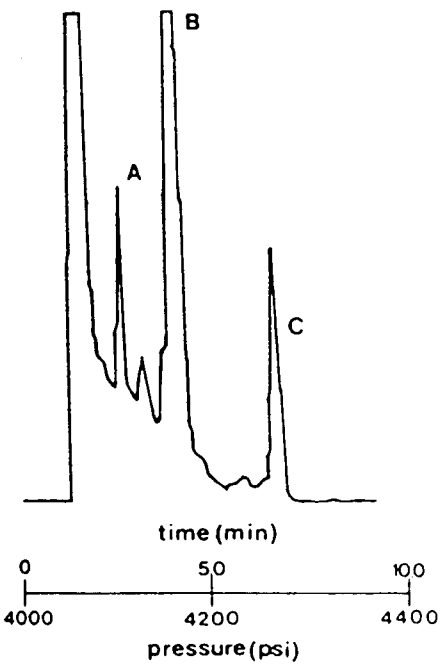

Fig. 4. Chromatogram of a mixture of insecticides and fungicides. Peaks: A = Hinosan; B = Parathion; C = DDVP.

composed. The change in voltage across the two electrodes was used as a measure of the water content of the environment surrounding the sensor. The resistance of the PFSI film changed according to the water content of the supercritical CO_2 fluid and the voltage difference between the two platinum wires was recorded.

As a control, air saturated with water was injected into the sensor at different time intervals. Air saturated with water was generated by bubbling air through water in two sequential bottles and was injected directly into the sensor through a three-way solenoid valve (Radio Shack). The results are shown in Fig. 5 and demonstrate that there is a good correlation between the voltage difference across the two electrodes of the sensor and the amount of water exposed to the sensor. Another parameter that affects the sensor response is the temperature of the environment surrounding the sensor. To consider the influence of temperature, Fig. 6 was obtained by measuring the sensor outputs with six different standard relative humidity streams at various temperatures. H_2SO_4 solutions of known composition [13] were used to generate the standard relative humidity streams.

Using the correlation of peak height and the percentage relative humidities at different temperatures (Fig. 6), the water content in supercritical CO_2 after passing through the μPorasil column saturated with water could be measured as a function of time (Fig. 7). Figure 7 shows that the amount of water in the mobile phase remained constant for about 35 min, but then decreased

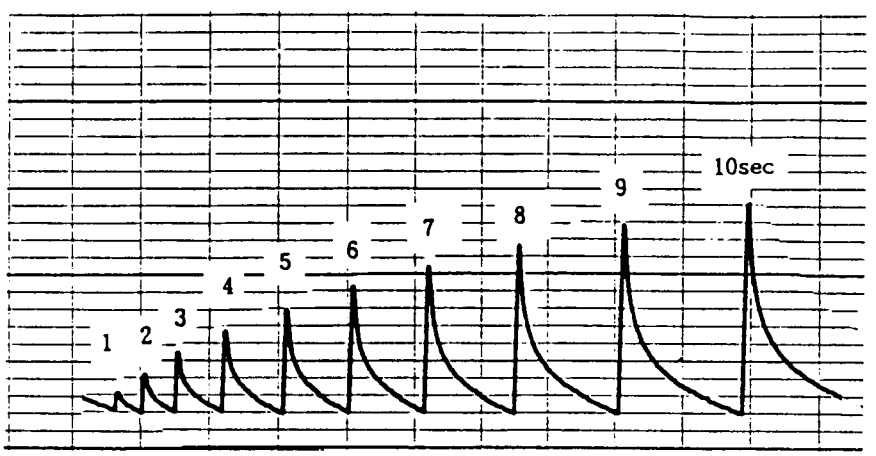

Fig. 5. Relative peak heights at different time intervals for air saturated with water. Flow-rate, 0.5 l min^{-1}; temperature, 20°C; ordinate scale, 200 mV cm^{-1}.

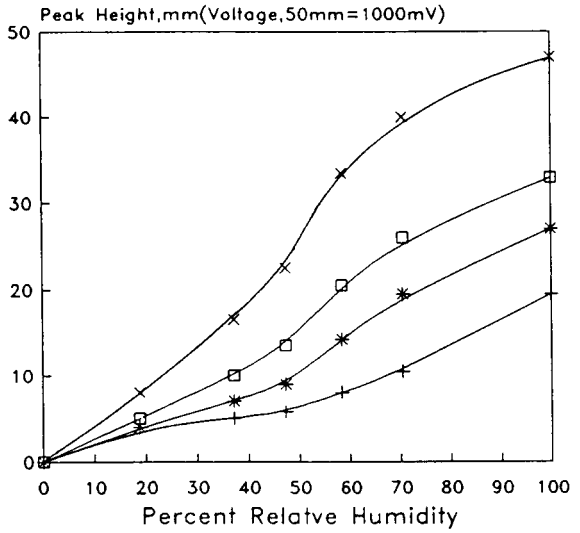

Fig. 6. Sensor response with various relative humidity levels (18.8, 37.1, 47.2, 58.3, 70.4 and 100%) at various temperatures: + = 10; * = 15; □ = 20; × = 25°C.

exponentially. This is, of course, because only limited amounts of water were held on the OH groups of the μPorasil. As supercritical CO_2 was passing through μPorasil column saturated with water, the fluid stripped water from the μPorasil and thus water held within the pores of the column was desorbed with time.

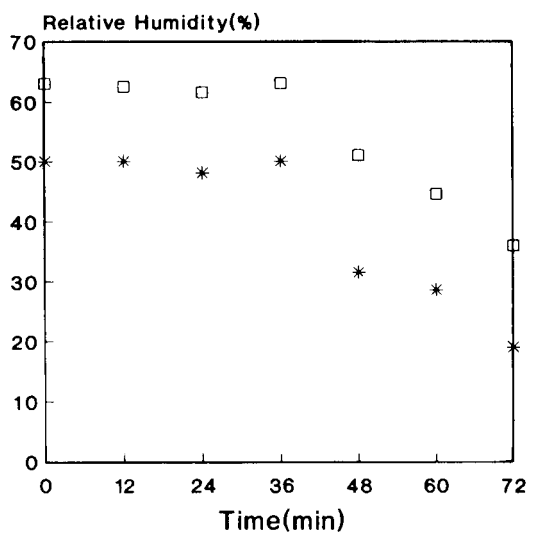

Fig. 7. Measurements of the water content in supercritical CO_2 as a function of time at (*) 100 and (□) 200 atm.

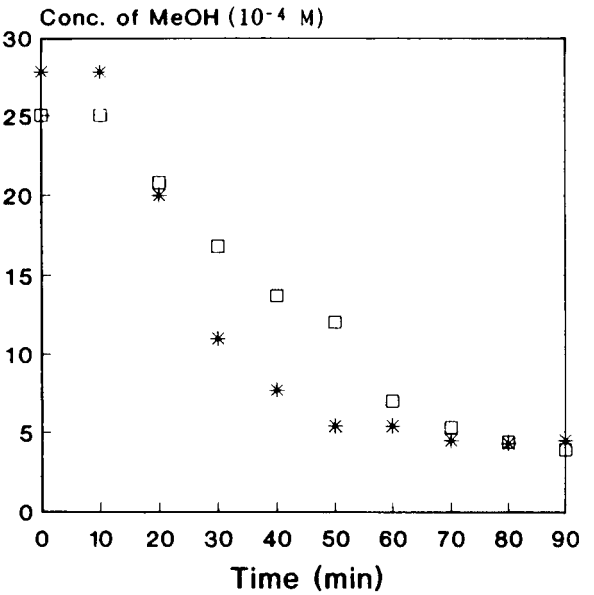

Fig. 8. Measurements of the methanol content in supercritical CO_2 as a function of time at (*) 100 and (□) 200 atm.

Another experiment was made using methanol as a modifier, in which the same μPorasil column and the same sensor were employed. The PFSI sensor is known to respond to alcohols in a way similar to water [11]. In this methanol-modified system using a saturator, the mobile phase composition could be monitored successfully in the same way. The results are shown in Fig. 8. With methanol, the time period during which a constant concentration of methanol was maintained in supercritical CO_2 was much shorter than that for water. The amount of methanol in the mobile phase remained constant for only 10 min and then decreased rapidly, probably because the solubility of methanol in supercritical CO_2 is greater than that of water [14].

Therefore, when a saturator column is used for addition of a modifier to carbon dioxide, it must be resaturated with modifier after a certain period of time. With the saturator column is used in this study, and using water as a modifier, the column must be resaturated with water every 35 min, and when methanol is used, it must be resaturated every 10 min to obtain reproducible separations. When methanol is used as a modifier, it is essential to maintain a constant level of

modifier in the mobile phase, otherwise it is almost impossible to obtain reproducible separations. A mixing device that can maintain the amount of modifier in the mobile phase constant for a much longer period is currently being developed.

This investigation was supported by a grant from the Korea Science and Engineering Foundation.

REFERENCES

1 E. Klesper, A.H. Corwin and D.A. Turner, J. Org. Chem., 27 (1962) 700.
2 C.R. Yonker, S.L. Frye, D.R. Lalkwarf and R.D. Smith, J. Phys. Chem., 90 (1986) 90, 3022.
3 R.E. Jentoft and T.H. Gouw, J. Chromatogr. Sci., 8 (1970) 138.
4 M. Novotny, W. Bertsch and A. Zlatkis, J. Chromatogr., 61 (1971) 17.
5 B.W. Wright and R.D. Smith, J. Chromatogr., 355 (1986) 367.
6 S. Schmidt, L.G. Blomberg and E.R. Campbell, Chromatographia, 25 (1988) 775.
7 A.L. Blilie and T. Greibrokk, Anal. Chem., 57 (1985) 2239.
8 C.R. Yonker and R.D. Smith, J. Chromatogr., 361 (1986) 25.
9 H. Engelhardt, A. Gross, R. Mertens and M. Petersen, J. Chromatogr., 477 (1989) 169.
10 H.E. Schwartz, P.J. Barthel, S.E. Moring, T.L. Yates and H.H. Lauer, Fresenius' Z. Anal. Chem., 330 (1988) 204.
11 H. Huang and P.K. Dasgupta, Anal. Chem., 62 (1990) 1935.
12 B.L. Karger, R.C. Castells, P.A. Sewell and A. Hartkopf, J. Phys. Chem., 75 (1971) 3870.
13 R.C. Weast (Ed.), CRC Handbook of Chemistry and Physics, CRC Boca Raton, FL, 70th edn., 1989, p. E-43.
14 B.A. Charpentier, in M.R. Sevenants (Ed.), Supercritical Fluid Extraction and Chromatography (ACS Symposium Series, No. 366), American Chemical Society, Washington, DC, 1987, p. 16.

Analytica Chimica Acta, 280 (1993) 111–117
Elsevier Science Publishers B.V., Amsterdam

Evaluation of the open-loop stripping technique used for the determination of volatile organic compounds in water

Nina K. Kristiansen

National Institute of Public Health, Department of Environmental Medicine, Geitmyrsvn. 75, N-0462 Oslo (Norway)

Elsa Lundanes

Department of Chemistry, University of Oslo, P.O. Box 1033, Blindern, N-0315 Oslo (Norway)

May Frøshaug and Georg Becher

National Institute of Public Health, Department of Environmental Medicine, Geitmyrsvn. 75, N-0462 Oslo (Norway)

(Received 4th December 1992; revised manuscript received 2nd February 1993)

Abstract

Open-loop stripping analysis (OLSA) was evaluated for the determination of volatile organic compounds that are often found as contaminants in drinking water produced offshore. The recoveries of alkylbenzenes, halogenated hydrocarbons, alkanes and some polar compounds were, in addition to their physico-chemical properties, also affected by the adsorbent filters, concentration level and storage conditions. Compounds with boiling points < 150°C showed significantly lower recoveries at the 1000 than at the 100 ng l^{-1} level. The within- and between-filter reproducibility were examined by using analysis of variance. A significant difference in recoveries was found for seven out of nine compounds for six adsorption filters with the same filter resistance. Using a single filter, the average precision for the determinations measured as standard deviation was about 4%. Water samples preserved with 1 g l^{-1} sodium azide could be analysed for purgeable components within 58 days without loss of compounds. The OLSA technique is simple, effective and suitable for concentrating volatile organic compounds present at levels down to ng l^{-1} in drinking water. However, for accurate determination care must be taken when the concentration of the contaminants in the samples varies greatly. Selection of adsorption filters for simultaneous parallel analysis also requires special precautions.

Keywords: Gas chromatography; Charcoal filters; Extraction; Volatile organic compounds; Waters

Open- and closed-loop stripping analysis (OLSA and CLSA, respectively) have been shown to be effective in concentrating relatively volatile organic contaminants from water matrixes at sub-μg l^{-1} levels [1,2]. The OLSA technique, with its flexibility, high sensitivity and low contamination level, has especially been applied to screening water quality for off-flavour problems [3,4]. A disadvantage of these methods is the often relatively high standard deviation that influences quantification. This is mainly caused by the variable stripping efficiency of organic compounds from the water and variable adsorption on and extraction from the charcoal filters [1,5–7].

The OLSA technique has recently been used for the examination of the quality of drinking water produced on offshore installations [8]. It was found that organic compounds leaking from

Correspondence to: N.K. Kristiansen, MATFORSK, Norwegian Food Research Institute, Osloveien 1, 1430 Ås (Norway) (present address).

coating materials in storage tanks and compounds formed during sea-water chlorination are the main causes of short-term variations in the water quality. Alkylated benzenes and brominated compounds were the main contaminants found in the tap water, with the first group being most important as a source of off-flavour problems.

In this work, the OLSA technique was used in combination with capillary gas chromatography (GC) with flame ionization detection (FID) and manual splitless injection. A sensitive, simple and rapid screening method which can easily be adopted by other laboratories was sought. In order to evaluate the method, the behaviour of compounds suspected of being present in this kind of water was examined with respect to recoveries and quantification. The concentration levels examined (100 and 1000 ng l^{-1}) correspond to the expected levels in the drinking water produced offshore. One of the critical steps in the analysis procedure is the choice of adsorbent filters [6]. To process a large number of samples in a reasonable time, it is necessary to operate parallel stripping systems using different filters. In the present study, the within- and between-filter reproducibilities were examined for different organic compounds using analysis of variance. The stability of selected compounds was examined in preserved and unpreserved water samples stored at 4°C over a 2-month period. The appropriateness of the OLSA technique as a reliable tool for screening the water quality offshore is discussed.

EXPERIMENTAL

Chemicals, reagents and glassware

All chemicals and reagents were of analytical-reagent grade. Carbon disulphide was of glass-distilled grade, obtained from Rathburn (Walkerburn, UK). Stock standard solutions of selected standards and internal standards of concentration 1 mg ml^{-1} were prepared in acetone by dissolving 50 mg of each compound in 50 ml; 100-fold dilutions in acetone or carbon disulphide were freshly prepared prior to use. Stock standard solutions were stored at 4°C. Glassware was cleaned with HCl and then successively rinsed with deionized water, ethanol and acetone. Nitrogen used for the enrichment procedure was purified with molecular sieves, charcoal and Tenax. For the open-loop stripping analysis, 1.5-mg charcoal filters (Bender und Hobein, Zurich, Switzerland) were rinsed with carbon disulphide and flushed with purified nitrogen prior to use. All filters used in the investigations had an identical filter resistance of 1.5 ml min^{-1} determined by measuring the time necessary for 0.6 ml of dichloromethane to flow through the filters by gravity.

Enrichment procedure

Open-loop stripping analysis (OLSA) has been described by Borén et al. [3]. Water samples (1 l) were purged with nitrogen (flow-rate 1 l min^{-1}) for 1.5 h at 60°C. The stripped organic compounds were trapped on an activated charcoal filter at 80°C. After concentration of the organic compounds, the filters were extracted three times with 10 μl of carbon disulphide.

Gas chromatography

A Perkin-Elmer Model 8320 gas chromatograph equipped with a flame ionization detector maintained at 250°C was used. Separations were achieved with a CP SIL 8 fused-silica capillary column (25 m × 0.32 mm I.D.; 0.4-μm film thickness) (Chrompack, Middelburg, Netherlands), using helium as carrier gas at a linear velocity of 25 cm s^{-1}. Volumes of 2 μl of the filter extracts were injected manually by splitless injection at 250°C. A temperature programme was operated from 50°C (5 min) to 250°C (5 min) at 5°C/min. Quantification was accomplished using peak-area ratios of the analytes and the internal standard.

Recovery studies

Carbon disulphide standard mixtures of the selected compounds were used for direct injection into the GC column to establish relative retention times and response factors for individual compounds. Ten or five replicate injections of the same standard solution were made and the average of the response factors was used for quantification. Acetone standard mixtures were

used for direct spiking of the water. To 1 l of laboratory tap water, 100 or 1000 ng of each compound in the standard mixtures were added, containing 200 ng of 1-chlorodecane as internal standard. OLSA was started immediately after mixing the spiked water samples. Relative recoveries were calculated with respect to the internal standard 1-chlorodecane; absolute recoveries were calculated with respect to 40 ng of 1-chloroctane (20 ng μl^{-1}) added to the carbon disulphide extracts [1]. Procedural blanks of the analytical charcoal filter and OLSA blanks of the water were determined before analysis. The contribution of components was negligible and correction was not necessary. Breakthrough loss was examined by connecting two filters in series and calculated as absolute recoveries.

Between- and within-filter variations

Relative recoveries were determined in triplicate for nine compounds using six different charcoal filters. From these data an analysis of variance (ANOVA) was performed utilizing the JMP software program (SAS Institute, Cary, NC).

Stability study

A 200-ng amount of each standard was added to 1 l of water. Sodium azide (1 g l^{-1}) was added to half of the samples to retard bacterial growth. The samples were sealed with glass stoppers and stored at 4°C with about a 200-ml headspace. Analyses were performed on days 0, 3, 7, 17, 28 and 58. Prior to analysis, 200 ng of 1-chlorodecane was added as an internal standard to correct for losses during storage, the enrichment procedure and analysis.

RESULTS AND DISCUSSION

Recovery studies

The relative response factors (RRFs) of the compounds examined were determined using ten or five consecutive 50-ng injections. Table 1 gives the RRFs with the analyses grouped into different chemical classes. The average relative standard deviation (R.S.D.) for the RRFs was 3.4%, which reflects an acceptable precision for this injection technique [9,10]. The observed variable FID responses between and within compound groups have been discussed previously [11], and demonstrate the need for the determination of the individual response factors for reliable quantitative analysis.

TABLE 1

FID relative response factors (RRF) (relative to 1-chlorodecane) and the relative standard deviation (R.S.D.) for model compounds

Compound	B.p. (°C)	RRF [a]	R.S.D. (%)
Alkanes			
n-Octane	125–127	1.45	4.7
n-Undecane	196	1.42	3.0
n-Hexadecane	287	1.12	2.9
n-Octadecane	305–307	1.12	3.1
n-Nonadecane	330	1.11	3.1
n-Eicosane	343	1.06	3.2
n-Docosane	369	0.97	3.8
Alkylbenzenes			
Toluene	111	1.64	5.6
Ethylbenzene	136	1.65	5.5
m-Xylene	139	1.65	4.9
n-Pentylbenzene	205	1.53	2.7
n-Decylbenzene	–	1.21	3.0
Halogenated hydrocarbons			
3,3-Dibromobutane	175	0.36 [b]	2.1
1,2-Dichlorobenzene	179	0.86	5.8
1-Bromo-4-chlorobenzene	196	0.61 [b]	1.8
2-Bromo-1,4-dimethylbenzene	200	0.81 [b]	1.5
2-Bromoethylbenzene	217–218 (734 mmHg)	0.81 [b]	2.2
1-Chlorodecane	223	1.00	
4-Bromobenzaldehyde	230	0.51 [b]	1.6
2,5-Dibromotoluene	236	0.46 [b]	2.0
1-Chlorododecane	260	1.01	2.4
Miscellaneous			
Benzaldehyde	179	1.04	5.9
Octan-1-ol	194	1.07	5.0
Naphthalene	217	1.51	1.4

[a] Means of ten determinations unless indicated otherwise.
[b] Means of five determinations.

Table 2 shows a comparison of the results for the relative recoveries (relative to 1-chlorodecane) for 24 compounds at two concentrations using the OLSA technique. The halogenated hydrocarbons were measured separately from the other compounds. Two charcoal filters in series

were utilized to examine possible breakthrough loss from the first filter, which was the same throughout the experiment.

The variable recoveries achieved (Table 2) in the stripping analysis reflect the differences in the physico-chemical properties of these compounds. In addition, lower recoveries are observed for some of the compounds at 1000 than at 100 ng l^{-1}. The detection limit varies with the recovery, but is ca. 10 ng l^{-1} for most of the compounds. Although Table 2 shows that the relative recovery of individual compounds varies from 10% to 100%, the average precision associated with the results is about 4%, and acceptable for all groups.

TABLE 2

Mean relative recoveries ($n = 5$) of the 24 selected compounds ± standard deviation (S.D.) at two concentration levels

Compound	Relative recovery (%)	
	100 ng l^{-1}	1000 ng l^{-1}
Alkanes		
n-Octane	94± 5	75± 4
n-Undecane	95± 2	96± 2
n-Hexadecane	91±12	82± 7
n-Octadecane	58± 7	58± 6
n-Nonadecane	43± 6	42± 5
n-Eicosane	31± 6	30± 5
n-Docosane	10± 3	8± 3
Alkylbenzenes		
Toluene	45± 5	9± 2
Ethylbenzene	82± 4	58± 4
m-Xylene	97± 3	74± 4
n-Pentylbenzene	99± 2	98± 4
n-Decylbenzene	88± 2	82± 6
Halogenated hydrocarbons [a]		
2-Bromo-1,4-dimethylbenzene	98± 3	n.a. [b]
1-Bromo-4-chlorobenzene	96± 3	n.a.
4-Bromobenzaldehyde	10± 1	n.a.
2-Bromoethylbenzene	90± 2	n.a.
1-Chlorodecane	100	100
1-Chlorododecane	95± 1	91± 4
1,3-Dibromobutane	60± 3	n.a.
2,5-Dibromotoluene	90± 9	n.a.
1,2-Dichlorobenzene	94± 7	85±11
Miscellaneous		
Benzaldehyde	24± 3	20± 4
Naphthalene	56± 2	63± 4
Octan-1-ol	48± 5	48± 6

[a] Experiments relating to brominated compounds were carried out at a concentration of 200 ng l^{-1}. [b] n.a. Not analysed.

The relative recoveries decrease linearly with increasing molecular weight for alkanes larger than *n*-hexadecane. This is due to the increasing boiling point, and therefore, less efficient vaporization from the water. This is confirmed by the finding that about 10% of these compounds are recovered when the water samples are re-stripped. Except for *n*-octane, no significant differences are observed in the recoveries at the two concentration levels.

The high recoveries for the alkylbenzenes are mainly due to their relative high vapour pressure in combination with their low water solubility [12]. For the lower molecular weight compounds, there are significant differences between the two concentration levels. Volatilization from the analytical charcoal filter is indicated by a breakthrough loss of about 16%, which is comparable to that reported by Borén et al. [1] for similar compounds. None of the compounds are found on re-stripping the samples, and the carbon disulphide is efficient in extracting these compounds as less than 2% is found on re-extraction of the filters. Therefore, the main reason for the difference in recoveries is the limited adsorption capacity of the carbon filter for the volatile compounds. This implies that special care must be taken for accurate quantification of relatively volatile compounds.

The three compounds in the miscellaneous group all have relatively low recoveries. For benzaldehyde and octan-1-ol this can possibly be explained by their higher polarity, and therefore better water solubility and lower vapour pressure, than the hydrocarbon classes.

Concerning the relative recoveries of the halogenated compounds, it is concluded (with a few exceptions) that the vaporization process from the water and the desorption from the charcoal are more efficient than for the other compound classes. Regarding the absolute/relative recovery ratio, a value of about 0.67 (which is also the absolute recovery of the internal standard 1-chlorodecane) is found for the alkanes, alkylbenzenes and the chlorinated hydrocarbons, whereas for the brominated hydrocarbons this ratio is about

0.45. The charcoal filters used were the same in all instances and therefore cannot explain the differences in the absolute/relative recovery ratios observed. On the other hand, the recovery of the chlorinated internal standard might have been affected by the presence of brominated compounds. An interaction of the brominated compounds with the chlorinated internal standard at relatively high stripping temperatures cannot be excluded. Other chemical interactions have been reported by Sävenhed et al. [4].

Between- and within-filter variations

The analysis of variance of the results for nine compounds on different filters is presented in Table 3. Except for benzaldehyde and *n*-pentylbenzene, significant differences between the within- and between-filter variations are found (according to their *F*-ratio). This is probably due to small differences in the characteristics of the filters used [13]. Hwang et al. [6] concluded that a set of filters would give similar results if the measured filter resistance was within ± 0.1 ml min^{-1}. However, in spite of the fact that filters with the same flow-rate (0.6 ± 0.1 ml min^{-1}) were utilized in this study, significant differences in recoveries between the filters were obtained. The within-filter variations found in this experiment correspond to the values given in Table 2 as expected. As the use of different "identical" filters may give relatively large standard deviations in the results, it is necessary for accurate quantification to determine the (relative) recoveries for each compound on each filter used in the OLSA.

TABLE 3

Within- and between-filter standard deviations (S.D.) of the relative recoveries (relative to 1-chlorodecane) of nine compounds on six filters ($n = 3$)

Compound	Mean relative recovery (%) (17 d.f.)	Between-filter S.D. (%) (5 d.f.)	Within-filter S.D. (%) (11 d.f.)	*F*-ratio (5, 11) [b]
n-Undecane	97	5	6	5.8
n-Dodecane	75	5	5	7.8
Toluene	37	22	2	798.0
Ethylbenzene	70	20	5	116.6
m-Xylene	79	16	4	80.1
n-Pentylbenzene	101	–	3	0.9
1-Chloroundecane	99	9	6	16.3
Octan-1-ol	41	3	4	6.1
Benzaldehyde	20	–	2	2.9

[a] d.f. = Degrees of freedom. [b] The theoretical *F*-ratio (5, 11) = 3.20.

Stability study

Addition of 1 g of sodium azide per litre of water sample has been shown to be an effective method of preventing bacterial growth. The stabilities of six compounds in preserved and unpreserved water stored at 4°C are shown in Fig. 1. A significant decrease in concentration is observed in the unpreserved water sample from day 17 for 1-chlorodecane and *n*-undecane, and from day 28 for *n*-pentylbenzene, octan-1-ol and benzaldehyde (Fig. 1A). These decreases are not observed (except for *n*-undecane) in samples with sodium azide added (Fig. 1B).

A slight increase in the level of bacteria during the storage period was observed in the unpreserved sample, which indicates biochemical degradation of the compounds. However, neither chemical degradation during storage [14] nor adsorption of organic compounds on the glass wall [15] can be excluded. It is not clear whether the degradation of *n*-undecane after 30 days in the preserved sample is the result of a chemical or an adsorption effect. Photodegradation cannot have occurred as all the samples were stored in the dark. The study shows that the maximum holding time for most volatile compounds in water can be increased to at least 58 days if samples are preserved with sodium azide. The commonly used preservatives hydrochloric acid and mercury(II) chloride [14,16] were avoided because of their corrosive properties and adverse environmental effects.

Conclusions

The OLSA technique is simple, effective and suitable for concentrating volatile organic compounds present at down to low ng l^{-1} levels in drinking water produced offshore. The relative recoveries of alkylated benzenes, halogenated hydrocarbons and alkanes with molecular weights lower than 250, were satisfactory, lying between

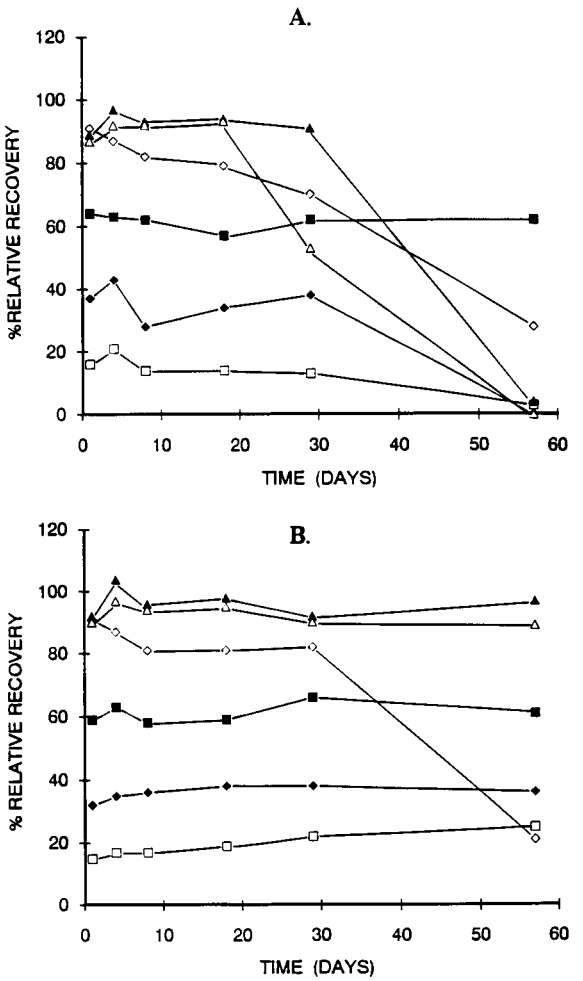

Fig. 1. Stability of volatile organic compounds during 58 days at 4°C in (A) unpreserved water and (B) water preserved with sodium azide. ■ = Ethylbenzene; □ = benzaldehyde; ◆ = octan-1-ol; ◇ = *n*-undecane; ▲ = *n*-pentylbenzene; △ = 1-chlorodecane.

80 and 100%. For higher molecular weight alkanes and some polar compounds, the recoveries were less than 60%.

However, special precautions must be taken for accurate determinations when the contaminant concentration in the samples varies widely at different sampling sites. Volatile compounds with boiling points < 150°C show a significant reduction in the recoveries at the 1000 relative to the 100 ng l^{-1} level. Both of these concentrations, or even higher, may be found in drinking water produced offshore. When appropriate quantification is necessary, e.g., in order to measure human exposure to contaminants, the samples should be diluted to an acceptable concentration in order to avoid overloading of the open-loop stripping system.

An important experimental parameter studied was the variance caused by the use of several analytical charcoal filters. Significant differences in recoveries were found for seven out of nine compounds, even though the six adsorption filters tested had the same filter resistance. Unfortunately, this gives a lower reproducibility and means that for accurate determination, the recoveries of all compounds under investigation have to be established for every filter. Identical filter resistance alone does not seem to be a reliable criterion for selecting filters for parallel analysis. When there is not complete control over the recoveries in different filters and at different concentrations, the results must be regarded as semi-quantitative.

Preserving the water samples with sodium azide at a concentration of 1 g l^{-1} was shown to prevent degradation by chemical or biochemical action of five of the six compounds investigated. Samples to be analysed for purgeable components by the OLSA technique can be stored for 58 days in the presence of sodium azide without associated loss of compounds.

The authors are grateful to Dr. Marcel P. van Berkel (DSM Chemlab, Netherlands) for his help with the statistical analyses and discussions on the manuscript. This research was sponsored by the Norwegian Directorate of Health, Royal Norwegian Council for Scientific and Industrial Research and the oil companies BP Exploration, Esso Norge, Phillips Petroleum Norway, Statoil and Elf Aquitaine.

REFERENCES

1 H. Borén, A. Grimvall, J. Palmborg, R. Sävenhed and B. Wigelius, J. Chromatogr., 348 (1985) 67.
2 K. Grob, J. Chromatogr., 84 (1973) 255.
3 H. Borén, A. Grimvall and R. Sävenhed, J. Chromatogr., 252 (1982) 139.

4 R. Sävenhed, H. Borén and A. Tjeder, Water Sci. Technol., 15 (1983) 139.
5 W.H. Glaze, M. Koga, D. Cancilla, K. Wang, M.J. McGuire, S. Liang, M.K. Davis, C.H. Tate and E. Marco Aieta, J. Am. Water Works Assoc., 81 No. 8 (1989) 66.
6 C.J. Hwang, S.W. Krasner, M.J. McGuire, M.S. Moylan and M.S. Dale, Environ. Sci. Technol., 18 (1984) 535.
7 W.E. Coleman, J.W. Munch, R.W. Slater, R.G. Melton and F.C. Kopfler, Environ. Sci. Technol., 17 (1983) 571.
8 N.K. Kristiansen, E. Lundanes, M. Frøshaug and H. Utkilen, Chemosphere, 25 (1992) 1631.
9 A.D. Sauter, L.D. Betowski, T.R. Smith, V.A. Strickler, R.G. Beimer, B.N. Colby and J.E. Wilkinson, J. High Resolut. Chromatogr. Chromatogr. Commun., 4 (1981) 366.
10 J.W. Eichelberger, E.H. Kerns, P. Olynyk and W.L. Budde, Anal. Chem., 55 (1983) 1471.
11 A.D. Jorgensen, K.C. Picel and V.C. Stamoudis, Anal. Chem., 62 (1990) 683.
12 L.C. Michael, R. Wiseman, L.S. Sheldon, J.T. Bursey, K.B. Tomer, E.D. Pellizzari, T.A. Scott, R. Coney, A.W. Garrison, J.E. Gebhart and J.F. Ryan, in L.H. Keith (Ed.), Advances in the Identification and Analysis of Organic Pollutants in Water, Vol. 1, Ann Arbor Sci. Publ., Ann Arbor, MI, 1981, pp. 87–114.
13 K. Grob, G. Grob and A. Habich, J. High Resolut. Chromatogr. Chromatogr. Commun., 7 (1984) 340.
14 M.P. Maskarinec, L.H. Johnson, S.K. Holladay, R.L. Moody, C.K. Bayne and R.A. Jenkins, Environ. Sci. Technol., 24 (1990) 1665.
15 P.M. Buszka, S.D. Zaugg and M.G. Werner, Bull. Environ. Contam. Toxicol., 45 (1990) 507.
16 V.D. Roe, M.J. Lacy and J.D. Stuart, Anal. Chem., 61 (1989) 2584.

Analytica Chimica Acta, 280 (1993) 119–127
Elsevier Science Publishers B.V., Amsterdam

Determination of xylose and glucose in a flow-injection system with PQQ-dependent aldose dehydrogenase

Maria Smolander

VTT, Biotechnical Laboratory, P.O. Box 202, SF-02151 Espoo (Finland)

Julia Cooper, Wolfgang Schuhmann, Martin Hämmerle and Hanns-Ludwig Schmidt

Lehrstuhl für Allgemeine Chemie und Biochemie, Technische Universität München, D-8050 Freising-Weihenstephan (Germany)

(Received 23rd September 1992; revised manuscript received 18th January 1993)

Abstract

Application of pyrroloquinoline quinone (PQQ)-dependent aldose dehydrogenase (ALDH) for the amperometric determination of xylose and glucose is described. Different flow injection configurations were investigated to optimize the measurement. The highest current densities could be obtained when the enzyme was immobilized directly on a graphite electrode. The best stability was achieved with controlled-pore glass (CPG)-immobilized ALDH. ALDH–CPG was also successfully used for the measurement of real fermentation samples. The measurement of samples containing only xylose as a carbon source correlated very well with high-pressure liquid chromatographic measurement, the correlation coefficient and conversion factor between the methods being 0.98 and 0.96, respectively. Also samples containing both xylose and glucose could be measured satisfactorily when the measurement with ALDH was combined with separate glucose measurement.

Keywords: Amperometry; Enzymatic methods; Flow injection; Aldose dehydrogenase; Glucose; Xylose

Determination of xylose is of importance especially in biotechnical applications, such as fermentation of xylose and application of xylanases for the hydrolysis of hemicellulose. At present xylose is mainly determined by liquid chromatography (LC) with refractive index as the most common detection method. So far only a few enzymatic methods for the detection of xylose have been published [1–4]. Similarly, very few biosensor constructions have been designed for xylose measurement. Immobilized pyranose oxidase was used in the determination of monosaccharides in cellulosic hydrolysates in a flow injection system [5]. Pyranoses, glucose, xylose and galactose were oxidized by the enzyme and the oxygen consumed in the reaction was measured. Xylulose and xylose were measured by Dominguez et al. [6] with an amperometric flow-injection system based on three successive reactions catalysed by xylose isomerase, mutarotase and NAD-dependent glucose dehydrogenase. Ikeda et al. [7] constructed a mediated, xylose-sensitive carbohydrate sensor based on NAD(P)-independent *Staphylococcus* sp. dehydrogenase. All these xylose detection systems based on amperometric detection are sensitive also to some other aldoses, including glucose. However, in many applications xylose is either the only or the dominating aldose sugar. The hemicellulose hydrolysates of hardwood, which can be used as raw materials for several biotechnical processes, contain mainly xylose [8].

Correspondence to: M. Smolander, VTT, Biotechnical Laboratory, P.O. Box 202, SF-02151 Espoo (Finland).

The aim of this work was to develop a flow-injection analysis (FIA) system for the amperometric measurement of xylose and glucose in real fermentation samples using PQQ-dependent aldose dehydrogenase (ALDH) from *Gluconobacter oxydans*. The enzyme oxidizes primarily glucose, xylose and galactose [9] and a large-scale applicable method has been developed for its purification [10].

Pyrroloquinoline quinone (PQQ)-dependent enzymes, or quinoproteins have some unique properties, which make them an excellent choice for biosensor applications. PQQ and the apoenzyme form a stable complex and oxygen does not affect the catalytic activity of bacterial quinoproteins [11]. Hence quinoproteins provide an ideal alternative to oxygen-dependent flavoproteins and dehydrogenases utilizing soluble nicotinamide coenzymes.

PQQ-dependent dehydrogenases have been succesfully applied in biosensor technology for the determination of glucose [12,13], fructose [14,15] and ethanol [16]. Most quinoprotein-based sensors are mediated biosensors, but direct electron transfer has also been reported between quinoprotein fructose dehydrogenase and a carbon paste electrode [15].

EXPERIMENTAL

Materials

PQQ-dependent aldose dehydrogenase (ALDH) was purified from *Gluconobacter oxydans* [10].

Pure aldoses were obtained from Sigma (D-xylose, D-mannose, D-arabinose, D-galactose), Merck (D-glucose, maltose, D-fructose, L-arabinose) and Serva (D-cellobiose).

Samples from xylose–yeast fermentation were obtained from VTT, Biotechnical Laboratory. Production of xylonic acid from xylose with *Gluconobacter oxydans* was done in shaking flasks according to Buchert and Viikari [17]. Centrifuged samples were incubated for 10 min at 80°C to stop enzymatic reactions and then filtered.

The electrochemical mediators phenazine methosulphate (PMS), benzoquinone (BQ) and dimethylferrocene (Fe) were obtained from Sigma, Merck and Fluka, respectively.

Activity assay of ALDH

Activity of the ALDH was measured spectrophotometrically at 600 nm at pH 6.5 as described by Buchert [9] with PMS and dichlorophenolindophenol (DCIP) as electron acceptors.

Immobilization of ALDH

Immobilization of ALDH on controlled-pore glass. ALDH was immobilized on glutaraldehyde-activated controlled-pore glass (CPG-10, 1400 Å) by the method of Weetall [18]. For the immobilization, 400 μl of ALDH (xylose oxidizing activity 17 nkat ml^{-1}) in 10 mM sodium acetate buffer containing 0.1% Triton X-100 as a detergent (pH 5.8) was used.

Immobilization of ALDH on graphite. ALDH was immobilized on heat-treated carbodiimide-activated graphite electrodes (Johnson Matthey) by the method of D'Costa et al. [13]. The inverted electrode was incubated in contact with 20 μl of enzyme solution (xylose oxidizing activity 28 nkat ml^{-1}) in 10 mM sodium acetate buffer (pH 5.8). Some of the electrodes were modified prior to the immobilization with dimethylferrocene (0.4 mg), which was adsorbed on the electrodes from toluene solution.

Immobilization of ALDH into osmium polymer. ALDH was immobilized into an osmium-containing redox polymer [19]. A 1-μl volume of enzyme solution in 10 mM *N'*-(2-hydroxyethyl)piperazine-*N*-ethanesulphonic acid (HEPES)–NaOH buffer (pH 8.0) (91 nkat ml^{-1}) was mixed with 1 μl of osmium polymer (10 mg ml^{-1}) and 0.5 μl of epoxy cross-linker (3 mg ml^{-1}) on the surface of a polished glassy carbon electrode (diameter 3 mm). The electrode was allowed to dry in the inverted position for 24 h at 4°C.

Electrochemical methods

Electrochemical detection of xylose and glucose was done with a flow-injection system connected to a potentiostat (Metrohm VA-Detector E611). The flow-through cell was equipped with a saturated calomel electrode (Metrohm) as a ref-

erence electrode and a platinum wire as a counter electrode. The working electrode was either glassy carbon (diameter 3 mm) or, for carbodiimide immobilization of ALDH, a graphite electrode (diameter 6 mm). The electrochemical surface of the working electrodes was determined using the Randles–Sevcik equation. Sample injection was performed with a computer (Commodore C64)-controlled peristaltic pump (Spetec, Germany) and an injection valve (Latek, Germany). The carrier buffer was pumped continuously at a flow-rate of 1.35 ml min^{-1} (Ismatec PMP duo-pump). The carrier electrolyte was 50 mM potassium phosphate (pH 6.5) throughout. When PMS was added to the carrier buffer, the reservoir was covered with aluminium foil in order to prevent the oxidation of PMS caused by light.

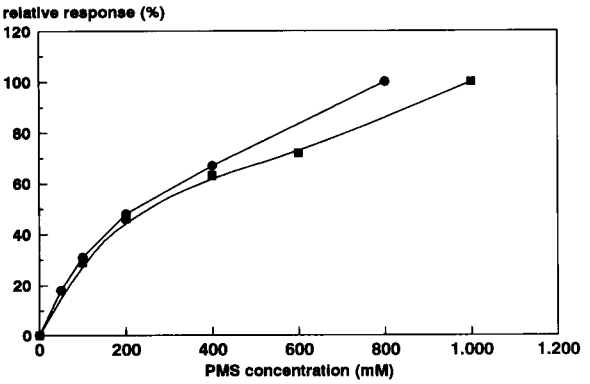

Fig. 1. Effect of soluble PMS concentration on a flow-injection measurement of 100 mM xylose with the ALDH–CPG system. ■ = PMS added to the carrier; ● = PMS added to the sample.

RESULTS AND DISCUSSION

Properties of the electrodes

PQQ-dependent aldose dehydrogenase (ALDH)-based electrodes were studied in a simple flow system. The system consisted of immobilized ALDH together with a mediator. ALDH was immobilized on CPG in an enzyme reactor column or at the electrode surface covalently or in an osmium redox polymer.

Prior to the investigation of the electrodes, the mediator and its concentration were optimized with CPG-bound ALDH. BQ and PMS were tested as mediators and hardly any difference could be seen in the current response (not shown). However, the oxidation potential of PMS is more favourable, it can be oxidized at 0 mV vs. SCE, whereas the oxidation of benzoquinone takes place only at potentials above 300 mV vs. SCE.

The effect of the concentration of PMS in the carrier buffer was studied by measuring the current response to 100 mM xylose (Fig. 1). The effect of increasing the PMS concentration on the response decreased above concentrations of 200 μM. At lower substrate concentrations than used in this experiment (100 mM xylose), the effect of the mediator concentration is expected to be less significant. Hence a PMS concentration of 500 μM was chosen to be used in the measurements when ALDH was immobilized on either CPG or unmodified graphite. When ALDH was immobilized on dimethylferrocene (Fe) or osmium polymer-modified electrodes no mediator was added to the buffer.

TABLE 1

Current densities of different flow systems [a]

Flow system	i (μA)	$a_{electrode}$ (cm^2)	i_a ($\mu A\ cm^{-2}$)	$Act_{immob.}$ (nkat)	$i_a/Act_{immob.}$ ($\mu A\ cm^{-2}\ nkat^{-1}$)
ALDH–CPG column, soluble PMS	0.22	0.05	4.0	7	0.6
ALDH covalently immobilized on the electrode, soluble PMS	3.2	0.20	16	0.6	29
ALDH covalently immobilized on the electrode, adsorbed Fe [b]	2.0	0.20	10	0.6	18
ALDH–osmium polymer	0.0056	0.05	0.1	0.1	1.0

[a] i = Current; a = electrode area; i_a = current density; Act = enzyme activity. [b] Dimethylferrocene.

In order to economize on the mediator, it would be beneficial to add it to the sample before injection instead of continuous pumping in the carrier buffer. This was also tested and the dependence of the response on the concentration was very similar to that with the mediator added to the carrier (Fig. 1).

Current and current density. The currents and current densities obtained after injection of a sample containing 100 mM xylose are shown in Table 1. The response obtained with the ALDH immobilized on CPG or carbodiimide-activated graphite were of the same magnitude whereas the current obtained with the ALDH–osmium polymer electrode was two magnitudes smaller than with the other systems.

When comparing these systems, it should be noted that the amount of enzyme immobilized and the location of the enzyme in relation to the electrode differ from one system to another, resulting in different response magnitudes. It can be seen that the ratio of the current density to the amount of enzyme activity used for the immobilization is of the same magnitude for both ALDH entrapped in the osmium polymer and immobilized on the CPG column, and this is significantly less than the same ratio for carbodiimide-immobilized ALDH. However, the current measured for carbodiimide-immobilized ALDH is of the same magnitude as that for the ALDH–CPG column, although the immobilized enzyme activity in the former instance is less than one tenth of that for the enzyme column. Also, it has to be taken into account that the carbodiimide immobilization was done by pipetting the enzyme solution on the electrode and the amount of the enzyme really immobilized is not known. The current magnitudes could be explained by faster electron transfer between the enzyme and the electrode if the enzyme is immobilized directly on the electrode. The same enzyme molecule can catalyse the oxidation of several substrate molecules as the electrode continuously accepts the electrons from the PQQ via the mediator, whereas for the ALDH–CPG column system it is very likely that only part of the reduced PMS molecules are re-oxidized on the electrode. The less efficient performance of the system based on the osmium-containing polymer compared with the other systems with the enzyme immobilized directly on the electrode surface could be due to the fact that the osmium-containing polymer is hydrophilic [20] whereas the enzyme is hydrophobic as it is a membrane-bound protein. It is therefore possible that the contact between the polymer and the enzyme is poor and the distance between PQQ and osmium is too long for fast electron transfer. Another reason for the low currents with the osmium polymer could be inactivation of the enzyme during the immobilization procedure. This is carried out at pH 8, which is incompatible with enzyme stability [10].

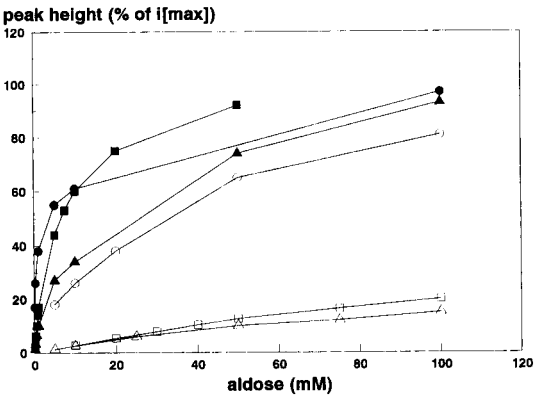

Fig. 2. Dependence of current on the xylose or glucose concentration with different flow systems. The maximum peak height was calculated according to a Hanes–Wolf plot for each system and the current values were calculated in comparison with it. ALDH–CPG column, soluble PMS: □ = xylose; ■ = glucose. ALDH covalently immobilized on the electrode, adsorbed Fe: △ = xylose; ▲ = glucose; ALDH–osmium polymer: ○ = xylose; ● = glucose.

The dependence of the current response on the concentration of xylose and glucose with three different systems is shown in Fig. 2. The maximum current (i_{max}) for each system was determined from Hanes–Wolf plots and the measured current values were plotted relative to this value. The i_{max} values and apparent Michaelis constants (K_M) are given in Table 2. The shape of the curves obtained with the systems based on covalent immobilization either on CPG or directly on the graphite electrode are fairly similar. Immobilization in the osmium polymer resulted in calibration graphs with a very different shape, espe-

TABLE 2

Kinetic constants for different flow systems

	Xylose		Glucose	
	K_M (mM)	i_{max} [a]	K_M (mM)	i_{max} [a]
Soluble ALDH	44		0.7	
Flow systems				
ALDH–CPG column, soluble PMS	206	371	5.2	599
ALDH covalently immobilized on the electrode, adsorbed Fe [b]	112	171	11	87
ALDH–osmium polymer	29	90	2.5	546

[a] i_{max} is given in arbitary units referring to the peak height.
[b] Dimethylferrocene.

cially that for xylose. This may be due to the different environment within the polymer, which may influence the accessibility of the substrate to the enzyme, or the enzyme kinetics directly.

Specificity. Specificity of ALDH was investigated in the flow system. The peak due to the injection of 100 mM glucose was taken as a reference and peaks for 100 mM solutions of other sugars were compared with it (Table 3). The specificity of ALDH in a flow system differs from that obtained with the soluble enzyme in a spectrophotometric assay using a substrate concentration of 73 mM [9]. This is probably due to the change in the apparent K_M values of the enzyme during the immobilization. Also, the substrate is in contact with the enzyme for only a short time in the flow system and, if it reacts slowly in the stationary system, the effect will be more critical in the flow system. With the ALDH–CPG flow system, the apparent K_M value for xylose (206 mM) is twice as high as the concentration used in the experiment (100 mM) and hence the concentration of the substrate can be limiting in the specificity experiment. For the soluble enzyme, K_M values of 0.7 and 44 mM for glucose and xylose, respectively, were determined.

TABLE 3

Specificity of ALDH in flow systems

Substrate	Peak height (relative values)		
	ALDH covalently immobilized on the electrode, adsorbed Fe [a]	ALDH–CPG column	
		Soluble PMS	Soluble BQ
D-Glucose	100	100	100
D-Xylose	14	15	12
D-Galactose	17	20	17
D-Mannose	5	6	3
D-Lactose	0.6	0	0
D-Arabinose	0	0	0
Maltose	5	5	3
Cellobiose	2	2	1
L-Arabinose	n.d	n.d	9
Fructose	n.d	n.d	0.7

[a] Dimethylferrocene. [b] n.d. = Not detected.

With the ALDH–CPG system, the linear measurement ranges for xylose and glucose extended to about 1 and 10 mM, respectively (Fig. 3). No substrate inhibition could be observed at xylose and glucose concentrations of less than 200 mM.

Stability. The stability of different systems in continuous use was investigated by injecting a sample containing 100 mM xylose into the flow system every 10 min. The peak height as a function of time is shown in Fig. 4. It can be seen that for the electrode with adsorbed mediator and covalently immobilized enzyme, the decrease in peak height is nearly linear as a function of time, 22% of the initial activity remaining after 10 h. At the end of the experiment we tried to add dimethylferrocene to the electrode from a Triton X-100 suspension (arrows 1 and 2) and from toluene solution (arrow 3). The response could be improved for few injections, but it soon decreased again. This indicated that the limiting factor in the stability of this kind of electrode was retention of the mediator, as could be expected on the basis of previously published studies on mediator leakage by Schuhmann et al. [21]. To confirm this, the same experiment was performed without adsorbed mediator, using soluble PMS added to the carrier buffer instead. Considerably better stability was achieved in this instance. A decrease in response of 41% took place during the first 5 h. However, the response decreased by only 9% during the next 5 h and the residual response after a 10-h experiment was 50%. The rapid decrease in the response at the beginning could

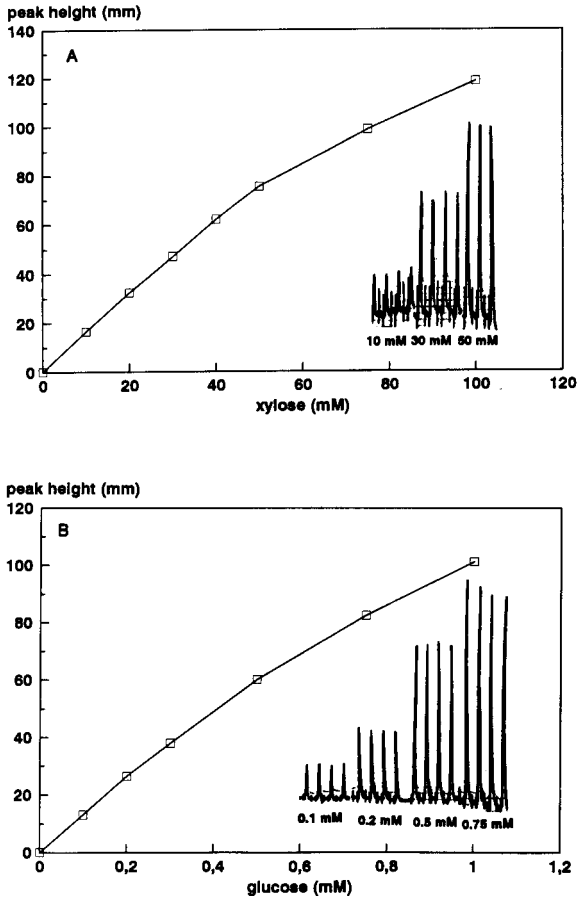

Fig. 3. Calibration graphs for (A) xylose and (B) glucose with the ALDH–CPG system. The insets show typical response peaks.

be due to the solubilization of weakly bound enzyme which is eluted from the system. This decrease is typical for immobilized enzymes. Interestingly, the residual response of the system with soluble PMS after 10 h of operation is very close to the improved response of the dimethylferrocene electrode after the re-addition of mediator at the end of the experiment. The system with the ALDH–CPG column and soluble PMS was most stable, the remaining response after 10 h of continuous operation being 87%. The experiment was performed at room temperature and without added stabilizers; optimization of the conditions might result in even better stability. A controlled temperature of, e.g., 18°C could possibly enhance the stability of the enzyme. Also, the addition of Triton X-100 as stabilizer to the carrier buffer could be beneficial, as ALDH is a membrane-bound protein and hence always needs the presence of a detergent to prevent precipitation and subsequent inactivation of the enzyme.

In the flow system with the enzyme column, a sample frequency of 25 samples per hour could be used. The reproducibility of the measurements was good, the standard deviation for 20 measurements of 20 mM xylose being 2.4%.

Application of ALDH based flow systems

FIA-system. On the basis of the preceding results, the ALDH–CPG enzyme column with soluble PMS (500 μM) as a mediator was the most suitable for the measurement of real fermentation samples. This system had the best stability and also the working potential needed for the re-oxidation of PMS is low (0 mV vs. SCE), which reduces the susceptibility to unspecific oxidation on the electrode.

If the sample contained both xylose and glucose, glucose was measured separately by incorporating a glucose oxidase column in the flow system. Hydrogen peroxide produced in the glucose oxidase column was measured at a platinum electrode at 700 mV vs. SCE. In addition to glucose oxidase-based FIA, a test kit and high-pressure liquid chromatography (HPLC) were also

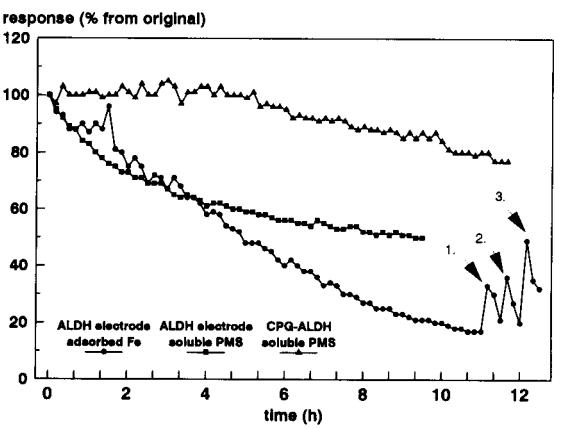

Fig. 4. Stability of different flow systems. ● = ALDH electrode, adsorbed Fe; ■ = ALDH electrode, soluble PMS; ▲ = ALDH–CPG, soluble PMS.

used for the measurement of glucose. When the glucose concentration was known, the corresponding peak height was traced from the ALDH FIA calibration graph. This peak height was multiplied by 0.9, because it was observed that for a peak due to two components, glucose and xylose, the peak height is 10% smaller than the sum of the corresponding individual peaks, even though the contribution from the xylose component is negligible. The sample containing both xylose and glucose was then measured with the ALDH FIA method and the peak height corresponding the glucose concentration was subtracted from that obtained for the sample. The remaining fraction of the peak was due to the xylose in the sample and xylose concentration was obtained from the ALDH FIA calibration graph for xylose. The procedure for the determination of the xylose concentration is shown in Fig. 5.

Measurement of samples from fermentation broths. ALDH was applied to the amperometric measurement of two sets of real samples. One set originated from a cultivation of yeast on xylose and contained 75–570 mM xylose. Another set of samples from *Gluconobacter* cultivation contained 28 mM glucose and 667 mM xylose at the start of the cultivation.

When real samples were measured, the decrease in the peak height was faster than with pure xylose samples, owing to fouling of the electrode, and after 30 samples the response had decreased to 80% of the initial value. Hence the

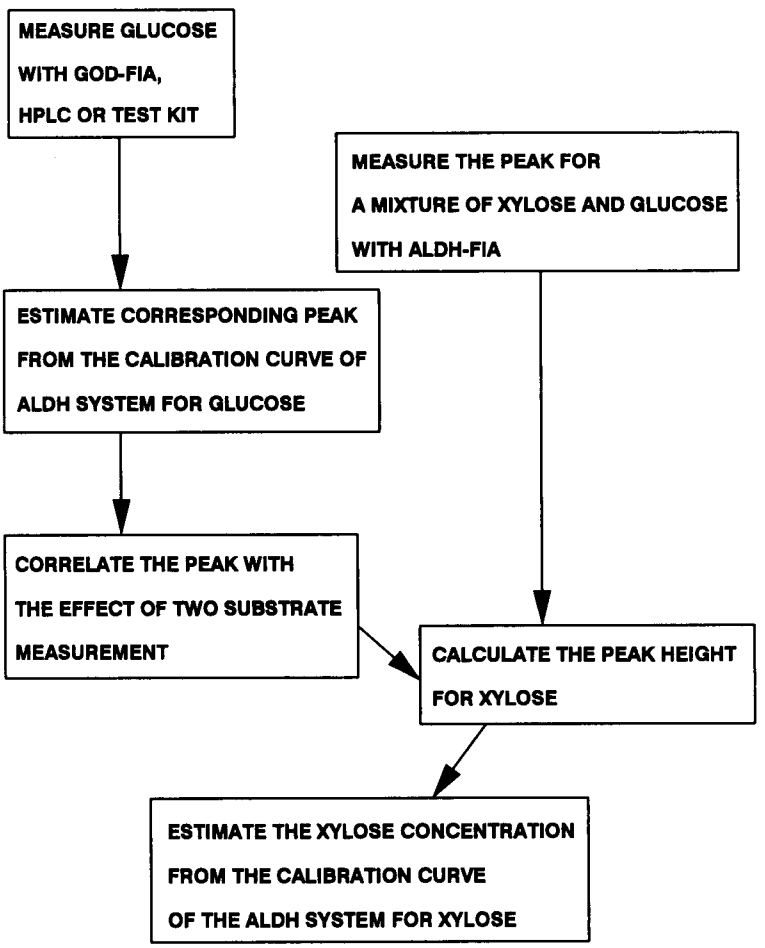

Fig. 5. Determination of xylose concentration in a sample containing both xylose and glucose.

peak heights obtained for real samples were correlated using a control sample, which was regularly injected into the system. The values obtained with the ALDH-based flow system were compared with those obtained by HPLC. Samples from the fermentation of yeast on xylose did not contain any glucose and the correlation between the two methods was good (Fig. 6). After cultivation for 1 day also the *Gluconobacter* samples were free of glucose and correlated well with the HPLC results (Fig. 6). The correlation coefficient for a plot of xylose concentrations determined by HPLC vs. FIA was 0.98 ($n = 21$) and the conversion factor between the two methods was 0.96.

When the samples taken at the beginning of the *Gluconobacter* cultivation were measured, the response obtained with the ALDH-based FIA system was due to both glucose and xylose. In order to calculate the individual aldose concentrations, glucose can also be measured separately and the xylose concentration calculated by subtracting the current due to glucose. Another possibility is to remove glucose with glucose oxidase (GOD), mutarotase and catalase [22]. Glucose was measured separately using either the GOD FIA system, HPLC or an enzymatic test kit (Boehringer, test kit for food analysis). Glucose measurement with the GOD-based flow system was not optimized and a very fast decrease in the signal occurred when real samples were measured. A mediated system including horseradish peroxidase [23,24] or inorganic mediator [25] would be better for this kind of measurement of biological samples.

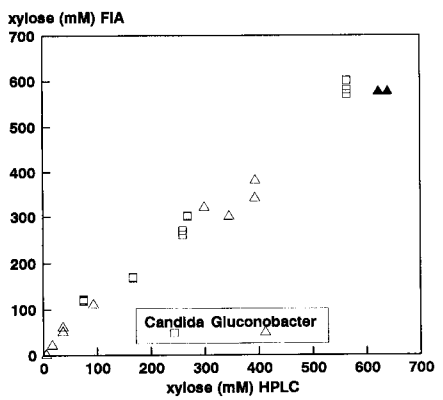

Fig. 6. Measurement of real samples with the ALDH-based flow system. The filled symbols are for the samples containing both xylose and glucose.

TABLE 4

Measurement of real samples containing xylose and glucose

Compound	Method	Concentration (mM)	
		Sample 1	Sample 2
Glucose	HPLC	27	25.5
	Test kit	25	25
	FIA (GOD)	27	27
Xylose	HPLC	623	640
	FIA (ALDH) + HPLC	575	650
	FIA (ALDH) + test kit	650	650
	FIA (ALDH + GOD)	575	575

The xylose concentration in glucose-xylose samples was measured using the ALDH column, together with either HPLC, the test kit or the flow-injection system based on glucose oxidase using the procedure shown in Fig. 5. The results for two glucose-xylose samples from *Gluconobacter* are given in Table 4, and the values obtained with the combined ALDH-GOD flow system are also shown in Fig. 6 (filled symbols). The estimated values for xylose concentration were fairly similar to the HPLC results.

Conclusions

Different flow-injection systems were compared in the application of PQQ-dependent aldose dehydrogenase to xylose and glucose measurement. The highest current densities were obtained when the enzyme was immobilized directly on the electrode. This could be explained by the better electron transfer in these systems.

When the stabilities of different systems were compared, the mediator leakage was clearly a limiting factor if a mediator-modified electrode was used. The best stability was achieved when CPG-immobilized ALDH was used. The ALDH–CPG system was also used for the measurement of real fermentation samples. If xylose was the only carbon source in the medium, a good correlation was found between the ALDH and HPLC results. Even if the samples contained both xylose and glucose, a fairly good estimation of the xylose concentration could be achieved when glucose

determination based on glucose oxidase was performed in addition to the measurement with ALDH. The measurement system can be successfully applied if the amount of xylose is high enough in comparison with glucose. This is often so because, e.g., in the hemicellulose hydrolysates of steamed birchwood, the xylose content is 10–50 times higher than the concentration of glucose [8]. If glucose is used as a carbon source, the sample can be diluted considerably owing to the low Michaelis constant for glucose and hence possible traces of other monosaccharides do not affect the measurement.

Ling Ye (Department of Chemical Engineering, University of Texas) is thanked for kindly providing the osmium polymer. The financial support of the Foundation for Biotechnical and Industrial Fermentation Research is gratefully acknowledged.

REFERENCES

1 J.H. Wissler and E. Logemann, Methods of Enzymatic Analysis, Vol. VI, Verlag Chemie, Weinheim, 1984, 3rd edn., pp. 449–465.
2 A.G. Williams and S.E. Withers, J. Microbial Methods, 4 (1986) 277.
3 H. Kerstens-Hilderson, E. van Doorslaer, C.K. de Bruyene and K. Yamanaka, Anal. Biochem., 80 (1977) 41.
4 J. Buchert, M. Smolander, L. Viikari, Method for Enzymatic Determination of Aldoses, Patent Application WO 92/07953, 1992.
5 L. Olsson, C.F. Mandenius and J. Volc, Anal. Chem., 62 (1990) 2688.
6 E. Dominguez, B. Hahn-Hägerdahl, G. Margo-Varga and L. Gorton, Anal. Chim. Acta, 213 (1988) 139.
7 T. Ikeda, T. Shibata, S. Todoriki, M. Senda and H. Kinoshita, Anal. Chim. Acta, 230 (1990) 75.
8 J. Buchert, Biotechnical Oxidation of D-Xylose and Hemicellulose Hydrolysates by *Gluconobacter oxydans*, Publication No. 70, Technical Research Centre of Finland, Helsinki, 1990.
9 J. Buchert, J. Biotechnol., 18 (1991) 103.
10 M. Smolander, J. Buchert and L. Viikari, J. Biotechnol., in press.
11 V.L. Davidson, Am. Biotechnol. Lab., 8, No. 2 (1990) 32.
12 W.H. Mullen, S.J. Churchouse and P.M. Vadgama, Analyst, 110 (1985) 925.
13 E.J. D'Costa, I.J. Higgins and A.P.F. Turner, Biosensors, 2 (1986) 71.
14 T. Ikeda, F. Matsushita and M. Senda, Agric. Biol. Chem., 54 (1990) 2919.
15 T. Ikeda, F. Matsushita and M. Senda, Biosensors Bioelectron., 6 (1991) 299.
16 Y. Kitagawa, K. Kitabatake, M. Suda, H. Muramatsu, T. Ataka, A. Mori, E. Tamiya and I. Karube, Anal. Chem., 63 (1991) 2391.
17 J. Buchert and L. Viikari, Appl. Microbiol. Biotechnol., 29 (1988) 375.
18 H.H. Weetall, Methods Enzymol., 44 (1976) 134.
19 B.A. Gregg and A. Heller, J. Phys. Chem., 95 (1991) 5976.
20 B.A. Gregg and A. Heller, J. Phys. Chem., 95 (1991) 5970.
21 W. Schuhmann, U. Löffler, H. Wohlschläger, R. Lammert, H.-L. Schmidt, H.-D. Wiemhöfer and W. Göpel, Sensors Actuators B, 1 (1990) 571.
22 A.F.P. Turner, I. Karube and G.S. Wilson, Biosensors, Fundamentals and Applications, Oxford University Press, Oxford, 1987, p. 337.
23 G. Jönsson-Pettersson, Electroanalysis, 3 (1991) 741.
24 J. Kulys and R.D. Schmid, Bioelectrochem. Bioenerg., 24 (1990) 305.
25 N.C. Foulds and C.R. Lowe, Anal. Chem., 60 (1988) 2473.

Analytica Chimica Acta, 280 (1993) 129–135
Elsevier Science Publishers B.V., Amsterdam

Use of stopped-flow fluorescence polarization immunoassay in drug determinations

A. Gaikwad [1], A. Gómez-Hens and D. Pérez-Bendito

Department of Analytical Chemistry, Faculty of Sciences, University of Córdoba, E-14004 Córdoba (Spain)

(Received 11th December 1992; revised manuscript received 28th January 1993)

Abstract

The stopped-flow technique was used jointly with fluorescence polarization immunoassay for the kinetic determination of haptens. Two different types of analytes, namely benzodiazepines and tricyclic antidepressants, were assayed in order to assess the advantages of this novel approach over the conventional equilibrium technique. Kinetic data can be obtained within a few seconds after the reactants have been mixed, which allows ready application of this technique to routine analyses. The within- and between-assay precision data are better and detection limits lower than those afforded by conventional fluorescence polarization immunoassay. The analytical recoveries ranged between 98.6 and 101.5% for nordiazepam in urine and between 97.1 and 102.0% for imipramine in serum. The results for serum and urine samples correlated well with those obtained by using the conventional method.

Keywords: Immunoassay; Fluorimetry; Kinetic methods; Imipramine; Pharmaceuticals; Serum; Stopped-flow technique; Urine

Immunological methods are routinely used in the clinical laboratory on account of their special features (particularly their high selectivity and the commercial availability of automatic instrumentation for their implementation). Since the first immunoassay involving the use of radioisotopes was reported, a wide variety of alternative immunoassay methods have been developed to overcome the shortcommings of radiolabelled reagents. However, only some of them are useful alternatives to radioimmunoassay (RIA). Thus, several homogeneous fluorescence immunoassays were developed [1] in order to avoid the separation required in RIA; however, their poor sensitivity and limited applicability hindered the use of many of them in the clinical laboratory. However, the special nature of fluorescence polarization and its dependence on the size of the molecules involved in the immunological reaction concerned are the chief reasons why fluorescence polarization immunoassay (FPIA) is widely used at present in clinical chemistry for the homogeneous determination of haptens such as therapeutic and abuse drugs [2]. Commercially available automated instrumentation has fostered its use even further. Of all the fluorescence immunoassays developed to date, FPIA has been by far the most successful.

Most immunoassays are based on measurements made after immunochemical reactions have approached equilibrium, so kinetic methodology has rarely been applied for this purpose. There are a few kinetic-based immunoassays for haptens such as gentamicin [3] and tobramycin, phenobarbitone and theophylline [4] by use of single-point measurements and a centrifugal analyser. Also, a multi-point kinetic method was

Correspondence to: D. Pérez-Bendito, Department of Analytical Chemistry, Faculty of Sciences, University of Córdoba (Spain).

[1] Present address: Regional Research Laboratory, CSIR, Trivandrum 695019, India.

developed for determination of theophylline by using a flavine–adenine dinucleoside as label [5]. This methodology has also been applied to the determination of immunoglobulin G with nephelometric measurements [6]. The stopped-flow mixing technique was used in this instance to evaluate a variety of kinetic parameters. Although this study provided very interesting results, no application to real samples was attempted. However, the stopped-flow mixing technique may offer complementary capabilities for routine analyses based on immunochemical reactions, just as it does with conventional reactions [7].

In order to study the potential advantages of kinetic methodology as applied to fluorescence polarization immunoassays, we investigated two different types of antigen–antibody system, namely benzodiazepines and tricyclic antidepressants, by monitoring changes in fluorescence polarization with time. For this purpose, we used a spectrofluorimeter in a T-format configuration where two emission paths symmetrically arranged on both sides of the sample compartment allowed simultaneous fluorescence measurements to be performed with the polarizers placed normal to each other. The response of both detectors was virtually the same if the emission monochromator was replaced with an interference filter to select the emission wavelength for each emission path of the instrument. This avoids the need to the use a correction factor [8] to compensate for the polarization caused by components such as a monochromator or a mirror on the emission side. This polarization bias is usually relatively small (ca. 0.98) and is routinely assumed to be unity [9]. Because the competitive antigen–antibody reactions involved are very fast, the stopped-flow mixing technique is required to obtain the kinetic curves and the corresponding reaction rate data. For this reason, the proposed approach is called stopped-flow fluorescence immunoassay.

The aim of this work was to assess the potential of kinetic methodology in FPIA and to compare the results obtained with those provided by conventional fluorescence polarization measurements. This is the first time this methodology has been used for measuring tracer binding directly in a competitive binding assay in which an antigen (analyte), a tracer and an antibody are involved. Hence, this approach can also be of use for conducting fundamental kinetic studies on immunochemical reactions.

EXPERIMENTAL

Instrumentation

An SLM-Aminco (Urbana, IL) Model 8000C photon-counting spectrofluorimeter equipped with a xenon arc source and three polarizers (Glan–Thompson calcite prism type), one in the excitation light path and the other two in the corresponding emission light path of the T-format configuration of the instrument, was used. The excitation wavelength was set at 494 nm by means of the excitation monochromator. The emission wavelength was selected by placing an interference filter with its band width centred at 550 nm in each of the two optical emission arms. The instrument was furnished with an SLM-Aminco MilliFlow stopped-flow reactor, a TWC computer and a Roland plotter. The stopped-flow module, with an observation cell of 0.2 cm path length, was controlled by the associated electronics, the computer and a pneumatic syringe drive system. The solutions in the stopped-flow module were kept at a constant temperature of 25°C by circulating water from a thermostated tank.

Chemicals

Test kits for the determination of benzodiazepines and tricyclic antidepressants by FPIA were supplied by Abbott Lab. (N. Chicago, IL). Working solutions were prepared by using TDx dilution buffer from Abbott Diagnostics. All other chemicals were of analytical-reagent grade.

Determination of benzodiazepines in urine

Of the two drive syringes of the stopped-flow module, one was filled with a solution containing 125-fold diluted tracer (fluorescein-labelled nordiazepam) and 20 μl of urine sample containing nordiazepam, in a final volume of 0.5 ml. The other syringe was filled with a solution containing a 25-fold diluted antibody solution in a final

volume of 0.5 ml. All dilutions were made with TDx dilution buffer. The concentration of nordiazepam in the final 0.5 ml solution volume must be between 0.15 and 8.0 ng ml^{-1} in order to obtain the calibration graph. In each run, 0.04 ml of each solution was mixed at a flow-rate of 20 ml s^{-1} in the mixing chamber. The variation of the fluorescence intensity in each emission arm of the T-format configuration was monitored at λ(em) = 550 nm [λ(ex) = 494 nm] by placing both emission polarizers normal for each other. Although the maximum emission of fluorescein occurs at 517 nm, the interference filter with the closest available wavelength, which was placed in each optical emission arm, was 550 nm. The use of two interference filters yielded an almost identical signal at each detector when the emission polarizer was placed in the same position. Data from the detectors were processed by the microcomputer to deliver the variation of the fluorescence polarization with time; also, by running a program for application of the initial-rate method, the reaction rate was determined in about 10 s. Each sample was assayed in triplicate and the blank signal was found to be negligible. All measurements were made at 25°C.

Determination of tricyclic antidepressants in serum

One of the two drive syringes was filled with a solution containing 125-fold diluted tracer (fluorescein-labelled imipramine) and 10 μl of human serum containing imipramine in a final volume of 0.5 ml. The other drive syringe was filled with a solution containing a 10-fold diluted antibody solution in a final volume of 0.5 ml. TDx dilution buffer was used for all dilutions. The imipramine concentration in the final 0.5 ml solution must be between 0.2 and 7.5 ng ml^{-1} in order to obtain the calibration graph. After this point, the procedure was similar to that described above for the benzodiazepines.

RESULTS AND DISCUSSION

FPIA is a homogeneous immunoassay based on the difference in molecular volume of a small fluorescent-labelled antigen or hapten when free and when bound to a large antibody. The competitive reactions between the antigen (analyte, Ag), antigen labelled fluorescein (tracer, Ag*) and the antibody (Ab) can be formulated as follows:

$$\begin{matrix} \mathrm{Ag} & & \mathrm{Ag{-}Ab} \\ & +\mathrm{Ab} \rightarrow & \\ \mathrm{Ag^*} & & \mathrm{Ag^*{-}Ab} \end{matrix}$$

The polarized light emitted by the free tracer is dim because of its fast rotational motion resulting from its small molecular volume, whereas that emitted by the tracer-bound antibody is bright as a result of its increased molecular volume and decreased Brownian motion. When the emitted light is polarized or partially polarized, the fluorescence intensity measured when the emission polarizer is placed parallel to the excitation polarizer is higher than when it is placed normal to it, whereas if the emitted light is not polarized, the fluorescence intensity obtained is the same for both positions of the emission polarizer.

The fluorescence polarization is usually quantified via the degree of polarization, which is given by

$$p = \frac{A-B}{A+B} = \frac{(A/B)-1}{(A/B)+1}$$

where A and B are the fluorescence intensities measured when the emission polarizer is placed parallel and normal, respectively, to the electric vector of the exciting light and p is a measure of the extent to which the emitted light has its electric vector pointing in the same direction as that of the exciting light. In the absence of analyte, p increases as the concentration of Ag*–Ab increases and, owing to the competitive reactions involved in the presence of analyte, p decreases as the analyte concentration increases. Thus, in conventional FPIA, p is the parameter to be used when the formation of the Ag*–Ab complex has approached equilibrium.

By measuring the variation of p with time, one can determine the rate of formation of the Ag*–Ab complex, which will be inversely proportional to the analyte concentration. By using the T-format configuration of the instrument, the initial

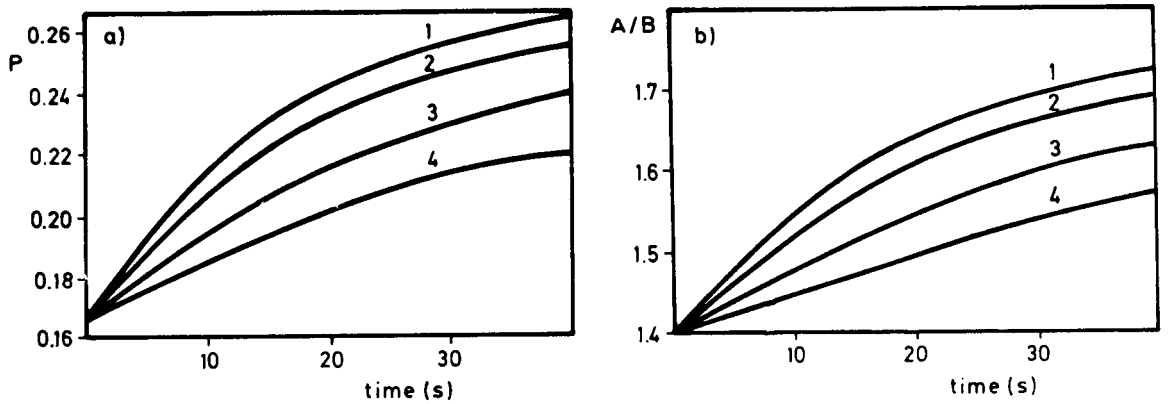

Fig. 1. Kinetic curves obtained for different concentrations of nordiazepam: (1) 0.5; (2) 1.0; (3) 2.0; (4) 3.0 ng ml^{-1}.

rate (dp/dt) can be obtained by placing the emission polarizers normal to each other and having the microcomputer process data in order to construct the polarization-time kinetic curve.

According to the definition of p, it depends on the concentration of species in the solution and on the experimental conditions through the ratio A/B; thus, by working under constant experimental conditions, this ratio can be used to determine the extent of development of the Ag*–Ab reaction and, by keeping the tracer and antibody concentrations constant, to determine the analyte concentration. Figure 1 shows the variation of p and A/B with time for different concentrations of nordiazepam. As can be seen, the kinetic curves are similar. These results shown that both paramenters, p and A/B, can be used to calculate the rate of formation of the Ag*–Ab complex,

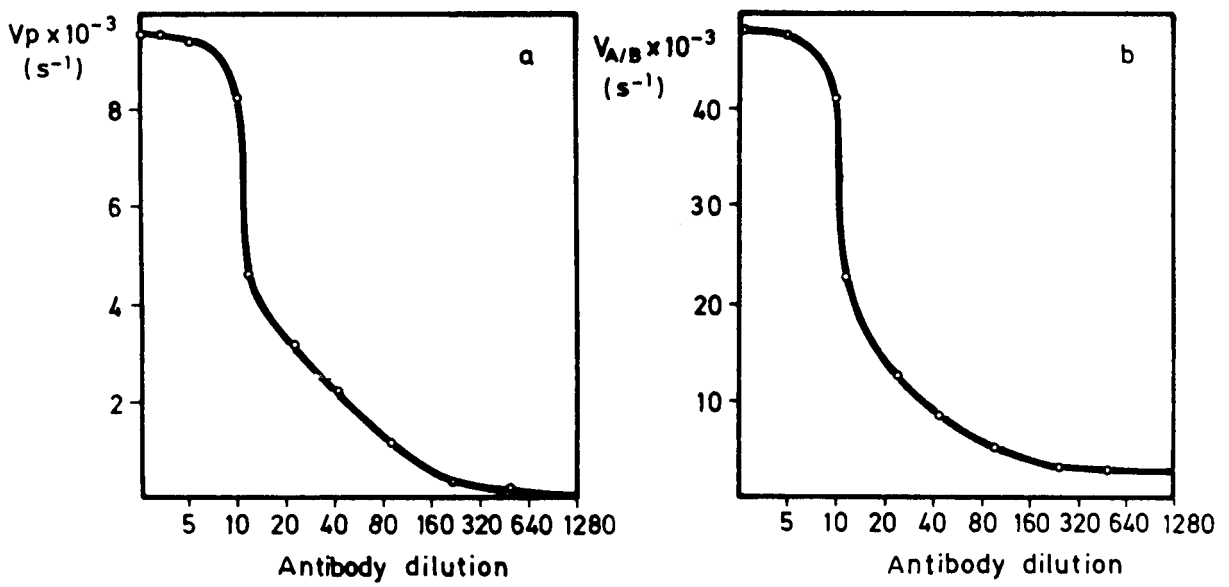

Fig. 2. Antibody dilution curves obtained with a 125-fold diluted tracer (fluorescein-labelled imipramine) by using the variation of (a) the fluorescence polarization and (b) the ratio A/B with time (i.e., V_p and $V_{A/B}$, respectively).

which is inversely proportional to the analyte concentration.

Antibody dilution study

After an appropriate tracer concentration had been chosen, the effect of adding decreasing amounts of antiserum to a constant amount of tracer (125-fold diluted tracer solution) on the reaction rate [dp/dt and $d(A/B)/dt$] was studied for both the benzodiazepines and the tricyclic antidepressants. The dilution curves obtained for fluorescein-labelled imipramine are shown in Fig. 2. As the antiserum concentration decreases, the variation of p or A/B with time decreases because binding of the antibody to the conjugate disminishes. This effect is similar to that observed when measurements are obtained at equilibrium. On the basis of these results, a solution with a 10-fold final of antibody was used for tricyclic antidepressants and a 25-fold dilution for benzodiazepines.

Features of the proposed method

Figure 3 shows the calibration graphs obtained for different concentrations of imipramine using the variations of p and A/B with time as measuring parameters. Both curves were obtained by using 125-fold diluted tracer and 10-fold diluted antibody. As can be seen, the dynamic range for imipramine, between 0.15 and 8.0 ng ml^{-1}, was the same in both instances. Obviously, such a dynamic range can be expanded by using higher concentrations of tracer and antibody, but the determination of low levels of analyte is bound to be less precise. The calibration graph of $d(A/B)/dt$ vs. nordiazepam concentration, obtained by using a 125-fold diluted tracer and 25-fold diluted antibody, is shown in Fig. 4. Nordiazepam can be determined under these conditions in the range 0.2–7.5 ng ml^{-1}. For both analytes, the calibration graphs are linear at low analyte concentrations (down to 3 ng ml^{-1} imipramine and 4 ng ml^{-1} nordiazepam). Table 1 summarizes the figures of merit of the proposed method; as can be seen, the linearity for nordiazepam is better than that for imipramine.

The detection limit, as defined by IUPAC [10], was 0.10 ng ml^{-1} for nordiazepam and 0.15 ng ml^{-1} for imipramine, equivalent to 2.5 ng ml^{-1} for nordiazepam and 7.5 ng ml^{-1} for imipramine in the samples. These detection limits are lower than those afforded by conventional FPIA (40 ng

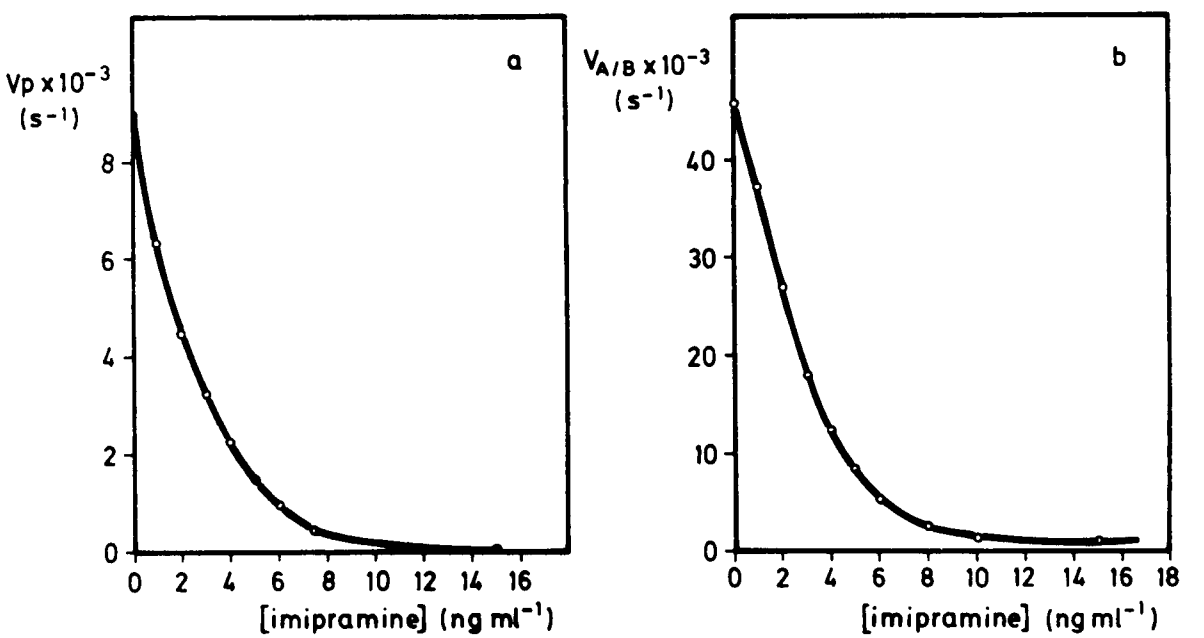

Fig. 3. Calibration graphs obtained for imipramine (tracer dilution 125:1; antibody dilution 10:1) ($V_p = dp/dt$, $V_{A/B} = d(A/B)/dt$).

TABLE 1

Quantification performance of the proposed stopped-flow method

Analyte	Linear range (ng ml^{-1})	Measuring parameter	(Slope ± S.D.) × 10^{-3} (s^{-1} ng^{-1} ml) [a]	(Intercept ± S.D.) × 10^{-3} (s^{-1}) [a]	r
Nordiazepam	0.15–4.0	dp/dt	1.5 ± 0.7	5.7 ± 0.2	0.973
		$d(A/B)/dt$	4.1 ± 0.9	16.9 ± 1.2	0.996
Imipramine	0.20–3.0	dp/dt	2.3 ± 1.0	9.0 ± 0.4	0.945
		$d(A/B)/dt$	9.3 ± 2.5	45.9 ± 1.2	0.988

[a] $n = 5$.

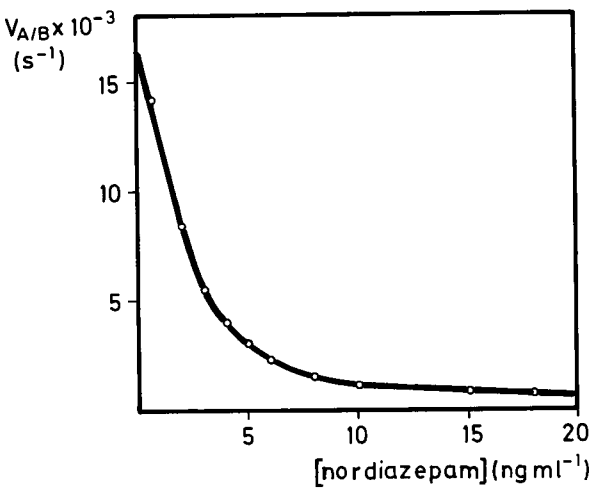

Fig. 4. Calibration graph obtained for nordiazepam (tracer dilution 125:1; antibody dilution 25:1) ($V_{A/B} = d(A/B)/dt$).

ml^{-1} for nordiazepam [11] and 20 ng ml^{-1} for imipramine [12]). Therefore, the joint use of kinetic methodology and the stopped-flow mixing technique substantially improves the determination capabilities of FPIA.

The within-day and between-day precisions for two different concentrations of nordiazepam and imipramine are given in Table 2. The values are smaller than those reported for conventional FPIA, which were in the range 1.36–4.11% for nordiazepam [11] and 2.51–7.70% for imipramine [12].

Analysis of real samples

Various amounts of nordiazepam were added to several urine samples, which were then analysed by taking 20-μl aliquots in each instance and treating them as described above. Similarly, several serum samples were spiked with various amounts of imipramine and analysed in 10-μl aliquots. The analyses were carried out with no pretreatment. Table 3 gives the results and analytical recoveries obtained. The mean recovery was 100.4% for nordiazepam and 98.7% for imipramine.

Table 4 summarizes the results obtained by using the least-squares regression technique [13] to calculate the slope and intercept of the linear

TABLE 2

Precision of the proposed stopped-flow method

Analyte	Within-assay ($n = 12$)			Between-assay ($n = 5$)		
	$\bar{X}$ (ng ml^{-1})	S.D. (ng ml^{-1})	R.S.D. (%)	$\bar{X}$ (ng ml^{-1})	S.D. (ng ml^{-1})	R.S.D. (%)
Nordiazepam in urine	0.1652	1.98×10^{-3}	1.20	0.1652	1.60×10^{-3}	0.97
	0.3107	8.89×10^{-3}	2.86	0.3076	7.42×10^{-3}	2.41
Imipramine in serum	0.298	7.88×10^{-3}	2.64	0.297	7.48×10^{-3}	2.52
	0.810	1.77×10^{-2}	2.18	0.807	7.84×10^{-3}	0.97

TABLE 3

Recovery of nordiazepam and imipramine from biological fluids

Analyte	No.	Drug concentration (ng ml^{-1})		Recovery (%)
		Added	Found [a]	
Nordiazepam in urine	1	1.20	1.21	100.8
	2	1.30	1.32	101.5
	3	1.42	1.40	98.6
	4	1.50	1.51	100.7
	5	1.62	1.63	100.6
Imipramine in serum	1	0.21	0.204	97.1
	2	0.26	0.250	96.15
	3	0.35	0.349	99.7
	4	0.75	0.751	100.1
	5	0.80	0.798	99.75
	6	1.00	0.999	99.9
	7	2.00	1.90	95.0
	8	5.00	5.10	102.0

[a] Average of three determinations.

TABLE 4

Representative least-squares statistics for comparison of the results provided by stopped-flow (y) and conventional (x) fluorescence polarization immunoassays

Analyte	Slope [a]	Intercept [a]	r
Nordiazepam in urine (ng ml^{-1}) ($n = 18$)	0.998 (0.02)	0.062 (0.26)	0.995
Imipramine in serum (ng ml^{-1}) ($n = 18$)	0.966 (0.081)	0.949 (1.79)	0.998

[a] Mean ± S.D.

relationship between the data obtained for benzodiazepines and tricyclic antidepressants using the stopped-flow and the equilibrium FPIA methods. As can be seen, the slopes are close to unity and the regression coefficients suggest good linearity, so the two sets of results are well correlated.

Conclusions

The results obtained by applying the stopped-flow technique to the kinetic determination of benzodiazepines and tricyclic antidepressants by FPIA show that this is a useful alternative to the automatic routine determination of these drugs in biological fluids. Compared with the conventional FPIA methods, the kinetic methodology improves the detection limits and precision; also, the use of the stopped-flow mixing technique reduces reactant manipulations and allows measurements to be made shortly after mixing. The time required to obtain analytical data is only about 10 s.

Unlike time-resolved immunoassay and enzyme immunoassay, where kinetic methodology is used to monitor the development of the indicator reaction, in the proposed approach the rate of the antigen–antibody reaction is measured directly. Thus, an additional interesting aspect is the possibility of conducting fundamental kinetic studies on immunochemical reactions (the stopped-flow technique has traditionally been used in studies of physico-chemical interest such as reaction kinetics and mechanisms). Work in progress under way at our laboratory is aimed at assessing the full potential of stopped-flow fluorescence immunoassay in this field.

Financial support from the CICyT (Grant No. PB91–0840) is gratefully acknowledged. A.G. is grateful to the Dirección General de Investigación Científica y Técnica for financing his stay in Spain.

REFERENCES

1 I. Hemmila, Clin. Chem., 31 (1985) 359.
2 M.C. Gutiérrez, A. Gómez-Hens and D. Pérez-Bendito, Talanta, 36 (1989) 1187.
3 J.W. Wu, S. Hoskin, S.M. Riebe, J.E. Gifford and S.P. O'Neill, Clin. Chem., 28 (1982) 659.
4 J.W. Wu, C. Bunyagidj, S. Hoskin, S.M. Riebe, J. Aucker, K. White and S.P. O'Neill, Clin. Chem., 29 (1983) 1540.
5 J.D. Lin and H.L. Pardue, Clin. Chem., 28 (1982) 2081.
6 J.W. Skong and H.L. Pardue, Anal. Chem., 58 (1986) 2306.
7 A. Gómez-Hens and D. Pérez-Bendito, Anal. Chim. Acta., 242 (1991) 147.
8 G.G. Guilbault, Practical Fluorescence, Dekker, New York, 2nd edn., 1990.
9 S.P. Popelka, D.M. Miller, J.T. Holen and D.M. Kelso, Clin. Chem., 27 (1981) 1198.
10 G.L. Long and J.D. Winefordner, Anal. Chem., 55 (1983) 712A.
11 W.N. Rawls, in M. Bottorff (Ed.), Drug Monitoring Forum, Vol. 4, Abbott Laboratories, Irving, TX, 1985, p. 3.
12 P. Jatlow, Clin. Biochem., 18 (1985) 143.
13 C.A. Parvin, Clin. Chem., 30 (1984) 751.

Analytica Chimica Acta, 280 (1993) 137–143
Elsevier Science Publishers B.V., Amsterdam

Elimination of interferences in the determination of arsenic and selenium in biological samples by inductively coupled plasma mass spectrometry

J. Goossens, F. Vanhaecke, L. Moens and R. Dams

Laboratory of Analytical Chemistry, Institute for Nuclear Sciences, Ghent University, Proeftuinstraat 86, B-9000 Ghent (Belgium)

(Received 17th November 1992, revised manuscript received 26th January 1993)

Abstract

The determination of As and Se in biological samples by inductively coupled plasma mass spectrometry is well known to be degraded by spectral interferences. The resolution of quadrupole mass analysers is insufficient to resolve As^+ and Se^+ ions from polyatomic species such as $ArCl^+$, $ArAr^+$ and SO_3^+. A study of this problem in human serum also revealed substantial non-spectral interferences on these elements occurring in the presence of organic compounds. It is shown that both problems can easily be overcome by a combination of chemical modification (addition of 4% ethanol) with nebulizer flow-rate gas adjustment. Under these conditions the use of standard additions for calibration allowed As and Se to be determined accurately in samples of biological origin. The method developed was applied to human serum and urine and for both As and Se excellent agreement with certified values was obtained.

Keywords: Inductively coupled plasma mass spectrometry; Arsenic; Biological samples; Interferences; Selenium; Urine

Soon after the introduction of inductively coupled plasma mass spectrometry (ICP-MS), users became aware of the existence of both non-spectral and spectral interferences that seriously affected the analytical performance of the technique.

Non-spectral interferences are usually defined as matrix-induced signal variations (both suppression and enhancement) and are therefore often referred to as matrix effects. However, the number and variety of the mechanisms proposed to explain these effects show a lack of consensus [1–5].

Internal standardization as a correction for matrix effects and multiplicative effects in general is widely applied in ICP-MS analyses and is based on the assumption that the analyte and the element added as an internal standard undergo an equal relative signal intensity shift. This implies that the relative signal variation should be indifferent of the chemical and physical properties of both nuclides. This is not entirely true. Matrix-induced signal variation is recognized to be dependent on the analyte mass number in a regular way and in this context several workers have reported on the importance of a close match in terms of mass number between analyte and internal standard [6–8]. Taking this into consideration, accurate correction is possible for numerous elements in a large variety of matrices.

However, experience shows that the calibration of As and Se may be difficult, especially in biological and clinical matrices, and that correction by internal standardization for matrix-in-

Correspondence to: R. Dams, Laboratory of Analytical Chemistry, Institute for Nuclear Sciences, Ghent University, Proeftuinstraat 86, B-9000 Ghent (Belgium).

TABLE 1

Spectral interferences on As and Se in biological samples [25,26]

Element	Nuclide (abundance, %)	Interfering species
Arsenic	^{75}As (100)	$^{40}Ar^{35}Cl$
	^{76}Se (9.0)	$^{40}Ar^{36}Ar$
	^{77}Se (7.5)	$^{40}Ar^{37}Cl$
Selenium	^{78}Se (23.5)	$^{40}Ar^{38}Ar$
	^{80}Se (50.0)	$^{40}Ar^{40}Ar$
		$^{32}S^{16}O_3$
	^{82}Se (9.0)	$^{34}S^{16}O_3$

duced signal variation in some instances results in systematic error.

In addition to this calibration problem, the accuracy of As and Se determinations is well known to be seriously affected by the occurrence of spectral interferences [9–25], as the resolution of quadrupole mass spectrometers is not sufficient to resolve atomic and molecular species having the same nominal mass. The main interferences occurring in biological samples are listed in Table 1. As can be seen, the presence of Cl and S in the sample matrix results in the formation of $ArCl^+$ and SO_3^+ species [25,26], prohibiting the direct determination of As at m/z 75 and Se at m/z 77 and 82. The application of alternative nuclides for Se at m/z 76, 78 or 80 is made impossible by the generation of $ArAr^+$, primarily at m/z 80, but also significantly at m/z 76 and 78. In the (rare) cases where Se contributes significantly to the total signal at m/z 78, correction for ArAr by blank subtraction is dubious as the extent to which polyatomic species are formed depends strongly on the matrix conditions [21]. ^{74}Se (0.9%) has been omitted from Table 1 as its abundance is too low for practical analytical purposes. Krypton, often present as a contaminant in the Ar plasma gas, may interfere at m/z 78, 80 and 82, but these contributions usually are very low and can be accurately corrected for by blank subtraction.

In this paper, a study of both spectral and non-spectral interferences in the determination of As and Se is described. The merits of internal standardization and standard addition in correction for matrix effects were compared.

Spectral interferences on As and Se were dealt with by a new approach. The addition of appropriate amounts of ethanol in combination with nebulizer gas adjustment was found to allow $ArCl^+$ and $ArAr^+$ interferences up to 50 times higher than the genuine As^+ and Se^+ signals to be eliminated completely.

EXPERIMENTAL

Instrumentation

The instrument used was a VG PlasmaQuad ICP mass spectrometer (VG Elemental, Winsford, UK) equipped with a Fassel torch, a Gilson Minipuls-2 peristaltic pump, a Meinhard-type Tr-30-A3 concentric glass nebulizer and a double-pass Scott-type spray chamber with surrounding liquid jacket, the temperature of which was controlled at 10°C with a recirculating refrigeration–heating system. The operating conditions are summarized in Table 2.

Reagents and solutions

Commercial 1 g l^{-1} standard solutions of As (Fluka, prepared from As_2O_3) and Ga (Johnson

TABLE 2

VG PlasmaQuad operating conditions and acquisition parameters

Operating conditions	
Plasma	
R.f. power	Forward: 1350 W
	Reflected: < 5 W
Gas flow-rates	Plasma: 13.5 l min^{-1}
	Nebulizer: variable
	Auxiliary: 0.9 l min^{-1}
Ion sampling	
Sampling cone	Nickel, 1.0-mm orifice
Skimmer cone	Nickel, 0.75-mm orifice
Vacuum	
Expansion stage	2.3 mbar
Intermediate stage	2.0×10^{-4} mbar
Analyser stage	4.6×10^{-6} mbar
Acquisition parameters	
Mass range	69–85 u
Number of channels	512
Dwell time	160 μs
Number of sweeps	500
Total acquisition time	40.9 s

Matthey) and a 1 g l^{-1} Se standard solution [prepared by dissolution of Se metal (purity > 99.99%) in concentrated nitric acid] were diluted to 1 mg l^{-1} with 1% HNO_3. A 20% (v/v) ethanol solution was prepared by dilution of absolute ethanol (analytical-reagent grade, Merck). High-purity HNO_3 (14 M) and HCl (10 M) were obtained by sub-boiling distillation of the analytical-reagent grade acids (UCB) from quartz apparatus. Water obtained from a Milli-Q system (Millipore) was used throughout.

For qualitative experiments, commercial 1 g l^{-1} standard solutions of Co, Cu, Zn, Ge, Br, Rb and Sr were used. A Se(VI) solution was prepared by dissolving H_2SeO_4 in water; Se(IV) and As(V) solutions were purchased from Alfa Products and Merck.

Experiments on non-spectral interferences

The signal intensities of As^+, Se^+ and a number of elements with a similar mass number (Co, Cu, Zn, Ga, Ge, Rb, Br, Sr) were measured as a function of the nebulizer gas flow-rate. This was done in two different matrices: 1% HNO_3 and 1% HNO_3 + 1% EtOH. The results for Co and As are presented in Figs. 1a and 1b, respectively.

Experiments on spectral interferences

In addition to the effect on the As^+ and Se^+ signals, the effect of addition of ethanol on the formation of interfering polyatomic ions, in particular $ArCl^+$ and $ArAr^+$, was also investigated. An As (50 μg l^{-1}) and Se (500 μg l^{-1}) standard solution was spiked with increasing amounts of EtOH (1%, 2% and 4% of the final volume) and the signal intensities at m/z 75 (As) and 77 (Se) were measured as a function of the nebulizer gas flow-rate. Similarly, a 1% HCl solution was spiked with EtOH (1%, 2% and 4%) and the $^{40}Ar^{35}Cl^+$ and $^{40}Ar^{38}Ar^+$ signals at m/z 75 and 78, respectively, were measured. For ease of survey, all the results are plotted together in Figs. 2a–d.

Preparation of serum and urine samples

For both human serum [27] and human urine (NIST SRM 2670 Low Level Toxic Metals in Human Urine) a similar sample pretreatment was applied. These freeze-dried reference materials were reconstituted with an appropriate amount of water and all solutions obtained were divided into two subsamples, one of which was spiked with an As and Se standard solution (100 μg l^{-1}) for calibration by standard additions. Samples were adjusted to volume with 1% HNO_3 after addition of Ga (200 μg l^{-1}) as an internal standard and EtOH (4% v/v) as a chemical modifier (concentrations in parentheses refer to the final solutions analysed). The whole procedure implied an eightfold sample dilution, which is desirable to reduce signal suppression and clogging of the nebulizer to an acceptable minimum [28].

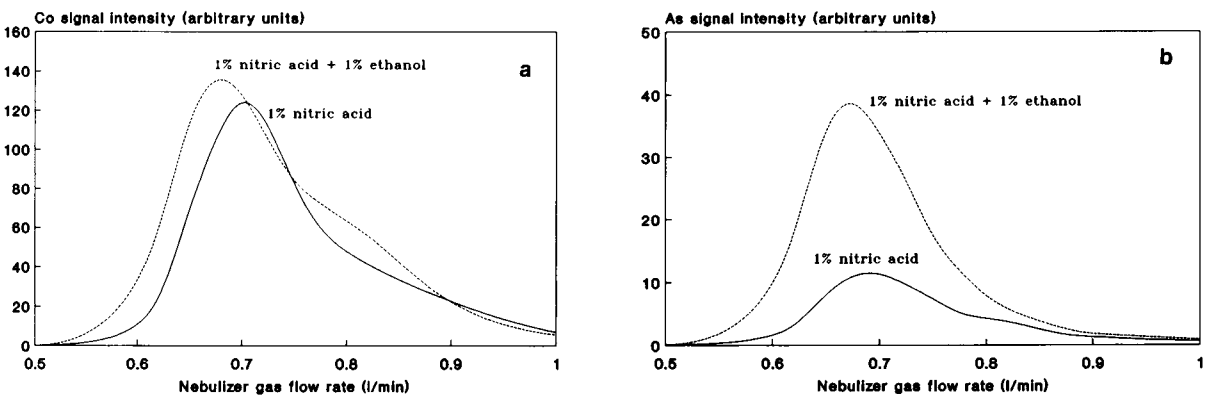

Fig. 1. Signal intensity as a function of nebulizer gas flow-rate for (a) $^{59}Co^+$ and (b) $^{75}As^+$ in two different matrices: 1% HNO_3 and 1% HNO_3 + 1% EtOH.

Procedure for serum and urine samples

Before each experiment the electrostatic lenses were tuned for maximum signal intensity of $^{71}Ga^+$ at a nebulizer gas flow-rate of ca. 0.74 l min^{-1}. The nebulizer gas flow-rate was then further adjusted by analysing a 0.2% HCl–4% EtOH solution with the quadrupole fixed at m/z 75 ($ArCl^+$ signal) and increasing the flow-rate until a minimum count rate was obtained. The mass scanning data acquisition mode was used and the acquisition parameters applied for all authentic samples are given in Table 2.

Standard addition (single addition) was applied as a calibration method and solutions were analysed in order of increasing concentration, i.e., blanks, unspiked samples, spiked samples. Each solution was measured five times and the As^+ and Se^+ signals were normalized to the $^{71}Ga^+$ signal.

RESULTS AND DISCUSSION

Non-spectral interferences on As and Se

Signal enhancement by the addition of a small amount of an organic solvent has been reported for several elements [6,29–31] and, in the present experiments, the phenomenon was observed to some extent (< 20%) for Co, Cu, Zn, Ga, Ge, Rb, Sr and Br on adding 1% EtOH to aqueous standard solutions. As illustrated for Co in Fig. 1a, the addition of 1% EtOH not only causes a

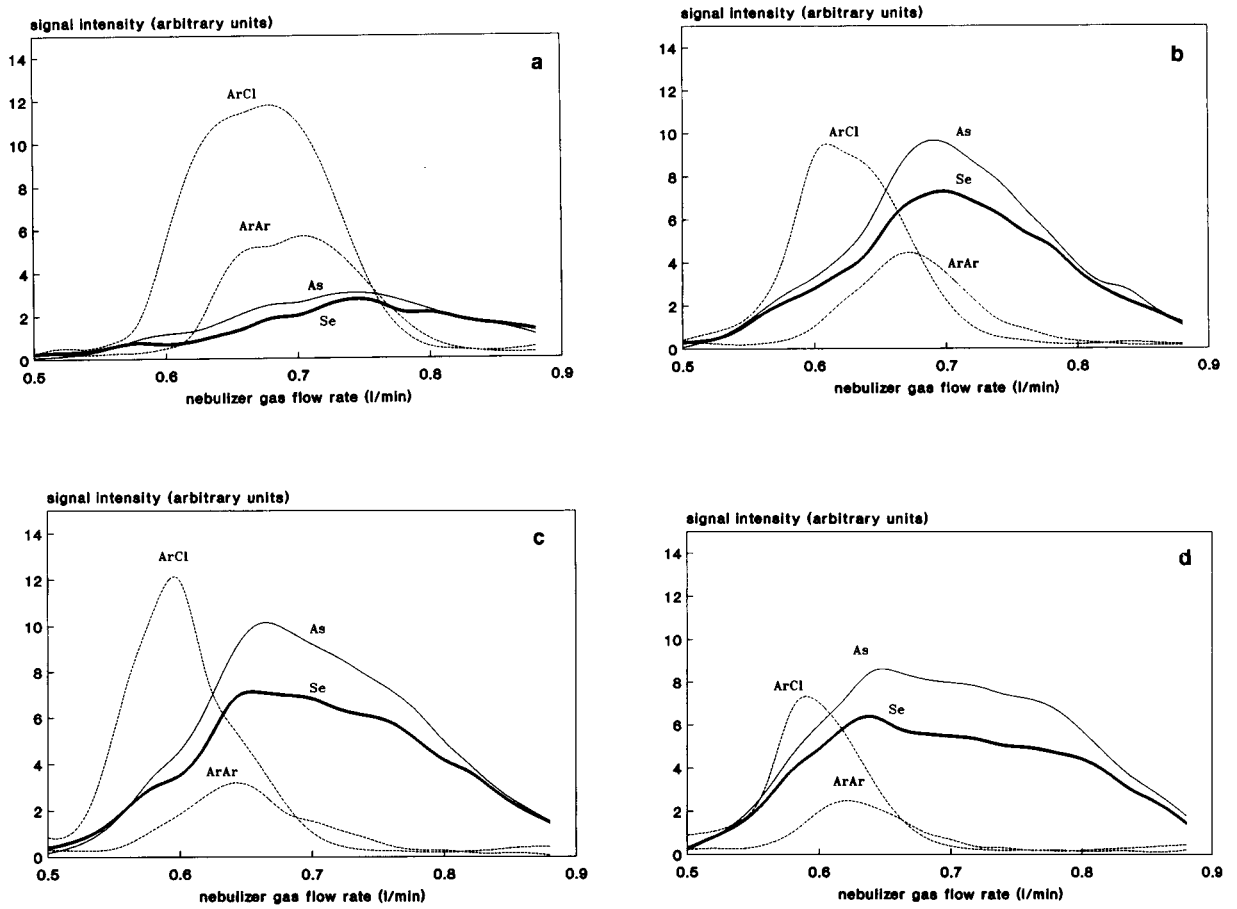

Fig. 2. $^{75}As^+$, $^{77}Se^+$, $^{40}Ar^{35}Cl^+$ and $^{40}Ar^{38}Ar^+$ signal intensity as a function of nebulizer gas-flow rate in (a) 1% HNO_3, (b) 1% HNO_3 + 1% EtOH (c) 1% HNO_3 + 2% EtOH and (d) 1% HNO_3 + 4% EtOH.

10% signal enhancement but also a shift of the maximum signal intensity to lower gas flow-rates. Both observations were recently explained by Vanhaecke et al. [5] as being caused by a contraction and spatial shift of the zone of maximum M^+ density in the plasma. However, this explanation seems insufficient with respect to the threefold As^+ and Se^+ signal enhancement observed on adding 1% EtOH to aqueous standard solutions (illustrated for As in Fig. 1b).

Additional studies showed that other organic matrices (e.g., 1% acetic acid) cause a similar As^+ and Se^+ signal enhancement, the magnitude of which was found to be indifferent of the oxidation state for both As(III or V) and Se(IV or VI). Comparative experiments made clear that the extreme signal enhancement cannot be completely attributed to the relatively high first ionization energy (As 9.81 eV, Se 9.75 eV) or to hydride formation as only a limited signal variation (< 15%) was observed for Br (ionization potential = 11.81 eV) and Ge, Sn, Sb and Pb, respectively. Possibly, volatilization effects contributed significantly to the signal enhancement as indicated by a similar behaviour for Hg in 1% EtOH. However, a conclusive explanation for the As^+ and Se^+ signal enhancement cannot be given and is the subject of current studies.

The most important conclusion to be drawn is that these matrix effects cannot be accurately corrected for by internal standardization. Matrix matching may offer a solution but, in view of the complex composition of most biological samples, standard addition seems to be a more practicable approach. However, whereas internal standardization (e.g., Ga) may not correct for the matrix effects described, it does for signal fluctuation and instrumental instability. This was confirmed experimentally as more accurate and precise results were obtained after normalization of both As^+ and Se^+ signals to the $^{71}Ga^+$ signal. Therefore, a combination of standard addition with internal standardization was applied in all analyses.

Spectral interferences on As and Se

Some interesting observations can be made from Fig. 2a–d: as indicated before, the absolute signal intensity of both As and Se is strongly matrix dependent; addition of ethanol results in a shift of the optimum nebulizer gas flow-rate to lower values both for analytes and ArCl interferences; the addition of increasing amounts of ethanol makes the signal intensity become less and less dependent on the nebulizer gas flow-rate, as reflected by a dilatation of the plots of As and Se; in contrast, the plot for ArCl shows a contraction as more ethanol is added and the maximum signal intensity of $ArCl^+$ is decreased by a factor of 2 on addition of 4% EtOH. Similar observations can be made when comparing the $^{40}Ar^{38}Ar$ plot with the ^{77}Se plot.

From Fig. 2d, it is clear that by the addition of ethanol (4%) to the samples in combination with nebulizer gas flow-rate adjustment, both As (m/z 75) and Se (m/z 77 and 78) can be determined sensitively, while the occurrence of spectral interferences is decreased significantly. The signal enhancement and the decreased dependence on the nebulizer gas flow-rate caused by the addition of an organic solvent permit accurate and precise measurement at non-ideal gas flow-rates. In fact, the sensitivity even increases on adding ethanol and adjusting the nebulizer gas flow-rate to 0.780 l min^{-1} in comparison with aqueous samples measured at ideal gas flow-rates. A 4% EtOH content was regarded as an optimum as both higher and lower contents resulted in decreased $^{75}As^+/^{40}Ar^{35}Cl^+$ and $^{77}Se^+/^{40}Ar^{37}Cl^+$ signal ratios.

Evans and Ebdon [17] reported that the addition of propan-2-ol to aqueous solutions could significantly decrease $ArCl^+$ and $ArAr^+$ interferences and suggested two mechanisms in explanation: suppressed ionization and increased breakdown of the polyatomic species due to altered plasma conditions and competitive formation of ArC^+. The present experiments confirmed the observations by Evans and Ebdon but it appeared that on addition of a small amount (< 5%) of an organic solvent the occurrence of spectral interferences is only shifted to lower carrier gas flow-rates and hence there is no actual suppression of the formation of polyatomic species. It can be seen from Fig. 2a–c that, at a given nebulizer gas flow-rate, the addition of 1–2% EtOH may im-

prove the $^{75}As^+/^{40}Ar^{35}Cl^+$ and $^{77}Se^+/^{40}Ar^{37}Cl^+$ signal ratios to a substantial extent whereas the absolute $ArCl^+$ signal intensity is hardly decreased but only shifts to lower flow-rates.

Analysis of human serum and urine

Two typical chlorine matrices (human serum and urine) were analysed using the procedure described. The nebulizer gas flow-rate was adjusted as described above and over a period of several months the value obtained ranged between 0.770 and 0.790 l min^{-1}. Further increase in the nebulizer gas flow-rate would unnecessarily decrease the As^+ and Se^+ signal intensity (cf., Fig. 2d). At a flow-rate of ca. 0.780 l min^{-1}, the blank at m/z 78 is approximately double that at m/z 75 and 77 owing to residual $^{40}Ar^{38}Ar$, but can at this (low) level be accurately corrected for by blank subtraction.

A drawback of the method is that the significance of residual spectral interferences cannot be determined directly. A comparison can be made with an appropriate HCl–EtOH mixture but the extent to which $ArAr^+$ and $ArCl^+$ are formed will differ as the matrix conditions are changed. However, the signal at m/z 76 or 80 due to residual $^{40}Ar^{36}Ar^+$ or $^{40}Ar^{40}Ar^+$ can be regarded as a monitor of the occurrence of or change in the $^{40}Ar^{38}Ar^+$ interference at m/z 78. In addition, the good agreement between the results obtained for ^{78}Se and ^{77}Se indicates to some extent the absence of significant contribution of residual ArCl at m/z 77 and, for sufficiently high As concentrations, also at m/z 75.

As a second solution, appropriate amounts of HCl can be added to the sample while the signals at m/z 75 and 77 are observed. This was done for the analysis of both human serum and urine: eightfold diluted samples (containing 4% EtOH) were spiked with 0.2% (v/v) HCl (ca. 0.7 g l^{-1} Cl). Although the Cl content of the samples was thus more than doubled, no significant signal enhancement was observed on measuring at a nebulizer gas flow-rate of ca. 0.780 l min^{-1}.

For human serum, four replicates were prepared and analysed as described above. Certified concentrations for As and Se in human serum are 1.78 and 95.5 $\mu g\ l^{-1}$, respectively [27]. When no ethanol is added and when using a gas flow-rate appropriate for maximum signal intensity of the internal standard, ArCl interferences at m/z 75 and 77 would cause the signals to be enhanced by a factor of 50 and 4, respectively. Further, $^{40}Ar^{38}Ar$ and $^{34}S^{16}O_3$ interferences at m/z 78 and 82 result in a fourfold signal increase. As can be seen from Table 3, the procedure described allows the accurate and precise determination of both As and Se, for the latter element based on two different isotopes. Determination of Se at m/z 82 resulted in a concentration of 93.0 ± 6.9 $\mu g\ l^{-1}$, which is also in good agreement with the certified value. However, the influence of ethanol addition on the SO_3^+ signals was not fully investigated.

TABLE 3

Determination of As and Se in human serum reference material [27]

Element	m/z value monitored	ICP-MS result ($\mu g\ l^{-1}$) [a]	Certified concentration ($\mu g\ l^{-1}$)
Arsenic	75	1.60 ± 0.04	1.78 ± 0.36
Selenium	77	99.3 ± 3.1	95.5 ± 4.6
	78	97.0 ± 4.4	

[a] Uncertainties are expressed as 95% confidence intervals.

For human urine, again four replicates were analysed. Without chemical modification and nebulizer gas flow-rate adjustment, $^{40}Ar^{37}Cl^+$ would cause a fifteenfold signals enhancement on m/z 77 while the signal at m/z 75 would be approximately 50% higher than expected from the As concentration. The results are given in

TABLE 4

Determination of As and Se in human urine reference material

Element	m/z value monitored	ICP-MS result ($\mu g\ l^{-1}$) [a]	Certified or indicative concentration ($\mu g\ l^{-1}$)
Arsenic	75	86.9 ± 1.4	60 [b]
Selenium	77	35.6 ± 6.4	30 ± 8 [c]
	78	36.4 ± 2.2	

[a] Uncertainties are expressed as 95% confidence intervals. [b] Indicative. [c] Certified.

Table 4 and are in good agreement with the certified (Se) or indicative (As) values. In this instance, determination of Se at m/z 82 resulted in systematically higher results (ca. 42 $\mu g\ l^{-1}$).

Conclusions

A combination of chemical modification with nebulizer gas flow-rate adjustment allows As and Se to be accurately determined in chlorine matrices. The method requires a minimum of sample pretreatment and therefore can be easily applied in routine analysis. Under these conditions, standard addition as a calibration method permits the accurate determination of As and Se in biological samples, as illustrated by the excellent agreement with the certified values of results obtained for As and Se in human serum and urine.

REFERENCES

1 D. Beauchemin, J.W. McLaren and S.S. Berman, Spectrochim. Acta, Part B, 42 (1987) 467.
2 J.A. Olivares and R.S. Houk, Anal. Chem., 58 (1986) 20.
3 D.C. Gregoire, Spectrochim. Acta, Part B, 42 (1987) 895.
4 G.R. Gillson, D.J. Douglas, J.E. Fulford, K.W. Halligan and S.D. Tanner, Anal. Chem., 60 (1988) 1472.
5 F. Vanhaecke, R. Dams and C. Vandecasteele, J. Anal. At. Spectrom., in press.
6 F. Vanhaecke, H. Vanhoe, R. Dams and C. Vandecasteele, Talanta, 39 (1992) 373.
7 J.J. Thompson and R.S. Houk, Appl. Spectrosc., 41 (1987) 801.
8 W. Doherty, Spectrochim. Acta, Part B, 44 (1989) 263.
9 A.L. Gray, Spectrochim. Acta, Part B, 41 (1986) 151.
10 A.R. Date, Y.Y. Cheung and M.E. Stuart, Spectrochim. Acta, Part B, 42 (1987) 3.
11 D. Beauchemin and J.M. Craig, Spectrochim. Acta, Part B, 46 (1991) 603.
12 J.W. McLaren, D. Beauchemin and S.S. Berman, J. Anal. At. Spectrom., 2 (1987) 277.
13 L.C. Alves, D.R. Wiederin and R.S. Houk, Anal. Chem., 64 (1992) 1164.
14 S. Branch, L. Ebdon, M. Ford, M. Foulkes and P. O'Neill, J. Anal. At. Spectrom., 6 (1991) 151.
15 S. Branch, W.T. Corns, L. Ebdon, S. Hill and P. O'Neill, J. Anal. At. Spectrom., 6 (1991) 155.
16 W.T. Buckley, J.J. Budac, D.V. Godfrey and K.M. Koenig, Anal. Chem., 64 (1992) 299.
17 E.H. Evans and L. Ebdon, J. Anal. At. Spectrom., 4 (1989) 299.
18 E.H. Evans and L. Ebdon, J. Anal. At. Spectrom., 5 (1990) 425.
19 S.H. Hansen, E.H. Larsen, G. Pritzl and C. Cornett, J. Anal. At. Spectrom., 7 (1992) 629.
20 T.D.B. Lyon, G.S. Fell, R.C. Hutton and A.N. Eaton, J. Anal. At. Spectrom., 3 (1988) 265.
21 T.D.B. Lyon, G.S. Fell, R.C. Hutton and A.N. Eaton, J. Anal. At. Spectrom., 3 (1988) 601.
22 S. Munro, L. Ebdon and D.J. McWeeny, J. Anal. At. Spectrom., 1 (1986) 211.
23 P.S. Ridout, H.R. Jones and J.G. Williams, Analyst, 113 (1988) 1383.
24 B.S. Sheppard, J.A. Caruso, D.T. Heitkemper and K.A. Wolnik, Analyst, 117 (1992) 971.
25 S.H. Tan and G. Horlick, Appl. Spectrosc., 40 (1986) 445.
26 H. Vanhoe, PhD Thesis, Ghent University, Ghent, 1992.
27 J. Versieck, L. Vanballenberghe, A. De Kesel, J. Hoste, B. Wallaeys, J. Vandenhaute, N. Baeck and F.W. Sunderman, Anal. Chim. Acta, 204 (1988) 63.
28 H. Vanhoe, C. Vandecasteele, J. Versieck and R. Dams, Anal. Chem., 61 (1989) 1851.
29 H.P. Longerich, J. Anal. At. Spectrom., 4 (1989) 665.
30 J. Marshall and J. Franks, J. Anal. At. Spectrom., 6 (1991) 591.
31 P. Allain, L. Jaunault, Y. Mauras, J.M. Mermet and T. Delaporte, Anal. Chem., 63 (1991) 1497.

Analytica Chimica Acta, 280 (1993) 145–155
Elsevier Science Publishers B.V., Amsterdam

Simulation of ^{13}C nuclear magnetic resonance spectra of indoles

M.L. Ranc and P.C. Jurs

152 Davey Laboratory, Department of Chemistry, Penn State University, University Park, PA 16802 (USA)

(Received 14th December 1992; revised manuscript received 28th January 1993)

Abstract

Linear models are developed to predict the ^{13}C NMR chemical shifts of carbons in indole moieties based on a critical review. These models fill a gap in the spectral simulation database which is used to simulate the ^{13}C NMR spectra of a wide range of organic compounds, illustrating that this is a viable method for the expansion of the database. The models are based on calculated numerical parameters (descriptors) which encode the topological and topological-electronic environments of the eight indole carbons. The 56 indoles in the reference set have a mean r.m.s. error of 0.93 ppm and the 42 indoles in the prediction set have an error of 2.04 ppm. The spectral error for *N*-substituted indoles is higher than that of *N*-unsubstituted indoles.

Keywords: Nuclear magnetic resonance; Indoles; Simulation

Naturally occurring and synthetic indoles and indole alkaloids often exhibit important pharmacological properties. ^{13}C nuclear magnetic resonance spectroscopy (^{13}C NMR) is a valuable tool in the structure elucidation of these compounds; for example, Erra-Balsells and Frasca [1] used ^{13}C NMR data to identify isolated indole alkaloids and photochemical products. However, it is often difficult to unambiguously assign the peaks in these spectra. In 1987, Morales-Ríos et al. [2] attempted to provide a reference set of shifts for future comparison through a critical review of existing literature. This review dealt with indole derivatives containing an unsubstituted benzenoid ring. Comparison of the shifts in the review, many of which have been reassigned, with unknown indoles was intended to lead to more accurate identification of the peaks.

A different approach to the identification of an unknown indole, and unambiguous assignment of its chemical shift peaks, is spectrum simulation. One method of spectrum simulation involves the development of linear equations, or models, based on structural parameters which describe the chemical environments of carbon atoms. Such models have the form

$$S = b_0 + b_1 X_1 + b_2 + \cdots + b_d X_d$$

where S is the estimated chemical shift for the carbon center of interest, the X_i are numerical descriptors (parameters) which encode the chemical environment of the carbon center, the b_i are coefficients determined by multiple linear regression analysis, and d denotes the number of descriptors used in the model.

The goal of our research is to develop the capability to simulate ^{13}C NMR spectra for a wide range of organic compounds. A major component of this has been the creation of a spectral simulation database containing predictive equations [3] and the development of methods to use

Correspondence to: P.C. Jurs, Department of Chemistry, Penn State University, University Park, PA 16802 (USA).

these equations to predict the chemical shifts of other compounds [3,4].

It was determined that the models in the spectral simulation database could not accurately predict the chemical shifts of indoles. This paper investigates the utility of developing models for a given moiety, in this case the indole moiety, as a method of expanding the database. In this regard the critical question to be answered is whether the ^{13}C NMR spectra for the eight carbons in the indole moiety can be accurately simulated despite small differences in the chemical shifts. A secondary goal of this research was to determine if the reassignments made in the review paper could be verified.

EXPERIMENTAL

Morales-Ríos et al. [2] reviewed the chemical shifts of several hundred indole derivatives. The following numbering system will be used:

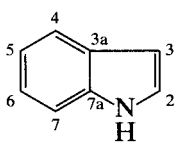

Shifts for the eight indole carbons were gathered from many primary literature sources. The authors reassigned some peaks, while they indicated that other peaks might be unreliable or interchangable. The variety of primary sources means that the spectra were collected under varying experimental conditions. Spectra were reported for 298 indole derivatives, with some compounds having ^{13}C NMR spectra recorded in more than one solvent (such as DMSO-d_6 and dioxane).

McIntyre and Small [5] have shown that ^{13}C NMR shift differences due to varying experimental conditions can be corrected for if overlap exists. This calibration method cannot be used with this data set due to the number of sources and lack of duplication among the ^{13}C NMR spectra. The chemical shifts of indoles are affected by solvent and concentration. To somewhat limit these effects, only spectra collected in $CDCl_3$ were used in our study. The concentrations are not reported. Of the 298 compounds, 32 were eliminated because they showed atypical chemical shifts for carbons 3, 3a, 6, and 7a. Additional compounds were eliminated due to ADAPT limitations, those with more than 40 non-hydrogen atoms and those containing a sulfur or phosphorus atom. A total of 145 spectra, in $CDCl_3$, were considered for use in this study. These were divided into two groups based on Morales-Ríos et al.'s evaluation of the spectra. The training set compounds generally were those which had the fewest reassigned, unreliable, and interchangable peaks. The molecular structures for the 98 indoles chosen for inclusion in this study are shown in Fig. 1. These indole alkaloids are generally known by common names, and since the structures are more informative than the compound names, only the structures have been shown.

The chemical structures and their associated ^{13}C NMR spectra were entered manually into computer files using the ADAPT software system [6–8]. The simulation of ^{13}C NMR spectra is a multistep procedure. Subsetting to divide the carbons into smaller, more homogeneous groups is performed. A series of atom-based descriptors are calculated and statistical analysis is used to reduce the number of descriptors. This reduced set is submitted to regression analysis to generate the linear models directly linking the calculated descriptors to the chemical shifts. The models are evaluated and then used to assemble the simulated spectra. These steps have been discussed in detail elsewhere [9,10] The computer programs implementing this methodology comprise ADAPT and are now running on a Sun 4/110 workstation.

RESULTS AND DISCUSSION

Evaluation of the spectral simulation database

The spectral simulation database consisted of 71 models capable of predicting the ^{13}C NMR chemical shifts of linear and branched alkanes [11], cycloalkanes [12], cyclohexanols and decalols [13], hydroxysteriods [14], cyclopentanes and cyclopentanols [15], norboranols [16], cyclohexanones and decalones [17], piperidines [18], polychlrinated biphenyls [19], alkyl-substituted ben-

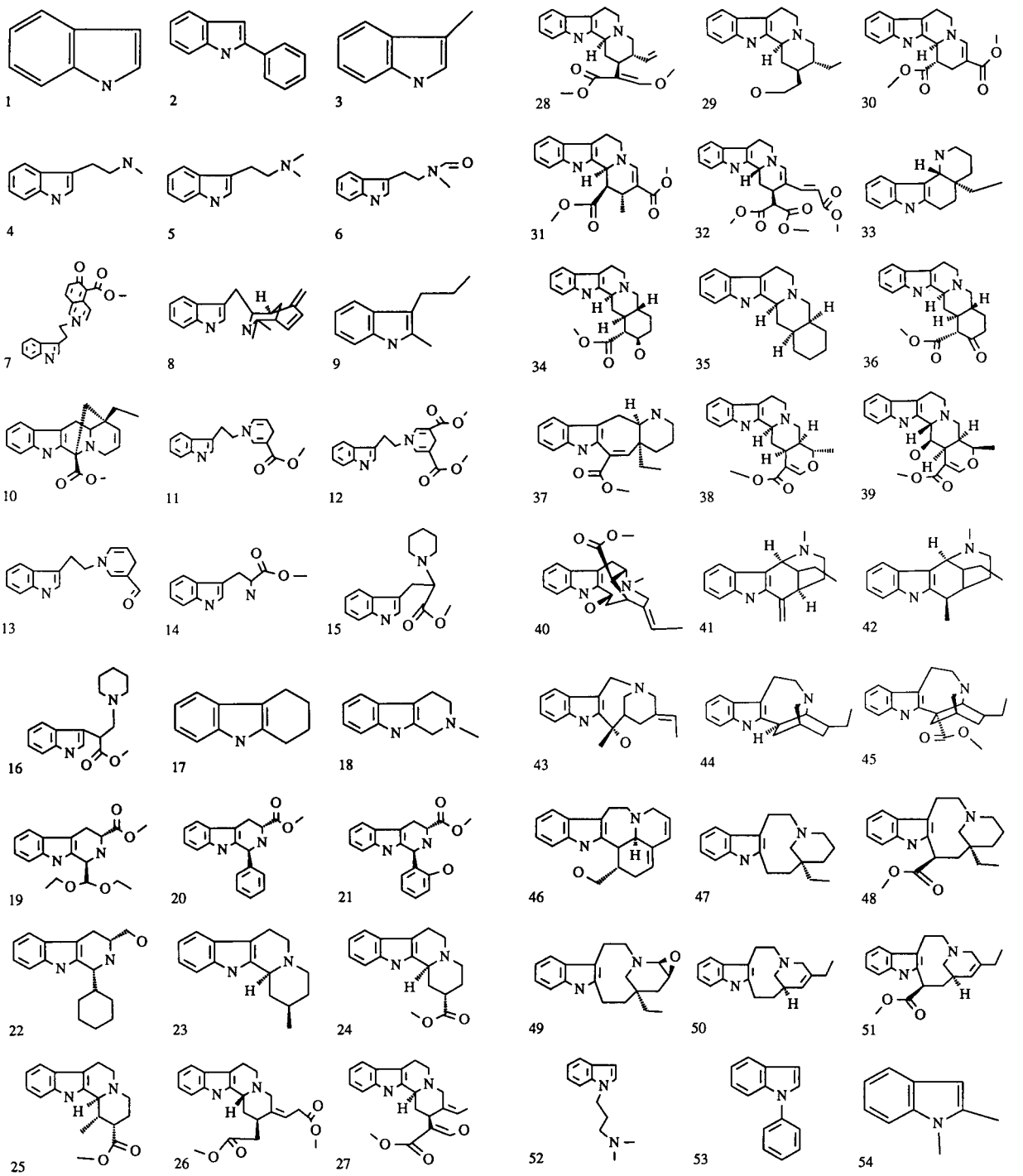

Fig. 1. The 98 indole compounds used in the study. The numbering of the indole moiety for all compounds follows the IUPAC numbering scheme for indole (1).

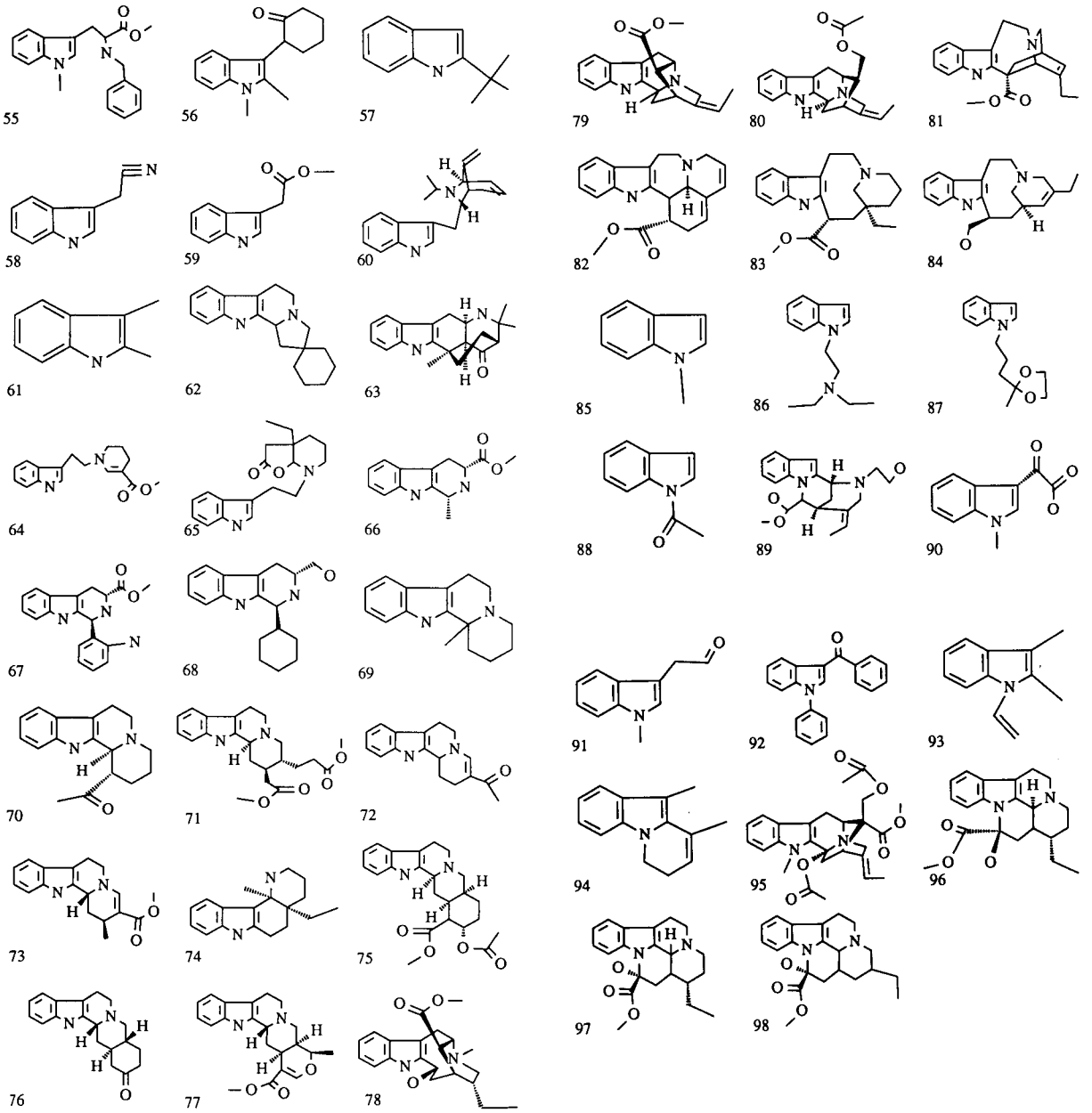

Fig. 1 (continued).

zenes and polyaromatics [20], ketosteriods [3] quinolines and isoquinolines [21], and cyclopentanones and cycloheptanones [4].

Twelve of the Indoles (**4**, **7**, **14**, **22**, **29**, **30**, **34**, **35**, **39**, **42**, **52**, **56**) were used to probe the database and verify that indole models would expand the scope of the existing database. Accurate three-dimensional atomic coordinates are needed for these compounds since most models in the database include geometric descriptors. These coordinates were generated with AMPAC [22,23].

Model selection has been described previously

[3,4] and therefore will only be briefly reviewed here. An atom-based approach to model selection [4], where each carbon is represented by a seven-dimensional vector, is used. Each carbon in the database is represented by the six descriptors used by MOS [14,24] and Randić's atomic ID descriptor [25]. The Euclidean distance from the carbon being evaluated, represented by a similar seven-dimensional vector, to each carbon in the database is calculated and the model associated with the closest carbon, or nearest neighbor, is used to predict the chemical shift of the query carbon.

For the carbons in the 12 probe indoles, models developed for quinolines and isoquinolines [21] are generally chosen. Other models selected were originally used to predict the chemical shifts of PAHs [20] and PCBs [19]. For example, quinoline/isoquinoline models are chosen for compound **4**. For carbons 3a and 7a the bridge carbon model was chosen. For carbons 3,4, and 7 the model for carbons one bond from a bridge carbon was chosen, while for the remaining carbons (2, 5 and 6) it was the model for those carbons two bonds from a bridge carbon. Table 1 shows the correlation coefficient and the standard error for each predicted spectrum. The large residual root mean square (r.m.s.) errors between the simulated and observed spectra, 10.55 to 58.95 ppm, indicate a gap in the database and justify the development of linear predictive models for the indole data set.

TABLE 1

Model selection evaluation

Compound [a]	R [b]	s [c]
4	0.338	13.43
7	0.244	12.72
14	0.289	12.12
22	0.189	18.90
29	0.082	15.08
30	0.175	15.41
34	0.074	15.39
35	0.075	13.28
39	0.140	13.87
42	0.548	58.95
52	0.021	17.27
56	0.516	10.55

[a] Compound number from Fig. 1. [b] R, multiple correlation coefficient. [c] s, standard error of estimate, in ppm.

Definition of study

This study involves 98 indoles (Fig. 1), 56 compounds in the training set and 42 in the prediction set. The prediction set is used in the final stage of the study to analyze the external predictive ability of the models generated from the training set.

The 56 training set compounds contain a total of 448 unique indole moiety carbons. In order to simplify the problem of chemical shift estimation, these carbons are divided into subsets. In the past, subsetting based on atom connectivity has proven useful, but this scheme is not applicable to the current data set. Instead, the 448 carbons were divided into six subsets based on relative position in the indole moiety. Subset A (carbons 5 and 6) and subset B (carbons 4 and 7) each contain 112 carbons, and subsets C (carbon 7a), D (carbon 3a), E (carbon 3), and F (carbon 2) contain 56 carbons each.

Descriptor generation and model formation

The environment surrounding each carbon center is encoded with a series of calculated topological and electronic descriptors. The compounds were not submitted to a molecular mechanics program to obtain three-dimensional atomic coordinates because of the flexibility of the indole substituents. Without these coordinates, geometric descriptors cannot be calculated. All relevant topological descriptors were investigated. Only those electronic descriptors which are topological in nature, σ and empirical atomic charges [26,27], were calculated.

For each of the subsets, the descriptors are screened using statistical procedures described previously [13,28] so that the information content is maximized while minimizing the number of descriptors. The remaining, statistically significant, descriptors are submitted to stepwise multiple linear regression analysis procedures. The resulting models are evaluated based on several statistical criteria, including standard error (s), correlation coefficient (R), outlier detection, and internal validation [29–32].

TABLE 2

Chemical shift models

p	Desc. [a]	Mean	S.D. [b]	Coefficient	Mean effect (ppm)
Subset A model: carbons 5 and 6					
1	NTAC 2	−0.0760	0.0474	17.2 ± 2.1	−1.31 ± 0.16
2	TESV 1	2.07	0.05	−4.34 ± 0.90	−8.98 ± 1.86
3	NTAC 4	−0.127	0.071	4.31 ± 1.40	−0.547 ± 0.178
4	Intercept			131	
Subset B model: carbon 4 and 7					
1	MNCG 2	−0.195	0.169	15.0 ± 0.4	−2.93 ± 0.08
2	WCG2 3	0.00971	0.00466	−343 ± 14	−3.33 ± 0.14
3	NNHY 4	2.56	1.21	−0.193 ± 0.038	−0.494 ± 0.097
4	Intercept			115	
Subset C model: carbon 7a					
1	TRAN 1	0.118	0.228	−1.37 ± 0.27	−0.162 ± 0.032
2	NTCG 2	0.0202	0.0355	−8.75 ± 2.74	−0.177 ± 0.055
3	MPAC 3	−0.00557	0.03815	14.5 ± 2.4	−0.0808 ± 0.0134
4	ICNC 4	0.881	0.381	−0.706 ± 0.310	−0.622 ± 0.273
5	Intercept			137	
Subset D model: carbon 3a					
1	NNHY 4	2.18	2.37	0.286 ± 0.056	0.623 ± 0.122
2	BDOX 1	3.96	3.25	−0.127 ± 0.028	−0.503 ± 0.111
3	MNCG 3	−0.0543	0.0608	5.70 ± 2.25	−0.310 ± 0.122
4	Intercept			128	
Subset E model: carbon 3					
1	WCG5 2	−0.114	0.036	−49.2 ± 8.5	5.61 ± 0.97
2	TESV 1	1.43	0.27	−5.03 ± 1.20	−7.19 ± 1.72
3	CB09 2	0.661	0.668	−1.16 ± 0.37	−0.775 ± 0.247
4	Intercept			111	
Subset F model: carbon 2					
1	NNAT 1	2.71	0.46	11.0 ± 0.8	29.8 ± 2.2
2	NNHY 2	3.32	1.38	1.59 ± 0.25	5.28 ± 0.83
3	MNAC 2	−0.143	0.117	11.1 ± 2.5	−1.59 ± 0.36
4	CB 10 1	0.946	0.353	−2.72 ± 0.76	−2.57 ± 0.72
5	Intercept			101	

[a] Descriptor definition ("heavy atoms" denotes all non-hydrogen atoms). *Topological*: BDOX 1, the number of bonds from the carbon center to the nearest oxygen; CB09 2, the number of carbons with three single bonds located β to the carbon center; CB10 1, the number of carbons with two single and one double bond located α to the carbon center; ICNC 4, the corrected connectivity index computed over bonds four bonds'from the carbon center; NNAT 1, the number of heavy atoms α to the carbon center; NNHY 2, the number of hydrogens attached to heavy atoms within two bonds of the carbon center; NNHY 4, the number of hydrogens attached to heavy atoms within four bonds of the carbon center. *Electronic*: MNAC 2, the most negative atomic charge among atoms β to the carbon center; MNCG 2, the most negative σ charge among atoms β to the carbon center; MNCG 3, the most negative σ charge among atoms γ to the carbon center; MPAC 3, the most positive atomic charge among atoms y to the carbon center; NTAC 2, the sum of the atomic charges for all heavy atoms β to the carbon center; NTAC 4, the sum of the atomic charges for all heavy atoms δ to the carbon center; NTCG 2, the sum of the σ charges for all heavy atoms β to the carbon center; TESV 1, the electrotopological state for the carbon of interest; TRAN 1, the square of the net atomic charge for all heavy atoms five bonds from the carbon center; WCG2 3, the weighted sum (by the inverse cubed topological distance) of the σ charges on heavy atoms within two bonds of the carbon center; WCG5 2, the weighted sum (by the inversed squared topological distance) of the σ charges on heavy atoms within five bonds of the carbon center. [b] S.D., standard deviation.

Model evaluation for subset C, carbon 7a, indicated the presence of two outliers. A check of the original literature [33–35] indicated that the chemical shifts were transcribed correctly in Morales-Ríos's review [2]. These two outliers, from compounds **10** and **37**, were removed. New models are generated for subset C, which now contains 54 carbons.

The performance of a set of models as a unit in simulating the complete spectrum is also considered in the selection of superior models. The best model found for each subset is shown in Table 2. The descriptor labels are defined in the footnote, and the mean, the standard deviation, the regression coefficient, and the mean effect on the estimated chemical shift are presented for each descriptor. The mean effect is a measure of the shielding or deshielding effects of each descriptor.

Model evaluation

In the past, a standard error of estimate (s) of approximately 1 ppm for each model was sufficient to simulate accurate ^{13}C NMR spectra. In this study, that was not the case due to the similarity of the chemical shifts. For example, the carbon shifts of the compounds in subset D have a range of 3.7 ppm and a standard deviation of 0.9 ppm. To generate accurate simulated spectra, an s of approximately 0.5 ppm is needed for subsets A–E and about 1 ppm for subset F.

The subset C model uses a transformed variable (TRAN 1) because the untransformed variable was nonlinear. Squaring the original variable corrected for this and the resulting variable was more highly correlated with the dependent variable (chemical shift).

A summary of some important statistics for each atom subset and their corresponding regression models is given in Table 3. The low, high, mean, and the standard deviation of the chemical shifts for each subset and the number of carbons in each group are presented. As discussed above, the subset for carbon 7a (subset C) has 54 carbons instead of 56 since two were discarded as outliers. The relatively low correlations, in conjunction with standard errors of less than 1 ppm, results from s being close to the standard deviation. How this effects the simulated spectra is discussed below. For all models the F value is statistically valid, indicating that a regression relation does exist.

The effects of substituents attached to the nitrogen are not well encoded, perhaps accounting for the relatively high s for carbons 2 and 3. This is not unexpected since N-substituted indoles are not well represented in the training set, only 5 of the 56 compounds are substituted at the nitrogen. This could be corrected for by adding additional compounds to the training set or by developing additional models for this class of compounds.

The primary objective of this work is to simulate observed spectra accurately. In order to eval-

TABLE 3

Summary of chemical shift data and model statistics

Model [a]	Observed chemical shifts					Model statistics				
	Low	High	Mean	S.D. [b]	n [c]	d [d]	R	R(adj) [e]	F [f]	s [g]
A	118.1	122.9	120.2	1.3	112	3	0.925	0.923	212.9	0.48
B	108.6	120.7	114.5	3.9	112	3	0.993	0.992	2411	0.48
C	134.5	137.4	135.9	0.6	54	4	0.751	0.733	15.8	0.42
D	126.2	129.9	127.6	0.9	56	3	0.725	0.712	19.2	0.64
E	98.5	113.9	108.5	3.2	56	3	0.868	0.862	52.8	1.66
F	121.1	141.9	131.7	6.1	56	4	0.956	0.954	136.7	1.84

[a] Model identification. A, carbons 5 and 6; B, carbons 4 and 7; c, carbon 7a; D, carbon 3a; E, carbon 3; F, carbon 2. [b] S.D., standard deviation. [c] n, number of carbons in the subset. [d] d, number of descriptors in the model. [e] R(adj), multiple correlation coefficient, adjusted for degrees of freedom. [f] F, F value for statistical significance of the model. [g] s, standard error of estimate, in ppm.

uate the utility of the generated models, the estimated chemical shifts were combined to form complete spectra for the 56 indole moities, and the residual mean square (r.m.s.) error between each simulated and observed spectrum was determined. The spectral r.m.s. error ranged from 0.20 to 1.84 ppm, with a mean error of 0.930 ppm.

Library searches

To further evaluate how well the simulated spectra approximate the observed spectra, a computer-aided library search procedure was employed. This qualitative evaluation procedure uses the Euclidean distance metric as the measure of similarity between the query spectrum and the library spectrum and reports the top five matches to each simulated spectrum. The library used for these tests consists of approximately 950 spectra. The library contains spectra of compounds ranging from simple alkanes to steroids and other complex, fused-ring compounds. In addition, 145 indole spectra (the 98 used in this study and 47 others from Morales-Ríos' paper) and the spectra of various quinolines, isoquinolines, PAHs, and PCBs, which nearest-neighbor model selection indicated were the most similar to indoles, are included in the library.

Search results indicate that the models are accurate enough to distinguish substitution patterns but not to identify a specific indole. Table 4 summarizes the library search results. All five matches correctly identified the substitution pattern for all of the 3-substituted indoles and 35 of 37 2,3-disubstituted. The two remaining 2,3-disubstituted indoles were **10** and **37**. These were the compounds where carbon 7a was identified as an outlier. Indole **10** was not found among the top five matches, but two 2,3-disubstituted and three 3-substituted indoles were found. The top matches for indole **37** were a 2,3-disubstituted indole (not **37**) and four 3-substituted indoles.

TABLE 4

Library search results (N/A = not applicable)

Substitution	Training set		Prediction set	
	n	Top 5	*n*	Top 5
–	1	1	0	N/A
2	1	1	1	1
3	12	6	5	0
2, 3	37	3	22	4
1	2	2	4	3
1, 2	1	1	1	1
1, 3	1	0	3	0
1, 2, 3	1	0	6	0
Total	56	14	42	9

The library contains the spectra of two 2-substituted indoles. The spectrum for 2-phenylindole (**2**) was identified as the closest match for the simulated spectrum; however, the other 2-substituted indole was not among the top five matches. Instead, the ^{13}C NMR spectra of four 1-substituted indoles were found.

As mentioned previously, the *N* -substituted indoles are not well modeled due to the lack of representation in the training set. As indicated in Table 4 only 5 of the 56 indoles are substituted at the nitrogen.

Simulation of prediction set

To test the external predictive ability of these six models, the ^{13}C NMR spectra of 42 indoles (**57–98**) not used in generating the regression models are simulated. The 336 unique carbons are divided into subsets similar to those used for the training set. The shifts are estimated using the coefficients of the regression models discussed above with descriptors values calculated for each atom in the prediction compounds. These shifts are then combined to produce simulated spectra. The mean r.m.s. spectral error is 2.04 ppm, ranging from 0.314 to 8.175 ppm. Library search results are summarized in Table 4.

The spectra simulated for *N*-substituted indoles were generally not as accurate as those for indoles with an unsubstituted nitrogen, due to the lack of representation in the training set. The three 1,3-disubstituted indoles (**90–92**) had a mean r.m.s. error of 7.34 ppm. None of the simulated spectra were matched with the corresponding observed spectra, and only indole **91** found a 1,3-disubstituted indole spectrum among the top five matches. Compared with the overal mean r.m.s. error of 2.04 ppm, the *N*-substitued indoles had an error of 3.44 ppm while the

N-unsubstituted indoles had an error of only 1.34 ppm.

One goal was to verify reassignments of chemical shifts in the critical review used as the basis for this study. Morales-Ríos et al. [36] reported the unambiguous assignment of ^{13}C NMR chemical shift peaks for a series of seven methylindoles. Two of these methylindoles, 1-methylindole (**85**) and 2,3-dimethylindole (**61**), were present in the prediction set. In the critical review [2], two peaks in the spectrum of 1-methylindole were considered unreliable while two chemical shifts were reassigned in the 2,3-dimethylindole spectrum. Table 5 shows the reported shifts and those calculated using the models developed in this study. The predicted chemical shifts support the reassignment of peaks for 2,3-dimethylindole and suggest that the assignments should be switched for carbons 4 and 5 in 1-methylindole. Results by Morales-Ríos et al. [36], which unambiguously assign these peaks, lead to the same conclusions. The higher standard error for models associated with carbons 2 and 3 may not allow the verification of reassignments for these two carbons; however, Table 5 indicates that the predictive models are accurate enough to verify the reassignment, made by Morales-Ríos et al. [2] in a critical review, of the chemical shift for the benzenoid carbons (carbons 3a–7a).

Model selection

As stated previously, the major objective of this research is to develop a system which allows the ^{13}C NMR spectral simulation of a wide range of organic compounds. Towards this end, a database has been formed [3,4] which can be used to predict the chemical shifts of various carbons. This study was undertaken In order to fill a gap in that database. As illustrated at the beginning of this paper (Table 1), the chemical shifts of indoles could not be predicted well. The models discussed in this paper have been added to that database. In order to evaluate how well the database gap has been filled, the prediction set was used to test the expanded database. Using the nearest neighbor, atom-based model selection described previously, the chemical shift of each carbon in the prediction set (336 carbons) was calculated. Table 6 summarizes the selection of models from the database. For a given carbon, the model considered correct is the indole model associated with that carbon. The model considered wrong is any other model. When the correct model is chosen the nearest-neighbor distance is much smaller than when the wrong model is chosen. The spectral r.m.s. error from use of the regression models and models chosen through model selection is shown in Table 7 for comparison. This table also includes a breakdown of models selected (correct vs. wrong). By definition, when eight correct models are chosen, the results are identical. In nearest-neighbor model selection, the models are chosen by the similarity between a query carbon and carbons in the database. The choice of a wrong model indicates that either the seven-dimensional vector used to describe the carbons is inadequate or that the query carbon is not well represented by the carbon subsets used to develop the correct models. The *n*-dimensional space which can be used to describe each carbon in the database is being investigated to determine the optimal vector on

TABLE 5

Chemical shift reassignments

Compound	Carbon	Shift [a] (review)	Shift [b] (pred.)	Shift [c] (paper)
85	4 [d]	119.1	120.38	120.8
85	5 [d]	120.7	119.38	119.2
61	5 [e]	119.0	118.78	118.9
61	6 [e]	120.8	121.22	120.8

[a] Shifts, in ppm, from Morales-Ríos et al. [2]. [b] shifts, in ppm, predicted from regression models. [c] Shifts, in ppm, from Morales-Ríos et al. [36]. [d] Carbons 4 and 5 considered unreliable [2]. [e] Carbons 5 and 6 were reassigned in Ref. [2].

TABLE 6

Nearest-neighbor model selection

Model selected	Number of carbons	Average distance	Average residual (ppm)
Correct	285	0.180	0.83
Wrong	17	0.975	13.27
Overall	336	0.300	2.72

TABLE 7

Linear regression vs. model selection

Compound	s_R [a]	s_M [b]	Correct	Wrong
57	1.94	1.94	8	0
58	2.59	6.61	7	1
59	1.17	1.17	8	0
60	1.79	1.79	8	0
61	2.57	2.57	8	0
62	2.225	2.22	8	0
63	2.37	12.38	6	2
64	0.60	0.60	8	0
65	0.84	0.84	8	0
66	0.64	0.64	8	0
67	0.37	0.37	8	0
68	0.76	0.76	8	0
69	1.15	1.15	8	0
70	2.85	6.10	7	1
71	0.31	0.31	8	0
72	1.01	1.01	8	0
73	0.90	0.90	8	0
74	0.88	0.88	8	0
75	0.33	0.33	8	0
76	1.87	1.87	8	0
77	0.69	0.69	8	0
78	1.32	1.32	8	0
79	2.07	2.07	8	0
80	1.02	1.02	8	0
81	1.05	2.70	7	1
82	1.74	7.98	6	2
83	1.48	1.48	8	0
84	0.89	0.89	8	0
85	1.05	1.05	8	0
86	1.11	1.11	8	0
87	1.59	1.59	8	0
88	4.22	7.94	4	4
89	1.76	18.59	4	4
90	7.86	16.14	3	5
91	5.99	7.02	7	1
92	8.17	8.66	0	8
93	4.180	15.75	3	5
94	3.72	15.42	5	3
95	1.80	10.71	6	2
96	2.22	14.72	3	5
97	2.27	14.42	3	5
98	2.16	15.81	3	5
Mean	2.04	5.04		

[a] s_R, spectral r.m.s. error in ppm from regression models.
[b] s_M, spectral r.m.s. error in ppm from model selection.

which the nearest-neighbor selection is based [37,38].

The high error (s_M) indicates that a gap still exists in the database; especially for the *N*-substituted indoles (**85–98**). Two approaches can be used to remedy this. The first, mentioned above, is to modify the *n*-dimensional vector used to describe the query and database carbons. The second approach is to increase the representation of *N*-substituted indoles in the training set.

Conclusions

This study has shown that simulation of spectra for a given moiety, instead of a compound, is a viable method for the expansion of the database used in model selection. Some major gaps in the database have been filled; however, a gap still exists for *N*-substituted indoles since 1,2-disubstituted, 1,3-disubstituted, and 1,2,3-trisubstituted indoles are not well modeled.

For the 56 indoles in the training set, the linear models have a mean r.m.s. error of 0.930 ppm. The 42 indoles in the external prediction set have a mean r.m.s. error of 2.04 ppm when the spectra are simulated using the predictive models developed in this study. When using models chosen from the database, including the six models presented here, the mean r.m.s. was 5.04 ppm. For the indoles with no substituent on the nitrogen, the r.m.s. error is 3.44 ppm from the regression models and 10.64 from model selection.

Future work should involve improving the models for the substituted carbons (2 and 3) to better account for substitution at the nitrogen (atom 1). This will involve the investigation of geometric and additional electronic descriptors (e.g., Hückel charge and the atomic charge calculated by AMPAC) which are geometry dependent. These models could also be improved through better representation of *N*-substituted indoles in the training set.

The simulated spectra were accurate enough to identify the substitution pattern but not to identify the correct indole. The predictive models were used to verify the reassignment of chemical shifts for two methylindoles. The shifts predicted by the models agreed with the unambiguous assignment of the shifts reported by Morales-Ríos et al. [36]. Further evaluation of the models can be accomplished by comparison of recent unambiguous assignment of chemical shifts for indoles (especially carbons 4, 5, 6 and 7) with the predicted shifts.

This opportunity is taken to thank J.W. Ball and L.S. Anker for their help with this project. This work was supported by the National Science Foundation under grant CHE-8815785. The Sun workstation was purchased with partial financial support of the National Science Foundation.

REFERENCES

1 R. Erra-Balsells and A.R. Frasca, J. Magn. Reson. Chem., 27 (1989) 134.
2 M.S. Morales-Ríos, J. Espineira and P. Joseph-Nathan, J. Magn. Res. Chem., 25 (1987) 377.
3 G.P. Sutton, L.S. Anker and P.C. Jurs, Anal. Chem., 63 (1991) 443.
4 J.W. Ball, L.S. Anker and P.C. Jurs, Anal. Chem., 63 (1991) 2435.
5 M.K. McIntyre and G.W. Small, Anal. Chem., 59 (1987) 1805.
6 W.E. Brugger and P.C. Jurs, Anal. Chem., 47 (1975) 781.
7 A.J. Stuper and P.C. Jurs, J. Chem. Inf. Comput. Sci., 16 (1976) 99.
8 R.H. Rohrbaugh and P.C. Jurs, UDRAW, Quantum Chemistry Exchange, Program 300, 1988.
9 P.C. Jurs, G.P. Sutton and M.L. Ranc, Anal. Chem., 61 (1989) 1115A.
10 M.L. Ranc, Computer-Aided Carbon-13 Nuclear Magnetic Resonance Spectrum Simulation of Nitrogen-Containing Cyclic Compounds, Ph.D. Dissertation, The Pennsylvania State University, 1988.
11 L.P. Lindeman and J.Q. Adams, Anal. Chem., 43 (1971) 1245.
12 D.H. Smith and P.C. Jurs, J. Am. Chem. Soc., 100 (1978) 3316.
13 G.W. Small and P.C. Jurs, Anal. Chem., 55 (1983) 1128.
14 G.W. Small and P.C. Jurs, Anal. Chem., 56 (1984) 1314.
15 D.S. Egolf and P.C. Jurs, Anal. Chem., 59 (1987) 1586.
16 D.S. Egolf, E.B. Brockett and P.C. Jurs, Anal. Chem., 60 (1988) 2700.
17 G.P. Sutton and P.C. Jurs, Anal. Chem., 61 (1989) 863.
18 M.L. Ranc and P.C. Jurs, Anal. Chem., 61 (1989) 2489.
19 D.S. Egolf and P.C. Jurs, Anal. Chem., 62 (1990) 1746.
20 G.P. Sutton and P.C. Jurs, Anal. Chem., 62 (1990) 1884.
21 M.L. Ranc and P.C. Jurs, Anal. Chim. Acta, 248 (1991) 183.
22 AMPAC, Quantum Chemistry Exchange, Program 539, 1988.
23 M.J.S. Dewar, E.G. Zoebisch, E.F. Healy and J.J.P. Stewart, J. Am. Chem. Soc., 107 (1985) 3902.
24 G.W. Small and P.C. Jurs, Anal. Chem., 56 (1984) 2307.
25 M. Randic, J. Chem. Inf. Comput. Sci., 24 (1984) 164.
26 S.L. Dixon and P.C. Jurs, J. Comp. Chem., 13 (1992) 492.
27 R.J. Abraham and P.E. Smith, J. Comp. Chem., 9 (1987) 288.
28 G.W. Small and P.C. Jurs, Anal. Chem., 55 (1983) 1121.
29 N.R. Draper and H. Smith, Applied Regression Analysis, 2nd edn., Wiley-Interscience, New York, 1981.
30 D.A. Belsley, E. Kuh and R.E. Welsch, Regression Diagnostics: Identifying Influential Data and Sources of Collinearity, Wiley-Interscience, New York, 1980.
31 D.M. Allen, Technical Report No. 23, Department of Statistics, University of Kentucky, Lexington, KY, 1971.
32 R.D. Snee, Technometrics, 19 (1977) 415.
33 W. Hofheinz, P. Schonholzer and K. Bernauer, Helv. Chim. Acta, 59 (1976) 1213.
34 J. Levy, C. Pierron, G. Lukacs, G. Massiot and J. Le Men, Tetrahedron Lett., (1976) 669.
35 G. Hugel and J. Levy, Tetrahedron, 39 (1983) 1539.
36 M.S. Morales-Ríos, R.E. del Rio and P. Joseph-Nathan, Magn. Reson. Chem., 26 (1988) 552.
37 L.S. Anker and P.C. Jurs, unpublished results.
38 J.W. Ball and P.C. Jurs, unpublished results.

Analytica Chimica Acta, 280 (1993) 157–162
Elsevier Science Publishers B.V., Amsterdam

Phenylglyoxal and glyoxal as fluorogenic reagents selective for *N*-terminal tryptophan-containing peptides

Eijiro Kojima, Yoshihito Ohba, Masaaki Kai and Yosuke Ohkura

Faculty of Pharmaceutical Sciences, Kyushu University 62, Maidashi, Higashi-ku, Fukuoka 812 (Japan)

(Received 20th January 1993)

Abstract

Methods are described for the determination of *N*-terminal tryptophan-containing peptides in which phenylglyoxal and glyoxal are used as fluorogenic reagents. Phenylglyoxal and glyoxal react selectively with the peptides when heated in a strongly acidic medium in the presence of potassium hexacyanoferrate(III) and in a moderately acidic medium, respectively, at 100°C for 30 min to produce fluorescence. The detection limits of *N*-terminal tryptophan-containing small peptides tested are 118–165 pmol ml^{-1} in the reaction mixtures. The reaction mixture of tryptophylalanine, a model peptide, with glyoxal afforded a single peak when separated by reversed-phase liquid chromatography whereas that with phenylglyoxal gave several peaks.

Keywords: Fluorimetry; Liquid chromatography; Peptides

The determination of peptides has generally been performed using detection techniques on the basis of UV absorption between 200 and 280 nm [1]. For more sensitive detection, fluorescence derivatization of the primary amino groups of peptides with fluorogenic reagents such as *o*-phthalaldehyde and fluorescamine [2,3] and electrochemical detection [4] have also been used. However, these methods do not have specificity for particular peptides.

However, a fluorogenic reagent that can recognize a certain amino acid residue in a peptide molecule is available for the facile determination of particular peptides. In this respect, fluorescence reactions have been developed of arginine-containing peptides and *N*-terminal tyrosine-containing peptides with benzoin reagent [5] and hydroxylamine–cobalt(II)–borate reagent [6], respectively, by which single fluorescent derivatives were produced from the respective peptides [7], and thus their reactions were applicable to pre- and post-column fluorescence derivatization liquid chromatography (LC) for the selective determination of several biogenic peptides in mammalian brain tissues [7–9].

It has been reported previously that phenylglyoxal (PGO) reacts selectively with tryptophan (Trp) in a strongly acidic medium to give a fluorescent compound, 1-(1-hydroxybenzyl)-β-carboline [10]. Recently, PGO was also found to react with *N*-terminal Trp-containing peptides to yield intense fluorescence especially in the presence of potassium hexacyanoferrate(III). This paper describes the reactivity of PGO and its analogues with Trp–Ala, a model peptide, which was examined for the screening of fluorogenic reagents selective for *N*-terminal Trp-containing peptides. The analogues used for the investigations were glyoxal (GO) and methylglyoxal (MGO) as aliphatic glyoxals, and 4-methoxyphenylglyoxal

Correspondence to: Y. Ohkura, Faculty of Pharmaceutical Sciences, Kyushu University 62, Maidashi, Higashi-ku, Fukuoka 812 (Japan).

(MPG), 3,4-dimethoxyphenylglyoxal (DMPG), 3,4,5-trimethoxyphenylglyoxal (TMPG) and 3,4-methylenedioxyphenylglyoxal (MDPG), which were synthesized as PGO derivatives substituted with electron-donating group(s), in the hope that promising reagents might be found. PGO and GO thus selected as the most sensitive reagents were employed to establish manual methods for the spectrofluorimetric determination of *N*-terminal Trp-containing peptides. The applicability of the methods to the derivatization of peptides in LC was also investigated using Trp–Ala.

EXPERIMENTAL

Apparatus

Uncorrected fluorescence excitation and emission spectra and intensities were measured with a Hitachi MPF-4 spectrofluorimeter using conventional quartz cells (10 × 10 mm); spectral band widths of 10 nm were used in both the excitation and emission monochromators. Electron impact mass spectra were obtained with a JEOL JMS-DX300 mass spectrometer (Nihon Denshi, Tokyo) interfaced to a JEOL JMS-3500 data system (Nihon Denshi). Uncorrected melting points were measured with a Yanaco MP-P3 melting point apparatus.

Reagents and solutions

The synthetic peptides were purchased from Sigma (St. Louis, MO). The peptides were used as received and dissolved in water or methyl Cellosolve. All other chemicals were of analytical-reagent grade.

Aqueous solutions of GO (21.9 M) and MGO (16.3 M) and PGO monohydrate were purchased from Sigma. GO and MGO solutions were diluted with water. PGO, MPG, DMPG, TMPG and MDPG were dissolved in dimethyl sulphoxide.

MPG, DMPG, TMPG and MDPG were synthesized from the corresponding acetophenones according to the synthesis procedure for PGO [11]. To a stirred solution of selenium dioxide (60 mmol, 7.0 g) in a mixture of dioxane (45 ml) and water (1.4 ml) was added 4-methoxy-, 3,4-dimethoxy-, 3,4,5-trimethoxy- or 3,4-methylenedioxyacetophenone (50 mmol, 7.5–10.5 g). The mixture was refluxed for 3–4 h and filtered after adding 50 ml of tetrahydrofuran, and the filtrate was concentrated in vacuo. To the resulting oily residue were added 150 ml of water and the mixture was refluxed for 20 min. The solution was filtered while hot. The precipitates thus obtained on cooling were recrystallized from water to give colourless needles. MPG: yield 4.5 g (58%); m.p. 100–102°C; mass spectrum, m/z 164 [M^+]; elemental analysis, calculated for $C_9H_{10}O_4$, C 59.3, H 5.5; found, C 60.5, H 5.4%. DMPG: yield 5.0 g (55%); m.p. 98–99°C; mass spectrum, m/z 194 [M^+]; elemental analysis, calculated for $C_{10}H_{12}O_5$, C 56.1, H 5.6; found, C 56.5, H 5.7%. TMPG: yield 5.3 g (50%); m.p. 86–88°C; mass spectrum, m/z 224 [M^+]; elemental analysis, calculated for $C_{11}H_{14}O_6$, C 54.6, H 5.8; found, C 55.0, H 5.6%. MDPG: yield 3.3 g (40%); m.p. 104–107°C; mass spectrum, m/z 178 [M^+]; elemental analysis, calculated for $C_9H_8O_5$, C 54.6, H 4.0; found, C 54.8, H 4.0%.

Screening procedure for glyoxal analogues

An aliquot (100 μl) of 0.1 mM Trp–Ala (or water for blank) was mixed with 50 μl of a 40–600 mM solution of an analogue, 50 μl of 20–100 μM potassium hexacyanoferrate(III) or water and 100 μl of 0.1–1.0 M hydrochloric acid or 40 mM Britton–Robinson buffer (pH 2–12). The mixture was heated at 100°C for 10–100 min. After cooling in a water-bath (20 ± 5°C), the fluorescence intensity of the mixture was measured at the wavelengths of their excitation and emission maxima.

Determination procedures with PGO and GO

A portion (1.0 ml) of aqueous test solution (or water for blank) was mixed with 1.0 ml each of 0.07 M PGO or 0.3 M GO and a mixture of 1.4 M hydrochloric acid and 0.2 mM potassium hexacyanoferrate(III) (1 : 1, v/v) for the PGO reaction or 0.2 M succinate buffer (pH 4.5) for the GO reaction. The mixture was heated at 100°C for 30 min. The fluorescence intensities of the reaction mixtures with PGO and GO were measured at emission wavelengths of 470 and 480 nm with

excitation wavelengths of 385 and 395 nm, respectively.

LC system and operating conditions

The LC system consisted of a Tosoh 803D liquid chromatograph with a Rheodyne Model 7125 syringe-loading sample injection valve (100-μl loop) and a Hitachi F-1000 spectrofluorimeter fitted with a 12-μl flow cell. The column was TSK gel ODS-80T$_M$ (150 × 4.6 mm i.d., particle size 5 μm) (Tosoh). The column temperature was ambient (25 ± 4°C). The mobile phases for the isocratic separation of the fluorescent products from Trp–Ala in the PGO and GO reaction mixtures, acetonitrile–50 mM phosphate buffer (pH 2.0)–water (35:20:45, v/v) and acetonitrile–50 mM phosphate buffer (pH 6.0)–water (20:20:60, v/v), respectively, were delivered at a flow-rate of 1.0 ml min^{-1}.

RESULTS AND DISCUSSION

Screening of glyoxal analogues

The commercially available and synthesized glyoxal analogues (seven in total) can afford fluorescence from Trp–Ala in acidic and neutral media in the presence and absence of potassium hexacyanoferrate(III) (Table 1). PGO gave the most intense fluorescence in strongly acidic solution in the presence of hexacyanoferrate(III); in its absence, the fluorescence intensity was diminished to 23% of that in its presence. GO gave more intense fluorescence in a moderately acidic medium (pH 4.5) in the absence of hexacyanoferrate(III) than in its presence; the oxidant reduced the fluorescence by 50%. In the presence of hexacyanoferrate(III), the aromatic analogues (MPG, DMPG, TMPG and MDPG) provided more intense fluorescence in an acidic medium than in neutral media; these aromatic analogues unexpectedly provided weak fluorescence. Therefore, PGO and GO were selected for further investigations.

Conditions of reactions with PGO and GO

Fluorescence spectra of the reaction mixtures of Trp–Ala with PGO and GO showed excitation maxima at 385 and 395 nm and emission maxima at 470 and 480 nm, respectively.

As the reaction of Trp–Ala with PGO occurred in acidic solutions, the concentrations of

TABLE 1

Optimal conditions for the fluorescence reactions of GO and its analogues with Trp–Ala and their relative fluorescence intensities (RFI) [a]

Analogue (mM)	Potassium hexacyanoferrate(III) (μM)	pH [b]	Reaction time (min)	Excitation maximum (nm)	Emission maximum (nm)	RFI [c]
GO (600)	50	4.5	30	395	480	53
	–	4.5	30	395	480	100
MGO (100)	50	7.0	30	405	445	11
	–	7.0	30	405	445	22
PGO (150)	100	0.2	40	385	470	115
	–	0.2	40	385	470	26
MPG (50)	60	2.0	90	375	470	25
	–	6.0	50	375	470	14
DMPG (50)	20	2.0	90	380	460	16
	–	7.0	90	380	460	7
TMPG (40)	40	2.0	90	380	460	11
	–	7.0	90	380	460	8
MDPG (40)	60	2.0	90	380	455	21
	–	7.0	90	380	455	8

[a] Portions (100 μl) of 0.1 mM Trp–Ala solution were treated according to the screening procedure. [b] Defined as the pH of 40 mM Britton–Robinson buffer used for the reaction. The acidic reaction mixture of pH 0.2 was prepared by using 0.7 M hydrochloric acid. [c] The fluorescence intensity obtained with GO in the absence of potassium hexacyanoferrate(III) was taken as 100.

diverse acids such as hydrochloric, phosphoric, sulphuric, nitric, trichloroacetic, perchloric and acetic acid were examined for fluorescence development; 0.7 M hydrochloric acid provided the most intense fluorescence and was selected for the determination procedure; pH of the reaction mixture was ca. 0.2.

The pH values of several buffers such as succinate, phthalate, acetate and citrate buffer (all 0.2 M) were examined for the fluorescence development with GO. The maximum fluorescence intensity was obtained at pH 4.5 of the buffers. Succinate buffer (pH 4.5) was used for the determination procedure as it gave the most intense fluorescence.

The highest fluorescence intensities in the PGO and GO reaction mixtures were produced at high temperatures (120–140°C) and higher temperatures allowed the fluorescence to develop more rapidly (Figs. 1 and 2). Heating at 100°C for 30 min was selected for convenience in the determination procedures in both reactions.

Of the oxidizing agents examined, such as sodium metaperiodate, hydrogen peroxide, potassium permanganate, sodium nitrite and potassium hexacyanoferrate(III) (0.01–1 mM each), hexacyanoferrate(III) gave the most intense fluo-

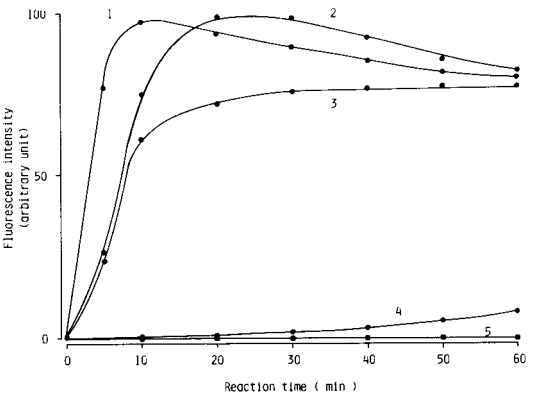

Fig. 1. Effect of reaction temperature and time on fluorescence development from Trp–Ala with PGO. Portions (1.0 ml) of 10 nmol ml^{-1} Trp–Ala solution were treated at different temperatures for various periods according to the determination procedure using PGO. Temperature: 1 = 140; 2 = 120; 3 = 100; 4 = 60; 5 = reagent blanks at the temperatures.

TABLE 2

Fluorescence excitation and emission maxima, relative fluorescence intensities (RFI) and limits of detection (LD) obtained by the reactions of Trp-related compounds with PGO and GO [a]

Compound (10 nmol ml^{-1})	Excitation maximum (nm)		Emission maximum (nm)		RFI [b]		LD [c] (pmol ml^{-1})	
	PGO	GO	PGO	PO	PGO	GO	PGO	GO
Trp–Ala	385	395	470	480	115	100	118	135
Trp–Leu	385	395	470	480	83	90	163	150
Trp–Trp	385	395	470	480	12	5	1131	2700
Trp–Gly–Gly	385	395	470	480	108	90	126	150
Trp–Met–Asp–Phe–NH_2	385	395	470	480	95	86	143	157
Ala–Trp	385	ND [d]	470	ND	4	ND	–	ND
Lys–Trp–Lys	ND	ND	ND	ND	ND	ND	ND	ND
pGlu–Trp–Pro–Arg–Pro–Gln–Ile–Pro–Pro	385	ND	470	ND	7	ND	1937	ND
pGlu–His–Trp–Ser–Tyr–Gly–Leu–Arg–Pro–Gly–NH_2	ND	ND	ND	ND	ND	ND	ND	ND
Tryptophan	385	385	470	460	180	111	75	121
Tryptophanamide	385	395	465	470	127	61	107	221
Tryptamine	385	395	470	470	6	80	2262	169
N-Acetyltryptophan	385	ND	470	ND	17	ND	798	ND
5-Hydroxytryptophan	385	370	530	490	2	4	–	–
Serotonin	ND	395	ND	510	ND	3	ND	–
Melatonin	ND	ND	ND	ND	ND	ND	ND	ND

[a] Portions (1.0 ml) of 10 nmol ml^{-1} solutions of the compounds were treated according to the determination procedures. [b] The fluorescence intensity from Trp–Ala with GO was taken as 100. [c] Defined as the concentration in the reaction mixture that gave a fluorescence intensity twice the blank. [d] Could not be determined.

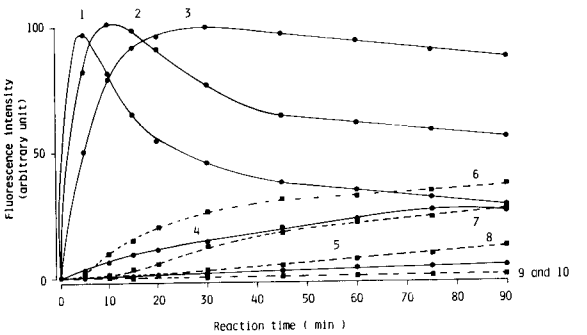

Fig. 2. Effect of reaction temperature and time on the fluorescence development from Trp–Ala with GO. Portions (1.0 ml) of 10 nmol ml^{-1} Trp–Ala solution were treated in the same manner as in Fig. 1, but using GO. Temperature: 1 and 6 = 140; 2 and 7 = 120; 3 and 8 = 100; 4 and 9 = 60; 5 and 10 = 37°C. 1–5 = Trp–Ala; 6–10 = reagent blanks.

rescence in the PGO reaction; in its absence, the fluorescence intensity was reduced 75%. The fluorescence intensity was not enhanced when the hexacyanoferrate(III) was added to the final reaction mixture of PGO.

Maximum and constant fluorescence intensities were attained at PGO concentrations greater than 0.1 M and at GO concentrations greater than 0.25 M; 0.1 and 0.3, respectively, were used in the PGO and GO reactions. PGO is insoluble in water and was dissolved in dimethyl sulphoxide.

The fluorescence in both the final reaction mixtures with PGO and GO was stable for at least 1 h in daylight at room temperature (25°C).

Validation of the methods

The calibration graphs for *N*-terminal Trp-containing small peptides (Table 2) with PGO or GO were all linear up to at least 100 nmol ml^{-1}. The within-day precision was established by repeated determinations ($n = 10$) using 10 nmol ml^{-1} Trp–Ala solution. The relative standard deviations were 1.6 and 1.1% in the PGO and GO reactions, respectively. Trp-related compounds and peptides were treated according to the recommended determination procedures and their fluorescence intensities and detection limits, which were measured at the respective fluorescence excitation and emission maximum wavelengths, are given in Table 2. The detection limits of *N*-terminal Trp-containing small peptides were 118–165 pmol ml^{-1} in the reaction mixtures, except for Trp–Trp. Trp and tryptophanamide fluoresced under the conditions of the determination procedures. Intense fluorescence from tryptamine was found in the GO reaction, but not in the PGO reaction. Weak fluorescence from Ala-Trp, *N*-acetyltryptophan and pGlu–Trp–Pro–Arg–Pro–Gln–Ile–Pro–Pro was observed when they were treated by the procedure with PGO; these compounds might be partially hydrolysed to Trp or *N*-terminal Trp-containing peptides by the acid used in the reaction.

The following substances did not fluoresce under the recommended conditions at concentrations as high as 100 nmol ml^{-1}: uric acid, adenine, guanine, thymine, cytosine, uracil, xanthine, hypoxanthine, nicotinamide, pyridoxine, cholesterol, nicotinic acid, ascorbic acid, α-ketoglutaric acid, glucose, fructose, erythrose, galactose, fucose, glyceraldehyde, glycolaldehyde, glucosamine, galactosamine, mannose, *N*-acetylgalac-

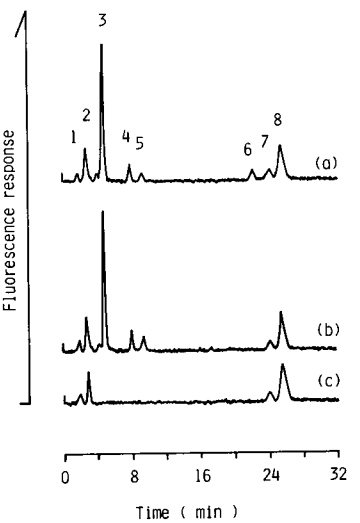

Fig. 3. Chromatograms of (a) Trp–Ala, (b) Trp and (c) reagent blank obtained with the reaction mixtures with PGO. Portions (1.0 ml) of 2.5 nmol ml^{-1} Trp–Ala, 0.25 nmol ml^{-1} Trp and water (for the blank) were treated according to the determination procedure using PGO and 100-μl portions of the reaction mixtures were subjected to chromatography. Peaks: 1, 2, 7 and 8 = reagent blank; 3, 4 and 5 = Trp–Ala and Trp; 6 = Trp–Ala.

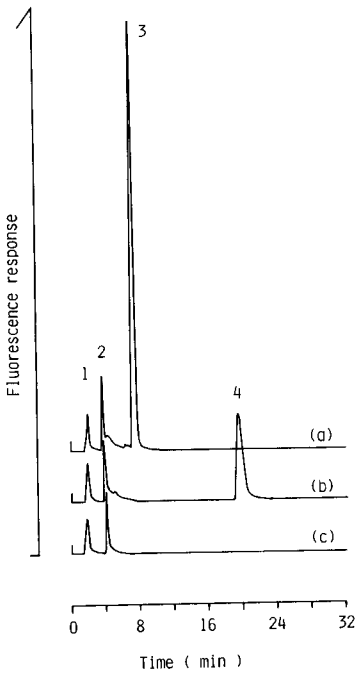

Fig. 4. Chromatograms of (a) Trp–Ala, (b) Trp and (c) reagent blank obtained with the reaction mixtures with GO. Portions (1.0 ml) of 5 nmol ml^{-1} Trp–Ala, Trp and water (for the blank) were treated in the same manner as in Fig. 3, but using GO. Peaks: 1 and 2 = reagent blank; 3 = Trp–Ala; 4 = Trp.

tosamine, glucuronic acid, ribose, deoxyribose, tyramine, histamine, epinephrine, norepinephrine, dopamine, spermine, spermidine, putrescine, guanidine and nineteen L-α-amino acids.

LC separation of the reaction mixtures

Figures 3 and 4 depict the chromatograms of the reaction mixtures of Trp–Ala treated according to the determination procedures with PGO and GO, respectively. The reaction mixture with PGO gave several peaks for the peptide, which were overlapped with the peaks from Trp except for one peak; the only peak characterized by the peptide was detected at a retention time of 22 min. On the other hand, the reaction mixture with GO showed a single peak for the peptide, the retention time of which was 8.1 min. These observations suggest that GO is usable in both pre- and post-column fluorescence derivatization LC but PGO only in post-column derivatization.

In conclusion, PGO and GO provided the selective fluorimetric determination of *N*-terminal Trp-containing peptides. Further, the reagents can be used for selective derivatization in the LC of these peptides.

This work was partly supported by a Grant-in-Aid for Scientific Research from the Ministry of Education, Science and Culture, Japan.

REFERENCES

1 J. River, R. McClintock, R. Galyean and H. Anderson, J. Chromatogr., 288 (1984) 303.
2 H. Nakamura, C.L. Zimmerman and J.J. Pisano, Anal. Biochem., 93 (1979) 423.
3 S. Stein and J. Moschera, Methods Enzymol., 79 (1981) 7.
4 S. Mousa and D. Couri, J. Chromatogr., 267 (1983) 191.
5 M. Kai, T. Miyazaki, Y. Sakamoto and Y. Ohkura, J. Chromatogr., 322 (1985) 473.
6 M. Kai and Y. Ohkura, Anal. Chim. Acta, 182 (1986) 177.
7 M. Nakano, M. Kai, M. Ohno and Y. Ohkura, J. Chromatogr., 411 (1987) 305.
8 M. Ohno, M. Kai and Y. Ohkura, J. Chromatogr., 392 (1987) 309.
9 G.Q. Zhang, M. Kai and Y. Ohkura, Anal. Sci., 6 (1990) 671.
10 E. Kojima, M. Kai and Y. Ohkura, Anal. Chim. Acta, 248 (1991) 213.
11 H.A. Riley and A.R. Gray, Org. Synth. Collect. Vol., 2 (1943) 510.

Analytica Chimica Acta, 280 (1993) 163–168
Elsevier Science Publishers B.V., Amsterdam

Stopped-flow determination of diphacinone based on lanthanide-sensitized luminescence

S. Panadero, A. Gómez-Hens and D. Pérez-Bendito

Department of Analytical Chemistry, Faculty of Sciences, University of Córdoba, E-14004 Córdoba (Spain)

(Received 7th December 1992; revised manuscript received 20th January 1993)

Abstract

The stopped-flow mixing technique was used to investigate the application of kinetic methodology to complex formation reactions involving energy transfer processes. By using initial rate measurements a very rapid fluorimetric method was developed for the determination of diphacinone by formation of the ternary complex Eu(III)–diphacinone–ammonia in the presence of Triton X-100. Kinetic data can be obtained only 2–3 s after the reactants are mixed, which allows ready application of the method to routine analyses. The linear response range of the proposed method is 0.5–5 μg ml^{-1} diphacinone and the mid-range relative standard deviation is ca. 2%. The mean recovery obtained in the analysis of serum samples was 98.3%.

Keywords: Fluorimetry; Kinetic methods; Diphacinone; Lanthanide-sensitized luminescence; Rodenticides; Serum; Stopped-flow technique

Lanthanide-sensitized luminescence is widely used for analytical purposes. The typically intense ion luminescence involved arises from an intrachelate energy transfer through the excited triplet state of the ligand to the emitting level of the central ion [1]. The features of lanthanide chelates (large Stokes shifts, narrow emission bands and long lifetimes) make them especially suitable as labels for time-resolved fluorescence immunoassay [2]. These chelates have also been used for the determination of the corresponding lanthanide ion [3–7] and, to a lesser extent, for the determination of the ligand [8]. Another phenomenon of analytical interest, the co-fluorescence effect, is the result of a highly enhanced excitation of the luminescent ion through light absorption by the chelates of non-emitting ions such as yttrium or gadolinium [4–7]. This involves inter-chelate energy transfer-sensitized luminescence. The efficiency of these processes can usually be greatly enhanced by employing a surfactant [9], which protects the complexes from non-radiative processes.

Energy transfer processes have been used for analytical purposes by measuring the emission intensity at equilibrium (conventional fluorimetry) or by making decay time measurements (time-resolved fluorimetry). However, no determinations have so far been developed in this context on the basis of reaction rate measurements. Because kinetic-based methods can offer complementary capabilities to transfer energy reactions, as they have to other types of reactions, it was decided to use the Eu(III)–diphacinone–ammonia system in the presence of Triton X-100, which was previously employed [4,5] for the de-

Correspondence to: D. Pérez-Bendito, Department of Analytical Chemistry, Faculty of Sciences, University of Córdoba, E-14004 Córdoba (Spain).

termination of Eu(III) from equilibrium fluorescence measurements.

Diphacinone is an anticoagulant rodenticide that has been used to control mouse and rat populations for several decades. The earliest determinations of diphacinone in ground bait and biological materials were spectrophotometric [10–12]. Later, various chromatographic techniques were used for its individual determination [13] and for the resolution of mixtures with other pesticides [14–17]. A competitive enzyme immunoassay for diphacinone has also been reported [18]. Because no kinetic methods have so far been reported for the determination of diphacinone, the Eu(III)–diphacinone–ammonia system was optimized to develop a simple, rapid, kinetic–fluorimetric method for the determination of this pesticide in human serum that could be readily applied in cases of suspected poisoning. The formation of this complex is very rapid, so the stopped-flow mixing technique is required to make reaction rate measurements and automate the method for routine analyses. In addition, because of its basis, viz., an energy transfer from diphacinone to Eu(III), the method avoids potential background interferences from serum samples owing to the large Stokes shift of the system.

EXPERIMENTAL

Instrumentation

A Perkin-Elmer Model LS-50 luminescence spectrometer fitted with a stopped-flow module [19] supplied by Quimi-Sur Instrumentation was used for fluorescence measurements. The instrument was controlled with a Hewlett-Packard Vectra computer. Reaction rate data were obtained by using the Kinetic Obey application program. The observation cell of the stopped-flow module had a path length of 1.0 cm and the excitation and emission slits were adjusted to provide a 15-nm band pass. The solutions in the stopped-flow module and the cell compartment were kept at a constant temperature (30°C) by circulating water from a thermostated tank.

Reagents

All chemicals were of analytical-reagent grade. A 100 μg ml^{-1} stock solution of diphacinone (Chem-Service, West Chester, PA) was prepared in ethanol and stored at 0–4°C. A 2×10^{-3} M europium(III) solution was prepared by dissolving the appropriate amount of $Eu(NO_3)_3 \cdot 5H_2O$ (Sigma) in distilled water. A 0.1% Triton X-100 aqueous solution and an ammonium chloride–ammonia buffer solution (0.4 M, pH 8.5) were also used.

Procedure

A solution containing 0.4 ml of 2×10^{-3} M europium(III), 0.25 ml of 0.1% Triton X-100 and 0.5 ml of 0.4 M ammonium chloride–ammonia buffer (pH 8.5) in a final aqueous volume of 5 ml was used to fill one of the two 5-ml reservoir syringes. The other syringe was filled with 5 ml of a premixed aqueous solution consisting of 0.25 ml of 0.1% Triton X-100, 0.5 ml of the same buffer and diphacinone standard solution at a final concentration between 0.5 and 5.0 μg ml^{-1}. After the two 2-ml drive syringes had been filled, 0.15 ml of each solution from these syringes was mixed in the mixing chamber in each run. The variation of the fluorescence intensity throughout the reaction was monitored at $\lambda(ex) = 336$ and $\lambda(em) = 619$ nm. Fluorescence values were obtained for 10 s and processed by linear regression by the microcomputer furnished with a program for application of the initial-rate method (Kinetic Obey). The reaction rate was determined in about 2–3 s and each sample was assayed in triplicate. The blank signal was found to be negligible. All measurements were made at 30°C.

Determination of diphacinone added to serum. Human serum (0.5 ml), spiked with appropriate amounts of diphacinone, was treated with 1.25 ml of ethanol and centrifuged at 4000 *g* and room temperature for 15 min. A volume of 0.75 ml of the supernatant was analysed as described above. The concentration of diphacinone in the samples was determined by interpolation on the calibration graphs constructed by adding 0.5 ml of a previously prepared serum pool to each diphacinone standard. The calibration graph was linear over the range 1.0–6.0 μg ml^{-1}.

RESULTS AND DISCUSSION

Zhu and co-workers [4,5] developed a method for the determination for europium based on the formation of a ternary complex with diphacinone and ammonia and on an intramolecular energy transfer from the excited triplet state of diphacinone to europium, which yields a fluorescent signal at 612 nm. Triton X-100 was used to avoid any loss of energy arising from collisions with solvent molecules, and analytical data were obtained at equilibrium. By optimizing the system, it could also be used for the fluorimetric determination of diphacinone. In order to develop the first kinetic method involving energy transfer, we exploited the attributes of the stopped-flow mixing technique as a means of accomplishing automation and expeditious handling of reagents for routine determinations, and applied it to the determination of diphacinone. The kinetic curve obtained when the europium solution is placed in a syringe of the stopped-flow module, the diphacinone solution in the other and Triton X-100 and the buffer solutions in both syringes corresponds to the formation of the ternary complex rather than the energy transfer process, which is much too fast to be recorded. The slope of the curve will be proportional to the concentration of diphacinone provided that the other variables are kept constant. Figure 1 shows the kinetic curves obtained at different concentrations of diphacinone. When measurements are carried out at equilibrium, one must wait for 5 min to allow the maximum fluorescence signal to be reached [4,5]. However, the rapid and thorough mixing of the streams from the drive syringes in the flow cell of the stopped-flow module increases the rate of formation of the complex, so it can be measured within few seconds. Although the reaction provided by the batch technique would be lower, it would still be fast enough to make it impossible to obtain kinetic data. Hence using the stopped-flow mixing technique is essential for a kinetic study of this system.

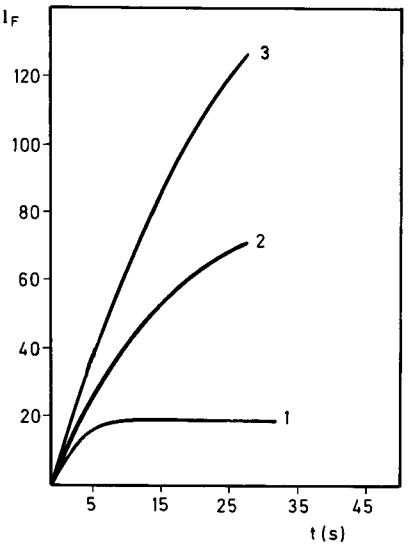

Fig. 1. Variation of the fluorescence intensity of the Eu(III)–diphacinone–ammonia system with time at different concentrations of diphacinone: 1.0; (2) 3.0; (3) 5.0 μg ml^{-1}.

Optimization of variables

The effect of variables affecting the performance of the proposed kinetic method for the determination of diphacinone was investigated by using the univariate method. All concentrations given below correspond to a stage prior to the dilution (1:2) in the stopped-flow cuvette. Each kinetic result was the average of three measurements.

The formation of the diphacinone–europium binary complex in the absence of ammonia was studied and results obtained showed the reaction rate to be ca. ten times lower than that of the ternary complex. In order to determine the influence of pH on the formation of the ternary complex, a constant amount of ammonium chloride–ammonia buffer was used in each sample and the pH was changed with either sodium hydroxide or hydrochloric acid. Figure 2 shows the effect of pH on the rate of formation of both complexes. That of the ternary complex was independent of pH over the range 8.0–8.6. The concentration of ammonium chloride–ammonia buffer used (pH 8.5) did not affect the reaction rate in the range 0.02–0.08 M. Figure 3 shows the effect of the europium(III) concentration on the system; a 1.6×10^{-4} M concentration was finally chosen.

The effect of the Triton X-100 content is shown in Figure 4. No fluorescence signal was obtained

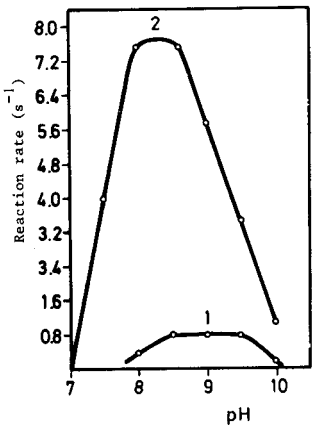

Fig. 2. Effect on pH on the reaction rate of the (1) Eu(III)–diphacinone and (2) Eu(III)–diphacinone–ammonia systems.

in the absence of the surfactant, which shows the significance of using an organized medium with systems involving energy transfer processes. The reaction rate remained constant above a Triton X-100 content of 2×10^{-3}% w/v. The highest reaction rate values were obtained when the surfactant was distributed between the two syringes. In order to determine the critical micelle concentration (c.m.c.), several samples containing Triton X-100 concentrations from 0 to 0.08% were prepared and their surface tension was measured with a stalagmometer. The c.m.c. obtained was 0.018%, which is ca. ten times higher than the content above which the reaction rate remained constant. These results show that optimum kinetic conditions are obtained only when submicellar aggregates are formed.

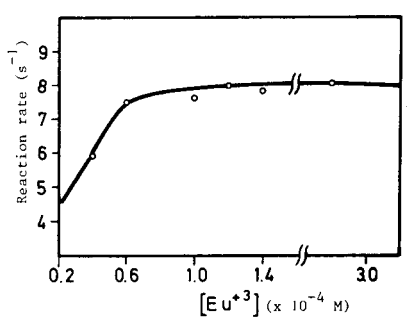

Fig. 3. Effect of Eu(III) concentration of the reaction rate of the Eu(III)–diphacinone–ammonia system.

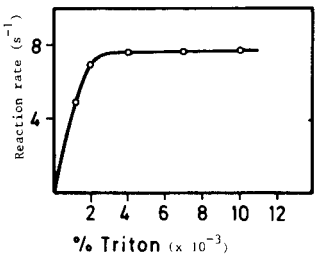

Fig. 4. Effect of Triton X-100 content on the reaction rate of the Eu(III)–diphacinone–ammonia system.

Because diphacinone is soluble in ethanol, the effect of the alcohol was also studied. The reaction rate decreased slightly with increase in ethanol content. Regarding temperature, the maximum reaction rate was obtained at 30°C, above or below which the rate was lower. The reaction rate also depends on the distribution of the reactants between the two syringes. The best results were obtained when the Triton X-100 and buffer solutions were distributed between the two syringes, diphacinone solution was placed in one of them and europium solution in the other.

The initial slopes of the fluorescence vs. time curves for solutions containing different amounts of diphacinone revealed the reaction to be first order in diphacinone. Under the working conditions used here, the other reactants showed a pseudo-zero-order dependence, thus the simple kinetic equation $v = k$[diphacione] is proposed, where v is the rate of formation of the complex and k the conditional rate constant.

Study of the co-fluorescence effect

As stated above, the co-fluorescence effect is commonplace in systems involving some energy transfer. Thus, the fluorescence intensity obtained at equilibrium for the Eu(III)–diphacinone–ammonia complex is increased by addition of excess of yttrium [4] or gadolinium [5] ion. This is explained by the fact that, for yttrium, each Eu(III)–diphacinone–ammonia moiety is surrounded by many Y(III)–diphacinone–ammonia moieties so europium is excited both by the intramolecular energy transfer from the excited triplet state of diphacinone in the complex of europium and by the intermolecular energy

transfer from the excited triplet state of diphacinone in the yttrium complex.

The effect of yttrium was studied by using the stopped-flow mixing technique. The results obtained showed that the co-fluorescence effect can be observed only when the ligand is in excess with respect to lanthanide ion, but the equilibrium is reached fairly slowly, which accounts for the need to wait for 5 min to measure the maximum fluorescence intensity in the determination of europium [4]. Under the analytical conditions used, viz., excess of europium for the kinetic determination of diphacinone, equilibrium is reached fairly rapidly, and not only was the co-fluorescence effect not observed but also yttrium had a negative effect on the reaction rate and maximum fluorescence intensity.

Figures of merit of the proposed method

The kinetic curves obtained for different amounts of diphacinone, with excitation and emission wavelengths of 336 and 619 nm, respectively, were processed by the initial rate method. The calibration graph was linear in the range 0.5–5.0 μg ml^{-1} and conformed to the equation v (s^{-1}) = 0.41[diphacinone (μg ml^{-1})] -9.8×10^{-2}, with a Pearson's correlation coefficient (r) of 0.997 ($n = 5$). The detection limit, calculated according to IUPAC recommendations [20], was 0.2 μg ml^{-1}.

The precision of the method was studied at two concentrations of diphacinone, viz., 1 and 3 μg ml^{-1}; the relative standard deviations obtained ($n = 11$) were 2.2 and 2.0%, respectively. The selectivity of the method was determined by assaying various potentially interfering anticoagulant rodenticides such as bromadiolone, warfarin and dicoumarol; all of them were tolerated at the same concentration level as diphacinone. Finally, the time required to obtain analytical data was only ca. 2–3 s.

Applications

Diphacinone was determined in various spiked human serum samples by using the above procedure. Several reagents, trichloroacetic acid, sodium tungstate and ethanol, were used to deproteinate the samples, the best results being obtained when ethanol was used. In order to simulate the sample matrix in the standards used for the calibration graph, 0.5 ml of a previously prepared serum pool was added to each standard sample. Because of the presence of the sample matrix and the ethanol used for deproteination, the calibration graph obtained under these experimental condition was linear over the range 1.0–6.0 μg ml^{-1} diphacinone. Table 1 summarizes the results obtained for the different serum samples analysed; the recoveries ranged between 82 and 112%.

TABLE 1

Recovery of diphacinone added to serum samples

Sample No.	Diphacinone (μg)		Recovery (%)
	Added	Found [a]	
1	20.0	19.5	98
	30.0	24.6	82
	40.0	43.2	108
2	20.0	18.7	94
	30.0	29.7	99
	40.0	38.9	97
3	20.0	22.5	112
	30.0	27.9	93
	40.0	39.5	99
4	20.0	18.8	94
	30.0	29.6	99
	40.0	38.9	97
5	20.0	19.2	96
	30.0	30.2	100
	40.0	43.2	108

[a] Average of three determinations.

Conclusions

The results obtained in the kinetic study of the Eu(III)–diphacinone–ammonia complex by using the stopped-flow mixing technique reveal the usefulness of the approach used to develop a rapid automatic method for the determination of diphacinone. Even though working with an Eu(III) excess with respect to diphacinone in the presence of Y(III) has an adverse effect and no co-fluorescence effect is observed, the reaction rate thus obtained is higher than in the opposite situation. However, the stopped-flow mixing technique can be used to study the kinetics of the

co-fluorescence effect provided that an adequate ligand–lanthanide ion molar ratio is used. Further studies aimed at the full assessment of the potential of the stopped-flow mixing technique are in progress.

The authors acknowledge financial support from the CICyT (Grant No. PB91-0840).

REFERENCES

1 G. Whan and G. Crosby, J. Mol. Spectrosc., 1 (1962) 314.
2 E.P. Diamandis, Clin. Biochem., 21 (1988) 139.
3 Z.-K. Si, G.-Y. Zhu and J. Li, Analyst, 116 (1991) 309.
4 G. Zhu, Z. Si, X. Wang and W. Zhu, Anal. Chim. Acta, 231 (1990) 295.
5 G.-Y Zhu, Z.-K. Si and W.-J. Zhu, Analyst 115 (1990) 115.
6 Y.-Y. Xu and I.A. Hemmilä, Anal. Chim. Acta, 256 (1992) 9.
7 Y.-Y. Xu and I.A. Hemmilä, Talanta, 39 (1992) 759.
8 L.M. Hirschy, E.V. Dose and J.D. Winefordner, Anal. Chim. Acta, 147 (1983) 311.
9 Y.-Y. Xu, I.A. Hemmilä and T.N.-E. Lövgren, Analyst, 117 (1992) 1061.
10 R.J. Caswell, J. Assoc. Off. Anal. Chem., 46 (1959) 104.
11 A. Danek and J. Kwiek, Diss. Pharm., 16 (1964) 359.
12 H.C. Hollifield and J.D. Winefordner, Talanta, 14 (1967) 103.
13 J.J.L. Hoogenboom and C.G. Rammell, Analyst, 109 (1984) 787.
14 B.R. Bennett and G.S. Grimes, J. Assoc. Off. Anal. Chem., 65 (1982) 927.
15 R.W. Bullard, G. Holguin and J.E. Peterson, J. Agric. Food. Chem., 23 (1975) 72.
16 V. Mallet, D. Surette and G.L. Brun., J. Chromatogr., 79 (1973) 217.
17 G.E. Caissie and V.N. Mallet, J. Chromatogr., 117 (1976) 129.
18 M.E. Mount, M.J. Kurth and D.Y. Jackson, J. Immunoassay, 9 (1988) 69.
19 A. Loriguillo, M. Silva and D. Pérez-Bendito, Anal. Chim. Acta, 199 (1987) 29.
20 G.L. Long and J.D. Winefordner, Anal. Chem., 55 (1987) 712A.

Analytica Chimica Acta, 280 (1993) 169–172
Elsevier Science Publishers B.V., Amsterdam

Flotation–spectrophotometric determination of praseodymium with 5,7-dichloroquinolin-8-ol and Rhodamine 6G

V. Bhagavathy, T. Prasada Rao and A.D. Damodaran

Regional Research Laboratory (CSIR), Trivandrum 695019 (India)

(Received 30th June 1992; revised manuscript received 21st January 1993)

Abstract

Praseodymium was determined by reaction with 5,7-dichloroquinolin-8-ol and Rhodamine 6G in a weakly alkaline medium. The flotation of the ion association complex was carried out with hexane, followed by dissolution in acetone for subsequent spectrophotometric determination. The molar absorptivity was 1.83×10^5 l mol^{-1} cm^{-1} at 530 nm. Beer's law was obeyed in the range 8–240 μg l^{-1} praseodymium. Praseodymium in aluminium metal and aluminium salts was determined by the proposed method in conjunction with an ion-exchange separation using Dowex 50W-X8 cation-exchange resin.

Keywords: Ion exchange; UV–Visible spectrophotometry; Aluminium; Flotation; Praseodymium

Flotation–spectrophotometry provides a sensitive and relatively simple approach to trace metal analysis [1–3]. The flotation separation of ion associates involves shaking an aqueous pseudo-solution containing a sparingly soluble hydrophobic compound with an appropriate less dense solvent. The sparingly soluble ion associate usually contains a multivalent anionic complex of the metal combined with more than one hydrophobic monovalent cation of the dye. Sometimes the floatable compound is not a simple ion associate but an adduct with salt molecules of the dye used. Normally, the precipitate separated by flotation is washed to remove the free dye and then dissolved in a polar organic solvent for spectrophotometric measurements. Flotation–spectrophotometric methods [4–6] for the determination of platinum metals and gold based on sparingly soluble ion associates of anionic complexes of these metals with basic dyes provide molar absorptivities (ϵ) of 2×10^5–1×10^6 l mol^{-1} cm^{-1}.

Flotation–spectrophotometric methods have not been reported for rare earth elements. However, in a weakly alkaline medium and the presence of 5,7-dichlorooxinequinolin-8-ol, praseodymium forms multivalent cluster compounds which give sparingly soluble, floatable ion associates with certain basic dyes. This paper deals with the flotation and spectrophotometric determination of praseodymium with 5,7-dichloroquinolin-8-ol and Rhodamine 6G. The developed procedure is highly sensitive ($\epsilon = 1.83 \times 10^5$ l mol^{-1} cm^{-1}) and applicable to the determination of praseodymium in aluminium metal and aluminium salts.

Correspondence to: T. Prasada Rao, Regional Research Laboratory (CSIR), Trivandrum 695019 (India).

EXPERIMENTAL

Reagents

All solutions were prepared with analytical-reagent grade chemicals and doubly distilled water. Hexane and acetone were distilled before use.

Praseodymium standard solution (1 mg Pr ml^{-1}) was prepared by dissolving 0.3020 g of praseodymium oxide (Rare Earth Products, Cheshire) in a minimum amount of 1 + 1 hydrochloric acid and diluting to volume with water in a 250-ml volumetric flask. The solution was standardised using EDTA. Working solutions were prepared by suitable dilution with water.

Rhodamine 6G was used as a 0.01% (w/v) aqueous solution.

5,7-Dichloroquinolin-8-ol, used as a 0.05% (w/v) solution in methanol, was freshly prepared daily.

Buffer solution (0.25 M) was prepared by dissolving 1.8 g of NH_4Cl in water, adding 2.5 ml of 25% (w/v) ammonia solution, adjusting the pH to 8.5 and diluting to 250 ml.

Apparatus

A Hitachi Model 220 microprocessor-controlled double-beam spectrophotometer was used with 1.00-cm quartz cells. An Elico Model LI-120 digital pH meter was used for pH measurements.

Procedure

To an aliquot of praseodymium solution containing up to 6 μg in 20 ml, add 1 ml of 5,7-dichloroquinolin-8-ol solution and 1.5 ml of NH_3–NH_4Cl buffer, adjust the pH to 8.5 and add 2.5 ml of Rhodamine 6G solution. Transfer the solution into a 60-ml separating funnel, add 10 ml of hexane and shake for 3 min. Slowly discard the aqueous layer, then wash the hexane phase and the separated precipitate by shaking with 5 ml of 0.25 M NH_3–NH_4Cl buffer for 3 min. Carefully remove the aqueous and organic layers and dissolve the precipitate adhering to the walls in 5 ml of acetone. Measure the absorbance at 530 nm against a reagent blank prepared in the same way.

RESULTS AND DISCUSSION

In weakly alkaline medium, praseodymium forms an anionic complex with 5,7-dichloroquinolin-8-ol. This anionic complex reacts with basic dyes to form sparingly soluble ion associates that accumulate on the walls of the separating funnel after shaking with a solvent of low polarity. Preliminary investigations showed that Rhodamine 6G was the most promising dye.

Optimization

The effect of pH on the flotation of the ion associate was investigated by varying the pH of the solution in the range 6.0–10.0 for 5 μg of praseodymium. The results obtained are shown in Fig. 1, from which it is clear that constant and maximum absorbance is obtained in the pH range 8.0–9.0. All further studies were carried out at pH 8.5 ± 0.5.

The 5,7-dichloroquinolin-8-ol concentration necessary for the formation of the praseodymium complex was studied over the range 0.1–3 ml of a 0.05% (w/v) solution. Curve A in Fig. 2 shows that a constant and maximum absorbance was obtained from 0.5 to 3.0 ml of 0.05% (w/v) 5,7-dichloroquinolin-8-ol solution and hence 1 ml of 0.05% (w/v) solution was used for all further studies.

The effect of Rhodamine 6G concentration on the flotation of the ion association complex was studied over the range 10–5.0 ml of a 0.01% (w/v) solution. It was found that the maximum

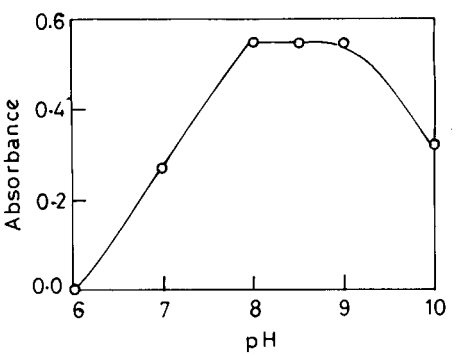

Fig. 1. Effect of pH (5 μg of praseodymium, 1 ml of 0.05% 5,7-dicholoroquinolin-8-ol, 2.5 ml of 0.01% Rhodamine 6G).

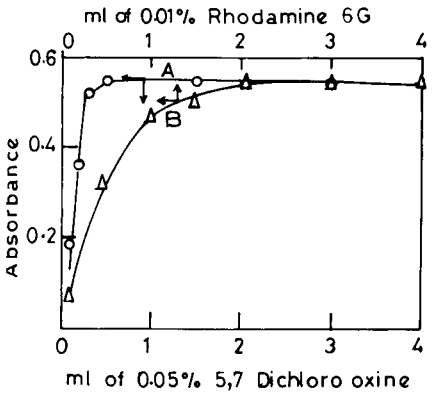

Fig. 2. Effects of (A) 5,7-dichloroquinolin-8-ol concentration (pH 8.5) and (B) Rhodamine 6G concentration (pH 8.5). Other conditions as in Fig. 1.

absorbance was obtained from 2.0 to 5.0 ml of 0.01% (w/v) Rhodamine 6G, as shown by curve B of Fig. 2. Hence 2.5 ml of 0.01% (w/v) Rhodamine 6G solution were used for all further investigations.

Shaking 25 ml of the aqueous phase with 10 ml of hexane for periods from 2.0–5.0 min resulted in a constant and maximum absorbance for the floated complex after dissolution in acetone. A 3-min equilibration time was chosen for all further experiments.

Flotation of the ternary ion associate with various solvents was examined and hexane was found to be the most suitable, as shown in Table 1. Constant and maximum absorbance was obtained by maintaining the aqueous phase volume between 15 and 30 ml; 25 ml of aqueous phase volume were chosen for further investigations.

TABLE 1

Choice of flotation solvent (5 μg of praseodymium in 25 ml)

Solvent	Absorbance
Hexane	0.550
Cyclohexane	0.297
Chloroform	0.080
Isoamyl acetate	0.020
Toluene	0.019
Isobutyl methyl ketone	0.011
Dichloroethane	0.006
Isobutyl alcohol	0.000
Butanol	0.000
Benzene	0.000

The order of addition of 5,7-dichloroquinolin-8-ol and Rhodamine 6G to the metal solution had no effect, but the addition of buffer directly to the praseodymium solution decreased the absorbance. Hence the buffer was added after the addition of 5,7-dichloroquinolin-8-ol.

Composition of the complex

The ratio of praseodymium to Rhodamine 6G and 5,7-dichloroquinolin-8-ol in the floated ion associate was established by both mole ratio and equilibrium shift methods. The results showed that the ratio of praseodymium to Rhodamine 6G is 1:2 and that of praseodymium to 5,7-dichloroquinolin-8-ol is 1:5.

Conformity with Beer's law and sensitivity

Under the optimum conditions, a linear calibration graph was obtained over the range 1–6

TABLE 2

Inteference study on the effect of 1 mg of the added ion on the response for 5 μg of praseodymium

Added in	Remarks
Li^+, Na^+, K^+, Be^{2+}, Ca^{2+}, Sr^{2+}, Ba^{2+}, As^{3+}, Te^{4+}, Br^-, F^-, ClO_4^-, Cl^-, I^-, SCN^-, CrO_4^{2-}, WO_4^{2-}, $S_2O_3^{2-}$, tartrate, thiourea, thioglycollic acid	No interference
Hg^{2+}	Masked by adding 2 ml of 5% thiourea
Bi^{3+}, Zr^{4+}, MoO_4^{2-}	Masked by adding 2 ml of 5% sodium tartrate
Pd^{2+}, Pt^{4+}	Masked by adding 2 ml of 5% thiogly collic acid

μg of praseodymium (with a gradient of 0.11 μg^{-1} of praseodymium) in 25 ml of the aqueous phase, i.e., 40–240 $\mu g\ l^{-1}$. The correlation coefficient of the present procedure was found to be 0.95. The molar absorptivity of the complex was 1.83×10^5 l mol^{-1} cm^{-1} at 530 nm. The detection limit corresponding to twice the standard deviation of the blank value was 8 $\mu g\ l^{-1}$. The proposed procedure showed good precision and the relative standard deviation ($n = 5$) for 200 $\mu g\ l^{-1}$ of praseodymium was 2.11%.

Interferences

The effects of 1-mg amounts of various ions on the determination of 5 μg of praseodymium were investigated. Table 2 lists those ions which did not interfere and those masked by various masking agents. Nonetheless, Fe^{3+}, Al^{3+}, Cu^{2+}, Ni^{2+}, Mg^{2+}, UO_2^{2+}, Co^{2+}, Zn^{2+}, Mn^{2+} and Ti^{4+} at the 1-mg level interfered in the determination. A simple ion-exchange procedure was therefore developed for the separation of praseodymium from these elements, based on the selective retention of trace amounts of praseodymium (as a solution in 1 M HCl) on a Dowex 50W-X8 (H^+) cation-exchange resin column. Subsequent elution of praseodymium with 0.5 M NH_4Cl resulted in its quantitative recovery. However, other rare earth elements behave similarly both in the ion-exchange separation and the flotation–spectrophotometric determination and therefore interfere if present.

Analysis of aluminium metal and aluminium salt samples

The proposed method (including the in-exchange step) was applied to the determination of praseodymium in aluminium metal and aluminium salts by adding known amounts of praseodymium prior to sample dissolution. The results obtained are given in Table 3, from which it can be seen that the recoveries are satisfactory and the results agree well with standard Arsenazo I method [7].

TABLE 3

Determination of praseodymium in aluminium and aluminium chloride after ion exchange

Sample	Amount per 100 ml (g)	Praseodymium added (μg)	Praseodymium found (μg)	
			Present method	Arsenazo I method
Aluminium metal	0.1	5	5.0	5.1
	0.25	50	49.0	49.5
	1.0	100	98.0	99.0
Aluminium chloride	0.5	5	4.9	5.0
	1.0	50	49.5	49.5
	2.0	100	98.5	98.0

Conclusions

Although many flotation–spectrophotometric procedures have been developed for the determination of noble metals, no such procedure has been reported for rare earth elements. The flotation–spectrophotometric procedure described here for the determination of praseodymium is more sensitive ($\epsilon = 1.83 \times 10^5$ l mol^{-1} cm^{-1}) than the commonly used Arsenazo I procedure ($\epsilon = 2.75 \times 10^4$ l mol^{-1} cm^{-1}). Even though other rare earth elements interfere, the method was successfully used for the determination of traces of praseodymium in aluminium and steel with a prior ion-exchange separation procedure.

REFERENCES

1 Z. Marczenko, CRC Crit Rev. Anal. Chem., 11 (1981) 195.
2 Z. Marczenko, Microchim. Acta, II (1977) 651.
3 Z. Marczenko and M. Jaroz, Analyst, 106 (1981) 751.
4 K. Kalinowski and Z. Marczenko, Microchim. Acta, I (1985) 167.
5 Z. Marczenko and K. Jankowski, Anal. Chim. Acta, 176 (1985) 185.
6 K. Kalinowski and Z. Marczenko, Anal. Chim. Acta, 186 (1986) 331.
7 I.M. Kolthoff and P.J. Elving, Treatise on Analytical Chemistry, Part II, Vol. 8, Interscience, New York, 1963.

Analytica Chimica Acta, 280 (1993) 173–177
Elsevier Science Publishers B.V., Amsterdam

Information extraction on efficient purification of organic reagents by using the branch and bound algorithm

Wei Zeng, Meihua Tu, Kean Li and Shenyang Tong

Department of Chemistry, Beijing University, Beijing 100871 (China)

(Received 16th November 1992; revised manuscript received 20th January 1993)

Abstract

Mixtures with a known range of possibly present species can be simultaneously analysed qualitatively and quantitatively by using the branch and bound algorithm. The computation time is much less than in the enumeration procedure and there is no risk of missing the real combination of co-existing components in the sample. Nitrophenol mixtures were analysed satisfactorily.

Keywords: UV–Visible spectrophotometry; Branch and bound algorithm; Nitrophenols; Organic reagent purification

When an organic reagent is synthesized, some by-products would be produced, such as isomers and derivatives, accompanying the main product. Because the chemical properties of the main product and the by-products may be similar, purification of the main product may be very difficult, and a selective method to determine the content of the main product is lacking. The problems are that it is difficult to know which by-products are present and what their contents are.

By using chemical knowledge, we can assume all the possible by-products of a reaction, and hence know the range of the impurities in the product of the reaction. However, we do not know what by-products will be produced and what will not. The characteristic of this problem is that the range of possible species present is known, but the exact components in the products are uncertain. This is the best variable selection problem in statistics. When the real components in the sample are not certain, some traditional methods, such as multiple linear regression [1] and the Kalman filter [2] cannot be used directly. Fortunately, some algorithms have been developed to solve this problem, such as all possible regression analysis, detailed by Garside [3], stepwise regression analysis [4] and best subset selection method, the branch and bound algorithm, advanced by Furnival and Wilson [5].

Stepwise regression analysis starts with no predictor variable in the model, then adds predictor variables one at a time to the regression model, according to the F statistic of the predictor variable. F statistics are calculated for each of the predictor variables in order to reflect the variable's contribution to the model. These calculated F statistics are then compared with the F-value of the prespecified selection criteria, namely SLE (significance level for entry). If the F statistic of some predictor variables is greater than the prespecified SLE value, then this method includes the predictor variables which have the largest F statistic contribution to the model. Before the next variable is added, the statistic of significance can be examined. Thus, after a variable has been added, the stepwise regression method looks at all the variables already in the

Correspondence to: Wei Zeng, Department of Chemistry, Beijing University, Beijing 100871 (China).

model and deletes any variable that does not produce an F statistic at a required significance level. Because this significance level sometimes is difficult to give properly, the model may be wrong.

The all possible regression method is adequate for small problems with only a few predictor variables. It is not difficult to carry out all the calculations by using high-speed computers. Because all the subsets of predictor variables must be calculated in this method, one can easily find the best subset which are good at explaining the data. However, if too many predictor variables are in the model, the computing time and internal storage needed for the all possible regression method will increase exponentially. For example, if ten predictor variables are in the model, 1024 (2^{10}) subsets would be calculated.

The computing time and internal storage needed for the all possible regression method can be greatly reduced if the branch and bound algorithm is used. This method only needs to compute a small fraction of all possible subsets of predictor variables. Because all the subsets which are not calculated are indifferent and unnecessary to the result, the result of this method is as precise as that of the all possible regression method. There is no risk of missing the real combination of co-existing components in the sample.

The chemical properties of compounds of the nitrophenol class are so similar that their spectra overlap heavily (Fig. 1). We simultaneously analysed the nitrophenols qualitatively and quantitatively by using the branch and bound algorithm and established the feasibility of the separation method for nitrophenol isomers and derivatives.

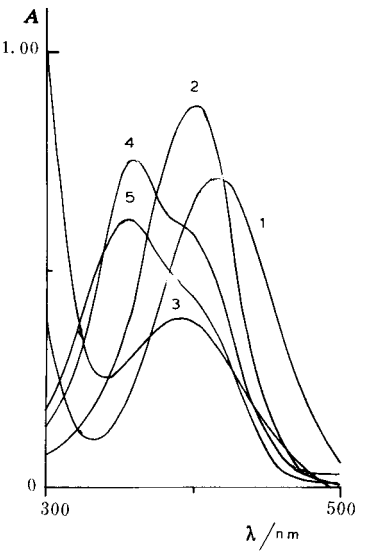

Fig. 1. Spectra of nitrophenols. 1 = *o*-Nitrophenol; 2 = *p*-nitrophenol; 3 = *m*-nitrophenol; 4 = 2,4-dinitrophenol; 5 = 2,4,6-trinitrophenol.

THEORY AND METHOD

According to the Lambert–Beer law, the general mathematical model of multi-component spectrophotometry is expressed as follows:

$$A = C_1E_1 + C_2E_2 + \cdots + C_mE_m + e \qquad (1)$$

where A is the absorbance vector of mixtures at different wavelengths, E_i the absorptivity vector of possibly present components at different wavelengths, e the error vector, i.e., the Gaussian distribution error of zero mean and uniform variance, C_i is the concentration of component i in the mixture and m is the number of possibly present components.

All possible variables were arranged from large to small according to the partial regression sum of squares. The branch and bound algorithm is based on the fundamental inequality

$$RSS(\mathrm{A}) \leqslant RSS(\mathrm{B})$$

where A is any set of independent variables and B is a subset of A. In other words, it is impossible to reduce the residual sum of squares (RSS) for a regression by deleting variables from that regression. The use of this inequality to restrict the number of subsets evaluated in a search for the best subset regression is illustrated by the inverse tree diagram in Fig. 2.

Figure 2 gives a five-variable inverse tree. The subset regression is computed by pivoting variables out of the regression from the top of the tree. The RSS for a node is obviously a lower bound for the RSS of its offspring. Hence, if we arrive at the node *.2345*, say, and had already computed one-, two- and three-variable regres-

sions with *RSS* smaller than that for *.2345*, then we could ignore the fourteen descendents of *.2345*.

In order to evaluate the importance of the variables and to eliminate the effects of dimension and range of values, the data are autoscaled to zero mean and uniform variance by subtracting from each variable the mean and dividing by the standard deviation.

In order to calculate effectively, a semi-sweep operator [6] is used, as follows.

For $A = (a_{ij})_{n\times n}$, if $a_{ii} \neq 0$, a new square matrix $B = (b_{ij})_{n\times n}$ is defined as follows:

$$b_{ii} = 1/a_{ii}$$

$$b_{ij} = a_{ij}/a_{ii}, \quad j \neq i$$

$$b_{ji} = -a_{ji}/a_{ii}, \quad j \neq i$$

$$b_{kl} = a_{kl} - a_{il} \cdot a_{ki}/a_{ii}, \quad k \neq i, \quad l \neq i$$

The above is called an S operator by pivot of a_{ii}, and expressed as $B = S_i A$.

A regression model can be expressed as follows:

$$Y = a1 + XB + e,\ E(e) = 0,\ \mathrm{cov}(e) = I$$

The matrix was divided as $X = (X_q : X_t)$, where X_q has q columns and X_t has t columns. S and A are defined as follows:

$$S = X^T X = \begin{vmatrix} X_q^T X_q & X_q^T X_t \\ X_t^T X_q & X_t^T X_t \end{vmatrix} = \begin{vmatrix} S_{11} & S_{12} \\ S_{21} & S_{22} \end{vmatrix}$$

$$A = \begin{bmatrix} S & X^T \bar{Y} \\ Y^T X & \|Y - \bar{Y}1\|^2 \end{bmatrix}$$

$$= \begin{bmatrix} S_{11} & S_{12} & X_q^T \bar{Y} \\ S_{21} & S_{22} & X_t^T \bar{Y} \\ Y^T X_q & Y^T X_t & \|Y - \bar{Y}1\|^2 \end{bmatrix}$$

With the S operator operating on matrix A, we obtained regression coefficients and the *RSS*. Because A is a symmetrical matrix, we can only operate the elements above the diagonal of the matrix.

Three common criteria are used for determining the best subset:

(1) Maximize R^2: $R^2 = 1 - RSS_q/SSY$

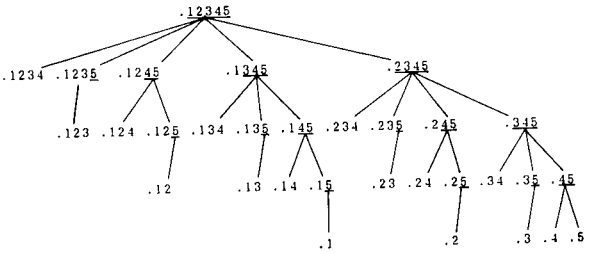

Fig. 2. Inverse tree.

(2) RMS_q: $RMS_q = RSS_q/(n-q)$

(3) Minimize Mallow's Cp statistic: $Cp = RSS_q/MSE - (n-2q)$

$$MSE = RSS_q/(n-q)$$

where RSS_q is the residual sum of squares containing q parameters, SSY is the total sum of squares containing q parameters, MSE is the residual mean squares from a regression model containing the total set of predictor variables, n is the number of collected data and q is the number of predictor variables present in the model.

EXPERIMENTAL

Instrumentation

Absorption spectra of the sample solution in 1.0 cm cuvettes were recorded every 2 nm in the range 300–500 nm on a Shimadzu UV-265 spectrophotometer. The program was written in TURBO PASCAL and run on an IBM PC-XT computer.

Reagents

Preparation of standard solutions and mixture samples. All reagents were of analytical-reagent grade. *o*-Nitrophenol was obtained from Merck, *m*-nitrophenol from Shanghai Reagents and *p*-nitrophenol, 2,4-dinitrophenol and 2,4,6-trinitrophenol from Beijing Chemical Factory. They were recrystallized many times under different conditions. The purified reagents were weighed accurately and dissolved in 0.1 mol l^{-1} NaOH and used to prepare mixture samples.

TABLE 1

Recoveries for unknown samples

Sample	Concentration (10^{-5} mol l^{-1})	Addition [a] (10^{-5} mol l^{-1})			Analytical results (10^{-5} mol l^{-1})			Recovery (%)		
m-Nitrophenol	44.0	A	C	D	A	C	D	A	C	D
		0	0	0	–	43.8	–			
		3.03	3.63	0.880	3.11	47.5	0.880	103	102	100
2,4-Dinitrophenol	7.42	A		D	A		D	A		D
		0		0	–		7.09			
		6.06		0.880	6.23		8.01	103		104
o-Nitrophenol	26.4	A		B	A		B	A		B
		0		0	26.1		0.019			
		6.06		1.74	32.3		1.77	102		101

[a] Added species A, B, C and D are *o*-nitrophenol, *p*-nitrophenol, *m*-nitrophenol and 2,4-dinitrophenol, respectively.

Preparation of unknown samples. Nitrophenol samples containing impurities were weighed accurately and dissolved in 0.1 mol l^{-1} NaOH.

Synthesis and separation of o-nitrophenol and p-nitrophenol [7]. To 60 ml of water in a flask immersed in an ice–water mixture, 21 ml of H_2SO_4 (sp. gr. 1.84) were added slowly, followed by 23 g of $NaNO_3$. A 14.1-g amount of phenol was dissolved in 4 ml of water, gently warmed to dissolve completely, then the solution was cooled to room temperature. The phenol solution was added to the $NaNO_3$ solution dropwise at 15–20°C and the mixture was kept for 0.5 h. A crude product (1), which contained mainly *o*- and *p*-nitrophenol, was obtained. The crude product was cooled with ice–water, washed several times with water, then steam distilled. The distillate was cooled to obtain a solid (2), which was mainly *o*-nitrophenol. The residual liquid in the distillation flask was diluted to 150 ml with water, 10 ml of concentrated HCl and 1 g of activated charcoal were added and the solution was boiled for 10 min, then filtered immediately. The filtrate was cooled with ice–water and allowed to stand overnight, giving *p*-nitrophenol (3) was obtained. The filtrate (4) after filtration was also kept for analysis.

RESULTS AND DISCUSSION

Study of mixture samples

Thirty sample mixtures with 1–5 components at concentrations between 0 and 3.73×10^{-4} mol l^{-1} were studied. The results indicate that the relative error for each component in the mixture samples was less than 3%, which is in the range of relative errors of spectrophotometric methods. The species in the mixtures selected by the program were exactly as expected. The species were neither mis-selected nor failed to be selected.

Study of unknown samples

The three nitrophenols were studied and the results are given in Table 1. The standard additions method was also used to support this method. Certain amounts of nitrophenols which were accurately added to other nitrophenols were determined by this method and their recoveries were close to 100%.

Analysis of synthetic samples

Samples of *o*- and *p*-nitrophenol synthesized in the laboratory were studied. The results are given in Table 2. It can be seen that the crude product (1) is a mixture of *o*-nitrophenol, *p*-

TABLE 2

Analytical results for synthetic samples

Sample [a]	A [b] (%)	B [b] (%)	C [b] (%)	D [b] (%)	E [c] (%)
1	33.4	61.7	–	–	5.0
2	100.0	–	–	–	–
3	12.8	86.4	–	–	0.9
4	–	96.3	–	–	3.7

[a] Samples 1–4 are explained in the text. [b] A–D are as in Table 1. [c] E is 2,4,6-trinitrophenol.

nitrophenol and 2,4,6-trinitrophenol. This result corresponds with the prediction of the theory of organic synthesis. Because of the inner molecular hydrogen bond in *o*-nitrophenol, the boiling point of *o*-nitrophenol is lower than that of the other compounds. When the crude product (1) was steam distillated, *o*-nitrophenol was extracted with the steam and separated from the crude product. Hence the *o*-nitrophenol (2) was very pure. Further, small amounts of *o*-nitrophenol and 2,4,6-trinitrophenol were also included in the *p*-nitrophenol (3). In the filtrate the main component was *p*-nitrophenol, and the content of 2,4,6-trinitrophenol was obviously higher than that of *p*-nitrophenol. This means that *p*-nitrophenol and 2,4,6-trinitrophenol can be separated efficiently by using dilute hydrochloric acid.

This work was supported by the National Natural Science Foundation of China.

REFERENCES

1 A. Lorber, L.E. Wangen and B.R. Kowalski, J. Chemometr., 1 (1987) 19.
2 Y.-M. Liu and R.-Q. Yu, Analyst, 112 (1987) 1135.
3 M.J. Garside, Appl. Statist., 20 (1971) 8.
4 R.R. Hocking, Technometrics, 14 (1972) 967.
5 G.M. Furnival and R.W. Wilson, Technometrics, 16 (1974) 499.
6 M.R. Schatzoff, S. Fienberg and R. Tsao, Technometrics, 10 (1968) 769.
7 Laboratory of Organic Chemistry in Lanzhou University and Fudan University, Organic Chemical Experiments, People's Educational Publishing House, Beijing, 1978, pp. 268–270.

PUBLICATION SCHEDULE FOR 1993

	S'92	O'92	N'92	D'92	J	F	M	A	M	J	J	A
Analytica Chimica Acta	267/1 267/2	268/1 268/2	269/1 269/2	270/1 270/2	271/1 271/2	272/1 272/2 273/1–2	274/1 274/2	275/1–2 276/1 276/2	277/1 277/2	278/1 278/2	279/1 279/2	280/1 280/2
Vibrational Spectroscopy		4/1			4/2		4/3	5/1		5/2		5/3

INFORMATION FOR AUTHORS

Detailed "Instructions to Authors" for *Analytica Chimica Acta* was published in Volume 256, No. 2, pp. 373–376. Free reprints of the "Instructions to Authors" of *Analytica Chimica Acta* and *Vibrational Spectroscopy* are available from the Editors or from: Elsevier Science Publishers B.V., P.O. Box 330, 1000 AH Amsterdam, The Netherlands. Telefax: (+31-20) 5862845.

Manuscripts. The language of the journal is English. English linguistic improvement is provided as part of the normal editorial processing. Authors should submit three copies of the manuscript in clear double-spaced typing on one side of the paper only. *Vibrational Spectroscopy* also accepts papers in English only.

Abstract. All papers and reviews begin with an Abstract (50–250 words) which should comprise a factual account of the contents of the paper, with emphasis on new information.

Figures. Figures should be prepared in black waterproof drawing ink on drawing or tracing paper of the same size as that on which the manuscript is typed. One original (or sharp glossy print) and two photostat (or other) copies are required. Attention should be given to line thickness, lettering (which should be kept to a minimum) and spacing on axes of graphs, to ensure suitability for reduction in size on printing. Axes of a graph should be clearly labelled, along the axes, outside the graph itself. All figures should be numbered with Arabic numerals, and require descriptive legends which should be typed on a separate sheet of paper. Simple straight-line graphs are not acceptable, because they can readily be described in the text by means of an equation or a sentence. Claims of linearity should be supported by regression data that include slope, intercept, standard deviations of the slope and intercept, standard error and the number of data points; correlation coefficients are optional.

Photographs should be glossy prints and be as rich in contrast as possible; colour photographs cannot be accepted. Line diagrams are generally preferred to photographs of equipment.

Computer outputs for reproduction as figures must be good quality on blank paper, and should preferably be submitted as glossy prints.

Nomenclature, abbreviations and symbols. In general, the recommendations of the International Union of Pure and Applied Chemistry (IUPAC) should be followed, and attention should be given to the recommendations of the Analytical Chemistry Division in the journal *Pure and Applied Chemistry* (see also *IUPAC Compendium of Analytical Nomenclature, Definitive Rules*, 1987).

References. The references should be collected at the end of the paper, numbered in the order of their appearance in the text (*not* alphabetically) and typed on a separate sheet.

Reprints. Fifty reprints will be supplied free of charge. Additional reprints (minimum 100) can be ordered. An order form containing price quotations will be sent to the authors together with the proofs of their article.

Papers dealing with vibrational spectroscopy should be sent to: Dr J.G. Grasselli, 150 Greentree Road, Chagrin Falls, OH 44022, U.S.A. Telefax: (+1-216) 2473360 (Americas, Canada, Australia and New Zealand) or Dr J.H. van der Maas, Department of Analytical Molecule Spectrometry, Faculty of Chemistry, University of Utrecht, P.O. Box 80083, 3508 TB Utrecht, The Netherlands. Telefax: (+31-30) 518219 (all other countries).

0003-2670/93/$06.00

This issue is printed on acid-free paper.

PRINTED IN THE NETHERLANDS

Methods for Experimental Design

Principles and Applications for Physicists and Chemists

by **J. Goupy**

Data Handling in Science and Technology Volume 12

The choice of ideal experiments is based on mathematical concepts, but the author adopts a practical approach and uses theory only when necessary. Written for experimenters by an experimenter, it is an introduction to the philosophy of scientific investigation. A method for organizing and conducting scientific experiments is described in this volume which enables experimenters to reduce the number of trials run, while retaining all the parameters that may influence the result.

Researchers with limited time and resources at their disposal will find this text a valuable guide for solving specific problems efficiently. The presentation makes extensive use of examples, and the approach and methods are graphical rather than numerical. All calculations can be performed on a personal computer; readers are assumed to have no previous knowledge of the subject. The presentation is such that the beginner may acquire a thorough understanding of the basic concepts. However, there is also sufficient material to challenge the advanced student. The book is, therefore, suitable for both first and advanced courses. The many examples can also be used in detail for self-study or as a reference.

Contents:

1993 xvi + 450 pages
Price: US $ 185.75 / Dfl. 325.00
ISBN 0-444-89529-9

ELSEVIER
SCIENCE PUBLISHERS

ORDER INFORMATION

For USA and Canada
ELSEVIER SCIENCE PUBLISHERS
Judy Weislogel
P.O. Box 945
Madison Square Station
New York, NY 10160-0757
Tel: (212) 989 5800
Fax: (212) 633 3880

In all other countries
ELSEVIER SCIENCE PUBLISHERS
P.O. Box 211
1000 AE Amsterdam
The Netherlands
Tel: (+31-20) 5803 753
Fax: (+31-20) 5803 705

US$ prices are valid only for the USA, Canada and are subject to exchange rate fluctuations; in all other countries the Dutch guilder price(s) is definitive. Customers in the European Community should add the appropriate VAT rate applicable in their country to the price(s). Books are sent post-free if prepaid.

0003-2670(19930802)280:1;1-H

11 FEB 36